

Metabolomic Studies by Capillary Electrophoresis-Electrospray Ionization-Mass Spectrometry

Comprehensive Metabolomics by Capillary Electrophoresis-Electrospray  
Ionization-Mass Spectrometry: Integrative Strategies for Biomarker Discovery

By

Richard Lee, MSc

A Thesis

Submitted to the School of Graduate Studies

In Partial Fulfillment of the Requirements

for the Degree

Doctorate of Philosophy

McMaster University

©Copyright by Richard Lee, Sept 2009

DOCTORATE OF PHILOSOLPHY (2009)

McMaster University

(Chemistry)

Hamilton, ON

TITLE : Comprehensive Metabolomics by Capillary Electrophoresis-Electrospray

Ionization-Mass Spectrometry: Integrative Strategies for Biomarker

Discovery

AUTHOR : Richard Lee, MSc (McMaster University)

SUPERVISOR : Dr. Philip Britz-McKibbin

NUMBER OF PAGES : xxvii, 250

## **Acknowledgments**

As I reflect on my journey through graduate school, I realize I could not have completed this part of my life without the support of several people. First I would like to thank my supervisor Dr. Philip Britz-McKibbin. Without his scientific direction and unwavering faith in our vision, this story may not have been possible. I would also like to thank the members of my committee, Dr. Jack Rosenfeld and Dr. John Brennan, for their guidance and advice. I would also like to thank past and present members of the Britz-McKibbin group for their support and entertainment on long days.

Graduate school can be a stressful environment but friends and family have always been there to encourage me through the tough times. Though the list is long and I cannot list everyone that had an impact I would specifically like to thank the “boys” - they have endured my struggles and supported me throughout my undergraduate and graduate years. To my family, and especially my sister Jackie I would not be here without you. Most of all, I would like to thank my wife Karin. For years she has been supported and encouraged me through the tough times of research, and reminded me on a number of occasions - when I wanted to wave the white flag, how much I wanted this and love research. Without her this would not have possible. Thank you.

**Abstract**

Metabolomics is a rapidly emerging area of post-genomic research aimed at the comprehensive analysis of all low molecular weight metabolites in a cell or biofluid, which heralds new advances in drug development, disease prognosis and nutritional intervention. The major goals of this thesis are aimed at addressing several key obstacles hampering the development of metabolomics in biological research that is presented in four major chapters in this thesis. *Chapter II* introduces an integrative strategy for the identification of unknown low abundance metabolites when using capillary electrophoresis-electrospray ionization-mass spectrometry (CE-ESI-MS) in conjunction with computer simulations when chemical standards are unavailable. The second project in *Chapter III* develops and validates an artifact-free method for analysis of labile metabolites in filtered red blood cell lysates by CE-ESI-MS that allows for accurate assessment of cellular redox status and antioxidant capacity based on the differential rates of glutathione oxidation. *Chapter IV* of the thesis introduces a differential metabolomics strategy for quantitative assessment of cellular oxidative stress and antioxidant efficacy with strenuous exercise. CE-ESI-MS together with univariate and multivariate data analysis was used to identify putative early- and late-stage biomarkers of oxidative stress in erythrocytes, which was applied to assess the attenuation of oxidative stress following high-dose oral *N*-acetyl-*L*-cysteine administration. The final project in *Chapter V* investigates the impact of low-dose  $\gamma$ -irradiation on intra-cellular metabolism and

cell membrane viability of leukocytes when using CE-ESI-MS and fluorescence-based flow cytometry, respectively. A distinct non-linear cellular response was measured for irradiated-leukocytes as reflected by a significant upregulation of metabolites and slower progression of late-stage apoptosis when exposed to a minimum-threshold dose of radiation. Metabolomics by CE-ESI-MS provides a novel and hypothesis-generating approach for investigating complex biological phenomena, which can improve our fundamental understanding of the underlying mechanisms of oxidative stress that is relevant to human health, aging and disease pathogenesis.

The following chapter material has been published previously and is reprinted with written permission :

**Chapter II :**

- Reprinted from : *Anal. Chem.*, **79**, R. Lee, A.S. Ptolemy, L. Niewczas and P. Britz-McKibbin, *Integrative Metabolomics for Characterizing Unknown low Abundant Metabolites by Capillary Electrophoresis-Mass Spectrometry with Computer Simulations*, 403-415, Copyright (2007) American Chemical Society.

**Chapter III :**

- Reprinted from : *Anal. Chem.*, **81** R. Lee and P. Britz-McKibbin, *Differential Rates of Glutathione Oxidation for Assessment of Intra-cellular Redox Status and Antioxidant Capacity by Capillary Electrophoresis-Electrospray Ionization-Mass Spectrometry: An Elusive Biomarker of Oxidative Stress*, 7047-7056, Copyright (2009) American Chemical Society.

**Chapter IV :**

- Reprinted from : submitted work, *J. Prot. Res.*, R. Lee, D. West, S.M. Phillips, and P. Britz-McKibbin, *Differential Metabolomics for Quantitative Assessment of Cellular Oxidative Stress and Antioxidant Efficacy with Strenuous Aerobic Exercise*, Copyright (2009) American Chemical Society.

**Chapter V :**

- Reprinted from : submitted work, *Electrophoresis*, R. Lee and P. Britz-McKibbin, *Metabolomic Studies of Radiation-induced Apoptosis of Human Leukocytes by Capillary Electrophoresis-Electrospray Ionization-Mass Spectrometry*, Copyright (2009) Wiley Interscience.

## Table of Contents

### I. Introduction to Metabolomics and Capillary Electrophoresis-Electrospray-Mass Spectrometry

1.1. Metabolomics .....	2
1.1.1. The Greatest omics of them all? .....	2
1.1.2. History of Metabolomics .....	4
1.2. Analytical Platforms for Metabolomic Studies .....	8
1.3. Capillary Electrophoresis Based Separation .....	14
1.3.1. Capillary Electrophoresis .....	14
1.3.2. Electrokinetic Phenomenon in CE .....	14
1.3.3. Electrophoretic Mobility ( $\mu_{ep}$ ) .....	15
1.3.4. Electroosmotic Flow (EOF) .....	17
1.3.5. Apparent Mobility .....	21
1.4. Mass Spectrometry – Ion Trap Mass Analyzer .....	24
1.4.1. Ion Trap Mass Analyzer .....	24
1.4.2. Ejection and Detection of Ions .....	25
1.4.3. Electrospray Ionization .....	27
1.4.4. CE-MS and Metabolomics .....	30
1.5. Data Analysis in Metabolomics .....	33
1.6. Applications of Metabolomics .....	37
1.7. Introduction to Oxidative Stress .....	42
1.7.1. Biomarkers of Oxidative Stress.....	42
1.7.2. Reactive Oxygen Species .....	44
1.7.3. Glutathione Metabolism .....	46
1.7.4. Functions of Glutathione .....	48
1.8. Research Objectives .....	50
1.9. References .....	51

## **II. Integrative Metabolomics for Characterizing Unknown Low Abundance Metabolites by Capillary Electrophoresis-Mass Spectrometry with Computer Simulations**

2.1. Abstract .....	66
2.2. Introduction .....	67
2.3. Experimental Section .....	73
2.3.1. Chemicals and Reagents.....	73
2.3.2. Apparatus and Conditions .....	73
2.3.3. <i>E. coli</i> Bacterial Incubation .....	75
2.3.4. Computer Simulation Using Simul 5.0 .....	76
2.4. Theory .....	78
2.4.1. Metabolite $\mu_0$ Determination .....	78
2.4.2. Metabolite $pK_a$ Determination.....	79
2.5. Results and Discussion .....	81
2.5.1. Optimization of On-Line Sample Preconcentration by CE-MS.....	81
2.5.2. Mechanism of t-CITP with Dynamic pH Junction.....	86
2.5.3. Prediction of RMT of Cationic Metabolites by Computer Simulations.....	90
2.5.4. Differential Metabolite Uptake during Bacterial Growth .....	93
2.5.5. De Novo Identification of Unknown Nutrients .....	96
2.5.6. Nutrient Uptake Patterns by <i>E. coli</i> during Growth .....	101
2.6. Conclusion .....	103
2.7. References .....	98

## **III. Differential Rates of Glutathione Oxidation for Assessment of Cellular Redox Status and Antioxidant Capacity by Capillary Electrophoresis-Mass Spectrometry: An Elusive Biomarker of Oxidative Stress**

3.1. Abstract .....	111
3.2. Introduction .....	112
3.3. Materials and Methods .....	116
3.3.1. Chemicals and Reagents.....	116

3.3.2. Apparatus and Conditions .....	117
3.3.3. Fingerprick Microsampling and Filtered RBC Lysate Preparation.....	119
3.3.4. <i>Ex-vivo</i> Oxidation Kinetic Studies of Filtered RBC Lysates for Anti-oxidant Capacity.....	120
3.3.5. <i>In-vitro</i> Incubation of Intact RBCs with Extrinsic Reagents.....	122
3.3.6. Protein-bound Glutathione Sample Preparation.....	122
3.3.7. Hemoglobin Assay .....	123
3.4 Results and Discussion.....	124
3.4.1. CE-MS Optimization for Artifact-free Glutathione Analysis .....	124
3.4.2. Ultrafiltration for Accurate Glutathione Determination in RBC Lysates .....	126
3.4.3. Equilibrium Free and Bound Glutathione Levels in Normal RBCs .....	128
3.4.4. Antioxidant Capacity of RBCs via Differential Rates of Glutathione Oxidation .....	132
3.4.5. <i>In-vitro</i> Preincubation of RBCs with Electrophilic Reagents .....	136
3.4.6. <i>In-vitro</i> Preincubation of RBCs with Antioxidant Supplements.....	139
3.5. Conclusions .....	144
3.6. References .....	146

#### **IV. Differential Metabolomics for Quantitative Assessment of Cellular Oxidative Stress and Antioxidant Efficacy with Strenuous Aerobic Exercise: Redox-Control of Cellular Metabolism by N-Acetyl-L-Cysteine.**

4.1. Abstract .....	154
4.2. Introduction .....	156
4.3. Materials and Methods .....	161
4.3.1. Chemicals and Reagents.....	161
4.3.2. Apparatus and Conditions .....	161
4.3.3. Strenuous Aerobic Exercise Regime.....	163
4.3.4. Blood Collection and Filtered RBC Lysate Preparation. ....	165
4.3.5. Data Processing and Statistical Analysis.....	167
4.4. Results .....	169

4.4.1. Unsupervised Data Exploration of Exercise-induced Oxidative Stress .....	169
4.4.2. Glutathione Metabolites as Early-stage Biomarkers of Oxidative Stress.....	175
4.4.3. Discovery of Unknown Biomarkers of Oxidative Stress .....	178
4.4.4. Concentration Profiles of Lead Biomarkers of Oxidative Stress .....	181
4.4.5. Global Metabolite Perturbations with High-dose NAC Intake Are Reversible.....	184
4.5. Discussion .....	186
4.5.1. Global Metabolite Profiling of Erythrocytes by CE-ESI-MS .....	186
4.5.2. Erythrocytes as Reporter Cells to Oxidative Stress.....	190
4.5.3. The Enigmatic Functions of NAC and Future Directions .....	193
4.5.4. Redox control of Global Metabolism and Future directions.....	193
4.6. Conclusions .....	198
4.7. References .....	200

## **V. Metabolomic Studies of Radiation-induced Apoptosis of Human Leukocytes by Capillary Electrophoresis-Electrospray Ionization-Mass Spectrometry and Flow Cytometry: Adaptive Cellular Response to Ionizing Radiation**

5.1. Abstract .....	209
5.2. Introduction .....	210
5.3. Materials and Methods .....	214
5.3.1. Chemicals and Reagents.....	214
5.3.2. Cell Culture and Irradiation.....	214
5.3.3. Flow Cytometric Assay .....	215
5.3.4. Metabolite Extraction .....	216
5.3.5. Apparatus and Conditions .....	216
5.3.6. Data Preprocessing and Statistical Analyses.....	218
5.4. Results and Discussion .....	220
5.4.1. Radiation-induced Apoptosis on Leukocytes .....	223

5.4.2. Untargeted Metabolite Profiling via CE-MS .....	224
5.4.3. Dose Dependant Metabolic Responses to Ionizing Radiation .....	225
5.4.4. Biological Interpretations of Low-level Irradiation of Leukocytes .....	227
5.5. Conclusion .....	232
5.6. References .....	233

## **VI. Future Directions in Capillary Electrophoresis-Electrospray Ionization-Mass Spectrometry for Biomarker Discovery**

6.1. Extension of Aerobic Exercise Induced Oxidative Stress .....	246
6.2. Integrated Sample Pretreatment of Thiol-Metabolites .....	248
6.3. Radiation-induced Metabolic Response .....	250
6.4. Critical Aspects of Metabolomics and Future Directions .....	252
6.5. References .....	253

## List of Figures

- Figure 1.1.** Schematic representing the major “omic” levels of functional genomics studies in systems biology ..... 3
- Figure 1.2.** Illustrates the classification of detected metabolites from *E. Coli* extracts by CE-MS. (a) Comprehensive list of 727 known metabolites in *E. Coli* classified according to their metabolic pathway from the Kyoto Encyclopedia of Genes and Genome. Class: I, primary metabolism; II, degradation of primary metabolites; III, Degradation of environmental compounds; IV, secondary or unconventional metabolism; V, pathway unknown; VI, intermediates in putative *in vitro* reaction. Further cataloging of metabolites in class I and II into (b) polar and non-polar metabolites, which are then further reduced into those which can be detected by CE-TOF-MS analysis for (c) hydrophilic metabolites..... 6
- Figure 1.3.** Bar graph showing the rapid increase in total metabolomics publications from 1989 to 2008 according to Web of Knowledge using a query search of “metabolomics and metabonomics” performed on June 21, 2009 relative to other major milestones in genomic and post-genomic research..... 9
- Figure 1.4.** Debye-Hückle-Stern model of the electric double layer showing the diffuse double layer and the zeta potential that generates the EOF near the capillary surface under an applied external voltage ..... 18
- Figure 1.5.** Comparison of the fluid transport profiles and corresponding analyte peak shapes for (a) a flat electrokinetic laminar flow in CE and (b) a parabolic flow generated by a pressure-driven pumping system ..... 20
- Figure 1.6.** Schematic showing separation of a mixture of ions based on differences in their  $\mu_{ep}$  using CE: (a) hydrodynamic injection, (b) zonal separation at pH >6 with strong EOF, (c) representative electropherogram under neutral/alkaline condition, (d) zonal separation at pH < 2 with suppressed EOF, and (e) representative electropherogram under strongly acidic conditions. .... 23

**Figure 1.7.** Schematic depicting (a) electrode configuration of a quadrupole 3D ion trap MS instrument. Stable and unstable ions are denoted in brown and red, respectively. Unstable ions do not have the correct trajectory and collide with the electrode and are neutralized. (b) stability regions where ions possess stable trajectories within the ion trap based on solutions of Mathieu equation ..... 26

**Figure 1.8.** Schematic diagram of a coaxial sheath liquid interface for CE-ESI-MS, as well as the ion evaporation process where gas-phase ions of solutes are generated from charged droplets..... 29

**Figure 1.9.** Total number of publications cited for CE-MS from 1989 to 2008 using ISI Web of Knowledge ..... 32

**Figure 1.10.** Principle component analysis (PCA) model estimates the variation in the matrix table. The analysis generates a score plot which can group data points which exhibit similar characteristics and identify possible outliers. The loadings plot represents the influence of the data points and their relation between them. .... 35

**Figure 1.11.** Schematic diagram depicting the circular workflow for untargeted metabolomic studies. Each step represents a critical aspect which must be carefully controlled for untargeted metabolomic analyses. Experimental design is vital for control of variables to limit any experimental variations, followed by the type of sample matrix and preparation. Method validation used on any analytical platform is imperative to have reproducible and valid results. Appropriate data preprocessing and mining are critical for identifying unique data changes, which can then be used for metabolite identification processes. Experimental data may confirm initial hypothesis or may lead to newly formed hypothesis ..... 38

**Figure 1.12.** Illustration of possible pathways for free radical generation and neutralization in erythrocytes. Oxidation of hemoglobin into methemoglobin releasing superoxide radical which is neutralized by superoxide dismutase into  $H_2O_2$ . Peroxide is neutralized by oxidation of GSH into GSSG by forming water and oxygen. .... 45

**Figure 1.13.** Schematic diagram of the biosynthetic pathway for production of

glutathione. The primary metabolism of glutathione consists of six coupled enzymatic reactions with the rate determining step associated with  $\gamma$ -glutamylcysteine biosynthesis. .... 47

**Figure 2.1.** On-line sample preconcentration via t-CITP with dynamic pH junction by CE-MS. (a) Plot depicting the impact of increasing sample injection bandwidth on amino acid ion count signal. (b) Overlay of three EIEs highlighting the influence of sample pH and co-ion on the extent of analyte band narrowing. Conditions: 1 M formic acid, pH 1.8, was used as the BGE, whereas the sample composition was 200 mM ammonium acetate, pH 7.0, in (a) and (b) red trace, 200 mM ammonium acetate, pH 1.8, in (b) green trace, and 1 M formic acid, pH 1.8, in (b) blue trace. Analyte peak numbering corresponds to 20  $\mu$ M concentration of the four different amino acids: (1) Trp, (2) Lys, (3) Glu, and (4) Ala... 83

**Figure 2.2.** Time-resolved electropherograms showing the dynamics of in-capillary Trp focusing by t-CITP with dynamic pH junction from experimental data and computer simulations using Simul 5.0 (insets). A long sample plug of 12.5 cm was placed at increasing distance from the distal end of the capillary ( $L_d$ ) from about (a) 7.5, (b) 25, and (c) 40 cm. Conditions: BGE, 1 M formic acid, pH 1.8; sample, 200 mM ammonium acetate, pH 7.0, 15 mM NaCl. Analyte peak numbering corresponds to the concentration profiles of (1) Trp (experimental), (1\*) Trp (simulated), (2)  $\text{NH}_4^+$ , (3)  $\text{Na}^+$ , and (4) pH. Note that concentration profiles of  $\text{NH}_4^+$  and  $\text{Na}^+$  co-ions were reduced relative to Trp for clarity purposes ..... 87

**Figure 2.3.** Comparison of experimental and simulated electropherograms for model amino acids using on-line sample preconcentration by CE-MS. (a) An overlay of EIEs for 20  $\mu$ M amino acids using the internal standard, MetS, and (b) predicted electropherogram using Simul 5.0 based on  $\mu_o$  and  $pK_a$  parameters listed in Table 2.1. Conditions: BGE, 1 M formic acid, pH 1.8; sample, 200 mM ammonium acetate, pH 7.0; sample injection, 6.2 cm;  $V$ , 23 kV; and  $L_c$ , 80 cm. Analyte peak numbering: (1) Lys, (2) His, (3) Gly, (4) Ala, (5) Ser, (6) Thr, (7) Glu, (7a) Lys ( $^{13}\text{C}$ ), (8) Trp, (9) Tyr, (10) Asp, and (11) MetS (IS)...92

**Figure 2.4.** Series of EIEs revealing selective nutrient uptake within complex LB broth media as a function of *E. coli* growth at (a) 0, (b) 1.5, and (c) 5 h by CE-MS. Conditions similar to Figure 2.3, except that analyte peak numbering corresponds to the following: (1) Lys, (1a) unknown (isobaric to Lys, 147 Da) 2-Ser, (3) unknown (267 Da), (4) Thr,

(4a) unknown (isobaric to Thr, 120 Da), (5) Trp, (6) Glu, (7) Tyr, (8) Asp, (9) MetS (IS), and (10) unknown (284 Da)..... 95

**Figure 2.5.** Integrative metabolomics strategy for unknown metabolite identification based on preliminary (a) multistage MS<sup>n</sup> and (b) dHDX experiments in conjunction with (c) computer simulations by Simul 5.0. Identification of two potential isomeric candidates ((3a) G and (3b) isoG) from KEGG database related to unknown nutrient 10 in Figure 2.4. Confirmation of G based on comparison of experimental with predicted RMTs using parameters in Table 2.2. Simulations were also applied to readily distinguish other isobaric ((1a) Lys vs (1b) Gln) and isomeric ((2a) Thr vs (2b) hSer) cations unresolved by conventional MS..... 97

**Figure 2.6.** Quantitative analysis of differential nutrient uptake patterns by *E. coli* in LB broth media as a function of total dried cell weight. Three distinct stages of bacterial growth are associated with specific nutrient uptake behavior from (a) 0-1.5, (b) 1.5-5, and (c) 5-8 h. Analyte peak numbering: (1) Asp, (2) Ser, (3) G, (4) Glu, (5) Trp, (5) Thr, (7) Lys, (8) Phe, and (9) Tyr..... 102

**Figure 3.1.** A comparison of (a) normal and (b) modified hydrodynamic sample injection sequences for avoiding oxidation artifacts at the anodic electrode interface when analyzing trace levels of GSSG in the presence of a 500-fold excess of GSH by CE-ESI-MS with on-line sample preconcentration. A series of extracted ion electropherogram overlays demonstrate a 3-fold improvement in method precision via the modified sample injection (CV  $\approx$  6.9%,  $n = 4$ ) when quantifying 3  $\mu$ M GSSG ( $MH_2^{2+} = 307$   $m/z$ ) that was independent of GSH concentration. .... 125

**Figure 3.2.** Recovery study highlighting the lack of oxidation artifacts occurring during sampling processing of filtered RBC lysates with ultrafiltration by spiking 100  $\mu$ M GSEE in ice-cold de-ionized water which was used for hemolysis. An overall recovery of reduced GSEE was determined to be (109  $\pm$  2)% without detection of the GSEE-GSEE disulfide homodimer ( $MH^+ = 336$   $m/z$ ) or GS-GSEE disulfide heterodimer ( $MH_2^{2+} = 321$   $m/z$ ) unlike low micromolar levels of GSSG ( $MH_2^{2+} = 307$   $m/z$ ) derived from filtered RBC lysates when using CE-ESI-MS. Black trace represents a section of the total ion electropherogram, whereas blue/red traces are extracted ion electropherogram overlays for peptides, which highlights the large dynamic range between high abundance GSH ( $MH^+ =$

308  $m/z$ ) and minor cationic metabolites present in erythrocytes, including various amino acids and amines. .... 129

**Figure 3.3.** *Ex-vivo* metal-catalyzed oxidation kinetic studies on filtered RBC lysates (normal) based on the apparent rates of GSH consumption ( $k_{GSH}$ ) and GSSG ( $k_{GSSG}$ ) formation for assessment of intra-cellular redox status and antioxidant capacity by CE-ESI-MS. (a) Extracted ion electropherograms highlighting qualitative changes in GSH and GSSG levels due to oxidation by  $\cdot\text{OH}$  as a function of incubation time. (b) Non-linear oxidation kinetic plots measured for GSH and GSSG in healthy RBCs as a biological reference ( $n = 3$ ), where the inset shows adherence to a pseudo-first order rate law ( $R^2 > 0.997$ ) with  $t_{CO}$  defined as the cross-over time interval at the intersection of GSH and GSSG linearized kinetic plots..... 134

**Figure 3.4.** *Ex-vivo* metal-catalyzed oxidation kinetic studies on filtered RBC lysates after preincubation of intact erythrocytes with NAC. (a) Extracted ion electropherograms highlighting qualitative changes in GSH and GSSG (initial concentrations unchanged relative to normal cells) due to oxidation by  $\cdot\text{OH}$  as a function of incubation time, which confirms the increased free radical scavenging efficiency of NAC-fortified cells. (b) Overall, attenuated oxidation kinetics were observed for NAC-enriched RBCs relative to normal cells as reflected by significantly slower apparent  $k_{GSSG}$  and longer  $t_{CO}$  in comparison to Figure 3.2 ..... 137

**Figure 3.5.** Metal-catalyzed oxidation kinetic studies on filtered RBC lysates after preincubation of intact erythrocytes with NAC. (a) Extracted ion electropherograms highlighting qualitative changes in GSH and GSSG (initial concentrations unchanged relative to normal cells) due to oxidation by  $\cdot\text{OH}$  as a function of incubation time, which confirms the increased free radical scavenging efficiency of NAC-fortified cells. (b) Overall, attenuated oxidation kinetics were observed for NAC-enriched RBCs relative to normal cells as reflected by significantly slower apparent  $k_{GSSG}$  and longer  $t_{CO}$  in comparison to Figure 3.3. .... 141

**Figure 3.6.** (a) Series of extracted ion electropherograms when using anionic CE conditions with negative-ion mode ESI-MS detection for simultaneous analysis of GSH and GSSG from NAC-enriched RBCs, as well as acidic metabolites not amenable to separations under acidic CE conditions, including NAC, NAC-NAC and GS-NAC (where

IS represents HQSA). Note that NAC-NAC and GS-NAC disulfide levels rapidly increase at early stages of metal-catalyzed oxidation (not detectable at  $t = 0$  min), but do not significantly change from 60 min to 180 min unlike GSH, GSSG and NAC. (b) ESI-MS spectra confirming the identification of disulfide adducts formed during metal-catalyzed oxidation reaction, namely NAC-NAC and GS-NAC..... 142

**Figure 3.7.** Proposed mechanism for describing the enhanced antioxidant capacity of NAC-enriched RBCs relative to normal cells based on competitive irreversible reactions (a-c) involving the direct reduction of free radicals ( $\cdot\text{OH}$ ) by GSH and/or NAC, as well as a reversible thiol-exchange reactions (d, e) associated with GSH and NAC-NAC, as well as NAC and GSSG. The latter reversible reaction is thermodynamically favored towards the forward direction with  $\Delta E_{hc2}^{\circ} \approx +63$  mV. The greater reduction potential of NAC provides a driving force for catalytic renewal of GSH during oxidative insult that is reflected by slower apparent  $k_{GSSG}$  and longer  $t_{CO}$  shown in Figure 3.4 of the supporting information section relative to normal RBCs ..... 143

**Figure 4.1.** 3D heat maps qualitatively display changes in the measured standardized response (*i.e.*, average relative peak area standardized at each time interval) for each metabolite defined as a paired variable ( $m/z$ :RMT) over a six hour time interval, which were arranged in a dendrogram using a HCA algorithm as an unsupervised method for pattern recognition. (a) The control trial without oral NAC supplementation, exhibits an oscillating pattern of metabolite profiles changing over the duration of the experiment that can be qualitatively classified into five distinctive groups. (b) Depicts the trial with NAC supplementation which illustrates the attenuation of metabolite fluctuations..... 171

**Figure 4.2.** Principle component analysis of all metabolites detected in control (blue) and oral NAC trials (red) (a) The scores plot of both control and NAC trials were overlaid on one PCA plot which revealed six metabolites denoted by their characteristic  $m/z$ :RMT as significant outliers which were observed for both trials. The inset represents the differential PCA which illustrates the same metabolites identified in (a) which undergoes significant change during the exercise regime. (b) Loadings plot of both control and oral NAC trials illustrates the global cellular stress during the oxidative stress event and the return to homeostatic levels after the event. The distinct metabolite attenuation of NAC can be seen by the reduction of the breath/elongation of its loadings curve along PC1...173

**Figure 4.3.** (a) Depicts the overlay plot of relative ion response for GSH and GSSG

during the exhaustive exercise regime. GSH and GSSG undergo significant changes during the exercise protocol as demonstrated by the over 20 fold increase of GSSG and the concomitant decrease of GSH in the control trial. GSH depletion and GSSG formation is modulated during the oral NAC trial. The inset displays the reduction of total RBC oxidation by 14% by oral supplementation of NAC. (b) Illustrates the half cell reduction potential of GSH, ( $E_{GSSG/2GSH}$ ). Both trials initially start with highly reduced state then undergo oxidation during the exhaustive exercise regime. This highly reversible process is attenuated by the consumption of NAC as shown by the more reduced state at the peak oxidation levels and the significantly shorter recovery time....176

**Figure 4.4.** (a) Base peak electropherogram of RBC lysate during T=0 min of control trial. Inset illustrates the extracted ion electropherograms of putative unknown biomarkers of oxidative stress. A large dynamic range is observed for the metabolites in RBC lysate with GSH in excess with the putative biomarkers in low abundance. (b) Multistage MS<sup>n</sup> spectra were acquired for the unknown biomarkers and compared against available database spectra. Identification of metabolites were (i) 3Me-His, (ii) C0, (iii) Cre, and (iv) C2 ..... 180

**Figure 4.5.** Time-dependent concentration profiles of six lead biomarkers of oxidative stress in control (blue) and oral NAC trials (red). (a) GSH and (b) GSSG profile depicts the enormous change during the oxidative stress event but returns to baseline levels during the recovery period for both control and oral NAC trials. (c) C2, (d) C0, and (e) Cre shared similar oscillating patters during exhaustive exercise in the control trial until stabilizing the end of the recovery period but were significantly elevated. During oral NAC trial C2, C0, and Cre were downregulated and did not exhibit significant increase at the end of the exercise protocol . (f) 3-MeHis was observed to have a unique concentration profile as it was not elevated at the end of the exercise protocol during the control trial but was downregulated and greatly attenuated by oral NAC supplementation. .... 182

**Figure 4.6.** Univariate analysis comparing the fold change of oral NAC trial at rest (blue) and 5 days after NAC trial (purple) relative to control trial at rest. Identified metabolites are labeled above their corresponding (m/z:RMT) values. Metabolites exhibited an overall significant down regulation with oral NAC..... 187

**Figure 4.7.** A summary of four major metabolic reactions associated with oxidative stress biomarkers identified in this study, namely GSH, GSSG, C0, C2, Cre and 3-MeHis. The efficacy of NAC pretreatment in attenuating oxidative stress while delaying the onset of fatigue during strenuous exercise is associated with inhibition of key cellular energy metabolic pathways involving skeletal muscle tissue, such as fatty acid catabolism involving acylcarnitine transport and creatine kinase activity for ATP regulation. Reduced energy demands at rest and during prolonged cycling with NAC pretreatment generates lower levels of RONS corresponding to a decrease in the extent of glutathione oxidation (GSSG) and a slower rate of proteolysis in muscle tissue as indicated by lower amounts of 3-MeHis uptaken by RBCs. .... 196

**Figure 5.1.** Average flow cytometry histogram for differentiating sub-populations of irradiated-leukocytes following a 44 hr incubation period that were exposed to a) 0 Gy, b) 2 Gy, c) 4 Gy, and d) 8 Gy. Lower left quadrant represents the double-negative staining region representing viable cells, lower right quadrant reflects the Annexin V-FITC positive-staining region corresponding to early-stage apoptosis, and the upper right quadrant represents the double-positive staining region of both AnxV and 7-AAD indicative of late-stage apoptosis..... 221

**Figure 5.2.** A series of extracted ion electropherograms (EIE-offset) for four major unknown metabolites and other identified isobaric ions derived from filtered WBC lysates exposed to increasing levels of  $\gamma$ -irradiation. Arrows qualitatively highlight the net depletion or upregulation of metabolites relative to control at increasing radiation dosages when using CE-ESI-MS. (a) unknown X1,  $m/z$  104, (b) unknown X3,  $m/z$  116 with isobar Pro (c) unknown X5,  $m/z$  131 (d) unknown X8,  $m/z$  132 with isobars Cre and Leu, whereas (e) depicts the non-linear dose-response relationship of eight known metabolites identified from irradiated-leukocytes that exhibited significant upregulation at the 4 Gy level in terms of their relative concentration levels in comparison to the control..... 226

**Figure 5.3.** Histogram illustrating the impact of irradiation dosage on intra-cellular cellular metabolism that shows the non-linear changes in identified and unknown metabolite levels derived from human leukocytes relative to the control at 0 Gy. Blue, red, and green bar graphs represent fold-change in average normalized ion responses measured for metabolites at 2, 4, and 8 Gy radiation relative to the control, where error bars represent  $\pm 1\sigma$  (triplicate measurements from two sets of cell batches,  $n=6$ ). A major

depletion in metabolites was consistently measured for most metabolites at the 2 and 8 Gy doses, whereas a significant upregulation or recovery to control levels were detected for the majority of metabolites at the intermediate 4 Gy dose level, notably for Gln, Arg, Pro, Cre and GSH..... 228

**Figure 6.1.** Reaction of maleimide with thiol moiety to form the stable thiol-maleimide conjugate..... 245

**Figure 6.2.** Extracted ion electropharograms of free thiol (black) and thiol-MM conjugate (red). (a) Standard 20  $\mu$ M solutions of both NAC and NAC-MM conjugate under alkaline conditions and negative ESI conditions. Approximately 20% increase in signal for NAC-MM compared to NAC. The inset illustrates the mass spectrum of the NAC-MM conjugate with  $[M-H]^-$  at  $m/z$  273 (b) Standard 20  $\mu$ M solution of hCys-MM and Cys-MM both display a dramatic increase in ionization efficiency with maleimide conjugation. Enhancement of 40 and 19 fold increase is exhibited by hCys-MM and Cys-MM, respectively ..... 246

## List of Tables

<b>Table 1.1.</b> Major classes of primary metabolites, representative structure of each class of metabolite major pathways, and electric charge state. Metabolites classified as polar can be amendable for CE-MS analysis. ....	7
<b>Table 2.1.</b> Fundamental Physicochemical Parameters for Modeling Ion Mobility Using Computer Simulations Based on the Hubbard–Onsager Model. ....	80
<b>Table 2.2.</b> Identification of Unknown Nutrients and Isobaric Cationic Metabolites in Broth Medium by CE-ESI-ITMS Using On-Line Sample Preconcentration with Computer Simulations .....	100
<b>Table 3.1.</b> Impact of deproteinization method on the accuracy of glutathione determination from hemolysates by CE-ESI-MS .....	127
<b>Table 3.2.</b> Impact of sample storage on the accuracy of glutathione analysis from filtered RBC lysates using CE-ESI-MS due to artifactual oxidation.....	130
<b>Table 3.3.</b> Artifact-free glutathione analysis of filtered RBC lysates from a healthy adult volunteer using CE-ESI-MS with fingerprick blood microsampling and ultrafiltration. ....	130
<b>Table 3.4.</b> Comparison of various thermodynamic and kinetic parameters for assessing the intra-cellular redox status and antioxidant capacity of filtered RBC lysates by DIRGO using CE-ESI-MS. ....	133
<b>Table 4.1.</b> Summary of forty-two identified and unknown metabolites reliably quantified in RBCs during both exercise-induced oxidative stress trials by CE-ESI-MS, which highlights the global impact of high-dose oral NAC intake in downregulating metabolite levels that is reversible with its discontinued use. ....	188
<b>Table 5.1.</b> Dual-staining fluorescence assay using flow cytometry for assessment of viable cells (double-negative), early stage (AnxV+), and late stage (double-	

positive) apoptosis of normal leukocytes exposed to increasing levels of low-dose ionizing radiation ..... 222

**Table 5.2.** A summary of fold-change in measured ion responses relative to 0 Gy control for twenty two identified and unknown metabolites quantified in irradiated-leukocytes by CE-ESI-MS as a function of radiation dose. Unidentified metabolites were internally labeled by numerical sequence in their *m/z*:RMT..... 230

**LIST OF ABBREVIATIONS**

3D	Three Dimensional
7-AAD	7-Amino-Actinomycin
A	Adenosine
AC	Alternating Current
ACN	Acetonitrile
ADP	Adenosine Diphosphate
AnxV	Annexin V-FITC
APCI	Atmospheric Pressure Chemical Ionization
Arg	L-Arginine
ATP	Adenosine Triphosphate
BGE	Background Electrolyte
C0	L-Carnitine
C2	O-Acetyl-L-Carnitine
CDNB	1-Chloro-2,4-Dinitro Benzene
CEC	Capillary Electrochromatography
CE-ESI-MS	Capillary Electrophoresis-Electrospray Ionization- Mass Spectrometry
Cl-Tyr	3-Chlorotyrosine
CV	Coefficient of Variance
Cys	L-Cysteine
CySS	L-Cystine

CZE	Capillary Zone Electrophoresis
Da	Daltons
DC	Direct Current
diAla	D-Alanyl-D-Alanine
DIRGO	Differential Rates of Glutathione Oxidation
DTT	1,4-Dithiotheitol
DNA	Deoxyribonucleic acid
<u>E</u>	Electric Field Strength
EE2	Estrogen Ethinylestradiol
EIE	Extracted Ion Electropherograms
EOF	Electroosmotic Flow
FA	Formic Acid
G	Guanosine
GABA	$\gamma$ -Aminobutyric Acid
GC	Gas Chromatography
Gln	L-Glutamine
Glu	L-Glutamic Acid
GSSG	Glutathione (Disulfide)
GSH	Glutathione (Reduced)
Hb	Hemoglobin
HCA	Hierarchal Cluster Analysis
HCy	L-Homocystine

His	L-Histidine
HisN	Histamine
HMDB	Human Metabolome Database
HPLC	High Performance Liquid Chromatography
Ile	L-Isoleucine
IS	Internal Standard
IT	Ion Trap
KEGG	Kyoto Encyclopedia of Genes and Genomes
$K_a$	Weak Acid Dissociation Constant
Leu	L-Leucine
$L_d$	Effective capillary length to the detector
LIF	Laser Induced Fluorescence
LOD	Limit of Detection
Lys	Lysine
$\mu_o$	Absolute Electrophoretic Mobility
$\mu_{ep}^A$	Apparent Electrophoretic Mobility
$\mu_{ep}$	Electrophoretic Mobility
$\mu_{eo}$	Electroosmotic Mobility
M	Molarity
MCO	Metal Catalyzed Oxidation
Me-Asp	N-Methyl-L-aspartic Acid
Me-His	N-Methyl-L-histidine

MEKC	Micellar Electrokinetic Chromatography
MetS	Methionine Sulfone
MeOH	Methanol
Met	L-Methionine
MM2	Molecular Mechanics 2
mRNA	Messenger Ribonucleic Acid
m-Tyr	Meta-L-Tyrosine
MV	Molecular Volume
m/z	Mass to Charge Ratio
$\eta$	Viscosity
NADPH	Nicotinamide Adenine Dinucleotide Phosphate
NMR	Nuclear Magnetic Resonance
NAm	Nicotinamide
NA	Nicotinic Acid
NIST	National Institute of Standards and Technology
NO <sub>2</sub> -Tyr	3-Nitrotyrosine
o-Tyr	Ortho-L-Tyrosine
PABA	Para-Aminobenzoic Acid
PCA	Principle Component Analysis
Phe	L-Phenylalanine
PLS	Partial Least Squares
Pro	L-Proline

PS	Phosphatidylserine
p-Tyr	Para-L-Tyrosine
$Q_{\text{eff}}$	Effective Charge
R	Hydrodynamic Radius
RBC	Red Blood Cell
RNA	Ribonucleic Acid
RMT	Relative Migration Time
RPM	Revolutions Per Minute
RNS	Reactive Nitro Species
ROS	Reactive Oxygen Species
RPMI	Roswell Park Memorial Institute
TCA	Tricarboxylic Acid
TCA	Trichloroacetic Acid
t-ITP	Transient Isotachopheresis
TOF-MS	Time of Flight-Mass Spectrometry
TIE	Total Ion Electropherograms
Trp	L-Tryptophan
TrpN	Tryptamine
Tyr	L-Tyrosine
UPLC	Ultra-performance liquid chromatography
UV	Ultraviolet
$v$	Velocity

Val	Valine
$\zeta$	Zeta Potential
WBC	White Blood Cell
$Z_{\text{eff}}$	Effective Charge

*Chapter I*

Introduction to Metabolomics and Capillary Electrophoresis Electrospray  
Ionization- Mass Spectrometry

## **I. Introduction to Metabolomics and Capillary-Electrophoresis-Electrospray-Mass Spectrometry**

### **1.1. Metabolomics**

#### **1.1.1. The Greatest omics of them all?**

In a post-genomic era, several “omics” technologies have been developed to assess the complex dynamics associated with gene expression that impact the phenotype of an organism. Despite the sequencing of the human genome (and an increasing number of other organisms) using high-throughput multiplexed capillary array gel electrophoresis,<sup>1</sup> a functional understanding of gene activity on human health, development and disease is still lacking. In this context, complementary approaches for quantitative assessment of the downstream biochemical products of gene transcription in relation to the phenotype of an organism are urgently needed. Transcriptomics is a well developed area of functional genomics aimed at studying gene expression using DNA microarray hybridization technology for the quantification of messenger RNA (mRNA) levels in a cell. However, the major limitation of transcriptomics is that it is dependent on *a priori* knowledge of a gene sequence, while suffering from high background levels and limited dynamic range due to non-selective hybridization.<sup>2</sup> Moreover, both hybridization and sequencing based transcriptomic techniques are not applicable to the assessment of gene activity involving combinations of known and/or unknown spliced gene regions within a polyploid genome. The advent of proteomics promises a more complete functional understanding of gene expression in an organism since biological activity is strongly associated with

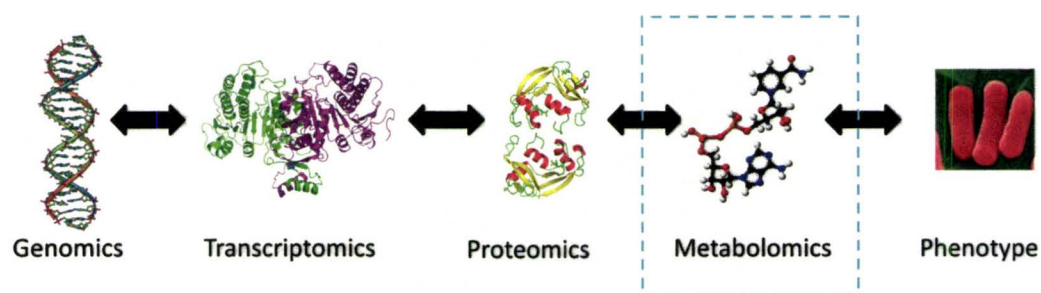


**Figure 1.1.** Schematic representing the major “omic” levels of functional genomics research in systems biology.

protein expression encoded by the genome. Despite breakthroughs in high resolution analytical technologies for comprehensive protein analysis based on 2D gel electrophoresis, liquid chromatography and/or mass spectrometry, functional understanding is elusive due to the large number, wide dynamic range and sheer complexity of protein states, including post-translational covalent modifications and various forms of non-covalent interactions involving protein-protein, protein-ligand and/or protein-membrane complexes that modulate activity *in-vivo*.<sup>3</sup> Metabolomics is an emerging yet complementary field of post-genomic research, which is aimed at the comprehensive analysis of metabolites in a cell, tissue or biological fluid. Indeed, metabolomics now represents a viable component of systems biology research<sup>4</sup> and an important counterpart to transcriptomic and proteomic research as highlighted in Figure 1.1. Since metabolites represent dynamic molecular endpoints of gene, transcript, protein expression and/or environment, metabolomics offers an insightful way to assess real-world changes in biological activity closely associated with the phenotype of an organism. This thesis is aimed at developing new strategies for comprehensive analysis of

metabolites in biological samples that addresses major analytical challenges associated with sample pretreatment, unknown metabolite identification/quantification and multivariate data analysis for biomarker discovery.

### **1.1.2. History of Metabolomics**

The term “metabolome” was first introduced by Fiehn as representing the full complement of small molecules in an organism analogous to the genome or proteome.<sup>5, 6</sup> Metabolomics was later defined as the comprehensive analysis of all low molecular weight molecules (< 1000 Da) which can be detected, identified and quantified. In contrast, metabolite fingerprinting offers a qualitative strategy for distinguishing changes in metabolite levels associated with different states or external conditions, but it does not identify nor quantify detectable metabolites that is critical for deeper insight into the underlying mechanism(s) of biological activity.<sup>7</sup> Metabolite profiling of specific metabolite classes or targeted metabolic pathways has long been the cornerstone of biological research. In this context, metabolomics introduces the paradigm of unbiased global metabolite analyses, which provides a “hypothesis-free” or “hypothesis-generating” approach for investigating complex biological phenomena, ranging from the discovery of biomarkers for early detection of disease to the elucidation of genes/proteins of unknown function.<sup>8-10</sup>

Early confusion arose with the parallel introduction of “metabonomics” coined by Nicholson and co-workers, which is defined as the ability to

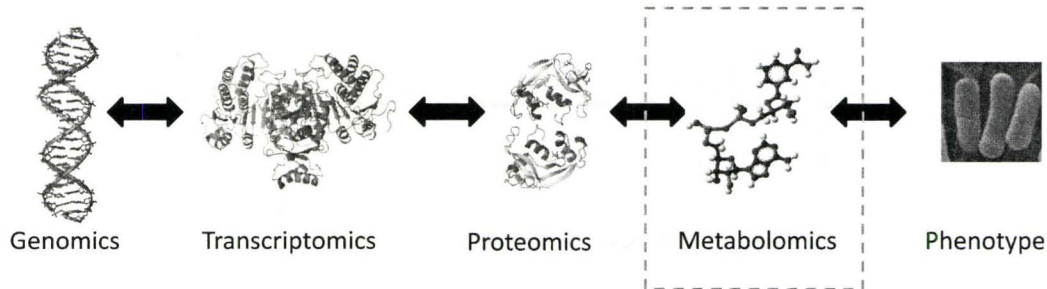


**Figure 1.1.** Schematic representing the major “omic” levels of functional genomics research in systems biology.

protein expression encoded by the genome. Despite breakthroughs in high resolution analytical technologies for comprehensive protein analysis based on 2D gel electrophoresis, liquid chromatography and/or mass spectrometry, functional understanding is elusive due to the large number, wide dynamic range and sheer complexity of protein states, including post-translational covalent modifications and various forms of non-covalent interactions involving protein-protein, protein-ligand and/or protein-membrane complexes that modulate activity *in-vivo*.<sup>3</sup> Metabolomics is an emerging yet complementary field of post-genomic research, which is aimed at the comprehensive analysis of metabolites in a cell, tissue or biological fluid. Indeed, metabolomics now represents a viable component of systems biology research<sup>4</sup> and an important counterpart to transcriptomic and proteomic research as highlighted in Figure 1.1. Since metabolites represent dynamic molecular endpoints of gene, transcript, protein expression and/or environment, metabolomics offers an insightful way to assess real-world changes in biological activity closely associated with the phenotype of an organism. This thesis is aimed at developing new strategies for comprehensive analysis of

metabolites in biological samples that addresses major analytical challenges associated with sample pretreatment, unknown metabolite identification/quantification and multivariate data analysis for biomarker discovery.

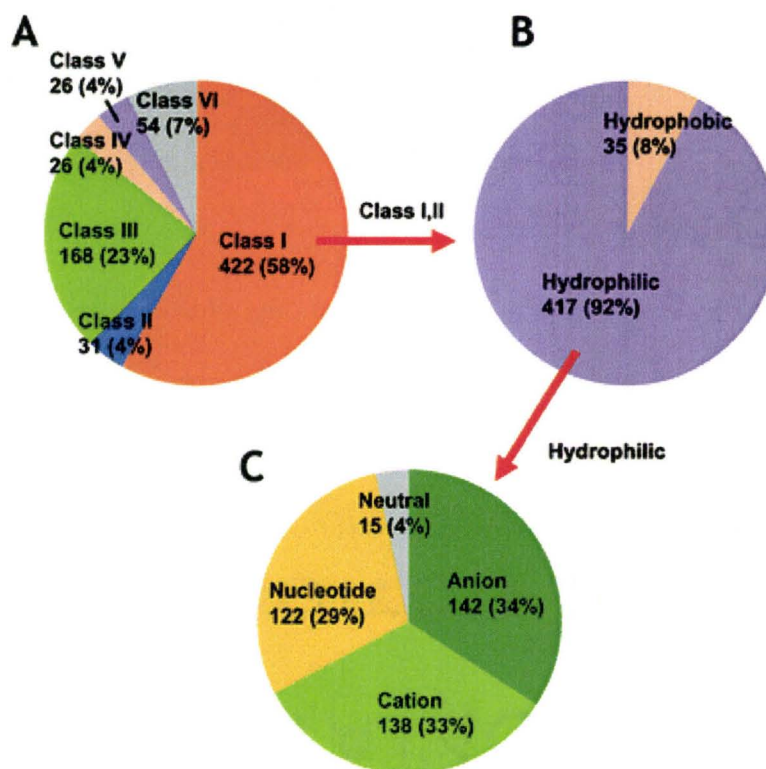
### **1.1.2. History of Metabolomics**

The term “metabolome” was first introduced by Fiehn as representing the full complement of small molecules in an organism analogous to the genome or proteome.<sup>5, 6</sup> Metabolomics was later defined as the comprehensive analysis of all low molecular weight molecules (< 1000 Da) which can be detected, identified and quantified. In contrast, metabolite fingerprinting offers a qualitative strategy for distinguishing changes in metabolite levels associated with different states or external conditions, but it does not identify nor quantify detectable metabolites that is critical for deeper insight into the underlying mechanism(s) of biological activity.<sup>7</sup> Metabolite profiling of specific metabolite classes or targeted metabolic pathways has long been the cornerstone of biological research. In this context, metabolomics introduces the paradigm of unbiased global metabolite analyses, which provides a “hypothesis-free” or “hypothesis-generating” approach for investigating complex biological phenomena, ranging from the discovery of biomarkers for early detection of disease to the elucidation of genes/proteins of unknown function.<sup>8-10</sup>

Early confusion arose with the parallel introduction of “metabonomics” coined by Nicholson and co-workers, which is defined as the ability to

differentiate time-related metabolic changes in an organism due to an external stimuli or genetic modifications.<sup>11, 12</sup> Indeed, metabolomics and metabonomics have been used interchangeably in the literature, but essentially relate to the same area of research although the experimental design and instrumental method/data processing used for conducting untargeted metabolite profiling may be different. In general, depending on the discretion of the research group, most nuclear magnetic resonance (NMR)<sup>11, 13</sup> based studies have used the term metabonomics, whereas researchers involved with mass spectrometry (MS)<sup>14, 15</sup> have adopted metabolomics. Due to the wider availability of bench-top MS instrumentation for laboratory research, the majority of reports in the literature use metabolomics as the primary term of choice, which will be used throughout this thesis. The discrepancies in terminology in reporting scientific data during the early development of metabolomics highlights that it is still a quite a nascent field of post-genomic research. With the growing interest in metabolomic applications across various fields of science, an international metabolomics standards initiative has recently been organized to develop a broad consensus on accepted syntax/semantics used in published reports, as well as ensure an adequate description of experimental protocols involving chemical analysis, data mining and biological context.<sup>16</sup>

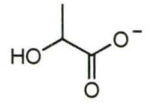
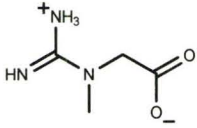
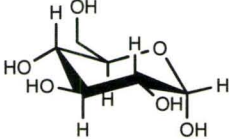
Unlike DNA, RNA or protein biopolymers, metabolites represent chemically diverse set of small molecules that vary significantly in terms of their physicochemical properties, such as polarity, solubility, electric charge and



**Figure 1.2.** Illustrates the classification of detected metabolites from *E. Coli* extracts by CE-MS. (a) Comprehensive list of 727 known metabolites in *E. Coli* classified according to their metabolic pathway from the Kyoto Encyclopedia of Genes and Genome. Class: I, primary metabolism; II, degradation of primary metabolites; III, Degradation of environmental compounds; IV, secondary or unconventional metabolism; V, pathway unknown; VI, intermediates in putative *in vitro* reaction. Further cataloging of metabolites in class I and II into (b) polar and non-polar metabolites, which are then further reduced into those which can be detected by CE-TOF-MS analysis for (c) hydrophilic metabolites.

volatility. The disparity in the chemical properties (including stability) of metabolites represents a significant analytical challenge for their comprehensive separation and detection under a single instrumental platform and/or sample preparation method. Moreover, the metabolome represents a large number of small molecules that are expressed over a wide dynamic range, notably secondary metabolites found within sessile organisms, such as plants. Indeed, it has been estimated that over 200 000 different metabolites may exist within the plant

**Table 1.1.** Major classes of primary metabolites, representative structure of each class of metabolite major pathways, and electric charge state. Metabolites classified as polar can be amendable for CE-MS analysis.

<b>Intrinsic Charge</b>	<b>Representative structure</b>	<b>Metabolite class</b>	<b>Polarity</b>	<b>Major metabolomic pathway</b>
Cationic		<b>Amines</b> (ie. <i>cadaverine</i> )	Polar	Urea Cycle
Anionic		<b>Organic Acids</b> <b>Nucleotides/cofactors</b> (ie. <i>lactate</i> )	Polar	Krebs Cycle
Zwitter-ionic		<b>Amino acids</b> <b>peptides/acylcarnitines</b> (ie. <i>Creatine</i> )	Polar	Glutathione Metabolism
Neutral*		<b>Sugars, steroids</b> (ie. <i>glucose</i> )	Non-polar	Glycolysis

\*Neutral metabolites normally are not separated by CE-ESI-MS unless additives are used in the background electrolyte that are compatible with the ion source.

kingdom alone, which poses considerable obstacles for attaining truly global metabolomic coverage.<sup>17</sup> Although the metabolome of animals or microbes are considerably less complex than plants, significant hurdles still remain due to the large fraction of unknown metabolites detected and the corresponding lack of purified commercial standards available, which limits unambiguous identification and quantification to only a few hundred metabolites by current analytical methodologies.<sup>18</sup> A recent survey performed by Ohashi *et al.* revealed about 727 known metabolites present in *E. coli* with a majority (> 62%) comprising primary metabolites and their degradation products (class I/II) as shown in Figure 1.2.<sup>19</sup> The authors highlighted that instrumental methods amenable to the separation and

detection of complex mixtures of polar/charged metabolites present in biological samples are preferred given their predominance within the metabolome, such as liquid chromatography or capillary electrophoresis-electrospray ionization-mass spectrometry (CE/LC-ESI-MS). Table 1.1 illustrates the classification of primary metabolites based on their intrinsic charge and associated metabolic pathways. In general, polar metabolites are amenable to CE-ESI-MS analysis provided they have an intrinsic charge state that permits their migration under an external electric field (*i.e.*, electrophoretic mobility) at a given buffer pH condition, which will be discussed in greater detail later in the introduction of this thesis.

## **1.2. Analytical Platforms for Metabolomic Studies**

A rigorous optimization and validation of analytical strategies used in metabolomics studies is essential for realizing truly unbiased metabolite coverage in biological samples, including sample pretreatment (pre-analysis), chemical analysis (choice of instrumental platform) and data exploration (post-analysis). The selectivity of the analytical method is one of the most important criteria to consider for metabolomic applications given the complexity of most biological samples that can result in significant interferences, such as the resolution of isobaric and/or isomeric metabolites. Indeed, the performance of an analytical technique is often compromised by background matrix effects unless sample pretreatment is performed accordingly prior to analysis. In addition, method sensitivity and its compatibility for the detection of a variety of different

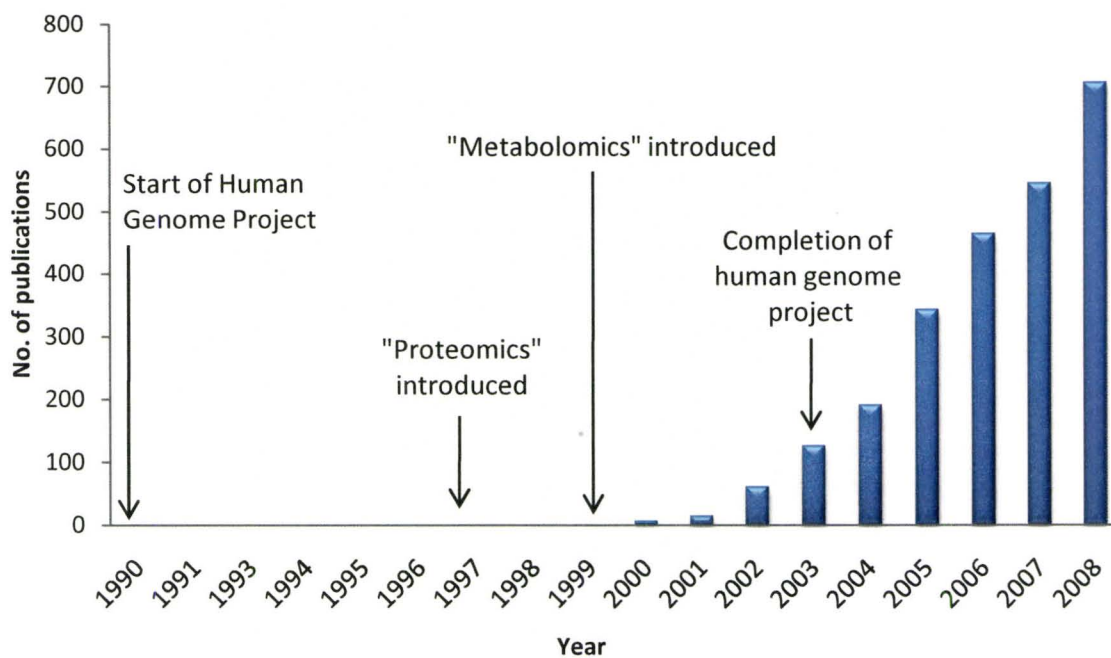


**Figure 1.3.** Bar graph showing the rapid increase in total metabolomics publications from 1989 to 2008 according to Web of Knowledge using a query search of "metabolomics and metabonomics" performed on June 21, 2009 relative to other major milestones in genomic and post-genomic research.

metabolite classes over a wide dynamic range is also a major feature to consider when selecting an analytical technique. For instance, the detection of low abundance metabolites (sub-micromolar) can provide insightful information regarding biological active hormones, xenobiotics or biomarkers of disease that would remain undetected by conventional methods with inadequate sensitivity. Figure 1.3 highlights the rapid rise in NMR and MS based metabolomics research reported in the scientific literature since 2000. However, one of the most daunting obstacles in metabolomic research remains the identification of a large fraction of unknown metabolites.<sup>20</sup> Several public databases have been established to assist in the identification of metabolites using a number of different query searches (*e.g.*, accurate mass, MS/MS *etc.*), such as KEGG,<sup>21</sup>

Metlin,<sup>22</sup> and Human Metabolome Project,<sup>23</sup> however unambiguous identification remains elusive when authentic chemical standards are lacking. An *in silico* strategy for improved identification of unknown metabolites based on simulation of their electromigration behavior from their fundamental physicochemical properties is introduced in *Chapter II* of this thesis when using CE-ESI-MS in conjunction with computer modeling. Thus, quantitative analytical techniques that can also provide qualitative characterization of unknown yet biologically relevant metabolites are highly desirable.

Several analytical platforms have been adopted for metabolomic studies, the majority involving nuclear magnetic resonance (NMR)<sup>24</sup> and increasingly chromatographic separation hyphenated to mass spectrometry (MS). NMR is a non-destructive method that can provide a wealth of information for structural elucidation of unknown metabolites with minimal sample preparation, however sensitivity is still limited to micromolar levels when using high magnetic fields (800 MHz) in conjunction with cryogenic probe technology.<sup>25</sup> NMR also suffers from high infrastructure/operating costs, complex data processing and slow acquisition times when detecting minor metabolites in biological fluids, which limits its suitability for high-throughput metabolomic studies. Gas chromatography coupled to mass spectrometry (GC-MS) provides a highly robust format for the separation of complex sample mixtures together with superior sensitivity for the detection of sub-micromolar levels of metabolites.<sup>26, 27</sup> Unlike electrospray ionization-mass spectrometry (ESI-MS), electron impact (EI) is the

primary ionization source used in GC-MS, which is less susceptible to matrix effects while generating equivalent responses for metabolites. Despite being considered the gold standard for chemical analyses due to its long history of validated use in the laboratory, GC-MS requires complicated sample handling (*e.g.*, desalting, chemical derivatization etc.) when analyzing polar/charged metabolites derived from biological samples that is time-consuming while contributing to increased assay bias and poorer precision. In addition, GC-MS is not applicable to the analysis of thermally unstable or chemically labile polar metabolites. Chemical derivatization of polar metabolites can also result in incomplete or multiply-labeled derivatives, which convolutes chromatographic separation and subsequent data interpretation.<sup>26</sup> However, metabolite identification is facilitated when using GC-MS by access to the National Institute of Standards and Technology (NIST) reference library, which comprises mass spectra of over 190 000 organic compounds and 45 000 GC retention indices.<sup>28</sup> Recently, Oliver Fiehn privatized their in-lab developed mass spectral and GC indices database of over 800 metabolites into a commercially available software package in collaboration with Agilent Technologies.<sup>29</sup> Increasingly, liquid chromatography coupled to mass spectrometry (LC-MS) represents an increasingly viable separation format for metabolomics since it reduces the extent of sample preparation required for polar metabolite analysis that is endemic to GC. Since LC selectivity is constrained by the choice of stationary phase used for metabolite separation, reverse-phase, hydrophilic interaction and other types of

columns are required to be tested to ensure adequate coverage of the metabolome encompassing both polar and non-polar metabolites.<sup>30</sup> Analysis times can vary for LC-MS depending on the complexity of the sample, although with the advent of ultra-high performance liquid chromatography (UPLC), separation times can be reduced down to a few minutes due to high flow rates with greater separation efficiency.<sup>31</sup> Nevertheless, multiple ionization sources (ESI, APCI) and polarity settings (positive/negative ion mode) are needed to attain global metabolomic coverage when using LC-MS since ion responses are highly variable and dependent on the physicochemical properties of different classes of metabolites.<sup>32</sup>

An alternative to GC/LC-MS is capillary electrophoresis-mass spectrometry (CE-MS). CE is a highly efficient microseparation technique ideal for polar metabolite analyses that requires minimal off-line sample preparation, small sample volumes and short total analysis times when using low cost aqueous buffer systems and open tubular fused silica capillaries. Recently, Willams *et al.* conducted an inter-laboratory comparison of the performance of GC-MS versus CE-MS for the analysis amino acids from *Medicago truncatula* root cell extracts.<sup>26</sup> The authors reported several distinct advantages of CE-MS relative to GC-MS for amino acid profiling from plant extracts, which included less complex sample pretreatment steps and faster total analysis times that resulted in about a three-fold higher throughput for analysis. In addition, CE-MS provided similar reproducibility and lower cost per sample since no chemical reagents, expensive consumables and chromatographic columns are needed.

To date, there is no single analytical platform amenable for comprehensive metabolomic analysis, which has prompted some research groups to integrate data generated across multiple yet complementary platforms, such as LC-MS and NMR.<sup>33</sup> Recently, Zamboni *et al.* reported a cross-platform investigation for quantitative metabolomics by comparing the performance between GC-MS, LC-MS, and CE-MS using 91 metabolite standards of primary metabolism and <sup>13</sup>C labeled yeast extracts.<sup>34</sup> The authors criteria for comparing the performance of the three different analytical platforms were based on the extent of metabolite coverage, time required for sample preparation as well as overall reproducibility. Based on these criteria, LC-MS was concluded as the preferred platform due to its convenient sample pretreatment protocol and robustness of methodology. Although LC-MS and CE-MS were comparable with respect to the total number of metabolites resolved and detected, Zamboni *et al.* reported that the robustness for anionic metabolite analysis by CE-MS was poor relative to LC-MS when adopting the method introduced by Soga *et al.*<sup>35</sup> which requires a complicated dynamic coating procedure to modulate the electroosmotic flow (EOF). However, this cross-platform instrumental evaluation did not consider the long-term cost of performing analyses, as well as recent advances in CE-MS methodologies for the detection, identification and quantification of unknown low abundance metabolites without complicated sample pretreatment,<sup>20, 36, 37</sup> which will constitute one of the major contributions of this thesis.

### **1.3. Capillary Electrophoresis Based Separation**

#### **1.3.1. Capillary Electrophoresis**

Capillary electrophoresis (CE) represents one of the most versatile separation techniques due to its ability to generate highly efficient separations, where selectivity can be readily tuned by modifications in the properties of the electrolyte solution. High separation efficiency (number of theoretical plates,  $N > 100,000$ ) is attributed to the physical and chemical properties of the capillary, the high voltages applied and the unique separation mechanisms operative in CE. The use of narrow bore fused-silica capillaries allows for the generation of the electroosmotic flow (EOF), which minimizes the extent of solute axial diffusion when compared to pump-driven LC formats undergoing parabolic flow due to its unique flat profile (*i.e.*, laminar flow). In addition, the use of fused-silica capillaries with narrow internal diameters ( $\approx 50 \mu\text{m}$ ) leads to efficient heat dissipation that reduces the extent of Joule heating when applying high voltages (up to 30 kV) due to its high surface area to volume ratio. These features have allowed for the development of an array of CE separation modes to resolve diverse classes of solutes within complex sample mixtures, ranging from metals to small molecules to biopolymers and intact cells.

#### **1.3.2. Electrokinetic Phenomena in CE**

Separations in CE are dictated by two discrete electrokinetic processes, namely the electrophoretic mobility of the solute ( $\mu_{ep}$ ) and the electroosmotic mobility ( $\mu_{eo}$ ) of the bulk solution.  $\mu_{ep}$  represents the ion migration velocity under

an electric field, which is dependent on the intrinsic physiochemical properties of a solute and its local environment. The EOF is a natural electrokinetic pumping mechanism generated by the interaction of the capillary surface with the electrolyte solution under an external voltage. The vector sum of both these parameters constitutes the apparent mobility of an analyte ( $\mu_{ep}^A$ ), which influences its overall migration time in CE.

### 1.3.3. Electrophoretic Mobility ( $\mu_{ep}$ )

$\mu_{ep}$  is defined as the ion velocity ( $v$ ) per unit of electric field strength ( $E$ ). Since the size of a small molecule can be approximately described as a sphere,  $\mu_{ep}$  is dependent on the ratio of the effective charge ( $Q_{eff}$ ) to hydrodynamic radius ( $R_H$ ) of an ion, as well the viscosity of the surrounding electrolyte solution ( $\eta$ ) at a specific temperature, which is defined by the Hückel equation:<sup>38, 39</sup>

$$\mu_{ep} = \frac{v}{E} = \frac{Q_{eff}}{6 \cdot \pi \cdot \eta \cdot R_H} \quad (1)$$

As indicated in eq. (1), the direction and magnitude of  $\mu_{ep}$  is dependent on the effective charge density of an ion which controls the selectivity in CE. Separation optimization is most often performed by altering the composition of the electrolyte solution, such as buffer type, pH, ionic strength and organic solvent content. Buffer pH is one of the most important parameters for improving resolution as it effectively controls  $\mu_{ep}$  for weakly ionic analytes, as well as the magnitude of the EOF. Indeed, CE is particularly well suited for metabolomics studies since the majority of metabolites are hydrophilic/polar species<sup>40</sup> that are

intrinsically charged in aqueous solutions.<sup>41</sup> In addition, the selectivity of CE separations can be extended to include neutral and enantiomeric solutes through the use of specific additives in the electrolyte solution, such as surfactants<sup>42</sup> and cyclodextrin macrocycles.<sup>43, 44</sup> Terabe *et. al* first introduced micellar electrokinetic chromatography (MEKC) as a novel separation mode in CE for the separation of neutral analytes based on their dynamic partitioning with charged micelles that migrate through the capillary during voltage application.<sup>45</sup> Similarly, high-throughput sequencing of DNA can be realized by CE via the use of dilute solutions of neutral entangled polymers that function as size-dependent sieves to differentially retard DNA fragments during electromigration.<sup>46</sup> Thus, unlike conventional LC columns that require covalent binding of a stationary phase to a solid support matrix, CE allows for unlimited ways to alter selectivity since single or multiple additives can be used in free solution with unmodified capillaries. Noteworthy, separations in CE are influenced by two complementary mechanisms, namely differential electrokinetic (*i.e.*, mobility) and thermodynamic (*i.e.*, equilibrium) processes unlike conventional chromatography. Since  $\mu_{ep}$  is an intrinsic physicochemical parameter of a solute that can be measured with excellent precision when using commercial thermostated instruments, CE is increasingly being used as a unique biophysical tool for studying the thermodynamics and kinetics of biomolecular interactions, such as protein-ligand binding.<sup>47, 48</sup>

#### 1.3.4. Electroosmotic Flow (EOF)

The EOF is an electrokinetically-driven bulk flow of solution that is generated by the application of an external voltage across a narrow bore capillary. The surface of a fused-silica capillary is comprised of weakly acidic silanol functional groups ( $pK_a \approx 6.5$ ) when in contact with an aqueous electrolyte solution.<sup>38</sup> The Debye-Hückle-Stern model describes the formation an electric double layer due to the ionization of the capillary surface, which comprises a rigid layer of adsorbed cations (Stern layer) followed by a diffuse region of mobile cations/anions.<sup>38</sup> In the case of a negatively charged surface, excess cations in the electrolyte solution are electrostatically adsorbed within the Stern layer, where the magnitude of the potential difference at this boundary relative to the bulk solution is referred to as the zeta potential ( $\zeta$ ). In general, the EOF is directly proportional to both the sign and magnitude of  $\zeta$  near the capillary surface, which can be altered by changes in the properties of the background electrolyte, such as buffer pH, ionic strength and viscosity of the solution. Figure 1.4 illustrates that the diffuse double layer is prevalent when using buffer conditions at  $pH > 3$ , whereas under strongly acidic conditions the fused-silica capillary is protonated and thus the EOF is effectively suppressed. When an external voltage is applied across the capillary, a net migration of excess cations within the diffuse double layer is induced towards the cathode. Since these mobile cations are solvated, a uniform electrokinetic flow of the bulk solution gives

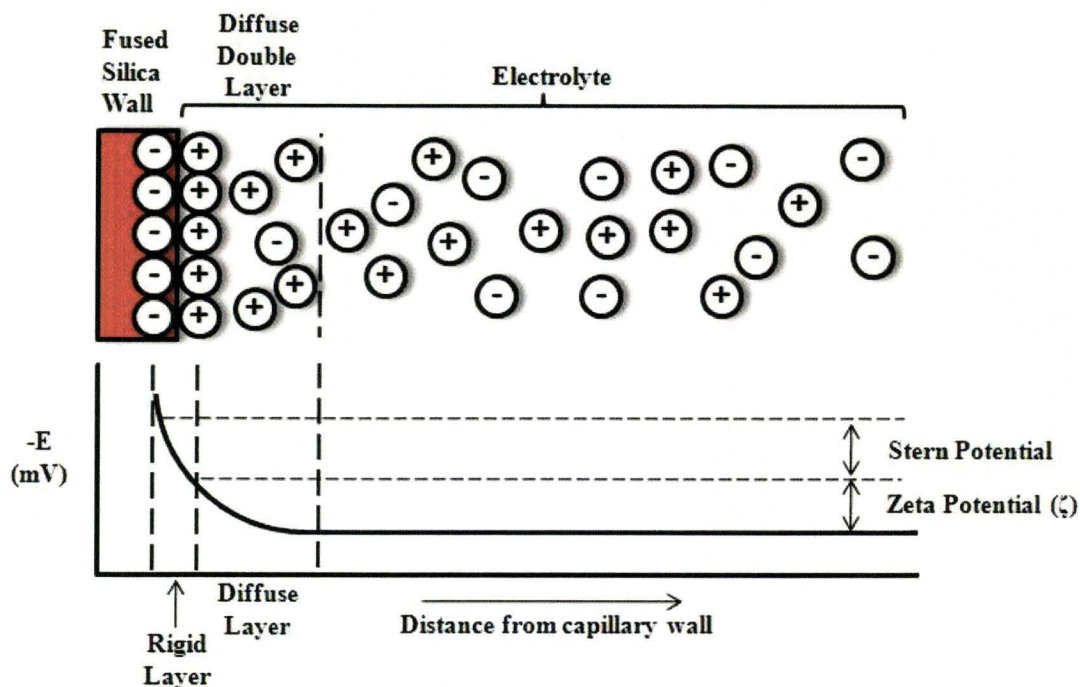


**Figure 1.4.** Debye-Hückle-Stern model of the electric double layer showing the diffuse double layer and the zeta potential that generates the EOF near the capillary surface under an applied external voltage.

rise to flat profile or laminar flow characteristic to the EOF. Thus, the EOF acts as a natural electrokinetic pump which transports all analytes within a complex mixture towards a fixed detector. The direction and magnitude of the EOF are dictated by the chemical properties of the capillary surface and electrolyte properties of the solution, which can be described by the Smoluchowski equation:<sup>38</sup>

$$\mu_{eo} = \frac{\varepsilon \cdot \zeta}{6 \cdot \pi \cdot \eta} \quad (2)$$

where,  $\varepsilon$  is the dielectric constant,  $\zeta$ , is zeta potential of the double layer and  $\eta$  is the viscosity of the buffer solution. In general, low ionic strength/alkaline buffer condition generates a large  $\zeta$  and thus a strong cathodic EOF, whereas a high ionic

strength/acidic buffer conditions can significantly suppress the EOF. Similarly, cationic surfactants in the background electrolyte (BGE) can be used to reverse the direction of the EOF (anodic) due to formation of a positively charged bilayer at the capillary surface.<sup>38</sup>

Although the EOF represents a simple and effective pumping mechanism for fluid transport in CE and microfluidic devices, a high variance in apparent migration times can occur relative to external pressure-based pumping systems used in LC due to changes in capillary surface properties and electrolyte conditions in sample or run buffer. Various strategies have been developed to either suppress or stabilize the EOF to improve migration time reproducibility. Suppression of the EOF is most commonly performed by neutralizing the silanol surface of the capillary using strongly acidic buffers, which reduces the extent of ion adsorption onto the neutral capillary surface. However, under these conditions only cationic metabolites (*e.g.*, amines, amino acids, nucleosides etc.) can be analyzed as they are fully protonated and migrate with a positive mobility towards a fixed detector, which has been successfully applied to complex biological samples, such as urine,<sup>49</sup> blood,<sup>37</sup> and bacterial extracts.<sup>18</sup> Other methods to manipulate the EOF have been applied by using covalent or non-covalent modifications to the surface of the bare fused-silica capillary. For instance, Soga *et al.* used a cationic polymer solution (polybrene) to reverse the EOF for analysis of anionic metabolites by CE-MS, including various organic acids and nucleotides.<sup>50</sup> However, additional rinsing/equilibration steps are

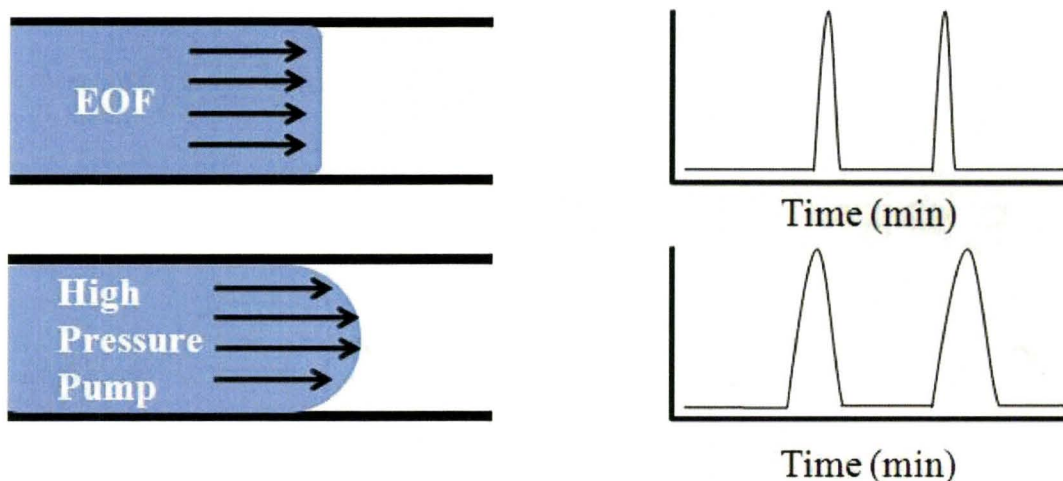


**Figure 1.5.** Comparison of the fluid transport profiles and corresponding analyte peak shapes for (a) a flat electrokinetic laminar flowing CE and (b) a parabolic flow generated by a pressure-driven pumping system.

required to generate stable non-covalently modified capillaries that are not suitable for high-throughput analyses, while reducing method sensitivity due to high background signals caused by polymer desorption when using ESI-MS detection. Nevertheless, proper conditioning of the capillary in conjunction with the use of high ionic strength buffers under strongly acidic or alkaline conditions ( $\text{pH} < 3$  or  $\text{pH} > 8$ ) provide the simplest strategy to ensure a stable EOF for reproducible performance in CE. In addition, normalization of apparent migration times relative to an internal standard provides an effective way to improve precision in terms of the relative migration time (RMT) of an analyte with coefficient of variance (CV)  $< 2\%$ .<sup>20</sup>

Axial diffusion is a drawback of pressure-driven LC separations due to increased frictional forces near the column surface, which leads to a non-uniform

parabolic flow with increased band broadening of analyte zones during elution. In contrast, the EOF exhibits a uniform flow profile when using an open tubular capillary in CE, where its velocity approaches zero only at the capillary surface in association with the Stern layer. Figure 1.5 compares the different flow profiles for fluid transport in CE and LC, as well as its impact on separation efficiency which is a kinetic parameter related to the magnitude of analyte dispersion. In essence, the higher separation efficiency in CE allows for the separation of complex mixtures with greater resolution and higher peak capacity relative to LC due to the favorable fluid transport properties of the EOF. Similarly, capillary electrochromatography (CEC) represents a hybrid separation format where the electrokinetic pumping mechanism of the EOF is used for efficient elution of solutes in columns packed with sub-micron sized particles without the need for expensive ultra-high pressure pumping systems since no back pressure is generated.<sup>51</sup>

### 1.3.5. Apparent Mobility

The apparent mobility of an analyte ( $\mu_{ep}^A$ ) in CE is dictated by both the direction and magnitude of  $\mu_{ep}$  and  $\mu_{eo}$  as described below:

$$\mu_{ep}^A = \mu_{ep} + \mu_{eo} \quad (3)$$

Thus,  $\mu_{ep}$  can be experimentally determined by measuring the apparent migration time of an analyte relative to the migration time of a neutral EOF marker (*e.g.*,

caffeine) with knowledge of the dimensions of the capillary and the applied voltage as shown below.<sup>52</sup>

$$\mu_{ep} = \frac{L_t \cdot L_d}{V} \left( \frac{1}{t_A} - \frac{1}{t_{EOF}} \right) \quad (4)$$

where,  $L_t$  represents the total capillary length,  $L_d$  describes the effective length to the detector,  $V$  is the applied voltage,  $t_A$  and  $t_{EOF}$  represents the apparent migration time of an analyte and the migration time of an EOF marker, respectively. Indeed,  $\mu_{ep}$  represents a fundamental physicochemical property of an ion that can be measured with excellent precision by CE, as well as accurately predicted when using computer molecular modeling based on the Hubbard-Onsager model for describing the electrohydrodynamics of ion migration.<sup>20</sup> The latter feature will represent a major strategy introduced in *Chapter II* of the thesis that allows for qualitative identification of unknown metabolites *in silico* that is complementary to ESI-MS in cases when authentic commercial standards are unavailable.

In general, the migration order of analytes in CE is highly dependent on the electrolyte conditions used for separation and the voltage polarity. Figure 1.6 illustrates the migration behavior of charged and neutral metabolites in free solution CE when using post-capillary detection by ESI-MS. A strong cathodic EOF occurs under neutral and/or alkaline buffer conditions in CE, which transports all species towards the detector with a migration order of cations < neutrals < anions due to differences in their  $\mu_{ep}$  which reflects their effective

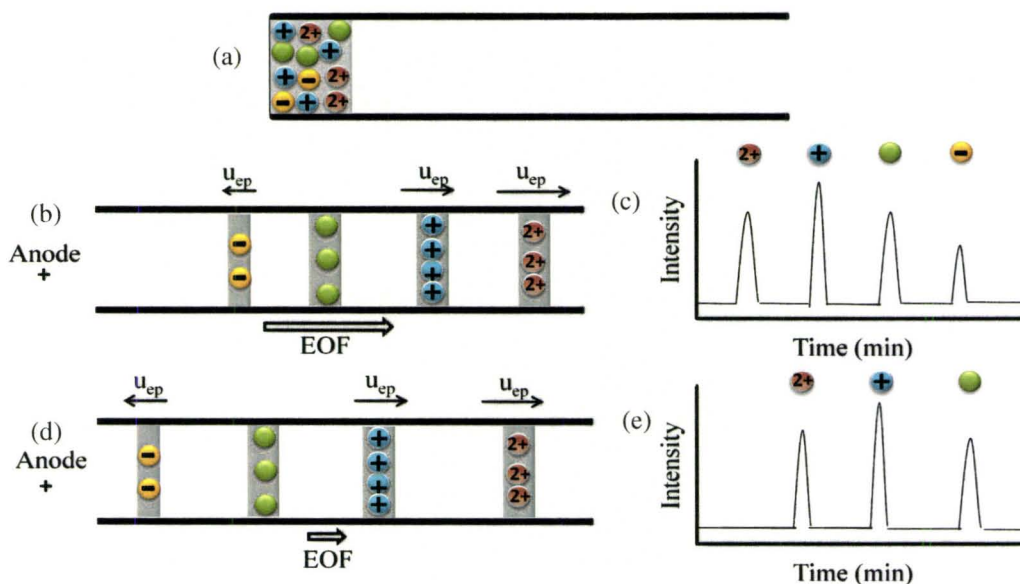


**Figure 1.6.** Schematic showing separation of a mixture of ions based on differences in their  $\mu_{ep}$  using CE: (a) hydrodynamic injection, (b) zonal separation at pH >6 with strong EOF, (c) representative electropherogram under neutral/alkaline condition, (d) zonal separation at pH < 2 with suppressed EOF, and (e) representative electropherogram under strongly acidic conditions.

charge density. However, under strongly acidic conditions, only cations can be effectively resolved in CE under suppressed EOF conditions, since anions derived from strong acids (e.g.,  $\text{Cl}^-$ ) migrate out of the capillary inlet entirely due to a weak EOF, whereas other weakly acidic species are neutralized. The high mobility of most inorganic salts (e.g.,  $\text{Na}^+$ ,  $\text{Cl}^-$ ,  $\text{K}^+$ ) relative to bulkier metabolites that migrate with a slower  $\mu_{ep}$  is a useful feature in CE since it allows for on-column desalting of biological samples without ionization suppression when using ESI-MS detection.

## 1.4. Mass Spectrometry – Ion Trap Mass Analyzer

### 1.4.1. Ion Trap Mass Analyzer

The quadrupolar ion trap mass analyzer or 3D-ion trap is a versatile, robust yet low cost mass spectrometer with unit mass resolution, which has the ability to trap and fragment selected gas-phase ions, as well as scan for ions of variable mass to charge ratio ( $m/z$ ). The 3D ion trap was developed concurrently with the linear quadrupolar mass filter by Wolfgang Paul and it is often referred to as the Paul Trap.<sup>53</sup> The ions are trapped within an electrostatic field by the manipulation of AC voltages under RF frequencies or “trapping potentials.” The theory behind trapping ions is defined by a series of equations describing the trajectory of an ion within a quadrupolar field. These equations are often referred to as the Mathieu equations,<sup>53, 54</sup> which form the basis of ion trap theory as described below:

$$\frac{d^2u}{dt^2} + (a_u - 2q_u \cos 2\varepsilon)u = 0 \quad (5)$$

In this equation,  $u$  represents the Cartesian axes ( $x, y, z$ ),  $\varepsilon$  represents  $\Omega t/2$  where  $\Omega$  is the frequency and  $t$  denotes time, whereas  $a_u$  and  $q_u$  are place holders which have no dimensions but represent trapping potentials. By substituting in  $\Omega t/2$ , and multiplying by  $m$ , which represents the mass of an ion, eq. (6) can be transformed to:

$$m \frac{d^2u}{dt^2} = \frac{-m\Omega^2}{4} (a_u - 2q_u \cos \Omega t)u \quad (6)$$

The left hand side of the equation is now expressed as the electric force that the ion experiences along any axis, where force is equivalent to the ion mass

multiplied by its acceleration. By a series of substitutions, the force of an ion in a quadrupole field can be

expressed by the following along the x-axis:

$$a_z = \frac{-8eU}{mr_0^2\Omega^2} \quad \text{and} \quad q_z = \frac{4eV}{mr_0^2\Omega^2} \quad (7)$$

Similar expressions can be derived for the y and z axis.  $q_z$  corresponds to the operation of ion traps, since the equation includes the mass to charge ratio ( $m/z$ ), the radius or size of the trap,  $r_0$ , and amplitude of the RF voltage in  $V$ , and the radial frequency represented by  $\Omega$ . Solutions to the Mathieu equation reveal regions where ions can be trapped along the z (axial) and r (radius) axes as depicted in Figure 1.7.<sup>55</sup> The overlap of both stability regions will reveal conditions where ions possess stable trajectories to oscillate in a quadrupole field of the ion trap without contacting the ring/end-cap electrodes. In contrast, ions with unstable trajectories can be rejected by colliding with the ring electrode or directed through an endcap electrode for detection by an electron multiplier.

#### 1.4.2. Ejection and Detection of Ions

Ion traps are often referred to as gas-phase test tubes since a variety of experiments/reactions can be performed on selective ions within an electrostatic field. The motion of ions within an ion trap mass analyzer is modulated by varying their axial (z) and radial (r) secular frequencies.<sup>53</sup> Ions that first enter the quadrupolar field experience a reduction in their kinetic energies (cooling) by collisional deactivation with an inert dampening gas at low pressure, such as

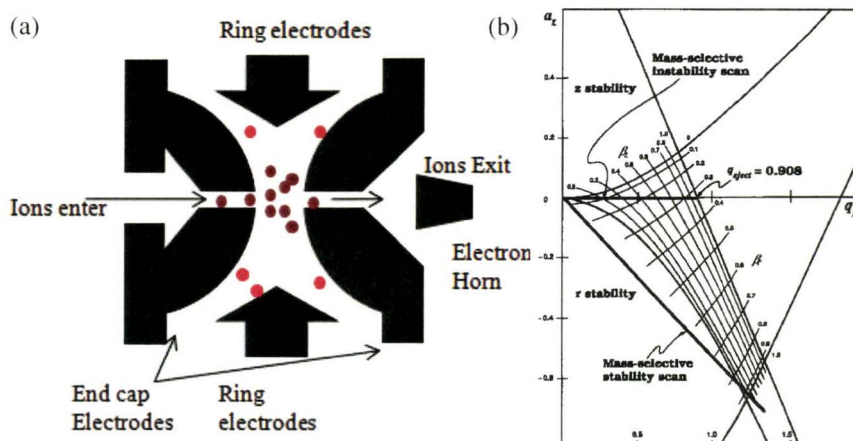


**Figure 1.7.** Schematic depicting (a) electrode configuration of a quadrupole 3D ion trap MS instrument. Stable and unstable ions are denoted in brown and red, respectively. Unstable ions do not have the correct trajectory and collide with the electrode and are neutralized. (b) stability regions where ions possess stable trajectories within the ion trap based on solutions of Mathieu equation.<sup>53</sup>

helium. The ions over a defined  $m/z$  range are then trapped within a confined region of the ion trap by the RF potential applied to the ring electrode. However, supplementation of a RF potential on the endcap electrodes can also be used to perturb the motion of ions confined within the ion trap, such as selective ejection of undesired ions of a defined  $m/z$  range from the trap. This mode is particularly useful when isolating a single ion of nominal  $m/z$  prior to additional experiments, such as collision-activated dissociation (CAD) or resonance excitation.<sup>53</sup> The latter process is frequently used to induce fragmentation of specific ions for structural elucidation, which can be performed in series for subsequent product or daughter ions generated referred to as multistage MS<sup>n</sup> experiments. Unlike quadrupole mass filters, ion traps offer improved sensitivity under full-scan ion monitoring as all ions over a defined range of  $m/z$  can be trapped simultaneously.

However, the upper capacity of the trap must not be exceeded when sampling large numbers of ions, since Columbic repulsion or space-charge effects will distort ion trajectories and result in a loss in mass resolution.<sup>56</sup>

### **1.4.3. Electrospray Ionization**

Despite recent advances in high resolution mass analyzers, such as the orbitrap,<sup>57</sup> the performance of MS instruments are ultimately limited by the robustness of the ion source. ESI was first suggested as an ion source for MS by Dole and co-workers in 1968,<sup>58</sup> which was then further developed by Fenn who was later awarded the Nobel Prize in Chemistry in 2003.<sup>59</sup> This method has been adopted as a near universal format for the ionization of polar analytes, as well as a compatible interface for liquid-based separation techniques, including LC and CE. In ESI-MS, a potential difference across the tip of a stainless steel needle (emitter/electrode) is used to disrupt solvent cohesion forces to facilitate aerosol formation that can be more readily desolvated prior to sampling into the mass analyzer. The high electric field strength near the emitter tip results in the generation of a Taylor cone, where electrostatic forces repel or accelerate negative or positive ions in solution (depending on voltage polarity) until formation of a fine spray of charged droplets. Recent evidence supports an ion evaporation mechanism for describing gas-phase ion formation involving the desolvation of low molecular weight solutes from charged droplets.<sup>60</sup> However, a fully quantitative model for predicting solute ionization response in biological samples

is still lacking.<sup>61, 62</sup> This is relevant given the wide disparity in solute ionization efficiency and ionization suppression effects, which can result in responses that differ by over three-orders of magnitude despite equimolar concentrations in solution. Recently, a multivariate strategy for predicting the relative response factor of polar metabolites based on their fundamental molecular, thermodynamic and electrokinetic properties was developed using CE-ESI-MS, which enabled semi-quantitative analysis of recently identified metabolites in cases when purified chemical standards are lacking.<sup>36</sup>

The main obstacle for direct coupling of LC to ESI-MS was the high flow rates ( $\mu\text{L}/\text{min}$ ) of solvent eluting from the column, which is not compatible with the low pressure requirements of MS.<sup>63</sup> The design of orthogonal ESI interfaces under high temperatures with counter-flow curtain gas technology have improved desolvation processes while reducing background noise levels in the mass analyzer. However, unlike LC, the flow rate in CE generated by the EOF is typically on the scale of  $\text{nL}/\text{min}$ , which is too low to generate a stable spray in conventional ESI-MS. To circumvent this issue, several groups have developed various ESI designs appropriate for CE-MS hyphenation with particular attention to sheathless and sheath-liquid interfaces over the last twenty years.<sup>64</sup> The coaxial sheath liquid interface<sup>36</sup> is currently the most widely used ESI design in commercial CE-MS instruments, which is depicted in Figure 1.8. The ion spray is composed of three concentric tubes, where the inner tube represents the distal end of the fused-silica capillary used for CE separation. In addition, two outer

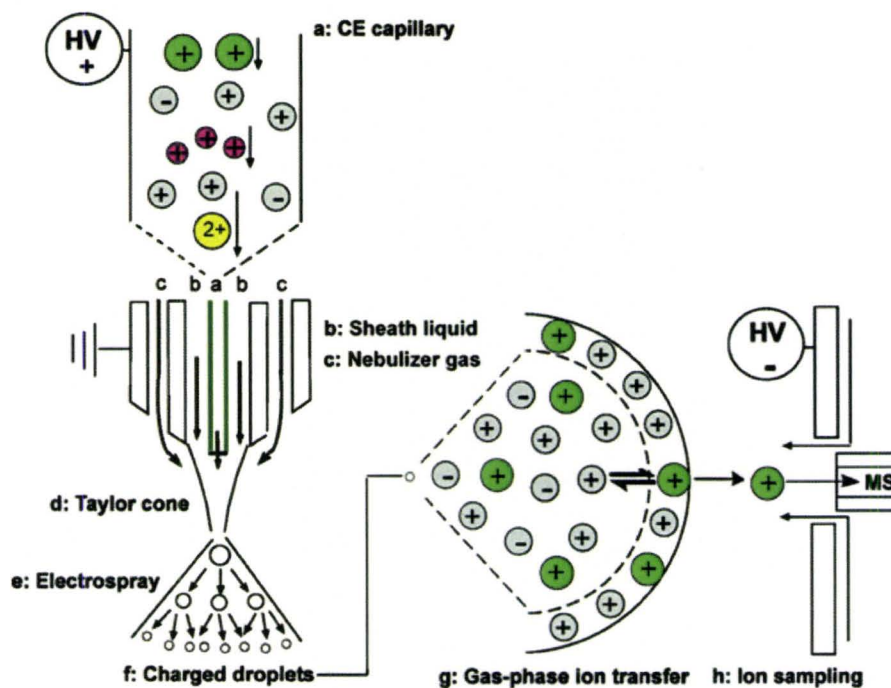


**Figure 1.8.** Schematic diagram of a coaxial sheath liquid interface for CE-ESI-MS, as well as the ion evaporation process where gas-phase ions of solutes are generated from charged droplets

stainless steel tubes are constructed around the central capillary to facilitate ion spray formation in CE-MS via the use of a sheath liquid and nebulizing gas, respectively. The sheath liquid, which is composed of an organic solvent/electrolyte mixture (*e.g.*, 50% MeOH/0.1% formic acid) serves to complete an electrical contact between the CE instrument and ESI interface, as well as provide a make-up flow to enhance spray formation. In contrast to LC-ESI-MS, the use of a sheath liquid allows independent optimization of conditions in CE for separation resolution from ionization conditions in ESI-MS required for improving sensitivity. The co-axial sheath liquid interface in CE-ESI-MS

represents a robust configuration that provides a stable spray without suffering from significant ionization suppression from sample matrix effects. Nevertheless, the sheath liquid flow can contribute to reduced concentration sensitivity due to post-capillary dilution effects on analyte zones prior to ionization.<sup>65</sup> In addition, the high flow rate of the nebulizing gas can create a siphoning effect within the capillary leading to parabolic flow instead of an ideal laminar flow by the EOF thereby reducing separation efficiency. Because to these shortcomings, various sheathless interface designs for CE-ESI-MS are still being investigated by various research groups,<sup>66</sup> however an alternative design with satisfactory robustness for routine operation has yet to be demonstrated. Recently, Hasimoto *et al.* reported the fabrication of a novel microelectrospray ( $\mu$ -ESI) interface for CE-MS using a reduced probe diameter that avoids the need for a nebulizer gas as a way to retain high separation efficiency.<sup>67</sup> Alternatively, on-line sample preconcentration techniques can be used to improve separation efficiency and concentration sensitivity in CE-MS when using conventional sheath flow ESI interfaces, which will be discussed in further detail in *Chapter II* of the thesis.

#### **1.4.4. CE-MS and Metabolomics**

In recent years, CE-MS has emerged as a promising platform for the analysis of complex mixtures of polar molecules that is complementary to GC-MS and LC-MS. Due to its high separation efficiency, tunable selectivity and small sample volume requirements, CE-MS provides a high resolution separation platform with qualitative information for structural elucidation of unknown

compounds. In essence, CE-MS represents an ideal orthogonal analytical platform since solutes are first resolved in the solution phase by their effective charge/size ratio by CE, which are then further resolved in the gas-phase by their mass/charge ratio by the mass analyzer. This complementary separation principle allows for expanded selectivity notably for stereoisomers and isobaric ions which cannot be distinguished by MS alone. In addition, CE can improve the performance of ESI-MS by resolving major co-ions/in-volatile salts from low abundance metabolites in complex biological samples without ionization suppression that is a serious limitation of direct-infusion ESI-MS. Olivares *et al.* reported the first successful coupling of CE with ESI-MS, where they were able to interface a home-built CE instrument with a quadrupole mass analyzer using a co-axial sheath liquid interface.<sup>68</sup> Since this first report, there has been considerable advancement in CE-MS, which has been applied to the analysis of complex biological samples, including proteins/peptides<sup>69-71</sup> and polar metabolites.<sup>14, 18, 72-75</sup> Figure 1.9 highlights the steady rise in the total number of research publications cited in the literature over the last twenty years. Nevertheless, LC-MS represents the most widely used liquid separation format for small molecules due to its longer historical usage and standardized ESI interface design that have been adopted by major commercial instrumental vendors. Indeed, LC-MS is still the method of choice for non-polar/neutral metabolite analyses due to compatibility issues when using non-volatile surfactant additives in MEKC-MS.<sup>76</sup>

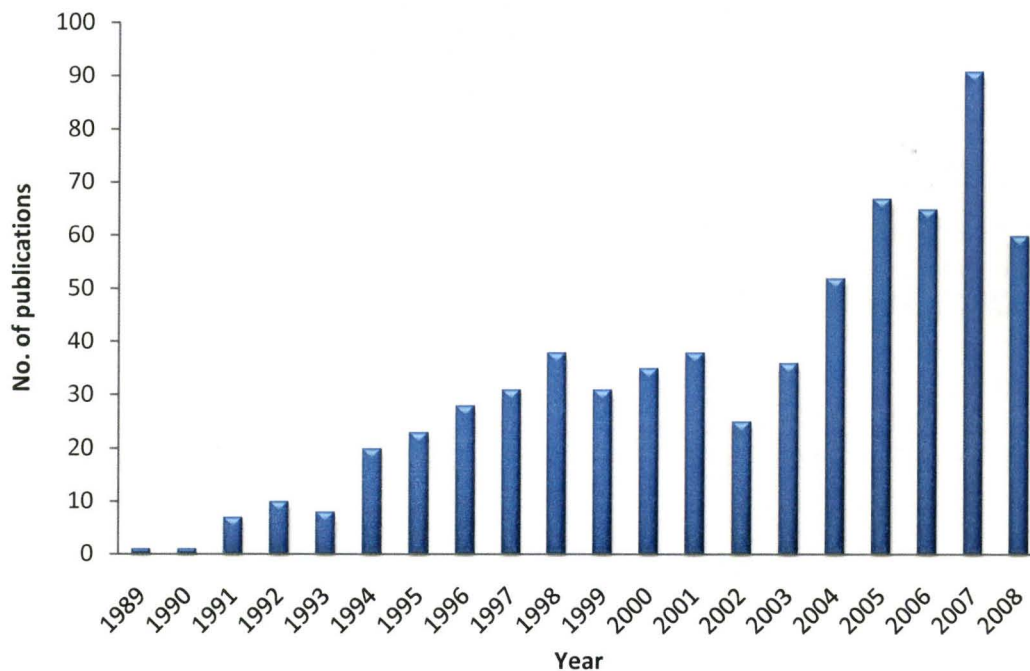


**Figure 1.9.** Total number of publications cited for CE-MS from 1989 to 2008 using ISI Web of Knowledge (<http://apps.isiknowledge.com>)

However, CE-ESI-MS offers unique advantages in terms of greater selectivity and improved sensitivity for charged metabolites that have widely different polarity, such as the simultaneous profiling of amino acids and acylcarnitines in dried blood spots for expanded newborn screening of inherited metabolic disorders.<sup>37</sup>

Soga and colleagues at the Institute for Advanced Biosciences at Keio University have been at the forefront of method development and biological applications of CE-MS technology for metabolomics research.<sup>41, 77</sup> Soga *et al.* first reported baseline resolution of all 20 amino acids was demonstrated under strongly acidic conditions to suppress the EOF.<sup>78</sup> Later, alkaline buffer conditions were optimized to increase coverage to include anionic metabolites by CE-MS using polybrene as polycation additive to reverse the EOF and stabilize ion spray

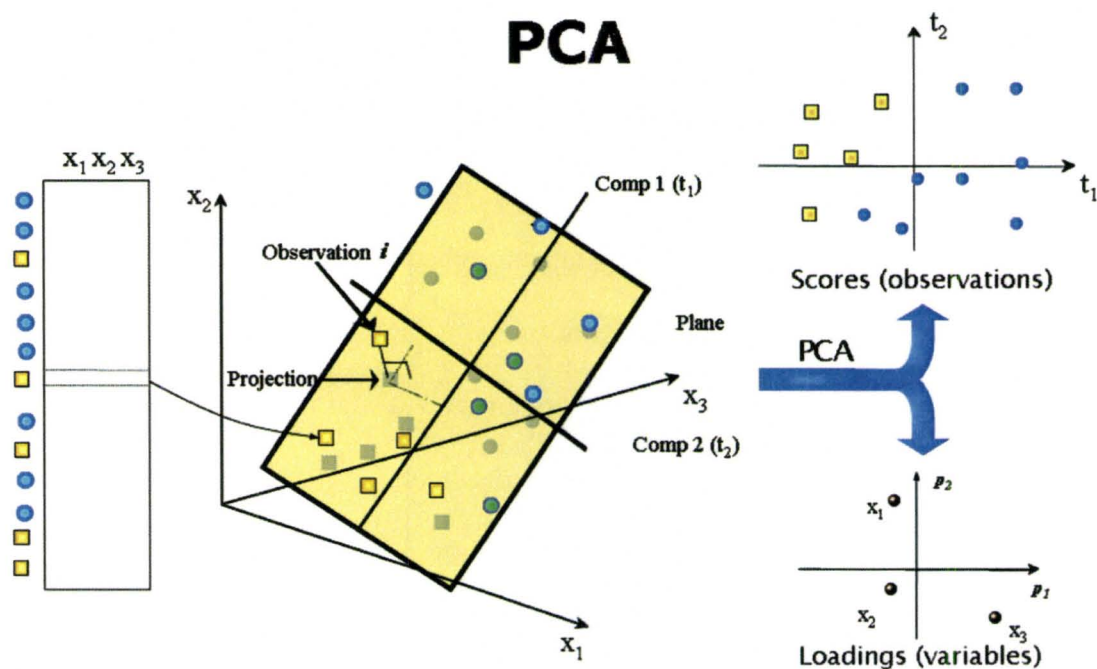


**Figure 1.10.** Principle component analysis (PCA) model estimates the variation in the matrix table. The analysis generates a score plot which can group data points which exhibit similar characteristics and identify possible outliers. The loadings plot represents the influence of the data points and their relation between them.<sup>81</sup>

variation (i.e., metabolites). The first principal component (PC1) represents the axis of maximum co-variance in the data set with each subsequent PC orthogonal and representing the next greatest direction of data-covariance. The scores plot of PCA provides an effective way to classify different objects (i.e., metabolites) that share similar co-variance in the data set, whereas outliers in a score plot highlight object with distinctive co-variance properties. Similarly, a score plot of PCA can be used to represent the inter-variable relationship impacting the data set of the experiment. The loading plot describes the relationship between the measured variables along the column at each time/progression point. The trajectory of the

loading plot is influenced by the score plot, thus, groupings on the scores plot can be identified by the variables on the loading plot. The correlation between these two plots can be used as a powerful tool to recognize underlying patterns as a function of certain stressors such as exogenous chemical perturbations,<sup>82</sup> analysis of food contamination<sup>83</sup> or biomarker discovery.<sup>84, 85</sup> Hierarchical cluster analysis (HCA) is another common type of non-supervised classification method.<sup>86-88</sup> HCA groups data together to visualize data sets as dendrograms. Similar observations or data are group together according to certain parameters step by step to form clusters until all observations are grouped into one cluster.<sup>86</sup> Both PCA and HCA will be applied as unsupervised data exploration methods for identifying putative biomarkers of oxidative stress induced by exhaustive exercise as described in *Chapter IV* of the thesis. Supervised classification is a type of multivariate analysis which takes into account additional information relating the data set to another set of qualitative or quantitative responses, which is often used to generate predictive models. Partial least squares (PLS) is the most common supervised analysis method.<sup>89, 90</sup> In PLS, the scores and loadings are paired together to enhance covariance between the data set and classification, which can allow to form a predictive model or can be used to explain which data sets are related.

Multivariate analysis can indeed be used to enhance and distinguish statistically relevant data, however, raw data from metabolomic experiments must first be appropriately aligned, filtered and normalized in order to improve data

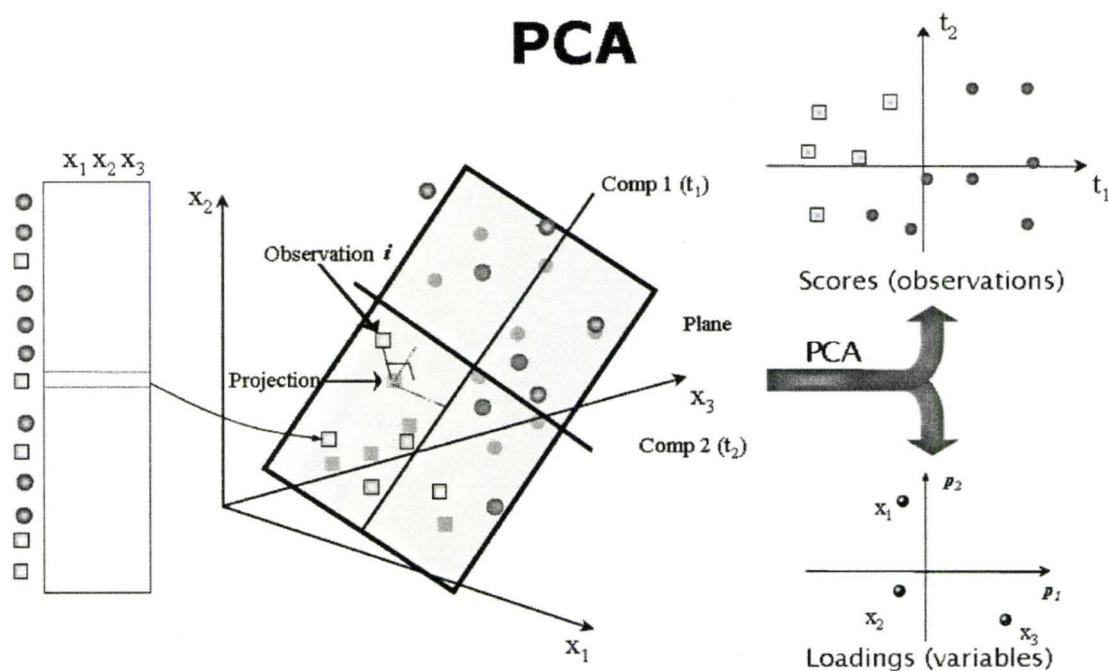


**Figure 1.10.** Principle component analysis (PCA) model estimates the variation in the matrix table. The analysis generates a score plot which can group data points which exhibit similar characteristics and identify possible outliers. The loadings plot represents the influence of the data points and their relation between them.<sup>81</sup>

variation (i.e., metabolites). The first principal component (PC1) represents the axis of maximum co-variance in the data set with each subsequent PC orthogonal and representing the next greatest direction of data-covariance. The scores plot of PCA provides an effective way to classify different objects (i.e., metabolites) that share similar co-variance in the data set, whereas outliers in a score plot highlight object with distinctive co-variance properties. Similarly, a score plot of PCA can be used to represent the inter-variable relationship impacting the data set of the experiment. The loading plot describes the relationship between the measured variables along the column at each time/progression point. The trajectory of the

loading plot is influenced by the score plot, thus, groupings on the scores plot can be identified by the variables on the loading plot. The correlation between these two plots can be used as a powerful tool to recognize underlying patterns as a function of certain stressors such as exogenous chemical perturbations,<sup>82</sup> analysis of food contamination<sup>83</sup> or biomarker discovery.<sup>84, 85</sup> Hierarchical cluster analysis (HCA) is another common type of non-supervised classification method.<sup>86-88</sup> HCA groups data together to visualize data sets as dendrograms. Similar observations or data are group together according to certain parameters step by step to form clusters until all observations are grouped into one cluster.<sup>86</sup> Both PCA and HCA will be applied as unsupervised data exploration methods for identifying putative biomarkers of oxidative stress induced by exhaustive exercise as described in *Chapter IV* of the thesis. Supervised classification is a type of multivariate analysis which takes into account additional information relating the data set to another set of qualitative or quantitative responses, which is often used to generate predictive models. Partial least squares (PLS) is the most common supervised analysis method.<sup>89, 90</sup> In PLS, the scores and loadings are paired together to enhance covariance between the data set and classification, which can allow to form a predictive model or can be used to explain which data sets are related.

Multivariate analysis can indeed be used to enhance and distinguish statistically relevant data, however, raw data from metabolomic experiments must first be appropriately aligned, filtered and normalized in order to improve data

quality/noise reduction caused by instrumental drift. The advent of high resolution and high sensitivity instrumental techniques has led to the ability to detect thousands of putative signals in complex biological samples. However, some recent metabolomic reports do not apply rigorous data preprocessing methods which can result in a significant overestimation of authentic metabolites detected in samples.<sup>88</sup> *Chapter IV* of this thesis will outline an extensive strategy for processing complex data sets generated from time-dependent changes in erythrocyte metabolism with strenuous aerobic exercise for the discovery of oxidative stress biomarkers.

Critical components of workflow for metabolomic studies are shown in Figure 1.11. Each aspect of the workflow is vital for thorough investigations for untargeted metabolomic studies from initial hypothesis, experimental design, sample type and preparation, to analytical platform. Data processing is a vital component as discussed previously to reveal pertinent data for identification of biomarkers. Data from untargeted metabolomic studies can often in unanticipated results which may lead to re-evaluation of original hypothesis to form newly generated hypothesis, such as the efficacy of antioxidant supplementation as described in *Chapter IV* of this thesis.

## **1.6. Applications of Metabolomics**

The rapidly growing interest in metabolomics is reflected by its diverse applications across various disciplines of scientific research. Since its early

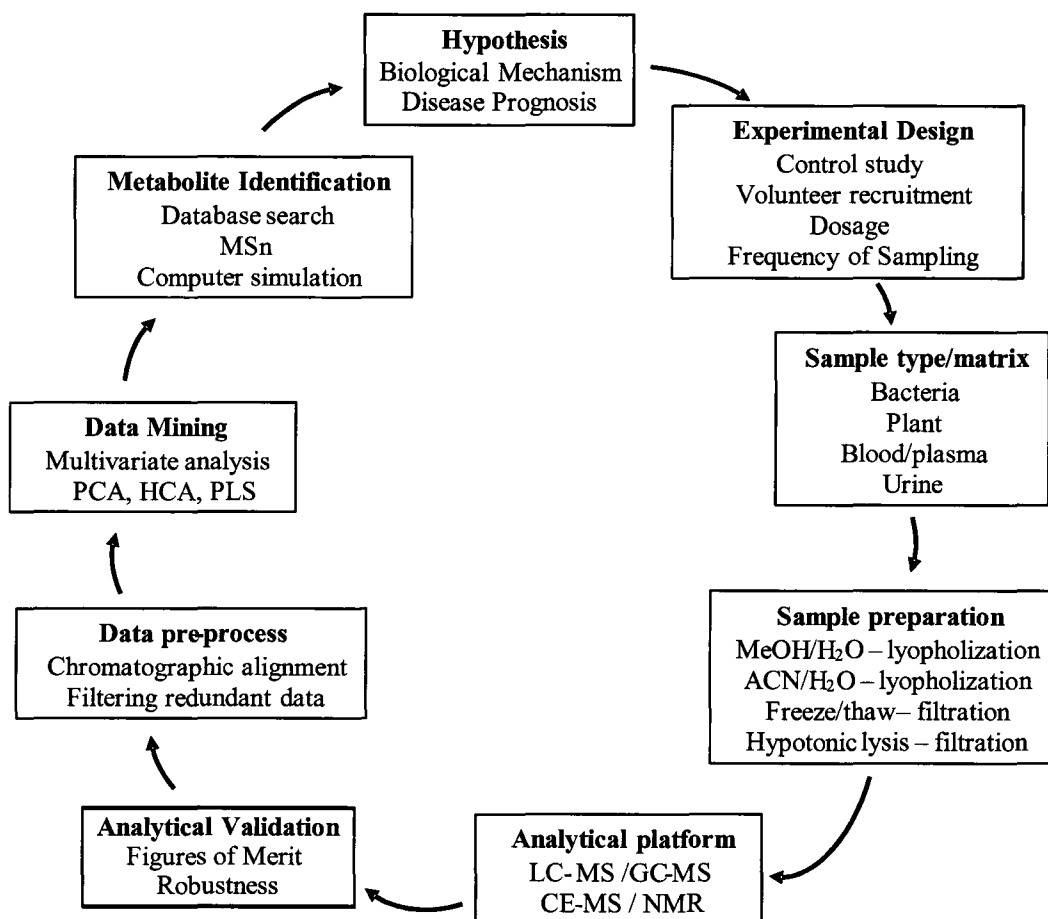


**Figure 1.11.** Schematic diagram depicting the circular workflow for untargeted metabolomic studies. Each step represents a critical aspect which must be carefully controlled for untargeted metabolomic analyses. Experimental design is vital for control of variables to limit any experimental variations, followed by the type of sample matrix and preparation. Method validation used on any analytical platform is imperative to have reproducible and valid results. Appropriate data preprocessing and mining are critical for identifying unique data changes, which can then be used for metabolite identification processes. Experimental data may confirm initial hypothesis or may lead to newly formed hypothesis.

introduction, plant biotechnology has embraced metabolomics as a missing link in functional genomic studies notably in the context of assessing the safety of genetically-modified crops.<sup>17</sup> The Fiehn group has spearheaded the expanding interest of metabolomics in plant research applications using high resolution GC-TOF-MS technology.<sup>5, 6, 91</sup> The major goals of plant biotechnology are to

genetically engineer crops that more resistant to environmental stress,<sup>92</sup> as well as increase the nutritional content or eliminate the toxicological properties of certain nutrients found within staple crops.<sup>93</sup> Recently, Fiehn *et al.* distinguished among four different *Arabidopsis* genotypes based on their distinct metabolomic profiles when using PCA analysis for differentiation of two wild type phenotypes and their mutant variants.<sup>5</sup> Givoanni and co-workers were able to demonstrate by incorporating the stilbene synthase gene found in grapes into transgenic tomatoes, they were able to induce synthesis of trans-resveratrol, a known antioxidant.<sup>94</sup> Not only was trans-resveratrol formed but other antioxidants such as GSH and ascorbic acid were found to be in elevated levels compared to wild-type counterparts. These reports highlight that a single gene mutation can have a significant impact on the phenotype an organism as revealed by untargeted metabolomic analyses.

Environmental research has recently emerged as a significant field of interest within metabolomics research. With increased awareness of the chronic effects of low level exposure to chemical pollutants in the environment, environmental metabolomics can provide an unbiased approach for assessing the impact of various stressors on the health of an organism. To date, most investigations have focused on the effects of various exogenous contaminants found in soil and water to model organism, such as earthworms and fish. For instance, the analysis of earthworms extracts was performed by NMR to identify responses upon exposure to different concentration levels of specific xenobiotics

based on global changes in metabolites.<sup>95</sup> Similarly, Warne *et al.* demonstrated the dose response of 3-trifluoromethylalaniline upon exposure to the earthworm *E. veneta*, where NMR in conjunction with PCA analysis was used to identify specific changes in metabolite levels associated with an organism's response to toxicity.<sup>96</sup> Samuelsson *et al.*<sup>97</sup> investigated the impact of the synthetic contraceptive and putative endocrine-disrupting substance, estrogen ethinylestradiol (EE2) based on metabolomic analyses of plasma extracts from male rainbow trout. Their study revealed significant changes in the levels of vitellogenin, alanine, phospholipids and cholesterol upon low level exposure to only 10 ng/L of the synthetic steroid.<sup>97</sup> The increase in plasma vitellogenin suggests that the reproduction system of male rainbow trout was exhibiting an adverse response with greater feminine characteristics which can be associated with changes in other low molecular weight metabolites.<sup>97</sup> Recently, Ekman *et al.* reported a similar metabolite profiling strategy using male flathead minnows upon exposure to EE2, whereas metabolite perturbations were not observed in their female counterparts.<sup>98</sup> Several studies have shown that the discharge of pharmaceuticals into the ecosystem represents an emerging area of environmental concern, however the long-term impact of these chemicals and their degradation products on the health of aquatic life and humans remains unclear.<sup>99, 100</sup>

Pharmaceutical research has slowly adopted metabolomics as a way to facilitate the identification of drug targets, as well as assess the toxicity of therapeutic agents at earlier stages of drug development. An area of particular

interest lies in the pre-clinical stage, where rat and mouse studies comprise the vast majority of animal testing. Recently, several major pharmaceutical and academic institutions have formed a conglomerate, Consortium on Metabonomic Toxicology, which aims to generate a public depository of NMR based data for toxins identified in rats.<sup>101</sup> For instance, Lenz *et al.* studied the impact of the immunosuppressant drug, cyclosporine A on Wistar rats based on untargeted urinary analysis of metabolites using NMR and LC-MS.<sup>87</sup> Elevated levels of citrate,  $\alpha$ -ketoglutarate, succinate and glucose were identified as key metabolites perturbed after administration with cyclosporine A, which suggested that the rats were unable to utilize carbohydrate sources leading to the observed reduction in weight gain relative to the control group. Similarly, elevated metabolite levels discharged in urine could be used as potential biomarkers of nephrotoxicity and reduced renal function.<sup>87, 102, 103</sup> Recently, Sreekumar *et al.* reported an extensive study that correlated specific metabolites found in urine, plasma, and tissue to the progression of prostate cancer.<sup>10</sup> Using a combination of GC-MS and LC-MS, over 1100 unique metabolites signatures were detected across the three different types of biological specimens, however elevated levels of sarcosine in urine was determined to be the statistically most significant biomarker associated with metastatic progression of prostate cancer relative to controls. Thus, biomarker discovery represents one the most promising applications of metabolomic research in the context of personalized medicine, which can lead to early detection, optimal treatment and improved health outcomes for individuals with

chronic disorders.<sup>104</sup> Indeed, *Chapters IV* and *V* of this thesis will focus on the use of CE-MS for the identification and validation of biomarkers of oxidative stress associated with strenuous exercise and ionizing radiation, respectively.

## **1.7. Introduction to Oxidative Stress**

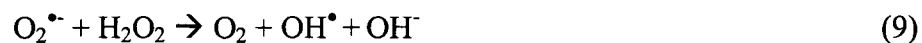
### **1.7.1 Biomarkers of Oxidative Stress**

Oxidative stress has been hypothesized as a mechanism underlying the pathogenesis of various disease states, as well as the natural consequence of aging.<sup>105</sup> Reactive free radicals generated as by-products of aerobic metabolism, immune defense and cellular signaling have been implicated in the oxidation of biological molecules resulting in altered cell activity. In 1928, Pearl introduced the “rate-of-living theory of aging”, which surmised a direct correlation between metabolism and ageing, such that organisms with faster metabolic rates will age faster.<sup>106</sup> Thirty years later, Harman proposed the “free radical theory of aging” in 1956, where free radicals were hypothesized as the causative agents of normal aging processes.<sup>107</sup> The integration of these two biochemical theories on aging results in the metabolic consequence of “live fast-die young”, where faster metabolic rates result in accelerated ageing due to the formation of various reactive oxygen and nitrogen species (ROS/RNS).<sup>108</sup> The damaging effects of ROS/RNS on biological systems has been termed oxidative stress, which occurs when the reducing capacity of a cell to neutralize these free radicals is compromised.<sup>109</sup> This results in the imbalance of the cellular redox states between pro-oxidants and antioxidants that has long been the dominant paradigm

in nutritional sciences.<sup>110</sup> Numerous studies have demonstrated that chronic oxidative stress has been associated with irreversible cellular damage leading to neurodegenerative disorders, such as Parkinson's<sup>111</sup> and Alzheimer's<sup>111-113</sup> disease. Nevertheless, there is growing evidence that oxidative stress based on an understanding of an imbalance in the levels of pro-oxidant-antioxidant is inadequate to describe universal oxidative stress. There is mounting evidence that suggests increased levels of ROS/RNS do not necessarily lead to oxidative stress. Redox imbalance has been shown to be involved in a number of normal cellular processes such as cell proliferation and specific redox involved pathways.<sup>114</sup> Studies have shown elevated levels of peroxide, a major source of free radicals, under specific conditions does not increase cellular oxidative stress and nor alter the redox balance with respect to reduced glutathione (GSH) levels as previously thought.<sup>115</sup> Physiological levels of ROS have been observed to be contained within subcellular compartments, where various proteins have been examined to undergo selective oxidation but cytosolic levels of GSH did not change.<sup>116</sup> These investigations suggest that the presence of intracellular ROS does not immediately lead to global changes in the reduced and oxidized glutathione (GSSG) redox couple, GSH/GSSG, and that perhaps a new definition of oxidative stress should be developed.

### **1.7.2. Reactive Oxygen Species**

Free radicals can be defined as reactive molecular species which possess an unpaired electron.<sup>117</sup> In biological systems, the two most prevalent free radicals are the superoxide anion radical,  $O_2^{\bullet-}$ , and hydroxyl radical,  $OH^{\bullet}$ .<sup>117</sup> The superoxide anion can be generated within the mitochondria where energy metabolism occurs as electrons leak from the mitochondria electron transport chain.<sup>118</sup> Once generated they can proceed to react with molecules to form other free radicals or ROS, such as hydrogen peroxide via superoxide dismutase (eq.7). The hydroxyl radical,  $OH^{\bullet}$ , is closely related to the intracellular availability of metal ions such as iron and copper particularly within erythrocytes where iron in hemoglobin is accessible. Under oxidative stress conditions, excess superoxide anions have been shown to increase intracellular levels of free iron from iron-bound protein.<sup>119</sup> These free  $Fe^{2+}$  ions are available to participate in Fenton-like reactions to generate hydroxide radicals with hydrogen peroxide (eq.8).<sup>120</sup> The superoxide anion radical can further participate to produce hydroxide radicals via Haber-Weiss reaction (eq.9) that combines the Fenton reaction and the reduction of  $Fe^{3+}$  by  $O_2^{\bullet-}$ .<sup>121</sup>



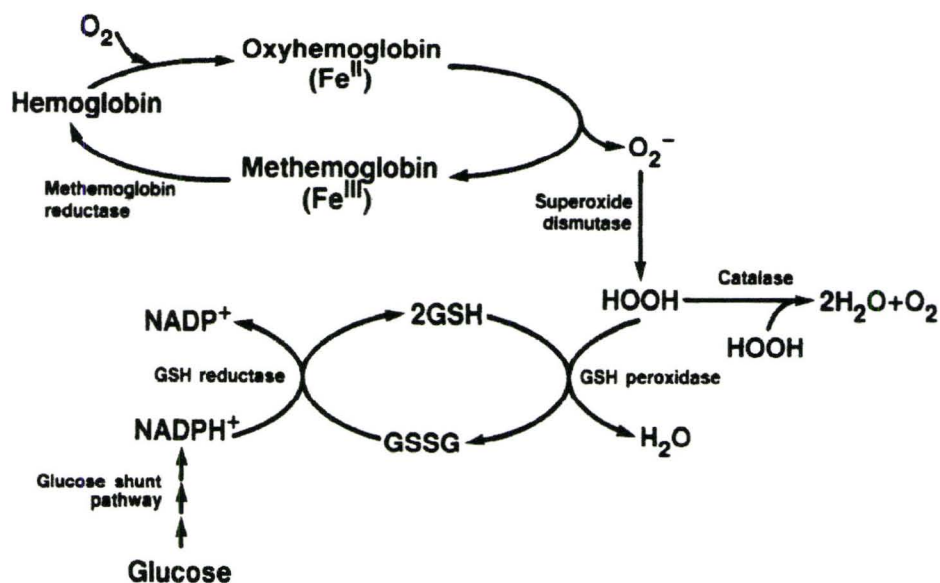


**Figure 1.12.** Illustration of possible pathways for free radical generation and neutralization in erythrocytes. Oxidation of hemoglobin into methemoglobin releasing superoxide radical which is neutralized by superoxide dismutase into H<sub>2</sub>O<sub>2</sub>. Peroxide is neutralized by oxidation of GSH into GSSG by forming water and oxygen.<sup>122</sup>

Once generated, these free radicals can cause disruption to normal cellular processes unless scavenged by antioxidants, such as GSH. Figure 1.12 illustrates a schematic diagram of the generation and neutralization of free radicals within erythrocytes,<sup>122</sup> which is a model cell type examined in *Chapter III* and *IV* of the thesis. A significant portion of literature has studied oxidative stress from modification of large biomolecules, including oxidative damage to protein and DNA.<sup>123, 124</sup> Increasing evidence suggests that oxidation of proteins by reactive free radicals could be involved in various diseases relating to protein misfolding or enzyme inactivation.<sup>117</sup> Reactive free radical species will most likely oxidize electron-rich side chains of amino acids such as tyrosine (Tyr), phenylalanine

(Phe), tryptophan (Trp), and cysteine (Cys).<sup>125, 126</sup> For instance, oxidation of Phe results in the formation of two unnatural isomers of Tyr, *meta*-Tyr and *ortho*-Tyr, which have been analyzed in urine as a measure of oxidative stress in association with chronic disease states.<sup>127-130</sup> High Met-content proteins have also been shown to be a substantial target of oxidation to generate two oxidized by-products, namely methionine sulfoxide and methionine sulfone.<sup>131</sup> Methionine sulfoxide has garnered much interest due to its reversible reduction by methionine sulfoxide reductase, implicating its role as a cellular redox switch possibly during cellular repair.<sup>132, 133</sup> Protein-bound Tyr has also been demonstrated to undergo covalent modification to form a number of oxidized by-products depending on the type of oxidant, such as 3-NO<sub>2</sub>-Tyr,<sup>134</sup> 3-Cl-Tyr<sup>135</sup> and dityrosine.<sup>136</sup>

### 1.7.3. Glutathione Metabolism

One of the most widely studied biomarkers of oxidative has been the analysis of thiol containing metabolites, such as Cys and GSH and their respective oxidized dimer by-products, namely cystine (CySS) and GSSG, respectively.<sup>137, 138</sup> GSH is a tripeptide comprised of three amino acids, Glu, Cys, and Gly. Physiological levels range from 1-10 mM depending on the cell type; highest concentration located in the liver and lungs as a majority of the detoxification processes occur in these organs. GSH is considered a major non-enzymatic antioxidant due to its high intracellular concentration levels and excellent free radical scavenging efficiency due to its labile thiol moiety.

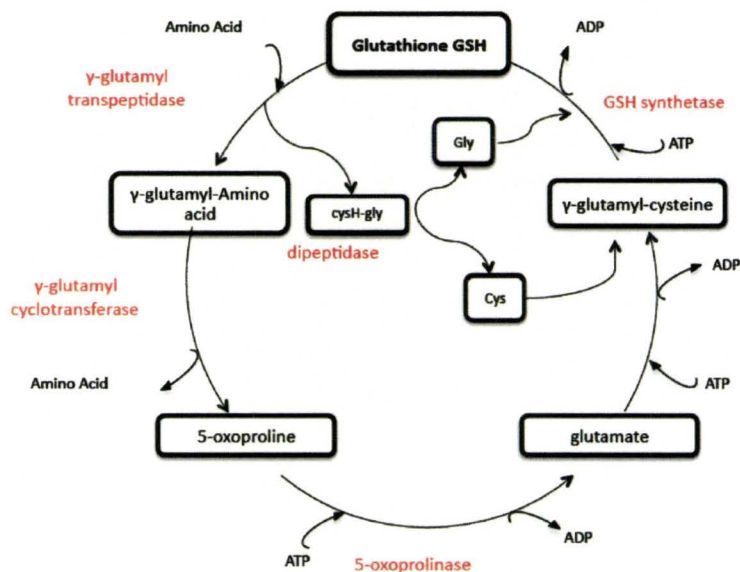


**Figure 1.13.** Schematic diagram of the biosynthetic pathway for production of glutathione. The primary metabolism of glutathione consists of six coupled enzymatic reactions with the rate determining step associated with  $\gamma$ -glutamylcysteine biosynthesis.

Consequently, the ratio between GSH and GSSG has been considered as a diagnostic marker for cellular oxidative status associated with the pathogenesis of various acute and chronic disorders.<sup>139</sup> The biosynthetic pathway for GSH is illustrated in Figure 1.13, it consists of a two step enzymatic processes which incorporates each of the three amino acids.<sup>140</sup> The first enzymatic reaction via  $\gamma$ -glutamylcysteine synthetase is responsible for the formation of  $\gamma$ -glutamylcysteine from glutamate and cysteine. The  $\gamma$ -peptic linkage prevents hydrolysis from a number of intracellular peptidases. Following formation of  $\gamma$ -glutamylcysteine, glycine is added by GSH synthetase as the final step for GSH production. GSH can also be synthesized through the catabolism of GSH conjugates, such as GSSG. Glutathione reductase can enzymatically reduce the disulfide bond with nicotinamide adenine dinucleotide phosphate (NADPH) to regenerate GSH. An

alternative catabolism pathway of GSH conjugates is mediated by  $\gamma$ -glutamyl transpeptidase which produces cysteinylglycine and  $\gamma$ -glutamyl conjugate. The dipeptide bond between cysteinylglycine can be hydrolyzed in order to allow Gly and Cys to be incorporated back into the GSH biosynthetic pathway.  $\gamma$ -glutamyl conjugate can undergo a subsequent enzymatic hydrolysis to form 5-oxoproline via  $\gamma$ -glutamyl cyclotransferase which can further be oxidized to generate glutamic acid (Glu). The availability of cysteine has been widely considered as the rate determining step in the biosynthesis of GSH.<sup>110</sup> Given the important role of GSH for cell protection, methods to increase or enhance GSH biosynthesis by nutritional supplements is an active field of research. One particular supplement that has garnered much attention has been *N*-acetyl-*L*-cysteine (NAC), which has been investigated extensively as a supplement to enhance GSH concentration.<sup>141</sup> <sup>142</sup> GSH can scavenge intracellular free radicals such as  $O_2^{\bullet-}$  and  $OH^{\bullet}$  by donating an electron and oxidizing to form  $GS^{\bullet}$  and  $H_2O$  which can then readily combine to form GSSG. In addition, detoxification of highly electrophilic species can be mediated by glutathione S-transferases to form water soluble GSH thioether/thioester conjugates that can be actively transported out of the cell for further metabolism or excretion.

#### **1.7.4. Functions of Glutathione**

The role of GSH has evolved considerably over the last 20 years. Initially thought of as an antioxidant, its function has expanded to include cell cycle modulation (regulation, proliferation, and apoptosis), metabolism of xenobiotics,

and thiol disulfide exchange mechanisms for proteins.<sup>117</sup> GSH levels have been linked with a variety of age-related degenerative diseases. It has been well documented that as individuals age, there is an overall decrease in antioxidant capacity associated with lower GSH levels.<sup>117</sup> As GSH is the major intra-cellular anti-oxidant, reduced levels of GSH can lead to an increase susceptibility to oxidative damage. This is reflected in the increase in age related eye disorders with the concomitant decline of GSH levels in human lens. Lens transparency and tissue hydration has been associated with high levels of GSH which can prevent the onset of cataracts.<sup>143</sup> The retina in particular is highly susceptible to oxidative stress with increased exposure to light and oxygen. Reduction of GSH levels has been associated with two retinopathies, glaucoma and macular degeneration.<sup>144-146</sup> The exact etiology of these two disorders are still unknown but oxidative damage to the retinal epithelium cells has been implicated as the underlying mechanism.<sup>147, 148</sup> Apart from age related conditions, abnormal levels of GSH and malfunction of its metabolism has been linked with a multitude of disease states, such as inborn errors of metabolism. Deficiency of  $\gamma$ -glutamylcysteine synthase can result in a number of disorders ranging spinocerebellar degeneration to amino-aciduria.<sup>149, 150</sup> Patients who exhibit glutathione synthase deficiency can suffer from spectrum of diseases ranging from hemolytic anemia in mild cases to more severe cases of recurring bacterial infections and central nervous system dysfunction.<sup>139, 150</sup> Although diminished concentrations of GSH have been linked with several disorders, increase in GSH

has also been demonstrated to be detrimental, specifically in treatment of various cancers. For instance, elevated levels of GSH in cancerous cells and tumors are observed to be more resistant to chemotherapy.<sup>151-154</sup> Tumor cells exhibiting chemoresistance have been shown to possess higher activities of enzymes associated with GSH biosynthesis.<sup>153, 154</sup> The importance of GSH to intracellular health cannot be underestimated. *Chapter III* and *IV* will develop and validate an artifact-free method for accurate quantification of cellular redox status and antioxidant capacity based on glutathione analysis in erythrocytes, which will also be applied for the assessment of exercise-induced oxidative stress as a way to elucidate the efficacy of antioxidant supplementation.

### **1.8. Research Objectives**

Metabolomic studies are directed at the comprehensive analysis of all metabolites in a biological sample which offers improved functional understanding of the impact of various extrinsic stressor on phenotype. The detection and identification of biomarkers which reflect specific cellular status are of particular interest as they can provide insight to the biochemical pathways which are affected. The goals of this thesis are aimed at addressing several major analytical challenges that hinder the future progress of metabolomics in biological research. To assist in this effort, the major research objectives associated with the work presented in this thesis are : (a) development of on-line sample preconcentration and desalting technique to enhance concentration sensitivity of

low abundance metabolites, (b) a virtual approach for the identification of unknown metabolites using computer electrophoretic simulations for prediction of ion electromigration behavior based fundamental physiochemical properties of metabolite candidates, (c) the validation of a robust artifact-free strategy for accurate determination of labile metabolites from red blood cell lysate without complicated sample handling, (d) a novel assay for the evaluation of intracellular antioxidant capacity and redox status of cells based on the differential rates glutathione oxidation, and (e) application of univariate and multivariate statistical tools for the discovery of putative oxidative stress biomarkers associated with strenuous exercise and low dose ionizing radiation. The ultimate goal of this thesis is to integrate these objectives as a foundation for biomarker discovery using an unbiased metabolomics strategy based on CE-ESI-MS.

### 1.9 References

- (1) Dovichi, N. J.; Zhang, J. Z. *Angew. Chem. Int. Ed.* **2000**, *39*, 4463.
- (2) Wang, Z.; Gerstein, M.; Snyder, M. *Nature Rev. Genetics* **2009**, *10*, 57-63.
- (3) Tyers, M.; Mann, M. *Nature* **2003**, *422*, 193-197.
- (4) Weckwerth, W. *Annu. Rev. P. Bio.* **2003**, *54*, 669-689.
- (5) Fiehn, O.; Kopka, J.; Dormann, P.; Altmann, T.; Trethewey, R. N.; Willmitzer, L. *Nat. Biotech.* **2000**, *18*, 1157.
- (6) Fiehn, O.; Kopka, J.; Trethewey, R. N.; Willmitzer, L. *Anal. Chem.* **2000**, *72*, 3573.

- (7) Fiehn, O. *Comp. Func. Genomics* **2001**, *2*, 155.
- (8) Saito, N.; Robert, M.; Kitamura, S.; Baran, R.; Soga, T.; Mori, H.; Nishioka, T.; Tomita, M. *J. Prot. Res.* **2006**, *5*, 1979-1987.
- (9) Griffin, J. L. *Curr. Opin. Chem. Biol.* **2006**, *10*, 309.
- (10) Sreekumar, A.; Poisson, L. M.; Rajendiran, T. M.; Khan, A. P.; Cao, Q.; Yu, J.; Laxman, B.; Mehra, R.; Lonigro, R. J.; Li, Y.; Nyati, M. K.; Ahsan, A.; Kalyana-Sundaram, S.; Han, B.; Cao, X.; Byun, J.; Omenn, G. S.; Ghosh, D.; Pennathur, S.; Alexander, D. C.; Berger, A.; Shuster, J. R.; Wei, J. T.; Varambally, S.; Beecher, C.; Chinnaiyan, A. M. *Nature* **2009**, *457*, 910-914.
- (11) Nicholson, J. K.; Lindon, J. C.; Holmes, E.; *Meta. Xeno.* **1999**, *29*, 1181.
- (12) Nicholson, J. K.; Connelly, J.; Lindon, J. C.; Holmes, E. *Nature Rev. Drug Discov.* **2002**, *1*, 153.
- (13) Reily, M. D.; Robertson, D. G.; Delnomdedieu, M.; Baker, J. D. *Am. Pharm. Rev.* **2003**, *6*, 105.
- (14) Soga, T. *Plant Cell Physi.* **2004**, *45*, S7-S7.
- (15) Fiehn, O. *Plant Mol. Biol.* **2002**, *48*, 155.
- (16) Sansone, S. A.; Fan, T.; Goodacre, R.; Griffin, J. L.; Hardy, N. W.; Kaddurah-Daouk, R.; Kristal, B. S.; Lindon, J.; Mendes, P.; Morrison, N.; Nikolau, B.; Robertson, D.; Sumner, L. W.; Taylor, C.; van der Werf, M.; van Ommen, B.; Fiehn, O. *Nature Biotech.* **2007**, *25*, 844-848.

- (17) Hall, R.; Beale, M.; Fiehn, O.; Hardy, N.; Sumner, L.; Bino, R. *Plant Cell* **2002**, *14*, 1437-1440.
- (18) Soga, T.; Ohashi, Y.; Ueno, Y.; Naraoka, H.; Tomita, M.; Nishioka, T. *J. Prot. Res.* **2003**, *2*, 488-494.
- (19) Ohashi, Y.; Hirayama, A.; Ishikawa, T.; Nakamura, S.; Shimizu, K.; Ueno, Y.; Tomita, M.; Soga, T. *Mol. Biosys.* **2008**, *4*, 135-147.
- (20) Lee, R.; Ptolemy, A. S.; Niewczas, L.; Britz-McKibbin, P. *Anal. Chem.* **2007**, *79*, 403-415.
- (21) Ogata, H.; Goto, S.; Sato, K.; Fujibuchi, W.; Bono, H. *Nucleic Acids Res.* **1999**, *27*, 29.
- (22) Smith, C. A.; O'Maille, G.; Want, E. J.; Qin, C.; Trauger, S. A.; Brandon, T. R.; Custodio, D. E.; Abagyan, R.; Siuzdak, G. *Ther. Drug. Mon.* **2005**, *27*, 747-751.
- (23) Wishart DS, T. D., Knox C, Eisner R, Guo AC, Young N, Cheng D, Jewell K, Arndt D, Sawhney S, Fung C, Nikolai L, Lewis M, Coutouly MA, Forsythe I, Tang P, Shrivastava S, Jeroncic K, Stothard P, Amegbey G, Block D, Hau DD, Wagner J, Miniaci J, Clements M, Gebremedhin M, Guo N, Zhang Y, Duggan GE, Macinnis GD, Weljie AM, Dowlatabadi R, Bamforth F, Clive D, Greiner R, Li L, Marrie T, Sykes BD, Vogel HJ, Querengesser L. *Nucleic Acids Res.* **2007**, *35*, D521-526.
- (24) Dunn, W. B.; Bailey, N. J.; Johnson, H. E. *Analyst* **2005**, *130*, 606.

- (25) Keun, H. C.; Beckonert, O.; Griffin, J. L.; Richter, C.; Moskau, D.; Lindon, J. C.; Nicholson, J. K. *Anal. Chem.* **2002**, *74*, 4588.
- (26) Brad J. Williams, C. J. C. R. W. C. D. B. L. W. S. J. T. S. *Electrophoresis* **2007**, *28*, 1371-1379.
- (27) Jonsson, P.; Johansson, A. I.; Gullberg, J.; Trygg, J. A. J.; Grung, B.; Marklund, S.; Sjostrom, M.; Antti, H.; Moritz, T. *Anal. Chem.* **2005**, *77*, 5635.
- (28) <http://www.nist.gov/srd/nist1a.htm>.
- (29) Fiehn, O. <http://www.chem.agilent.com/en-US/Products/Instruments/ms/fiehgcmstmetabolomicsrtlibrary/Pages/default.aspx>.
- (30) Yoshida, H.; Yamazaki, J.; Ozawa, S.; Mizukoshi, T.; Miyano, H. *J. Ag. Food Chem.* **2009**, *57*, 1119-1126.
- (31) Martin, F. P. J.; Wang, Y.; Yap, I. K. S.; Lundstedt, T.; Lek, P.; Lindon, J. C.; Sprenger, N.; Kochhar, S.; Fay, L. B.; Holmes, E.; Nicholson, J. K. *J. Prot. Res.*, to be submitted for publication.
- (32) Nordstrom, A.; Want, E.; Northen, T.; Lehtio, J.; Siuzdak, G. *Anal. Chem.* **2008**, *80*, 421-429.
- (33) Gipson, G. T.; Tatsuoka, K. S.; Ball, R. J.; Sokhansanj, B. A.; Hansen, M. K.; Ryan, T. E.; Hodson, M. P.; Sweatman, B. C.; Connor, S. C. *Mol. Biosys.* **2008**, *4*, 1015-1023.

- (34) Zamboni, G.; Capelli, P.; Scarpa, A.; Bogina, G.; Pesci, A.; Brunello, E.; Kloppel, G. *Arch. Path. Lab. Med.* **2009**, *133*, 439-453.
- (35) Soga, T.; Ueno, Y.; Naraoka, H.; Matsuda, K.; Tomita, M.; Nishioka, T. *Anal. Chem.* **2002**, *74*, 6224-6229.
- (36) Chalcraft, K. R.; Lee, R.; Mills, C.; Britz-McKibbin, P. *Anal. Chem.* **2009**, *81*, 2506-2515.
- (37) Chalcraft, K. R.; Britz-McKibbin, P. *Anal. Chem.* **2009**, *81*, 307-314.
- (38) Copper, C. L. *J. Chem. Ed.* **1998**, *75*, 343-347.
- (39) Copper, C. L.; Whitaker, K. W. *J. Chem. Ed.* **1998**, *75*, 347-351.
- (40) Nobeli, I.; Ponstingl, H.; Krissinel, E. B.; Thornton, J. M. *J. Mol. Bio.* **2003**, *334*, 697-719.
- (41) Monton, M. R. N.; Soga, T. *J. Chrom. A* **2007**, *1168*, 237-246.
- (42) Shamsi, S. A.; Miller, B. E. *Electrophoresis* **2004**, *25*, 3927-3961.
- (43) Kodama, S.; Yamamoto, A.; Matsunaga, A.; Soga, T.; Minoura, K. *J. Chrom. A* **2000**, *875*, 371-377.
- (44) Servais, A. C.; Fillet, M.; Mol, R.; Somsen, G. W.; Chiap, P.; de Jong, G. J.; Crommen, J. *J. Pharm. Biomed. Anal.* **2006**, *40*, 752-757.
- (45) Terabe, S.; Otsuka, K.; Ichikawa, K.; Tsuchiya, A.; Ando, T. *Anal. Chem.*, **1984**, *56*, 111-113.
- (46) Chang, H. T.; Yeung, E. S. *J. Chrom. B* **1995**, *669*, 113-123.
- (47) Gavina, J. M. A.; Mazhab-Jafari, M. T.; Melacini, G.; Britz-McKibbin, P. *Biochem.* **2009**, *48*, 223-225.

- (48) Yunusov, D.; So, M.; Shayan, S.; Okhonin, V.; Musheev, M. U.; Berezovski, M. V.; Krylov, S. N. *Anal. Chim. Act.* **2009**, *631*, 102-107.
- (49) Iio, R.; Chinaka, S.; Takayama, N.; Hayakawa, K. *J. Health Sci.* **2005**, *51*, 693-701.
- (50) Soga, T.; Ueno, Y.; Naraoka, H.; Ohashi, Y.; Tomita, M.; Nishioka, T. *Anal. Chem.* **2002**, *74*, 2233-2239.
- (51) Luedtke, S.; Adam, T.; von Doehren, N.; Unger, K. K. *J. Chrom. A* **2000**, *887*, 339-346.
- (52) Jorgenson, J. W.; Lukacs, K. D. *Anal. Chem.* **1981**, *53*, 1398-1302.
- (53) March, R. E. *J. Mass. Spectrom.* **1997**, *32*, 351-369.
- (54) March, R. E. *Int. J. Mass. Spectrom.* **2000**, *200*, 285-312.
- (55) March, R. E. *Rapid Commun. Mass. Spectrom.* **1998**, *12*, 1543-1554.
- (56) Splendore, M.; Lausevic, M.; Lausevic, Z.; March, R. E. *Rapid Commun. Mass. Spectrom.* **1997**, *11*, 228-233.
- (57) Hu, Q. Z.; Noll, R. J.; Li, H. Y.; Makarov, A.; Hardman, M.; Cooks, R. G. *J. Mass. Spectrom.* **2005**, *40*, 430-443.
- (58) Dole, M. M., L.; Hines, R.L.; Mobley, R.C.; Ferguson, D.; Alice, M. *J. Chem. Phys.* **1968**, *49*, 2240.
- (59) Yamashita, M. F., J.B. *J. Phys. Chem* **1984**, *88*.
- (60) Nguyen, S.; Fenn, J. B. *PNAS* **2007**, *104*, 1111-1117.
- (61) Cole, R. B. *J. Mass Spectrom.* **2000**, *35*, 763-772.
- (62) Kebarle, P. *J. Mass Spectrom.* **2000**, *35*, 804-817.

- (63) Fenn, J. B. *J. Biomol. Tech.* **2002**, *13*, 101-118.
- (64) Maxwell, E. J.; Chen, D. D. Y. *Anal. Chim. Act.* **2008**, *627*, 25-33.
- (65) Jens Ohnesorge, C. N. H. W. *Electrophoresis* **2005**, *26*, 3973-3987.
- (66) Zamfir, A. D. *J. Chrom. A* **2007**, *1159*, 2-13.
- (67) Hashimoto, M.; Ishihama, Y.; Tomita, M.; Soga, T. *Rapid Commun. Mass Spectrom.* **2007**, *21*, 3579-3584.
- (68) Olivares, J. A.; Nguyen, N. T.; Yonker, C. R.; Smith, R. D. *Anal. Chem.* **1987**, *59*, 1230-1232.
- (69) Gomez-Ruiz, J. A.; Ramos, M.; Recio, I. *Electrophoresis* **2007**, *28*, 4202-4211.
- (70) Haselberg, R.; de Jong, G. J.; Somsen, G. W. *J. Chrom. A* **2007**, *1159*, 81-109.
- (71) Miksik, I.; Sedlakova, P.; Mikulikova, K.; Eckhardt, A.; Kasicka, V. **2008**; S89-S96.
- (72) Tanaka, Y.; Higashi, T.; Rakwal, R.; Wakida, S.; Iwahashi, H. *J. Pharm. Biomed. Analysis* **2007**, *44*, 608-613.
- (73) Soga, T.; Ishikawa, T.; Igarashi, S.; Sugawara, K.; Kakazu, Y.; Tomita, M. *J. Chrom. A* **2007**, *1159*, 125-133.
- (74) Sugimoto, M.; Kikuchi, S.; Arita, M.; Soga, T.; Nishioka, T.; Tomita, M. *Anal. Chem.* **2005**, *77*, 78-84.
- (75) Tanaka, Y.; Higashi, T.; Rakwal, R.; Wakida, S.-i.; Iwahashi, H. *J. Pharm. Biomed. Anal.* **2007**, *44*, 608-613.

- (76) Amundsen, L. K.; Kokkonen, J. T.; Siren, H. *J. Sep. Sci.* **2008**, *31*, 803-813.
- (77) Soga, T. *Meth. Mol. Bio.* **2007**, 129-137.
- (78) Soga, T.; Heiger, D. N. *Anal. Chem.* **2000**, *72*, 1236-1241.
- (79) Morohashi, M.; Shimizu, K.; Ohashi, Y.; Abe, J.; Mori, H.; Tomita, M.; Soga, T. *J. Chrom. A* **2007**, *1159*, 142-148.
- (80) Soga, T.; Baran, R.; Suematsu, M.; Ueno, Y.; Ikeda, S.; Sakurakawa, T.; Kakazu, Y.; Ishikawa, T.; Robert, M.; Nishioka, T.; Tomita, M. *J. Bio. Chem.* **2006**, *281*, 16768-16776.
- (81) Trygg, J.; Holmes, E.; Lundstedt, T. *J. Prot. Res.* **2007**, *6*, 469-479.
- (82) Beckwith-Hall, B. M.; Nicholson, J. K.; Nicholls, A. W.; Foxall, P. J.; Lindon, J. C.; Connor, S. C.; Abdi, M.; Connelly, J.; Holmes, E. *Chem. Res. Toxicol.* **1998**, *11*, 260.
- (83) Guillermina Font, M. J. R. M. F. Y. P. *Electrophoresis* **2008**, *29*, 2059-2078.
- (84) Holmes, E.; Nicholson, J. K.; Nicholls, A. W.; Lindon, J. C.; Connor, S. C.; Polley, S.; Connelly, J. *Chemom. Intell. Lab. Syst.* **1998**, *44*, 245.
- (85) Constantinou, M. A. P. E.; Benaki, D.; Spraul, M.; Shulpis, K.; Koupparis, M. A.; Mikros, E. *Anal. Chim. Acta* **2004**, *511*, 303.
- (86) Griffiths., W. J. *Metabolomics, Metabonomics, and Metabolite Profiling* **2008**, 323.

- (87) Lenz, E. M.; Bright, J.; Knight, R.; Wilson, I. D.; Major, H. *J. Pharm. Biomed. Analysis* **2004**, *35*, 599-608.
- (88) Patterson, A. D.; Li, H.; Eichler, G. S.; Krausz, K. W.; Weinstein, J. N.; Fornace, A. J.; Gonzalez, F. J.; Idle, J. R. *Anal. Chem.* **2008**, *80*, 665-674.
- (89) Wold, S.; Trygg, J.; Berglund, A.; Antti, H. *Chemom. Intel. Lab. Syst.* **2001**, *58*, 131.
- (90) Eriksson, L.; Antti, H.; Gottfries, J.; Holmes, E.; Johansson, E.; Lindgren, F.; Long, I.; Lundstedt, T.; Trygg, J.; Wold, S. *Anal. Bioanal. Chem.* **2004**, *380*, 419-429.
- (91) Roessner, U.; Luedemann, A.; Brust, D.; Fiehn, O.; Linke, T.; Willmitzer, L.; Fernie, A. R. *Plant Cell* **2001**, *13*, 11.
- (92) Fernie, A. R.; Schauer, N. *Trends Gen.* **2009**, *25*, 39-48.
- (93) Bovy, A.; Schijlen, E.; Hall, R. D. *Metabolomics* **2007**, *3*, 399-412.
- (94) Giovinazzo G, D'Amico L, Paradiso A, Bollini R, Sparvoli F, DeGara L., *Plant Biotech. J.* **2005**, *3*, 57-69.
- (95) Simpson, M. J.; McKelvie, J. R. *Anal. Bioanal. Chem.* **2009**, *394*, 137-149.
- (96) Warne, M. A.; Lenz, E. M.; Osborn, D.; Weeks, J. M.; Nicholson, J. K. *Biomarkers* **2000**, *5*, 56-72.
- (97) Samuelsson, L. M.; Forlin, L.; Karlsson, G.; Adolfsson-Eric, M.; Larsson, D. G. J. *Aquat. Toxicol.* **2006**, *78*, 341-349.

- (98) Ekman, D. R.; Teng, Q.; Villeneuve, D. L.; Kahl, M. D.; Jensen, K. M.; Durhan, E. J.; Ankley, G. T.; Collette, T. W. *Environ. Sci. Tech.* **2008**, *42*, 4188-4194.
- (99) Kolpin, D. W.; Furlong, E. T.; Meyer, M. T.; Thurman, E. M.; Zaugg, S. D.; Barber, L. B.; Buxton, H. T. *Environ. Sci. Tech.* **2002**, *36*, 1202-1211.
- (100) Heberer, T. *Toxicology Letters* **2002**, *131*, 5-17.
- (101) Lindon, J. C.; Keun, H. C.; Ebbels, T. M.; Pearce, J. M.; Holmes, E.; Nicholson, J. K. *Pharmacogen.* **2005**, *6*, 691.
- (102) Gartland, K. P.; Beddell, C. R.; Lindon, J. C.; Nicholson, J. K. *J. Pharm. Biomed. Anal.* **1990**, *8*, 963.
- (103) Williams, R. E.; Major, H.; Lock, E. A.; Lenz, E. M.; Wilson, I. D. *Toxicology* **2005**, *207*, 179.
- (104) Kell, D. B. *Expert Rev. Mol. Diag.* **2007**, *7*, 329-333.
- (105) Sohal, R. S.; Mockett, R. J.; Orr, W. C. *Free Radic. Biol. Med.* **2002**, *33*, 575-586.
- (106) Pearl, R. *University of London Press* **1928**.
- (107) Harman, D. *J. Geront.* **1956**, *11*, 298-300.
- (108) Dowling, D. K.; Simmons, L. W. *Proc. Royal Soc. B.* **2009**, *276*, 1737-1745.
- (109) Kovacic, P.; Pozos, R. S.; Somanathan, R.; Shangari, N.; O'Brien, P. J. *Curr. Med. Chem.* **2005**, *12*, 2601-2623.
- (110) Sies, H. *Free Radic. Biol. Med.* **1999**, *27*, 916-921.

- (111) Markesbery, W. R.; Lovell, M. A. *Antiox. Redox Signaling* **2006**, *8*, 2039-2045.
- (112) Haeffner, F.; Smith, D. G.; Barnham, K. J.; Bush, A. I. *J. Inorg. Biochem.* **2005**, *99*, 2403-2422.
- (113) Lovell, M. A.; Markesbery, W. R. *Nucleic Acids Res.* **2007**, *35*, 7497-7504.
- (114) Jones, D. P. *Antiox. Redox Signaling* **2006**, *8*, 1865-1879.
- (115) Go, Y.-M.; Gipp, J. J.; Mulcahy, R. T.; Jones, D. P. *J. Biol. Chem.* **2004**, *279*, 5837-5845.
- (116) Halvey, P. J.; Watson, W. H.; Hansen, J. M.; Go, Y.-M.; Samali, A.; Jones, D. P. *Biochem. J.* **2005**, *386*, 215-219.
- (117) Valko, M.; Leibfritz, D.; Moncol, J.; Cronin, M. T. D.; Mazur, M.; Telser, J. *Int. J. Biochem. Cell Bio.* **2007**, *39*, 44-84.
- (118) Cadenas, E.; Sies, H. *Free Radic. Res.* **1998**, *28*, 601-609.
- (119) Liochev, S. I.; Fridovich, I. *Free Radic. Biol. Med.* **1994**, *16*, 29-33.
- (120) Valko, M.; Morris, H.; Cronin, M. T. D. *Curr. Med. Chem.* **2005**, *12*, 1161-1208.
- (121) Liochev, S. I.; Fridovich, I. *Redox Report* **2002**, *7*, 55-57.
- (122) Gohil, K.; Viguie, C.; Stanley, W. C.; Brooks, G. A.; Packer, L. *J. Appl. Physiol.* **1988**, *64*, 115-119.

- (123) Bekman, E. M.; Baranova, O. A.; Gubareva, E. V.; Shulenina, L. V.; Moskvina, S. N.; Danilogorskaya, Y. A.; Azizova, O. A. *Bull. Exp. Bio. Med.* **2006**, *142*, 299-303.
- (124) Dalle-Donne, I.; Scaloni, A.; Giustarini, D.; Cavarra, E.; Tell, G.; Lungarella, G.; Colombo, R.; Rossi, R.; Milzani, A. *Mass Spec. Rev.* **2005**, *24*, 55-99.
- (125) Alvarez, B.; Radi, R. *Amino Acids* **2003**, *25*, 295-311.
- (126) Stadtman, E. R.; Levine, R. L. *Amino Acids* **2003**, *25*, 207-218.
- (127) Molnar, G. A.; Nemes, V.; Biro, Z.; Ludany, A.; Wagner, Z.; Wittmann, I. *Free Radic. Res.* **2005**, *39*, 1359-1366.
- (128) Molnar, G. A.; Wagner, Z.; Marko, L.; Koszegi, T.; Mohas, M.; Kocsis, B.; Matus, Z.; Wagner, L.; Tamasko, M.; Mazak, I.; Laczy, B.; Nagy, J.; Wittmann, I. *Kidney Int.* **2005**, *68*, 2281-2287.
- (129) Gurer-Orhan, H.; Aykin-Burns, N.; Ercal, N. *Free Radic. Biol. Med.* **2002**, *33*, 246.
- (130) Gurer-Orhan, H.; Ercal, N.; Mare, S.; Pennathur, S.; Orhan, H.; Heinecke, J. W. *Biochem. J.* **2006**, *395*, 277-284.
- (131) Davies, M. J. *Biochim. Biophysica. Prot. Proteom.* **2005**, *1703*, 93-109.
- (132) Swaim, M. W.; Pizzo, S. V. *J. Leukocyte Biol.* **1988**, *43*, 365.
- (133) Marnett, L. J.; Riggins, J. N.; West, J. D. *J. Clin. Invest.* **2003**, *111*, 583-593.
- (134) Duncan, M. W. *Amino Acids* **2003**, *25*, 351-361.

- (135) Fu, S.; Wang, H.; Davies, M. J.; Dean, R. T. *J. Biol. Chem.* **2000**, *275*, 10851.
- (136) Kato, Y.; Kitamoto, N.; Kawai, Y.; Osawa, T. *Free Radic. Biol. Med.* **2001**, *31*, 624-632.
- (137) Ballatori, N.; Krance, S. M.; Notenboom, S.; Shi, S.; Tieu, K.; Hammond, C. L. *Bio. Chem.* **2009**, *390*, 191-214.
- (138) Navarro, J.; Obrador, E.; Pellicer, J. A.; Asensi, M.; Vina, J.; Estrela, J. M. *Free Radic. Biol. Med.* **1997**, *22*, 1203-1209.
- (139) Ristoff, E.; Larsson, A. *Orpha. J. Rare. Dis.* **2007**, *2*, 16.
- (140) Franco, R.; Schoneveld, O. J.; Pappa, A.; Panayiotidis, M. I. *Arch. Physiol. Biochem.* **2007**, *113*, 234 - 258.
- (141) Matuszczak, Y.; Farid, M.; Jones, J.; Lansdowne, S.; Smith, M. A.; Taylor, A. A.; Reid, M. B. *Muscle Nerve* **2005**, *32*, 633-638.
- (142) Tirouvanziam, R.; Conrad, C. K.; Bottiglieri, T.; Herzenberg, L. A.; Moss, R. B.; Herzenberg, L. A. *PNAS* **2006**, *103*, 4628-4633.
- (143) Harding, J. J. *Biochem. J.* **1970**, *117*, 957-960.
- (144) Pau, H.; Graf, P.; Sies, H. *Graefes Arch. Clin. Experiment. Ophthalmol.* **1982**, *219*, 140-142.
- (145) Moreno, M. C.; Campanelli, J.; Sande, P.; Saenz, D. A.; Sarmiento, M.; Rosenstein, R. E. *Free Radic. Biol. Med.* **2004**, *37*, 803-812.
- (146) Samiec, P. S.; Drews, C. D.; Sternberg, P.; Chow, D. Y. K.; Reed, R. L.; Jones, D. P. *Invest. Ophthalmol. Vis. Sci.* **1993**, *34*, 1167-1167.

- (147) Young, R. W. *Surv. Opthal.* **1988**, *32*, 252-269.
- (148) Young, R. W. *Surv. Opthal.* **1987**, *31*, 291-306.
- (149) Ristoff, E.; Larsson, A. *Orpha. J. Rare. Dis.* **2007**, *2*.
- (150) Njalsson, R.; Norgren, S. *Act. Paedia.* **2005**, *94*, 132-137.
- (151) Balendiran, G. K.; Dabur, R.; Fraser, D. *Cell Biochem. Func.* **2004**, *22*,  
343-352.
- (152) Calvert, P.; Yao, K. S.; Hamilton, T. C.; O'Dwyer, P. J. *Chem. Bio. Inter.*  
**1998**, *112*, 213-224.
- (153) Estrela, J. M.; Ortega, A.; Obrador, E. *Crti. Rev. Clin. Lab. Sci.* **2006**, *43*,  
143-181.
- (154) Griffin, J. L.; Shockcor, J. P. *Nat. Rev. Cancer* **2004**, *4*, 551.

*Chapter II*

Integrative Metabolomics for Characterizing Unknown Low-Abundance  
Metabolites by Capillary Electrophoresis-Mass Spectrometry with Computer  
Simulations

## **II. Integrative Metabolomics for Characterizing Unknown Low-Abundance Metabolites by Capillary Electrophoresis-Mass Spectrometry with Computer Simulations**

### **2.1. Abstract**

Characterization of unknown low-abundance metabolites in biological samples is one the most significant challenges in metabolomic research. In this report, an integrative strategy based on capillary electrophoresis-electrospray ionization mass spectrometry (CE-ESI-MS) with computer simulations is examined as a multiplexed approach for studying the selective nutrient uptake behavior of *E. coli* within a complex broth medium. On-line sample preconcentration with desalting by CE-ESI-MS was performed directly without off-line sample pretreatment in order to improve detector sensitivity over 50-fold for cationic metabolites with nanomolar detection limits. The migration behavior of charged metabolites were also modeled in CE as a qualitative tool to support MS characterization based on two fundamental analyte physicochemical properties, namely, absolute mobility ( $\mu_0$ ) and acid dissociation constant ( $pK_a$ ). Computer simulations using Simul 5.0 were used to better understand the dynamics of analyte electromigration, as well as aiding de novo identification of unknown nutrients. There was excellent agreement between computer-simulated and experimental electropherograms for several classes of cationic metabolites as reflected by their relative migration times with an average error of <2.0%. Our studies revealed differential uptake of specific amino acids and nucleoside nutrients associated with distinct stages of bacterial growth. Herein, we demonstrate that CE can serve as an effective

preconcentrator, desalter, and separator prior to ESI-MS, while providing additional qualitative information for unambiguous identification among isobaric and isomeric metabolites. The proposed strategy is particularly relevant for characterizing unknown yet biologically relevant metabolites that are not readily synthesized or commercially available.

## **2.2. Introduction**

Metabolomics<sup>1</sup> represents an emerging aspect of chemical biology that is defined as the comprehensive and unbiased analyses of low molecular weight metabolites in a biological fluid or organism. Since metabolite levels are often closely associated with phenotype, there is growing interest in adopting metabolomics in functional genomic research applications ranging from personalized medicine, drug screening,<sup>2, 3</sup> plant biotechnology,<sup>4</sup> microbial engineering,<sup>5</sup> to protein discovery.<sup>6</sup> However, due to the extremely large chemical diversity and dynamic range of metabolites, there is still no single technique amenable to global metabolite analyses. To date, several different techniques have been reported for metabolomics primarily based on hyphenated chromatographic techniques coupled to MS or NMR detection.<sup>7</sup> Two of the most widely used formats for metabolomic studies have included GC/MS and NMR. Since a large fraction of minor (i.e., low-abundance) metabolites in organisms are unknown, new strategies for de novo elucidation of chemical structure are required. Although multidimensional NMR methods offer a powerful format for structural elucidation

of unknown metabolites, it is limited by poor concentration sensitivity. GC/MS offers improved sensitivity for low-abundance metabolite detection, but requires chemical derivatization for polar metabolites that are thermally stable and nonlabile. Multiple or incomplete labeling hinders reliable mass spectral interpretation, as well as universal database matches since they are dependent on the specific type of reagent. GC with time-of-flight (TOF)-MS offers high mass resolution and accuracy (<5 ppm) for metabolite characterization; however, it is still often insufficient for distinguishing among likely candidates selected within a database based on elemental composition after isotope abundance filtering.<sup>8</sup> This situation is particularly relevant for isomeric and isobaric metabolites that are not readily differentiated by MS alone. Although LC-ESI-MS<sup>9, 10</sup> can be directly applied to polar metabolites without chemical labeling, selection of a stationary phase with sufficient selectivity for both cationic and anionic metabolites is challenging, notably for resolving sugar phosphate isomers.<sup>11, 12</sup> Recently, Nicholson *et al.*<sup>12</sup> have introduced a statistical heterospectroscopic approach for metabolite analyses based on cross-correlation of NMR and LC-TOF-MS data sets. Although this multiplexed strategy provides richer spectral information for characterizing biomarkers in complex biofluids, it is still constrained to relatively abundant metabolites. Thus, effective analytical strategies that can be directly applied to characterize nanomolar levels of metabolites without chemical derivatization are required in metabolomics research. Evidence of the biological significance of newly discovered metabolites that exist outside of conserved

metabolic pathways can then pave the way for their subsequent synthesis and characterization.

Since its first introduction in 1987 by Smith *et al.*,<sup>13</sup> capillary electrophoresis-mass spectrometry (CE-MS) is emerging as a versatile hyphenated separation technique for the analysis of small amounts of complex sample mixtures, ranging from protein to pharmaceuticals.<sup>14-17</sup> Most commercial CE-MS instruments utilize an orthogonal electrospray ionization (ESI) configuration with a coaxial liquid-sheath interface in order to provide a suitable electric contact for generation of desolvated gas-phase ions.<sup>18</sup> Since a major fraction of metabolites are polar and ionic, CE represents a promising high-efficiency separation technique for their analysis. To date, there have been only a few reports that have applied CE-MS in the context of global metabolomic analyses.<sup>6, 19-22</sup> Soga *et al.* have developed three different CE-MS formats for detection of up to 1692 charged metabolites in bacterial cell extracts; however, less than 10% of these metabolites could be identified.<sup>22</sup> Due to poor ionization efficiency for some classes of metabolites along with postcapillary dilution effects when using a sheath liquid ESI interface, detection limits in CE-MS can vary over 3 orders of magnitude from low-micromolar to millimolar range. Improved concentration sensitivity can be achieved using sheathless ESI interfaces with CE-MS,<sup>19</sup> however, their long-term robustness for routine analyses has yet to be fully demonstrated. Otherwise, a narrow mass scanning range (30  $m/z$ ) can be used to improve CE-MS detection performance for metabolite analyses; however, this can

require up to 33 repeated runs to cover the entire mass range per sample.<sup>22</sup> In addition, tentative unknown confirmation based on nominal mass, measured isotopic ratio, and expected charge state by CE-MS is often insufficient to distinguish among isomers and metabolites with similar carbon numbers.<sup>22</sup> Thus, new approaches to improve concentration sensitivity, as well as unknown metabolite characterization that does not impact total analysis times, are needed for high-throughput metabolomics via new multiplexed CE-MS interfaces.<sup>23</sup>

There are two distinct features of CE-MS that can enhance its potential as a viable platform for metabolomic studies that have yet to be fully explored. First, there is growing interest in adopting "in-capillary" strategies for sample preconcentration in CE-MS in order to improve concentration sensitivity based on discontinuous electrolyte systems.<sup>16</sup> In addition to the benefit of an automated sample enrichment procedure with minimal sample handling, on-line sample preconcentration methods that are applicable to high-salt samples are needed to reduce ion suppression while maintaining high separation efficiency. Three major formats have been reported that require no necessary modification to instrumental configuration, including transient cation isotachopheresis<sup>24-27</sup> (t-CITP), isoelectric focusing<sup>28, 29</sup> (IEF), and field-enhanced sample injection (FESI).<sup>30, 31</sup> Although these methods have been primarily used to boost detection limits for protein or peptide analyses, they can also be applicable to low molecular weight metabolites. When combined with the full scan sensitivity of high-capacity mass analyzers,

CE-ESI-MS with on-line sample preconcentration offers a sensitive format for characterizing nanomolar levels of metabolites in complex samples.

A second distinct feature of CE-MS is the ability to model analyte migration processes in free solution<sup>32</sup> via intrinsic metabolite physicochemical properties, such as absolute mobility ( $\mu_0$ ) and acid dissociation constant ( $pK_a$ ). Recently, Gas *et al.*<sup>33</sup> released a freeware software version of Simul 5.0 for dynamic simulation of analyte electromigration behavior that is applicable to multivalent ions based on the principles of mass conservation, acid-base equilibria, and electroneutrality. This provides a convenient way to better understand electromigration processes within discontinuous electrolyte systems,<sup>34, 35</sup> as well as computer-aided optimization of separation conditions.<sup>36</sup> Computer simulations for electrophoresis also represent a promising tool in metabolomic studies by offering additional qualitative information for metabolite identification, in cases where MS structural elucidation methods are insufficient.

In this report, CE-ESI-MS with computer simulations is proposed as an integrative strategy for low-abundance metabolite analyses and their identification in biological samples. The optimized method was applied to study the extracellular nutrient uptake patterns in complex broth media during *Escherichia coli* growth. Comprehensive analysis of submicromolar levels of cationic metabolites under acidic conditions was feasible without sample pretreatment. CE-MS experiments in conjunction with computer simulations were used to assess the impact of buffer pH, ionic strength, and sample injection length on

analyte focusing based on a dual t-CITP with dynamic pH junction process. Identification of specific unknown metabolites in broth samples exhibiting bacterial uptake (i.e., influx) was performed via a two-stage process. First, CE-ESI-MS was used to identify likely candidates within the Kyoto Encyclopedia for Genes and Genomes (KEGG) database after preliminary multistage MS<sup>n</sup>, isotope ratio, and dynamic hydrogen-deuterium exchange (dHDX) experiments. Then, computer 3D molecular modeling of candidate structures was performed to calculate their molecular volume ( $V$ ) and intrinsic valence charge ( $z_0$ ), which was then used to estimate  $\mu_0$  based on a Hubbard-Onsager model.<sup>37, 38</sup> Thermodynamic  $pK_a$  parameters for metabolites were either based on literature values, measured experimentally by CE, or estimated by computer software. Input of  $\mu_0$  and  $pK_a$  values in Simul 5.0 allowed for a quantitative comparison between predicted and experimental relative migration times (RMTs) of several different metabolite candidates to confirm their identity with an average relative error under 2%. Moreover, these studies also permitted a qualitative comparison between experimental and simulated electropherograms. Noteworthy, this strategy enabled differentiation of both isomeric and isobaric amino acid and nucleoside metabolites identified as key nutrients during *E. coli* growth. Recently, Soga *et al.*<sup>20</sup> reported an empirical method for prediction of the RMTs of cations by CE-MS via artificial neural network ensembles, which was used for identification of metabolite standards defined within an original training set. In contrast, this report is focused on de novo characterization and quantification of extracellular

metabolites by CE-ESI-MS identified as specific nutrients undergoing bacterial uptake within a complex broth medium. Qualitative identification of unknown metabolites was aided via computer modeling of simulated electropherograms based on two characteristic physicochemical parameters of a metabolite.

### **2.3. Experimental Section**

**2.3.1. Chemicals and Reagents.** Deionized water used for buffer and sample preparations was obtained using a Barnstead EASYpureII LF ultrapure water system (Dubuque, IA). A 1 M formic acid buffer (pH 1.8) was prepared by dilution of concentrated formic acid derived from Sigma-Aldrich (St. Louis, MO). All amino acids and other metabolite standards were purchased from Sigma-Aldrich. Individual amino acid and nucleoside stock solutions of 10 mM were prepared in 1:1 methanol/water.

**2.3.2. Apparatus and Conditions.** CE-ESI-MS studies were performed on an automated Agilent CE system equipped with an XCT 3D ion trap mass spectrometer, an Agilent 1100 series isocratic pump, and a G16107 CE-ESI-MS sprayer kit (Agilent Technologies, Waldbronn, Germany). All separations were performed on uncoated fused-silica capillaries with 50- $\mu$ m i.d. and 80-cm total length. A 1 M formic acid, pH 1.8, solution was used as the background electrolyte (BGE) for CE separations. Prior to use, new capillaries were first rinsed for 30 min with methanol, deionized water, and 1 M formic acid and then

conditioned overnight prior to use. Samples were introduced into the capillary using a low-pressure (50 mbar) injection. On-line sample preconcentration using a discontinuous electrolyte system was performed by first injecting a sample prepared in 200 mM ammonium acetate, pH 7.0, for 75 or 150 s at 50 mbar unless otherwise noted, followed by replacement of the sample with the BGE at the inlet prior to voltage application. The average velocity of the low-pressure rinse was calculated to be 5.1 cm/min, which was used to estimate the sample injection plug length. Separations were performed at 20 °C with an applied voltage of 23 kV. An Agilent 1100 series pump with a 1:100 splitter was used to supply a volume of 10  $\mu$ L/min of 5 mM ammonium acetate in 1:1 methanol/H<sub>2</sub>O as the sheath liquid. All MS analysis was performed using 4 kV as the cone voltage in positive ion mode at 300 °C. Nitrogen gas was used as the nebulizing gas and drying gas at 15 psi and 10 L/min, respectively, whereas helium was employed as the damping gas for ITMS. All MS data were recorded with a range of 50-350 *m/z* using the ultrascan mode of 26 000 *m/z* per second. Multi-stage MS experiments by ITMS were also performed to aide in structural elucidation of unknown metabolites; however, the extent of sequential fragmentation was often limited by the original abundance of the molecular ion and the complexity of its inherent structure. dHDX experiments were performed by replacing the deionized water fraction with deuterated water (D<sub>2</sub>O) in the sheath liquid,<sup>39</sup> which allowed estimation of the number of active hydrogens associated with acidic or basic functional groups (e.g., NH<sub>2</sub>, SH, OH, COOH) within a metabolite after comparison with its

protonated molecular ion ( $MH^+$ ). Despite the short time frame for exchange ( $<ms$ ) in the ion source that often does not permit complete exchange, this provided a convenient way to distinguish among likely candidates for unknown characterization without substantial change in instrumental conditions. In fact, only mass changes are apparent in dHDX experiments using CE-ESI-MS, whereas the RMTs of analytes are the same due to identical separation conditions in the BGE. All regression analyses and figure schematics were performed using Igor Pro 5.0 (Wavemetrics Inc, Lake Oswego, OR).

**2.3.3. *E. coli* Bacterial Incubation.** The incubation procedure for batch cultures of the BL-21 (DE3) *E. coli* strain used in this study has been described previously.<sup>40</sup> Briefly, after the selection of a single *E. coli* colony from a Luria-Bertani (LB) Miller medium agar-treated plate (BioShop Canada Inc., Burlington, ON, Canada), a 500-mL flask containing 100 mM liquid LB Miller (Bioshop Canada Inc.) broth was inoculated. Bacteria was grown in this medium on rotary shakers for 24 h at 37 °C and then used to inoculate a separate flask containing LB broth with 5% seeding volume. The optical density of this sample was then measured with a DU general purpose UV/visible spectrometer (Beckman-Coulter Inc.) at 600 nm, after which it was centrifuged at 6000 rpm for 10 min to allow for the supernatant (extracellular medium) to be removed and frozen at -78 °C for future use. This procedure was repeated in 30-min intervals over 8 h to generate a bacterial growth curve. The dried cell weight (mg) of bacteria was also

measured in order to assess the total increase in biomass during growth, which increased ~13-fold over an 8-h period. All bacteria were handled safely in a microbiological facility until discarded in 10% sodium hypochlorite (bleach) solution. Due to the wide concentration range of nutrients present in broth solutions, samples were diluted 20-fold in ammonium acetate, pH 7.0, prior to CE-MS analysis in order to ensure that metabolite concentrations were within the linear range for quantification, which was typically 0.1-100  $\mu\text{M}$  depending on the specific metabolite.

**2.3.4. Computer Simulation Using Simul 5.0.** Computer modeling of analyte electromigration behavior for prediction of simulated electropherograms of cationic metabolites were performed using Simul 5.0 software.<sup>33,34</sup> Values for  $\mu_0$  and  $\text{p}K_a$  provided in the software were used for most standard amino acids with the exception of Asp, which was found to be anomalous with our experimental data. In order to enhance computational speed during simulations, the effective capillary length and applied voltage were reduced to 80 mm and 230 V, respectively, as recommended by Gas *et al.*<sup>33</sup> Since these conditions tend to generate greater longitudinal diffusion, all simulated electropherograms were normalized by a factor of 2 in order to reduce the extent of band broadening, which was more reflective of experimental conditions. Also, the number of grid points (NX) was set to 5000 and the electroosmotic flow was activated based on an average mobility measured in our experiments to be  $+ 29.2 \times 10^{-9} \text{ m}^2/\text{V}\cdot\text{s}$ . Due

to the added length of computational time, simulations were not performed with ionic strength corrections to  $\mu_o$  and  $pK_a$ . On-line sample preconcentration conditions for metabolites in simulations were performed by using a sample injection positioned at 4 mm with a plug length of either 6 or 12 mm composed of 200 mM ammonium, 200 mM acetate, pH 7.0, whereas the BGE was 1 M formic acid, pH 1.8. Samples contained different concentrations of metabolites adjusted according to their detector response in CE-MS. In addition, all samples contained 15 mM NaCl to mimic the high salt content of diluted broth samples in order to illustrate the principle of sample desalting by CE-MS. Simulations were monitored either in the distance or the time domain. In addition, the detector position were varied in order to compare simulated electromigration processes relative to time-resolved electrophoretic experiments. Changes in pH, conductivity, and concentration profile of buffer/salt co-ions were also monitored as a function of time. Computer simulations required up to 5 days to complete when using discontinuous electrolyte conditions including 20 metabolites with a 1.83-GHz Intel Centrino Duo processor T2400 with 1GB DD2 SDRAM laptop.

## 2.4. Theory

**2.4.1. Metabolite  $\mu_o$  Determination.** Determination of  $\mu_o$  for Asp, methionine sulfone (MetS, internal standard), and other unknown metabolite candidates identified in the broth media after CE-MS and KEGG database analyses was

performed first by estimating its  $V$  (i.e., Connolly solvent-excluded volume) by computer molecular modeling using Chem3D Ultra software, version 8.0 (CambridgeSoft, Cambridge, MA). All chemical structures were energy-minimized using an iterative molecular mechanics 2 (MM2) algorithm with molecular dynamics in order to determine a stable molecular configuration prior to computing relevant parameters. A group of 18 standard amino acids (excluding His and Asp) were selected as model cationic analytes for prediction of  $\mu_0$  based on their  $z_0$  and  $V$  as input parameters using a Hubbard-Onsager model, that includes the impact of hydrodynamic and dielectric friction for describing ion motion:

$$\mu_0 = \frac{az_0}{Vc + \left(\frac{bz_0^2}{V}\right)} \quad (1)$$

Nonlinear regression of eq 1 by allowing all three parameters to float independently resulted in coefficient terms of  $a = 0.00132 \pm 0.00027$ ,  $b = -18.8 \pm 8.4$ , and  $c = 0.335 \pm 0.044$ , with a  $\chi^2$  of  $1.45 \times 10^{-9}$ . Note that the first term in the denominator is equivalent to the Hueckel model<sup>37</sup> for hydrodynamic friction of a rigid sphere with a theoretical value of about  $V^{1/3}$ , whereas the second term is associated with dielectric friction that is related to the charge density of a hydrated positive ion. There was good correlation between predicted and experimental  $\mu_0$  for the model amino acids as reflected by a slope ( $0.998 \pm 0.052$ ),  $y$ -intercept ( $3.8 \pm 1.8$ )  $\times 10^{-7}$ , and  $R^2$  (0.995). It was determined that parameters for molecular shape (ovality) for correcting nonspherical structures did not improve the accuracy of the model, as confirmed by a previous report.<sup>38</sup> Thus, eq

1 was then used to determine  $\mu_0$  for unknown metabolite candidates in this study based on characteristic  $z_0$  and  $V$  properties derived from their proposed chemical structure.

**2.4.2. Metabolite  $pK_a$  Determination.** Thermodynamic  $pK_a$  parameters for standard amino acids with the exception of Asp were provided in the database included in Simul 5.0 software. Otherwise,  $pK_a$  values for other metabolites were obtained from the literature,<sup>41, 42</sup> whereas other unknown metabolites not found in the literature (e.g., isoguanosine) were estimated by ACD/Lab  $pK_a$  DB (Advanced Chemical Development Inc., Toronto, Canada). These values were also compared with apparent  $pK_a$  corrected for ionic strength<sup>37</sup> determined by CE-MS experiments based on measured changes in analyte mobility ( $\mu_{ep}$ ) as a function of buffer pH for three major classes of cationic metabolites:

$$\mu_{ep} = \frac{[H^+]}{K_a + [H^+]} \mu_{ep,HA^-} \quad (2)$$

$$\mu_{ep} = \frac{[H^+]}{K_a + [H^+]} \mu_{ep,HA^{2+}} + \frac{K_a}{K_a + [H^+]} \mu_{ep,HA^+} \quad (3)$$

$$\mu_{ep} = \frac{[H^+]^2}{K_{a1}K_{a2} + [H^+]^2} \mu_{ep,H_2A^+} + \frac{K_{a1}K_{a2}}{K_{a1}K_{a2} + [H^+]^2} \mu_{ep,A^-} \quad (4)$$

where eq 2 is for neutral amino acids or monovalent amines (e.g., nucleosides), eq 3 is for cationic amino acids, and eq 4 is for acidic amino acids. Nonlinear

**Table 2.1.** Fundamental Physicochemical Parameters for Modeling Ion Mobility Using Computer Simulations Based on the Hubbard–Onsager Model.

<i>Metabolite (amino acid)</i>	<i>MW</i>	<i>V (Å<sup>3</sup>)</i>	<i>z<sub>o</sub></i>	<i>μ<sub>o</sub> × 10<sup>-4</sup> (cm<sup>2</sup>/V·s)<sup>a</sup></i>	<i>pK<sub>a</sub><sup>a</sup></i>
Gly	75.1	52.0	1	3.95	2.3
Ala	89.1	70.4	1	3.40	2.33
Ser	105.1	75.0	1	3.20	2.17
Pro	115.1	97.0	1	3.11	1.96
Val	117.2	107.2	1	2.96	2.26
Thr	119.1	93.0	1	2.96	2.15
Cys	121.2	87.7	1	2.92	1.94
Leu	131.2	124.0	1	2.76	2.31
<i>Iso-Leu</i>	131.2	124.2	1	2.83	2.30
Asn	132.1	94.8	1	3.06	2.12
Gln	146.2	113.7	1	2.81	2.15
Lys	146.2	130.6	2	5.93	1.70
Glu	147.1	111.5	1	2.76	2.16
Met	149.2	124.2	1	2.77	2.77
Phe	165.2	140.3	1	2.61	2.18
Arg	174.2	149.2	2	5.33	1.78
Tyr	181.2	143.4	2	2.47	2.22
Trp	204.2	164.7	1	2.49	2.32

<sup>a</sup>μ<sub>o</sub> and pK<sub>a</sub> values from Gas et al.<sup>3</sup> used in deriving three parameters in eq 1 based on the Hubbard–Onsager model.

regression was used to determine pK<sub>a</sub> and the acid (e.g., HA<sup>+</sup>) and/or conjugate base (e.g., A<sup>+</sup>) mobility terms. Note that acidic amino acids have two dissociation acid constants (pK<sub>a1</sub>, pK<sub>a2</sub>) that influence their mobility under acidic conditions. Reliable values for μ<sub>o</sub> and pK<sub>a</sub> are needed for accurate simulation of metabolite migration behavior and prediction of RMTs. A bias in pK<sub>a</sub> of ±0.1 used in computer simulations was estimated to generate an error in RMTs of ~2%. Table 2.1 summarizes all relevant parameters associated with model amino acids

required for computer simulations in this study, which were used to derive the coefficients used in eq 1.

## 2.5. Results and Discussion

**2.5.1. Optimization of On-Line Sample Preconcentration by CE-MS.** On-line sample preconcentration techniques in CE-MS are most readily achieved by in-capillary stacking based on analyte mobility differences within a discontinuous electrolyte system. Thus, direct injection of long sample plug lengths (>10% capillary length) can be performed since electrokinetic focusing of dilute analytes into narrow zones occurs prior to ionization. In general, t-CITP has been the most widely reported format for enrichment of biological samples in CE-ESI-MS, since IEF employs involatile ampholyte electrolytes that can suppress analyte ionization,<sup>43</sup> whereas FESI requires the use of low-conductivity samples that suffer from inherent injection bias and variability.<sup>16</sup> In CE-ESI-MS, t-CITP is most conveniently operated in the sample self-stacking<sup>44</sup> mode for protein analysis, typically using a volatile ammonium ion as the leading electrolyte in the sample and either acetic or formic acid as the terminating electrolyte that also serves as the BGE.<sup>25, 27, 45</sup> In most cases, the pH between the sample and BGE is the same with neutral coated capillaries recommended to prevent protein adsorption and suppress electroosmosis, which has been reported to disrupt ITP zone profiles.<sup>26</sup> However, mixed modes of electrokinetic focusing based on two or more distinct processes have been demonstrated for enhanced performance in CE,

such as dynamic pH junction-sweeping.<sup>46, 47</sup> In this study, t-CITP with dynamic pH junction is examined as a dual on-line sample preconcentration technique for enhancing the detection of zwitterionic amino acids and other cationic species by CE-ESI-MS using unmodified fused-silica capillaries.

Selective analysis of basic metabolites was performed in this study since they are cationic under 1 M formic acid (pH 1.8), which was used as the acidic BGE. Despite the extremely high concentration of formic acid, there was no significant Joule heating due to the relatively low  $\bar{z}$  concentration (~10 mM) of its conjugate base at this pH. Optimization of on-line sample preconcentration was performed via hydrodynamic injection of long sample plugs using ammonium acetate, pH 7.0, as the sample electrolyte. Since most amino acids are weakly ionic metabolites with mobilities lower than ammonium co-ion, t-CITP with dynamic pH junction can be used in tandem to induce efficient sample stacking. In this study, three factors were optimized for maximizing the extent of amino acid in-capillary preconcentration by CE-MS,  $\bar{z}$  namely, sample injection plug length, ionic strength, and pH.

Figure 2.1a depicts the influence of sample injection plug length on the magnitude of amino acid signal enhancement in CE-MS when using a discontinuous electrolyte system consisting of 1 M formic acid, pH 1.8, and 200 mM ammonium acetate, pH 7.0, as BGE and sample electrolyte, respectively. Formic acid was selected as the volatile acidic BGE compatible with CE-MS due to previous reports of applying it in high-efficiency separations of amino acid<sup>48</sup>

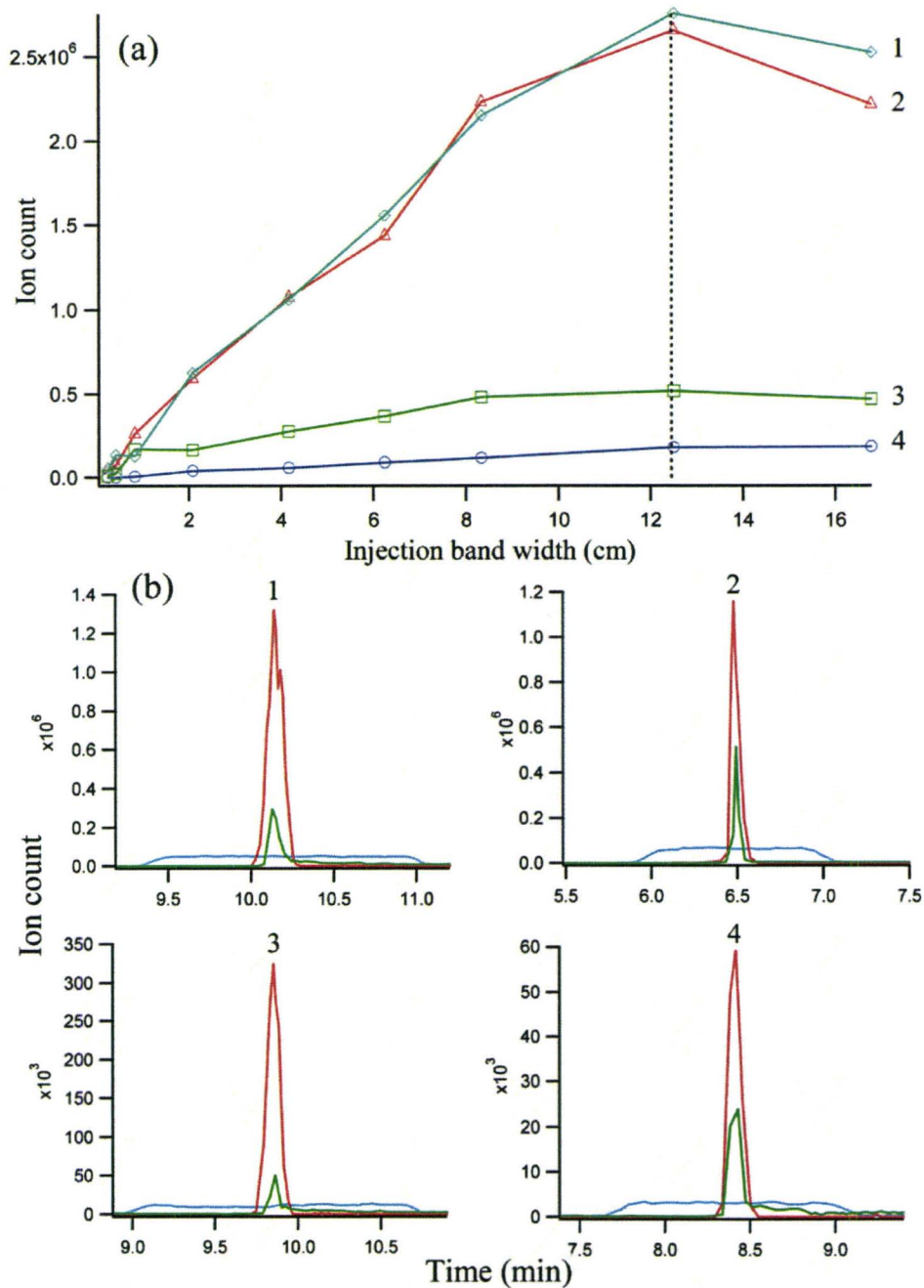


**Figure 2.1.** On-line sample preconcentration via t-CITP with dynamic pH junction by CE-MS. (a) Plot depicting the impact of increasing sample injection bandwidth on amino acid ion count signal. (b) Overlay of three EIEs highlighting the influence of sample pH and co-ion on the extent of analyte band narrowing. Conditions: 1 M formic acid, pH 1.8, was used as the BGE, whereas the sample composition was 200 mM ammonium acetate, pH 7.0, in (a) and (b) red trace, 200 mM ammonium acetate, pH 1.8, in (b) green trace, and 1 M formic acid, pH 1.8, in (b) blue trace. Analyte peak numbering corresponds to 20  $\mu$ M concentration of the four different amino acids: (1) Trp, (2) Lys, (3) Glu, and (4) Ala.

and protein<sup>43</sup> mixtures. Under these conditions, the electroosmotic flow was suppressed ( $+2.93 \times 10^{-5} \text{ cm}^2/\text{V}\cdot\text{s}$ ) to ensure improved resolution of cationic (i.e., basic or zwitterionic) metabolites with similar mobilities. A neutral sample electrolyte consisting of 200 mM ammonium acetate was selected in order to reduce amino acid positive mobilities at pH 7.0 (e.g., neutral amino acids have zero mobility) with excess ammonium serving as the leading co-ion. 2.1a highlights a near-linear increase in detector response of four different amino acids (20  $\mu\text{M}$  Ala, Trp, Glu, and Lys) as the sample injection plug length is increased from 0.25 to 16.8 cm, which corresponds to  $\approx 3.1\text{-}21\%$  of the total capillary length, respectively. There are a number of observations to note in this study. First, there was an apparent upper limit to the extent of sample preconcentration above 12.5 cm, since a lower detector response was measured at longer injection plug lengths. Second, the detector bandwidth ( $w_{\text{det}} \approx 1.2 \text{ cm}$ ) of amino acids was measured to be similar throughout the injection series despite using up to a 70-fold longer sample injection. This demonstrates that there was no loss of separation efficiency in CE-MS when using longer sample injections to enhance detector sensitivity. The loss in detector response at 16.8 cm was attributed to insufficient time to complete sample stacking under these conditions as reflected by partial peak fronting, which will be addressed later in the paper. Third, it was apparent that there was over a 14-fold difference in detector response among amino acids (e.g., Trp vs Ala) since ionization efficiency in ESI is highly dependent on the intrinsic chemical properties of an analyte.<sup>49</sup> Thus, on-line

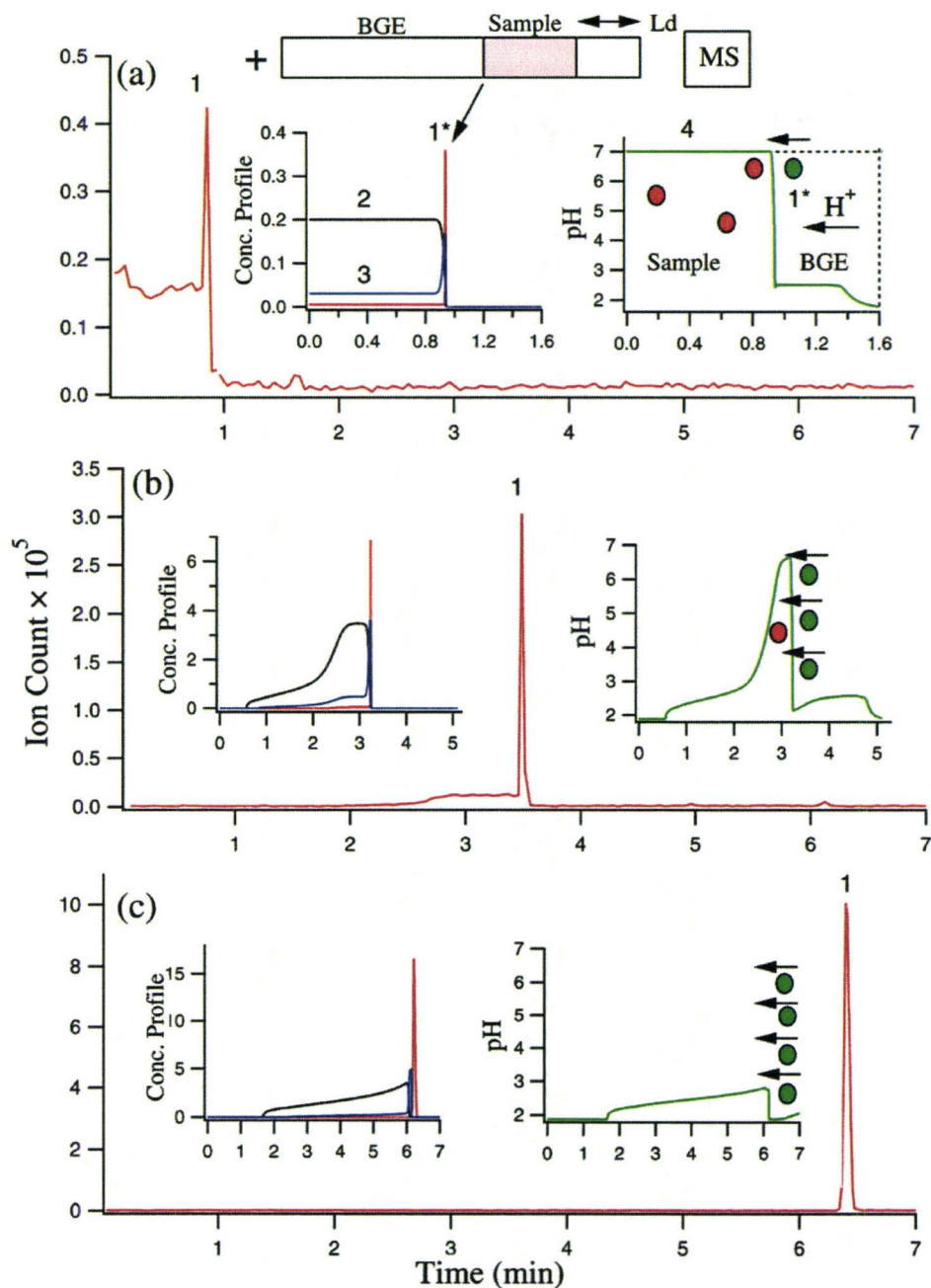
sample preconcentration in CE-ESI-MS is particularly relevant for enhancing the concentration sensitivity of less responsive metabolites with poor ionization efficiency. Overall, up to a 50-fold enhancement in concentration sensitivity can be achieved under optimum conditions relative to conventional injections, which is ultimately limited by the separation resolution required for analysis. For instance, the limit of detection ( $S/N \approx 3$ ) under these conditions was  $\sim 1$  and 25 nM for calibration solutions of Lys and Glu, respectively.

Figure 2.1b shows a series of extracted ion electropherogram (EIE) overlays, which highlights the impact of sample co-ion and pH on the stacking efficiency of amino acids by CE-MS when using a 12.5-cm injection plug. As noted by the broad blue traces, the use of a continuous electrolyte system (i.e., BGE/sample, 1 M formic acid) with the long sample injection results in detrimental sample overloading with a  $w_{det}$  up to 18 cm. In contrast, the red traces show the influence of both co-ion and pH when using 200 mM ammonium acetate, pH 7.0, as the sample electrolyte. It was apparent that a  $\sim 10$ -fold focusing of the original sample plug is realized using t-CITP with dynamic pH junction by CE-MS. However, when the ammonium acetate sample pH was reduced to 1.8 (pH adjusted with HCl) as shown in the green traces, incomplete focusing of amino acids by t-CITP was observed as reflected by peak tailing. This results in up to an 8-fold loss in sensitivity enhancement notably for Glu relative to t-CITP with dynamic pH junction. Thus, sample pH plays an important role in improving the efficacy of sample stacking when using long sample injection plugs ( $>10\%$

capillary length) in t-CITP that has yet to be examined. The optimum sample ionic strength was determined to be 200 mM ammonium acetate (data not shown) under these conditions since low ionic strength solutions generated broad peak shapes with poor separation efficiency, whereas ionic strength above 200 mM resulted in highly focused yet unresolved peaks. In general, optimization of on-line sample preconcentration in CE-MS strives to maximize sensitivity enhancement while achieving sufficient separation resolution. The latter property is dependent on the complexity of the sample matrix and the mass resolution of the MS. Hence, CE can be designed to serve multiple functions prior to ESI-MS, namely, as a preconcentrator, desalter, and separator, which will be demonstrated in the next study.

### **2.5.2. Mechanism of t-CITP with Dynamic pH Junction.**

In order to gain a deeper understanding of analyte electromigration dynamics when using in-capillary preconcentration, a series of time-resolved electrophoretic experiments were performed by CE-MS via placement of a long sample plug (12.5 cm, 20  $\mu$ M Trp, 15 mM NaCl, 200 mM ammonium acetate, pH 7.0) at various positions from the distal end of the capillary using a low-pressure rinse. Figure 2.2 depicts three major transitions experimentally observed in the process: (a) initial Trp focusing at the back end of the sample-BGE boundary, (b) partial focusing of Trp with residual peak fronting, and (c) complete focusing of Trp



**Figure 2.2.** Time-resolved electropherograms showing the dynamics of in-capillary Trp focusing by t-CITP with dynamic pH junction from experimental data and computer simulations using Simul 5.0 (insets). A long sample plug of 12.5 cm was placed at increasing distance from the distal end of the capillary ( $L_d$ ) from about (a) 7.5, (b) 25, and (c) 40 cm. Conditions: BGE, 1 M formic acid, pH 1.8; sample, 200 mM ammonium acetate, pH 7.0, 15 mM NaCl. Analyte peak numbering corresponds to the concentration profiles of (1) Trp (experimental), (1\*) Trp (simulated), (2)  $\text{NH}_4^+$ , (3)  $\text{Na}^+$ , and (4) pH. Note that concentration profiles of  $\text{NH}_4^+$  and  $\text{Na}^+$  cations were reduced relative to Trp for clarity purposes.

within the original sample plug. It is apparent that, under these conditions, electrokinetic focusing of Trp required greater than 5 min to complete prior to the transition to zonal separation and normal broadening by diffusion. Computer simulations of the dynamics of electrokinetic focusing were also performed by Simul 5.0 under the same experimental conditions by changing the detector position relative to the back end of the sample injection plug. The major advantage of performing simulations is that changes in analyte(s), as well as BGE and pH profiles, can be monitored simultaneously during electromigration. The concentration profiles of Trp (1\*),  $\text{NH}_4^+$  (2),  $\text{Na}^+$  (3), and pH (4) derived from computer simulations are illustrated as separate insets in Figure 2.2. Note that the concentration profile scales of  $\text{NH}_4^+$  and  $\text{Na}^+$  were reduced by a factor of 100- and 20-fold, respectively, relative to Trp in order to improve clarity. In general, there was good agreement between simulated (1\*) and experimental (1) Trp concentration profiles in the study. In addition, the simulations served to clearly highlight the impact of the leading co-ion ( $\text{NH}_4^+$ ) in the sample and the pH discontinuity between sample and BGE. In the early stages of Trp focusing as shown in Figure 2.2a, it was evident that excess  $\text{NH}_4^+$  started to migrate ahead of the Trp zone while electromigration of  $\text{H}^+$  (i.e.,  $[\text{H}^+] \approx 16 \text{ mM}$ ) from the BGE titrated the back end of the neutral sample plug. This process enhances analyte focusing since Trp has a local high positive mobility (green circles) in the acidic BGE, whereas its mobility is reduced to zero (red circles) within the neutral sample zone at the pH boundary. In fact,  $\text{H}^+$  also serves as the terminating co-ion

in t-CITP since its apparent mobility is significantly reduced under these conditions due to proton transfer to high concentrations of acetate within the sample zone. Also, note that excess  $\text{Na}^+$  ions begin to stack between  $\text{NH}_4^+$  and Trp due to its intermediate ion mobility. In the inset of Figure 2.2b, when on-line preconcentration of Trp was near completion, it was apparent that a major fraction of the original pH discontinuity was dissipated as the moving pH boundary or terminating co-ion (i.e.,  $\text{H}^+$ ) migrated throughout the original sample plug. At the same time, note the extended concentration profiles of leading co-ions,  $\text{NH}_4^+$  and  $\text{Na}^+$ , in front of the Trp zone as t-CITP transitions into zonal separation by CE. The inset of Figure 2.2c demonstrates that zonal separation of the fully stacked Trp coincided with dissipation of the original pH junction, as well as zonal separation of both  $\text{NH}_4^+$  and  $\text{Na}^+$  ahead of Trp. It is at this juncture when cationic metabolite separations occur by conventional CE within a reduced effective capillary length prior to ESI ionization.

Three important conclusions can be derived from this work. First, as the ionic strength or injection length of the sample plug is increased, the longer it takes for the transition from stacking to zonal separation to occur due to the slow rate of electrokinetic focusing under these conditions. Thus, there is an upper limit to the extent of sensitivity enhancement while still maintaining adequate resolution prior to ESI-MS detection. Although this on-line sample preconcentration technique can tolerate high concentrations of salt, excess  $\text{Na}^+$  (>100 mM) can further delay the transition to zonal separation as examined in a

recent report.<sup>34</sup> Second, the desalting function of CE that is important to minimize ion suppression in ESI-MS is effective as long as the analyte co-ion mobility is lower than the stacked  $\text{Na}^+$  ions generated by t-CITP. Thus, sample desalting in CE is effective for cationic metabolites that have a lower effective mobility than  $\text{Na}^+$  (i.e.,  $5.19 \times 10^{-4} \text{ cm}^2/\text{V}\cdot\text{s}$ ). It is important to note that, due to the low EOF under these conditions, excess  $\text{Cl}^-$  anions migrate directly out of the capillary inlet upon application of voltage and do not impact ESI-MS detection. Last, when computer simulations were performed under conventional t-CITP conditions (data not shown) without a pH discontinuity, on-line preconcentration of Trp occurred by a different process as reflected by stacking at the front portion of the BGE-sample boundary. In addition, the extent of sensitivity enhancement was reduced since only a fraction of the long sample plug was effectively focused. Thus, enhanced in-capillary sample preconcentration with desalting was achieved in CE-ESI-MS by a dual t-CITP with dynamic pH junction process, where analyte stacking occurred distinctly at the back end of the sample-BGE boundary prior to zonal separation and subsequent ESI-MS detection.

### **2.5.3. Prediction of RMT of Cationic Metabolites by Computer Simulations.**

Recently, Gas *et al.*<sup>33</sup> have demonstrated that computer simulations using Simul 5.0 can be useful for modeling electromigration behavior of multivalent ionic analytes, as well as predicting their separations in CE and ITP. Computer simulations can also be used as a promising tool in metabolomics research for

prediction of RMTs in order to confirm the identity of unknown metabolites among several candidates selected after CE-MS analyses. As a first step in this direction, Simul 5.0 was assessed to predict the separation of a group of 10 model amino acids with MetS as the internal standard. Figure 2.3a shows an experimental overlay of EIEs from a 20  $\mu\text{M}$  standard amino acid mixture under optimum conditions for on-line sample preconcentration with CE-ESI-MS. Note that the sample injection plug was reduced to 6.2 cm in order to have sufficient separation for the closely migrating isobaric species ( $\text{MH}^+ = 182 \text{ Da}$ ), Tyr (9) and MetS (11), due to the limited resolution of the mass analyzer. Also, it was clear that, among the amino acids, Gly had the lowest ionization efficiency, that was  $\sim 3000$ -fold lower than either Lys or Trp. In general, the migration order in CE-MS under these conditions was observed as follows, cationic > small neutral > aromatic  $\approx$  acidic amino acids, which is reflective of their characteristic  $\mu_0$  and  $\text{p}K_a$ . Figure 2.3b shows the simulated electropherogram under the same electrolyte conditions based on  $\mu_0$  and  $\text{p}K_a$  parameters<sup>33</sup> listed in Table 2.1. In the case of the internal standard, MetS, which did not have literature values reported, its two fundamental parameters ( $\mu_0 = 2.60 \times 10^{-4} \text{ cm}^2/\text{V}\cdot\text{s}$  and  $\text{p}K_a = 2.01$ ) were determined as described in the Experimental Section. Briefly,  $\mu_0$  was derived after computer molecular modeling and incorporation of  $V$  and  $z_0$  parameters into the Hubbard-Onsanger expression in eq 1, whereas the ionic strength-corrected  $\text{p}K_a$  was determined experimentally by CE-MS by apparent mobility changes as a

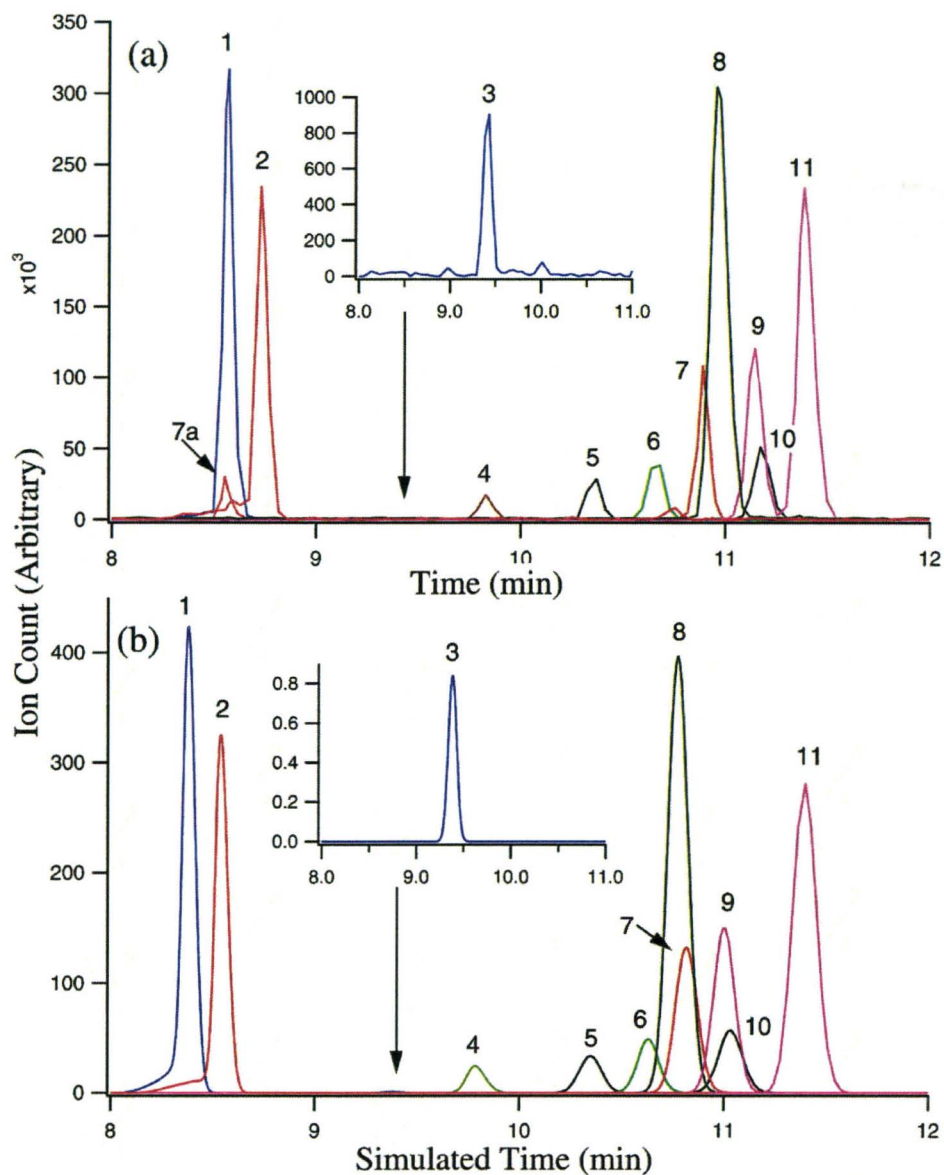


**Figure 2.3.** Comparison of experimental and simulated electropherograms for model amino acids using on-line sample pre-concentration by CE-MS. (a) An overlay of EIEs for 20 fM amino acids using the internal standard, MetS, and (b) predicted electropherogram using Simul 5.0 based on  $f^*$  and  $pK_a$  parameters listed in Table 2.1. Conditions: BGE, 1 M formic acid, pH 1.8; sample, 200 mM ammonium acetate, pH 7.0; sample injection, 6.2 cm;  $V$ , 23 kV; and  $L_c$ , 80 cm. Analyte peak numbering: (1) Lys, (2) His, (3) Gly, (4) Ala, (5) Ser, (6) Thr, (7) Glu, (7a) Lys (<sup>13</sup>C), (8) Trp, (9) Tyr, (10) Asp, and (11) MetS (IS).

function of buffer pH using eq 2. It was evident that there was a good qualitative agreement between experimental and predicted electropherograms in Figure 2.3 based on the similarity in the overall migration order. Although there was an average relative error of ~5.6% in terms of absolute migration times for amino acids due to run-to-run variances in EOF, a reduced error of only 1.7% was achieved when comparing predicted with experimental ( $n = 20$ , 2 days) RMT of amino acids using MetS as an internal standard. A small negative bias was noticed by linear correlation of predicted and experimental amino acid RMTs, as reflected by a slope of 1.10,  $y$ -intercept of -0.106, and  $R^2$  of 0.990. Thus, computer simulations can be used to reliably predict RMTs of metabolites in CE-MS even within discontinuous electrolyte systems provided that  $\mu_0$  and  $pK_a$  are accurate. Subsequent figures in this study will use RMT as the normalized time domain for improved reliability when applied to metabolomic studies of selective nutrient uptake behavior of *E. coli* by CE-MS.

**2.5.4. Differential Metabolite Uptake during Bacterial Growth.** An integrative metabolomic strategy using CE-ESI-MS with computer simulations was next developed to study the differential extracellular uptake of nutrients by bacteria within an undefined broth solution. LB is a complex nitrogen-rich carbon source medium derived from bactotryptone, yeast extract, and salt mixtures, which is often used to accelerate bacterial growth in *E. coli* cultures for enhanced expression of recombinant wild-type or mutant protein.<sup>50</sup> Since the growth rate of

bacteria is highly dependent on the amount and specific type of carbon source, optimization of the composition of a broth medium for selected microbes to maximize biomass yield is important in various biochemical and bioengineering applications. Although metabolomic studies are often directed at analysis of intracellular metabolites using glucose minimal media,<sup>11, 51</sup> this study was directed at identifying and quantifying extracellular metabolites that are taken up as key nutrients within an undefined growth media. Our earlier study of enantioselective metabolite flux using on-line sample preconcentration with chemical derivatization by CE<sup>52</sup> revealed selective uptake of different amino acids by *E. coli* without evidence of D-amino acid efflux into the broth medium. However, the method was limited in selectivity due to comigration of several unknown interferences when using CE with UV absorbance detection. Figure 2.4 depicts a series of overlay EIEs representing cationic metabolites identified as undergoing significant uptake by *E. coli* during different stages of bacterial growth at (a) 0, (b) 1.5, and (c) 5.0 hrs. The major advantage of using on-line sample preconcentration with CE-ITMS for comprehensive metabolite analyses is that it offers excellent full scan sensitivity with qualitative information provided by multistage MS experiments. In addition to several standard amino acids undergoing uptake from the medium, there were also several minor unidentified isobaric species (e.g., 1a, 4a), as well

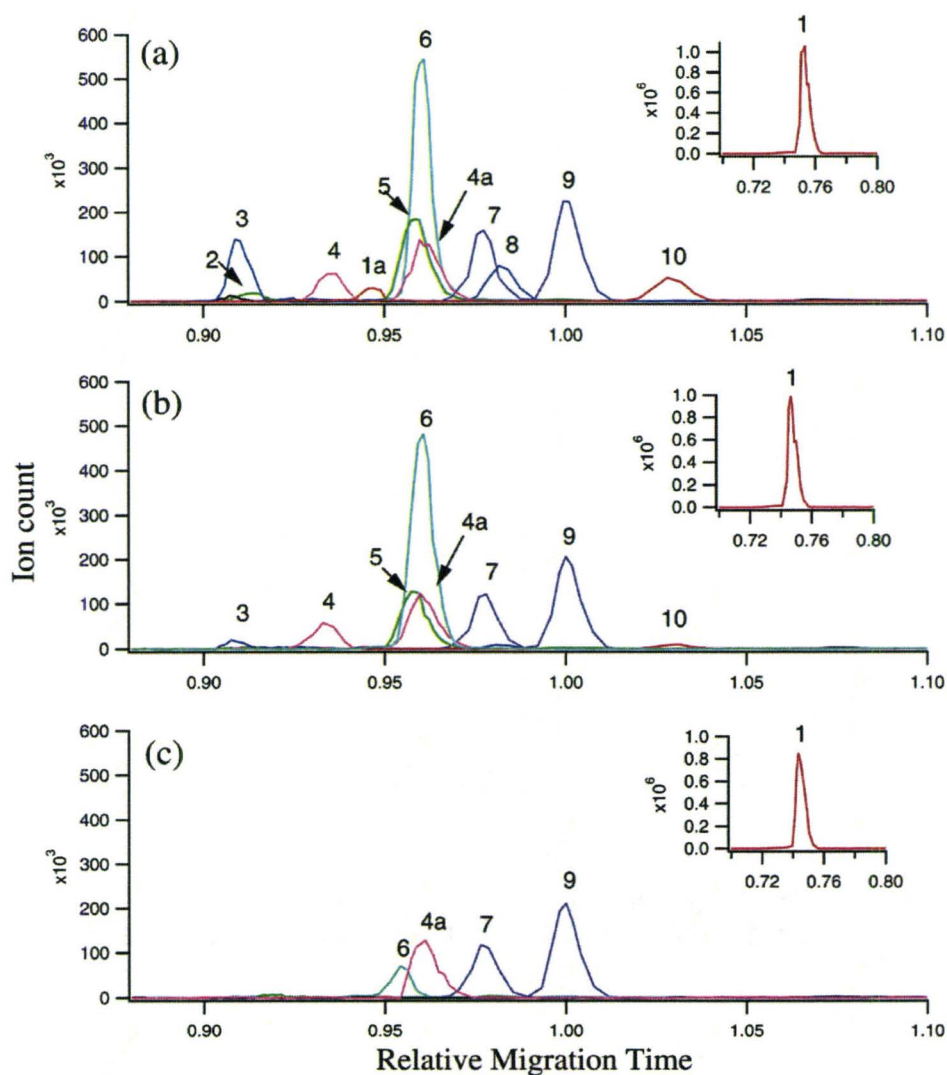


**Figure 2.4.** Series of EIEs revealing selective nutrient uptake within complex LB broth media as a function of *E. coli* growth at (a) 0, (b) 1.5, and (c) 5 hrs by CE-MS. Conditions similar to Figure 2.3, except that analyte peak numbering corresponds to the following: (1) Lys, (1a) unknown (isobaric to Lys, 147 Da), (2) Ser, (3) unknown (267 Da), (4) Thr, (4a) unknown (isobaric to Thr, 120 Da), (5) Trp, (6) Glu, (7) Tyr, (8) Asp, (9) MetS (IS), and (10) unknown (284 Da).

as other major unknown metabolites (e.g., 3, 10) detected. Figure 2.4 qualitatively demonstrated that *E. coli* cultures showed preferential uptake of specific nutrients (e.g., Asp, Ser) at early stages of growth until their depletion

with subsequent usage of other metabolites despite their overall higher abundance. Also, some amino acids were not used significantly as nutrient sources even after 8 hrs of incubation (e.g., Tyr, Lys). This feature reflects selective bacterial cometabolism in complex media, where multiple carbon sources that can be most efficiently used as direct sources in central energy metabolism are preferentially influxed within cells, such as Ser. Prior to quantitative analysis of differential metabolite uptake by *E. coli*, CE-ESI-MS in conjunction with computer simulations was first applied for identification of several unknown nutrients detected in Figure 2.4.

**2.5.5. De Novo Identification of Unknown Nutrients.** CE-MS in conjunction with computer simulations was used to identify several unknown metabolites used as key nutrients in LB broth medium. For instance, metabolite 10 in Figure 2.4 that was observed to undergo rapid uptake at early stages of bacterial growth (<1.5 hrs) was first characterized by preliminary CE-MS studies. Figure 2.5 highlights the overall strategy, where multistage MS<sup>3</sup> and dHDX experiments were used to identify characteristic fragments and total number of exchangeable protons in the unknown metabolite 10, respectively. Due to the relatively poor mass precision of ITMS, apparent isotopic ratio was used only qualitatively to detect the presence of heteroatoms or halogens (e.g., Cl, S). Figure 2.5 reveals that the unknown metabolite is a nucleoside based on its nominal mass (MH<sup>+</sup>

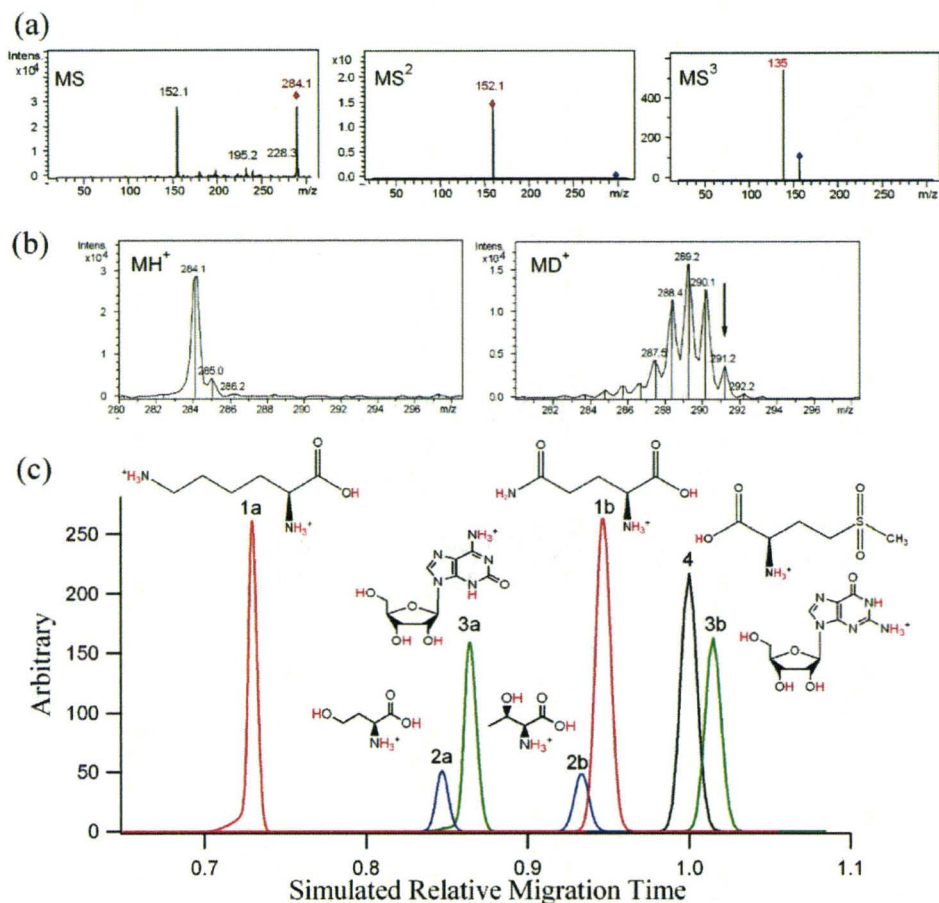


**Figure 2.5.** Integrative metabolomics strategy for unknown metabolite identification based on preliminary (a) multistage MS<sup>n</sup> and (b) dHDX experiments in conjunction with (c) computer simulations by Simul 5.0. Identification of two potential isomeric candidates ((3a) G and (3b) isoG) from KEGG database related to unknown nutrient 10 in Figure 2.4. Confirmation of G based on comparison of experimental with predicted RMTs using parameters in Table 2.2. Simulations were also applied to readily distinguish other isobaric ((1a) Lys vs (1b) Gln) and isomeric ((2a) Thr vs (2b) hSer) cations unresolved by conventional MS.

284 Da) and neutral fragment losses of ( $M^1 \rightarrow M^2$ , 132 Da;  $M^2 \rightarrow M^3$ , 17 Da), which correspond to a ribose and amine moiety, respectively. In addition, a comparison of the apparent mass change from water to deuterated sheath liquid during ESI ionization (e.g., MH<sup>+</sup> 284 Da; MD<sup>+</sup> 291 Da) indicated that the metabolite has a total of six exchangeable protons. A total of 16 isobaric metabolites were initially identified with the same nominal mass as the unknown

nutrient in the KEGG database among over 14 100 compounds. However, only two isomeric metabolites (i.e., guanosine, G, and isoguanosine, isoG) were selected as final candidates that satisfied CE-MS parameters in terms of being cationic, lacking halogen/heteroatoms isotopes, having six exchangeable protons, and containing both ribose and amine moieties. Computer simulations using Simul 5.0 were then used to further distinguish among selected candidates based on their characteristic  $\mu_o$  and  $pK_a$ , which was particularly relevant for isomeric and isobaric species unresolved by MS alone. Figure 2.5 also depicts simulated electropherograms that clearly demonstrates that the unknown metabolite 10 in Figure 2.4 was G, since the relative error between experimental and predicted RMT was only -1.3%. Table 2.2 demonstrates that the major factor for isomeric resolution by CE was differences in isomer  $pK_a$  since G is more acidic ( $pK_a \approx 2.10$ ) with a slower positive apparent mobility relative to isoG ( $pK_a \approx 3.65$ ) under the buffer conditions used in this study (pH 1.8). Thus, CE offers unique selectivity for resolution of complex metabolite mixtures with qualitative information complementary to MS. Figure 2.5 highlights that computer simulations can also be used to distinguish two other pairs of isobaric and isomeric metabolites based on predicted RMTs, namely Lys and Gln, as well as Thr and homoserine (hSer), respectively. The major advantage of computational approaches for metabolite identification by CE is that simulations can be performed from first principles based on the chemical structure of a candidate metabolite without the need for a purified standard. Table 2.2 also summarizes

other unknown metabolites identified in the broth that were observed to undergo bacterial uptake, such as Gln and adenosine (A), which were identified as 1a and 3 in Figure 2.4, respectively. In addition, Table 2.2 demonstrates that this strategy can be applied to identify other classes of cationic metabolites among several candidates with a relative error under 1.5%, such as tyramine (TyrN) and  $\gamma$ -aminobutyric acid (GABA), that were also present in the broth medium but were not observed to function as nutrients. However, it is important to ensure that proper data filtering is performed to account for  $^{13}\text{C}$  isotope and major fragment ions when interpreting MS spectra, which can result in a significant overestimate of total number of ions detected in a sample, as well as difficulty in finding a likely metabolite candidate for simulations. For example, unknown 4a in Figure 2.4 was determined to be a fragment ion from Phe ( $\text{MH}^+$  120 Da, isobaric to Thr) whose RMT did not correspond to any known metabolite candidate selected from the KEGG database search when MS spectra were not filtered. Noteworthy, our preliminary studies demonstrate that RMTs can be reliably predicted with a relative error approaching experimental error ( $\text{CV} < 1\%$ ) by CE-MS, which can be applied to several classes of unknown isomeric/isobaric metabolites, ranging from amino acids, amines, and nucleosides. Further insight into the selectivity and apparent uptake of metabolites in LB medium that served as nutrients for *E. coli* will next be examined.

**Table 2.2.** Identification of Unknown Nutrients and Isobaric Cationic Metabolites in Broth Medium by CE-ESI-MS Using On-Line Sample Preconcentration with Computer Simulations.

<i>Metabolite (candidates)</i>	<i>MH<sup>+</sup> (Da)</i>	<i>MS<sup>n</sup> (Da)</i>	<i>dHDx (no. xH)</i>	<i><math>\mu_o \times 10^{-4}</math> (cm<sup>2</sup>/V·s)<sup>a</sup></i>	<i>pK<sub>a</sub></i>	<i>RMT<sup>b</sup> (predicted)</i>	<i>RMT ± 1σ (CE-MS, n=5)</i>	<i>error (%)</i>	<i>uptake</i>
GABA (7)	104	104/87/69	3	3.08	4.23	0.804	0.801 ± 0.003	+0.49	No
Tyramine (6)	138	138/121/103, 93	3	2.74	9.74	0.835	0.833 ± 0.003	+0.21	No
Glutamine (5)	147	147/130/102	5	2.80	2.15	0.946	0.956 ± 0.002	-1.1	Yes
Adenosine (2)	168	268/138	5	2.20	3.00	0.912	0.910 ± 0.001	+0.28	Yes
Guanosine (2)	184	284/152/135	6	2.25	2.25	1.012	1.029 ± 0.001	-1.3	Yes

<sup>a</sup>Number of potential candidates identified from KEGG database after preliminary CE-ESI-MS analyses

<sup>b</sup>Predicted relative migration times using MetS as internal standard ( $\mu_o = 2.60 \times 10^{-4}$  cm<sup>2</sup>/V·s and pK<sub>a</sub> = 2.01) based on electrophoretic simulations using  $\mu_o$  and pK<sub>a</sub> as input parameters in Simul 5.0.

**2.5.6 Nutrient Uptake Patterns by *E. coli* during Growth.** Quantitative analysis of selective nutrient influx by *E. coli* is depicted in Figure 2.6 using dried cell weight as a measure of total biomass change. There were three distinct phases observed during bacterial growth, which were reflected by the differential extracellular nutrient uptake patterns identified in this study. It was apparent that *E. coli* displayed an inherent selectivity for five key nutrients, namely, Asp, Ser, Gln, A, and G, which were influxed rapidly within the first 1.5 hrs of bacterial growth. This stage represented the lag phase and early onset of *E. coli* replication where primary nutrients are directed for energy and protein biosynthesis. For instance, cometabolism of amino acid substrates such as Ser in complex media by *E. coli* has been previously demonstrated to enhance bacterial growth and biomass conversion.<sup>53</sup> Upon depletion of the primary nutrients in the broth solution, Figure 2.6 clearly demonstrates that secondary nutrients, namely, Glu, Trp, and Thr, were then utilized to continue bacterial replication during exponential growth between about 1.5 and 5 hrs. Surprisingly, the rate of biomass increase started to stagnate past this stage (5-8 hrs) despite the presence of other major metabolites in the nutrient-rich broth medium, such as Tyr, Lys, and Phe, whose concentration did not significantly change throughout the incubation. In addition to the inherent selectivity of nutrient uptake at different stages of bacterial growth, the rate of uptake (i.e., influx) from the extracellular medium was observed to be distinct for each nutrient. For example, the influx of Asp and Glu when normalized to dried cell weight was observed to undergo pseudo-first-order kinetics with an apparent

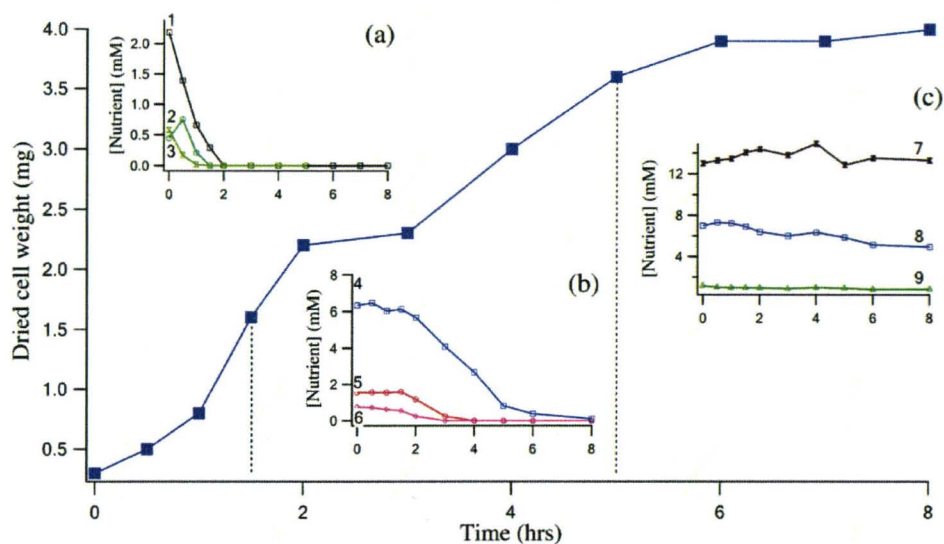


**Figure 2.6.** Quantitative analysis of differential nutrient uptake patterns by *E. coli* in LB broth media as a function of total dried cell weight. Three distinct stages of bacterial growth are associated with specific nutrient uptake behavior from (a) 0-1.5, (b) 1.5-5, and (c) 5-8 hrs. Analyte peak numbering: (1) Asp, (2) Ser, (3) G, (4) Glu, (5) Trp, (6) Thr, (7) Lys, (8) Phe, and (9) Tyr.

rate of  $41 \pm 3$  and  $18 \pm 1 \mu\text{M mg}^{-1} \text{min}^{-1}$ , respectively. Note that this technique allowed for direct analysis of metabolites present in complex broth samples present within over a 100-fold concentration range without labor-intensive sample pretreatment (e.g., chemical labeling, desalting, lyophilization, etc.). In general, these studies indicated rather inefficient biomass conversion when using standard LB broth media for recombinant expression of protein using *E. coli* since a significant fraction (~30%) of original nutrients were not utilized. Thus, metabolomic studies by CE-MS can be used as a tool to design customized broth solutions (e.g., Asp/Ser/Glu-rich media) for specific strains of microbes that reflect their inherent selectivity for nutrient uptake. Further studies will be

extended for simultaneous analysis and characterization of cationic and anionic (e.g., organic acid) metabolites in order to assess the global nutrient flux patterns of different strains of bacteria by CE-MS. It is anticipated that our integrative metabolomic strategy will offer a unique format for detection and unambiguous identification of unknown metabolites that is relevant in future drug discovery and clinical biomarker applications.

## 2.6 Conclusion

An integrative metabolomic strategy is proposed for the analysis of unknown low-abundance metabolites in complex samples using CE-MS in conjunction with computer simulations. On-line sample preconcentration was performed via t-CITP with dynamic pH junction in order to boost concentration sensitivity with nanomolar detection limits. Computer simulations along with time-resolved electrophoretic experiments provided a deeper insight into the dynamics of analyte band narrowing within a discontinuous electrolyte system, which permitted in-capillary sample preconcentration, desalting, and separation of metabolites prior to ESI-MS detection. Two fundamental analyte physicochemical parameters ( $\mu_0$  and  $pK_a$ ) were required to perform electrophoretic simulations, which enabled accurate prediction of the RMTs of several classes of cationic metabolites with a relative error under 2%. This strategy served as an important qualitative tool for aiding de novo identification of unknown nutrients among potential isobaric and isomeric candidates selected after preliminary CE-MS

experiments and ligand database search. Differential nutrient uptake patterns were revealed by CE-MS studies that highlighted the inherent selectivity of metabolite influx by *E. coli* during bacterial growth. Integrative metabolomics by CE-MS provides a simple yet powerful strategy for characterizing unknown metabolites without the requirement for purified standards. Future studies will be directed at expanding this approach to a wider array of metabolites for systemic understanding of extracellular and intracellular metabolite changes in bacteria as a function of specific stressors.

### **Acknowledgment**

This work is supported by funds provided by the National Science and Engineering Research Council of Canada, Premier's Research Excellence Award and the Canada Foundation for Innovation. R.L. acknowledges support in the form of an Ontario Graduate Scholarship in Science and Technology. The authors also thank Dr. Borislav Gas for helpful advice regarding use of Simul 5.0.

### **2.7 References**

- (1) Ryan, D.; Robards, K. *Anal. Chem.* **2006**, *78*, 7954.
- (2) Nicholson, J. K.; Connelly, J.; Lindon, J. C.; Holmes, E. *Nature Rev. Drug Discov.* **2002**, *1*, 153.

- (3) Catchpole, G. S.; Beckmann, M.; Enot, D. P.; Mondhe, M.; Zywicki, B.; Taylor, J.; Hardy, N.; Smith, A.; King, R. D.; Kell, D. B.; Fiehn, O.; Draper, J. *Proc. Natl. Acad. Sci. U.S.A.* **2005**, *102*, 14458.
- (4) Catchpole, G. S.; Beckmann, M.; Enot, D. P.; Mondhe, M.; Zywicki, B.; Taylor, J.; Hardy, N.; Smith, A.; King, R. D.; Kell, D. B.; Fiehn, O.; Draper, J. *Proc. Natl. Acad. Sci. USA* **2005**, *102*, 14458-14462.
- (5) Teusink, B.; Smit, E. J. *Nat. Rev. Microbiol.* **2006**, *4*, 46-56.
- (6) Saito, N.; Robert, M.; Kitamura, S.; Baran, R.; Soga, T.; Mori, H.; Nishioka, T.; Tomita, M. *J Prot. Res.* **2006**, *5*, 1979-1987.
- (7) Dunn, W. B.; Bailey, N. J.; Johnson, H. E. *Analyst* **2005**, *130*, 606.
- (8) Kind, T.; Fiehn, O. *BMC Bioinformatics* **2006**, *7*, 234-244.
- (9) Tolstikov, V. V.; Fiehn, O. *Anal. Biochem.* **2002**, *301*, 298-307.
- (10) Tolstikov, V. V.; Lommen, A.; Nakanishi, K.; Tanaka, N.; Fiehn, O. *Anal. Chem.* **2003**, *75*, 6737-6740.
- (11) Bajad, S. U.; Lu, W.; Kimball, E. H.; Yuan, J.; Peterson, C.; Rabinowitz, J. D. *J. Chromatogr. A* **2006**, *78*, 76-88.
- (12) Crockford, D. J.; Holmes, E.; Lindon, J. C.; Plumb, R. S.; Zirah, S.; Bruce, S. J.; Rainville, P.; Stumpf, C. L.; Nicholson, J. K. *Anal. Chem.* **2006**, *78*, 363-371.

- (13) Olivares, J. A.; Nguyen, N. T.; Yonker, C. R.; Smith, R. D. *Anal. Chem.* **1987**, *59*, 1230.
- (14) Simpson, D. C.; Smith, R. D. *Electrophoresis* **2005**, *26*, 1291-1305.
- (15) Klampf, C. W. *Electrophoresis* **2006**, *26*, 3-34.
- (16) Monton, M. R. N.; Terabe, S. *Anal. Sci.* **2005**, *21*, 5-13.
- (17) Smyth, E. F. *Electrophoresis* **2005**, *26*, 1334-1357.
- (18) Schmitt-Kopplin, P.; Frommberger, M. *Electrophoresis* **2003**, *24*, 3837.
- (19) Edwards, J. L.; Chisolm, C. N.; Shackman, J. G.; Kennedy, R. T. *J. Chromatogr. A* **2006**, *1106*, 80-88.
- (20) Sugimoto, M.; Kikuchi, S.; Arita, M.; Soga, T.; Nishioka, T.; Tomita, M. *Anal. Chem.* **2005**, *77*, 78-84.
- (21) Sato, S.; Soga, T.; Nishioka, T.; Tomita, M. *Plant Journal* **2004**, *40*, 151-163.
- (22) Soga, T.; Ohashi, Y.; Ueno, Y.; Naraoka, H.; Tomita, M.; Nishioka, T. *J. Prot. Res.* **2003**, *2*, 488-494.
- (23) Li, F. A.; Wu, M. C.; Her, G. R. *Anal. Chem.* **2006**, *78*, 5316.
- (24) Thompson, T. J.; Foret, F.; Vouros, P.; Karger, B. L. *Anal. Chem.* **1993**, *65*, 900-906.

- (25) Larsson, M.; Lutz, E. S. M. *Electrophoresis* **2000**, *21*, 2859.
- (26) Peterson, Z. D.; Bowerbank, C. R.; Collins, D. C.; Graves, S. W.; Lee, M. L. *J. Chromatogr., A* **2003**, *992*, 169.
- (27) Stutz, H.; Bordin, G.; Rodriguez, A. R. *Electrophoresis* **2004**, *25*, 1071.
- (28) Tang, Q.; Harrata, A. K.; Lee, C. S. *Anal. Chem.* **1996**, *68*, 2482.
- (29) Martinovic, S.; Berger, S. J.; Pasa-Tolic, L.; Smith, R. D. *Anal. Chem.* **2000**, *72*, 5356.
- (30) Yang, Y.; Boysen, R. I.; Hearn, M. T. W. *Anal. Chem.* **2006**, *78*, 4752.
- (31) Monton, M. R. N.; Imami, K.; Nakanishi, M.; Kim, J.-B.; Terabe, S. *J. Chromatogr. A* **2005**, *1079*, 266-273.
- (32) Reijenga, J. C.; Kenndler, E. *J. Chromatogr. A.*, **1994**, *659*, 417.
- (33) Hruska, V.; Jaros, M.; Gas, B. *Electrophoresis* **2006**, *27*, 984.
- (34) Breadmore, M. C.; Mosher, R. A.; Thormann, W. *Anal. Chem.* **2006**, *78*, 538-546.
- (35) Kim, J. B.; Britz-McKibbin, P.; Hirokawa, T.; Terabe, S. *Anal. Chem.* **2003**, *75*, 3986-3993.
- (36) Jaros, M.; Hruska, V.; Stedry, M.; Zuskova, I.; Gas, B. *Electrophoresis* **2004**, *25*, 3080-3085.

- (37) Fu, S.; Lucy, C. A. *Anal. Chem.* **1998**, *70*, 173.
- (38) Li, D.; Lucy, C. A. *Anal. Chem.* **2001**, *73*, 1324.
- (39) Palmer, M. E.; Tetler, L. W.; Wilson, I. D. *Rapid Commun. Mass Spectrom.* **2000**, *14*, 808.
- (40) Ptolemy, A.; LeBihan, M.; Britz-McKibbin, P. *Electrophoresis* **2005**, *26*, 4206.
- (41) Landers, J. P. **1997**.
- (42) Lide, D. R. *CRC Handbook of Chemistry and Physics*; CRC Press New York **1995**.
- (43) Storms, F. F.; Heijden, R.; Tjaden, U. R.; Greef, J. v. d. *Electrophoresis* **2004**, *25*, 3461.
- (44) Beckers, J. L. *J. Chromatogr.* **1993**, *641*, 363.
- (45) Sassi, A. R.; Bitter, H. M. L.; Brown, M. P. S.; Chapman, R. G.; Espiritu, J.; Greenquist, A. C.; Guyon, I.; Horchi-Alegre, M.; Stults, K. L.; Wainright, A.; Heller, J. C.; Stults, J. T. *Electrophoresis* **2005**, *26*, 1500.
- (46) Britz-McKibbin, P.; Terabe, S. *J. Chromatogr. A* **2003**, *1000*, 917-934.
- (47) Britz-McKibbin, P.; Otsuka, K.; Terabe, S. *Anal. Chem.* **2002**, *74*, 3736-3743.

- (48) Soga, T.; Heiger, D. N. *Anal. Chem.* **2000**, *72*, 1236.
- (49) Cech, N. B.; Enke, C. G. *Mass Spectrom. Rev.* **2002**, *20*, 362.
- (50) Gavina, J. M. A.; Das, R.; Britz-McKibbin, P. *Electrophoresis* **2006**, *27*, 4196.
- (51) Soga, T.; Ohahsi, Y.; Ueno, Y.; Naraoka, H.; Tomita, M.; Nishioka, T. *J. Proteome Res.* **2003**, *2*, 488-494.
- (52) Ptolemy, A.; Tran, L.; Britz-McKibbin, P. *Anal. Biochem.* **2006**, *354*, 192.
- (53) Netzer, R.; Peters-Wendisch, P.; Eggeling, L.; Sahm, H. *Appl. Environ. Microbiol.* **2004**, *70*, 7148-7155.

*Chapter III*

Differential Rates of Glutathione Oxidation for Assessment of Cellular Redox Status and Antioxidant Capacity by Capillary Electrophoresis-Mass Spectrometry: An Elusive Biomarker of Oxidative Stress

### **III. Differential Rates of Glutathione Oxidation for Assessment of Cellular Redox Status and Antioxidant Capacity by Capillary Electrophoresis-Mass Spectrometry: An Elusive Biomarker of Oxidative Stress**

#### **3.1 Abstract**

Glutathione metabolism plays a fundamental role in maintaining homeostasis and regulating the redox environment of a cell. Despite the widespread interest in quantifying glutathione metabolites in oxidative stress research, conventional techniques are hampered by complicated sample handling procedures in order to prevent significant oxidation artifacts generated during sample collection, sample pretreatment and/or chemical analysis. In this report, a simple and validated method for glutathione analysis from filtered red blood cell (RBC) lysates was developed using capillary electrophoresis-electrospray ionization-mass spectrometry (CE-ESI-MS) in conjunction with fingerprick microsampling and ultrafiltration. About a three-fold improvement in precision with nanomolar detection limits was achieved when using on-line sample preconcentration with CE-ESI-MS via a modified injection sequence, which permitted accurate determination of the intracellular reduced/oxidized glutathione ratio (GSH/GSSG), as well as other glutathione species, including protein-bound glutathione mixed disulfide (PSSG), free glutathione mixed disulfides (GSSR) and glutathione thioether conjugates (GSX). In this work, the redox status of filtered hemolysates was determined by the equilibrium half-cell reduction potential for glutathione ( $E_{GSSG/2GSH}$ ), whereas its intrinsic antioxidant capacity was assessed by the apparent rate of metal-catalyzed oxidation of glutathione. *In-*

*vitro* incubation studies of intact RBCs with 1-chloro-2,4-dinitrobenzene (CDNB) and *N*-acetyl-*L*-cysteine (NAC) were found to significantly alter  $E_{GSSG/2GSH}$  and/or glutathione oxidation kinetics (*e.g.*,  $k_{GSSG}$ ) relative to normal controls based on their function as a toxic electrophilic compound and a competitive free radical scavenging/reducing agent, respectively. Differential rates of glutathione oxidation (DIRGO) using CE-ESI-MS offers a novel strategy for global assessment of the impact of intrinsic metabolite constituents (*i.e.*, metabolome) and/or extrinsic perturbants on cellular redox status that is relevant to improved understanding of aging and the pathogenesis of acute or chronic disease states.

### 3.2 Introduction

Reduced glutathione (GSH) represents the most abundant intra-cellular thiol ( $\approx$  1-10 mM), where it functions as an important non-enzymatic antioxidant towards reactive oxygen and nitrogen species generated as by-products of aerobic metabolism, host defense and cell signaling.<sup>1-3</sup> The redox couple of GSH and oxidized glutathione disulfide (GSSG) interacts with other cyclical redox reactions that prevent oxidative damage to biological molecules by free radicals, including ascorbic acid and vitamin E.<sup>4</sup> Recent studies have demonstrated that glutathionylation of accessible cysteine residues is a key redox-control mechanism for regulating protein function<sup>5</sup> via a reversible thiol-sulfhydryl exchange involving GSSG or the nitric oxide donor *S*-nitrosoglutathione.<sup>6</sup> GSH also functions as an essential cofactor to glutathione peroxidases and glutathione *S*-transferases for the detoxification of non-radical oxidants, such as hydrogen

peroxide, electrophilic drugs and other types of xenobiotics.<sup>2</sup> The critical role of GSH for maintaining cell viability is exemplified by cases of adverse drug toxicity, such as primaquine-induced hemolytic anemia among susceptible individuals with glucose-6-phosphate dehydrogenase or glutathione synthetase deficiency.<sup>7</sup> Similarly, acetaminophen overdose represents an on-going health concern that can lead to acute liver damage as a result of excessive glutathione depletion upon accumulation of the reactive intermediate *N*-acetyl-*p*-benzoquinone imine.<sup>8, 9</sup> These examples highlight that sufficient recycling capacity and biosynthetic pathways for GSH during oxidative insult are vital to prevent deleterious cell injury and irreversible organ failure. GSH depletion, a low GSH/GSSG ratio or a high GSSG/2GSH half-cell reduction potential ( $E_{GSSG/2GSH}$ ) are hallmarks of oxidative stress that has been implicated in the regulation of cell differentiation, gene expression, signal transduction and apoptosis.<sup>10, 11</sup> Indeed, GSSG and protein-glutathione mixed disulfides (PSSG) have been demonstrated to be sensitive biomarkers of oxidative stress complementary to classical assays that quantify oxidative damage, such as protein carbonyl content and products of lipid peroxidation (*e.g.*, malondialdehyde).<sup>12</sup>

The development of robust yet accurate assays for glutathione analysis has long been hampered by the inherent reactivity and high abundance of GSH in whole blood, tissue homogenates or cell lysates, which can lead to significant artifacts during sample collection, sample pretreatment and/or chemical analysis.<sup>13</sup> To date, a variety of techniques have been reported for glutathione

determination in biological samples, including spectrophotometric assays, nuclear magnetic resonance (NMR), as well as liquid chromatography (LC) in conjunction with UV, fluorescence, electrochemical detection and electrospray ionization-mass spectrometry (ESI-MS).<sup>14, 15</sup> However, only a handful of reports<sup>12, 16-21</sup> have demonstrated adequate validation to ensure accurate recovery after sample deproteinization, which has contributed to the wide disparity of GSH and GSSG concentrations in whole blood or hemolysates reported in the literature.<sup>18</sup> For instance, acidification of whole blood samples induces partial oxidation of GSH upon denaturation of oxyhemoglobin (*i.e.*,  $\text{Fe}^{3+}/\text{O}_2^-$ ) with concomitant generation of hydrogen peroxide ( $\text{H}_2\text{O}_2$ ) that results in artificially elevated basal levels of GSSG.<sup>18, 20</sup> The addition of *N*-ethylmaleimide for protection of labile GSH has been proposed to prevent oxidation artifacts prior to sample acidification,<sup>22-24</sup> however the procedure is time-consuming since back-extraction of excess reagent and subsequent pH-adjustment of sample are required prior to chemical derivatization when using LC with photometric detection.<sup>12, 18</sup> Alternatively, membrane filtration with centrifugation (*i.e.*, ultrafiltration) offers a simple method for sample deproteinization that avoids oxidative artifacts.<sup>25, 26</sup> Reliable methods for quantifying glutathione metabolites are critical for better understanding of the underlying mechanisms of oxidative stress,<sup>27, 28</sup> which is relevant to the study of ageing, as well as the pathogenesis of various chronic disorders, ranging from cancer, diabetes to neurodegenerative and cardiovascular diseases.<sup>15</sup>

Herein we introduce a new strategy for assessment of the redox status and antioxidant capacity of cells via the differential rates of glutathione oxidation (DIRGO) by capillary electrophoresis-electrospray ionization-mass spectrometry (CE-ESI-MS). Reliable analysis of various glutathione metabolites from filtered red blood cell (RBC) lysates was achieved without complicated off-line sample pretreatment or oxidation artifacts, including GSH, GSSG, PSSG, glutathione-thiol mixed disulfides (GSSR) and glutathione thioether conjugates (GSX). Noteworthy, significant in-capillary oxidation of GSH was observed when performing sample injections at the anode by CE-ESI-MS, which was resolved by displacement of the sample plug within the capillary past the electrode interface prior to voltage application. Excellent reproducibility and sensitivity was realized by the optimized method when using CE-ESI-MS without chemical labeling unlike previous CE methods for glutathione analysis that are constrained by poor detection limits and/or limited selectivity.<sup>25, 29-35</sup> In addition, on-line sample preconcentration with desalting by CE-ESI-MS<sup>36-38</sup> enabled artifact-free quantification of low nanomolar levels of endogenous GSSG from hemolysates without ionization suppression effects. This feature is advantageous since concentration sensitivity in CE-ESI-MS can be significantly compromised due to post-capillary dilution effects when using a co-axial sheath liquid interface in conjunction with a reference sprayer that is required for high mass accuracy in TOF-MS.<sup>8</sup> In this work, *ex-vivo* metal-catalyzed oxidation (MCO) studies on filtered hemolysates were performed in order to assess the apparent kinetics of

glutathione oxidation as a quantitative measure of cytosolic antioxidant capacity and hydroxyl radical scavenging activity.<sup>39</sup> In addition, *in-vitro* incubation studies of intact erythrocytes with 1-chloro-2,4-dinitrobenzene (CDNB) and *N*-acetyl *L*-cysteine (NAC) were examined by DIRGO in order to characterize the impact of exogenous reagents on cell redox status based on perturbations in the initial equilibrium GSH/GSSG concentration ratio and/or apparent rates of glutathione oxidation. To the best of our knowledge, this work demonstrates for the first time that complementary thermodynamic (*e.g.*,  $E_{GSSG/2GSH}$ ) and kinetic (*e.g.*,  $k_{GSSG}$ ) parameters associated with glutathione metabolism serve as sensitive indicators of oxidative stress, which can provide deeper insight into the putative toxicity of chemical exposure and/or the efficacy of nutritional intervention on cell viability.

### 3.3 Materials and Methods

**3.3.1. Chemicals and Reagents.** De-ionized water used for buffer and sample preparations was obtained using a Barnstead EASY Pure II LF ultrapure water system (Dubuque, IA). All chemical standards and buffers were purchased from Sigma-Aldrich Inc. (St. Louis, MO, USA), including acetonitrile (ACN), *N*-acetyl-*L*-cysteine (NAC), *D*-alanyl-*D*-alanine (diAla), ammonium acetate, 1-chloro-2,3-dinitrobenzene (CDNB), dithiothreitol (DTT), formic acid (FA), hemoglobin (Hb), 8-hydroxyquinoline-5-sulfonic acid (HQSA), methanol (MeOH), oxidized glutathione (GSSG), reduced glutathione (GSH) and

trichloroacetic acid (TCA). Individual stock solutions of free thiol metabolite standards (*e.g.*, GSH, NAC) were prepared fresh daily in water. All solvents were degassed and chilled to 4°C prior to use on a daily basis.

**3.3.2. Apparatus and Conditions.** CE-ESI-MS studies were performed on an automated Agilent CE system equipped with an XCT 3D ion trap mass spectrometer, an Agilent 1100 series isocratic pump, and a G16107 CE-ESI-MS sprayer kit (Agilent Technologies, Waldbronn, Germany). All separations were performed on uncoated fused-silica capillaries (Polymicro Technologies Inc., Phoenix, USA) with 50- $\mu\text{m}$  i.d. and 80-cm total length. 1.0 M formic acid, pH 1.8 was used as the acidic background electrolyte (BGE) for cationic glutathione metabolite separations in CE. An Agilent 1100 series pump with a 1:100 splitter was used to supply a volume of 10  $\mu\text{L}/\text{min}$  of 0.1 % formic acid in 1:1 MeOH/H<sub>2</sub>O as the sheath liquid. Prior to first use, open tubular fused-silica capillaries were conditioned for 20 min with MeOH, de-ionized H<sub>2</sub>O and 1.0 M formic acid. Samples were then introduced into the capillary using a low-pressure (50 mbar) hydrodynamic injection. On-line sample preconcentration using a discontinuous electrolyte system<sup>36-38</sup> was performed by first injecting a sample prepared in 200 mM ammonium acetate, pH 7.0 for 75 s at 50 mbar followed by a 60 s injection of the acidic BGE at 50 mbar prior to voltage application. The latter (second) injection sequence was used to displace the original sample plug within the capillary past the electrode interface at the inlet (anode), which was required to avoid CE-induced oxidation artifacts when analyzing low micromolar

levels of GSSG in the presence of excess GSH. Filtered RBC lysates were typically diluted two-fold with ammonium acetate prior to CE-ESI-MS analysis. In some cases, CE separations were also performed under basic conditions with 50 mM ammonium acetate pH 8.5 as the alkaline BGE using negative-ion mode ESI-MS in order to analyze anionic metabolites, including NAC, NAC-NAC disulfide homodimer and GSH-NAC mixed disulfide heterodimer. In this case, on-line sample preconcentration of acidic metabolites was performed by preparing an acidic sample in 10 mM HCl/5 mM ammonium acetate, pH 2.0, which was injected for 150 s followed by a 60 s injection of alkaline BGE at 50 mbar prior to voltage application. An Agilent 1100 series pump equipped with a 1:100 splitter was used to supply a volume of 10  $\mu$ L/min of 5 mM ammonium acetate in 1:1 MeOH/H<sub>2</sub>O as the sheath liquid. Separations were performed at 20°C with an applied voltage of 30 kV. All CE-ESI-MS analysis was performed at 300°C using  $\pm$  4 kV as the capillary voltage depending on the ionization mode (*i.e.*, acidic BGE/+ESI; alkaline BGE/-ESI). Nitrogen gas was used as the nebulizing gas and drying gas at 5 psi and 10 L/min, respectively, whereas helium was employed as the damping gas for the ion trap mass analyzer. All MS data were recorded with a range of 50-750  $m/z$  using the ultrascan mode of 26 000  $m/z$  per second. All regression analyses and figures were processed using Igor Pro 5.0 (Wavemetrics Inc, Lake Oswego, OR).

### **3.3.3. Fingerprint Microsampling and Filtered RBC Lysate Preparation.**

Human blood samples were collected from a healthy volunteer by a disposable

“pin-prick” method using a mini-capillary blood collection vial (SAFE-T-FILL, Ram Scientific Inc, Yonkers, New York, USA) coated with K<sub>2</sub>EDTA. The blood sample was then centrifuged at 4°C under 2000 rpm for 5 min to fractionate plasma from erythrocytes. The plasma was removed and then the RBCs were washed with phosphate buffer saline (PBS: 10 mM NaH<sub>2</sub>PO<sub>4</sub>, 150 mM NaCl, pH 7.4, 4°C), vortexed and centrifuged at 4°C under 7000 rpm for 1 min to isolate RBCs. The washing steps were repeated three times until the supernatant was clear and colorless with no evidence of hemolysis. 200 µL of RBCs were aliquoted using Superslik surface pipette tips (VWR, Mississauga, Canada) and then lysed by addition of 600 µL of pre-chilled de-ionized water at 4°C. The hemolysate was then centrifuged at 4°C under 7000 rpm for 1 min to remove cell debris. Ultrafiltration of the RBC lysate supernatant (100 µL) was performed using a Nanosep 3kDa Omega microfilter (PALL Corporation, Ann Arbor, MI, USA) at 4°C under 14,000 rpm for 15 min to deproteinize the sample without oxidation artifacts. The filtered RBC lysate was then used for subsequent experiments and/or diluted in buffer prior to CE-ESI-MS analysis. In some cases, the protein retentate on the microfilter was recovered to assess the extent of protein glutathionylation as described later in the experimental. Overall, processing of microlitres (~ 500 µL) of blood samples was completed within 30 min, which yielded a minimum of 390 µL of filtered RBC lysate for *ex-vivo* glutathione oxidation studies. In general, a volume of only 10 µL was sufficient for performing sample injections when using CE-ESI-MS. Sample

deproteinization of RBC lysates using acid (TCA, 920 mM) and organic solvent (3:1 dilution with ACN) was compared to ultrafiltration in order to validate the method for glutathione quantification, which also included the impact of sample storage conditions (*e.g.*, freeze/thaw cycles). Spike and recovery experiments were also conducted on RBCs ( $n=3$ ) to confirm the lack of auto-oxidation during sample processing by using 100  $\mu\text{M}$  of glutathione ethyl ester (GSH-EE) as a recovery standard which was prepared in ice cold de-ionized water used for hemolysis.

**3.3.4. *Ex-vivo* Oxidation Kinetic Studies of Filtered RBC Lysates for Antioxidant Capacity.** Metal-catalyzed oxidation (MCO) studies were performed on standard glutathione solutions, as well as various filtered RBC lysate samples as a way to assess glutathione oxidation kinetics by CE-ESI-MS. In general, two 55  $\mu\text{L}$  aliquots of  $\text{H}_2\text{O}_2$  and  $\text{CuSO}_4$  (35  $\mu\text{M}$  each) were added simultaneously to 390  $\mu\text{L}$  of filtered RBC lysate or standard solution to initiate the MCO reaction within a final volume of 500  $\mu\text{L}$ . This oxidation process represents a Fenton-like catalytic reaction for *in-situ* generation of hydroxyl radical ( $\cdot\text{OH}$ ) as the reactive oxygen species on a slower time scale as compared to pulse radiolysis methods.<sup>40</sup>

<sup>41</sup> Higher concentrations of  $\text{H}_2\text{O}_2/\text{Cu}^{2+}$  were initially explored in this work, but resulted in observed oxidation kinetics for GSH that were too rapid ( $< 4$  min) to assess within the timeframe of the experiment. The optimum concentration levels for  $\text{H}_2\text{O}_2/\text{Cu}^{2+}$  was determined empirically by induction of a moderate yet steady rate of glutathione oxidation (*i.e.*, GSH depletion/GSSG formation) when using

normal filtered RBC lysate samples as a biological reference. This is in contrast to the high H<sub>2</sub>O<sub>2</sub> concentration levels ( $\approx 1$  mM) used to characterize the oxidation kinetics of standard solutions of GSH relative to other peptide analogues *in-vitro* for comparing their hydroxyl radical scavenging activity.<sup>41, 42</sup> Upon initiation of the reaction, the sample was mixed by vortex, covered with aluminum foil and then incubated at 37°C while various aliquots (19  $\mu$ L) were removed at increasing time intervals for up to 24 hrs. Each aliquot was then immediately quenched by addition of 1  $\mu$ L of 180 mM acetic acid containing 20  $\mu$ L of ammonium acetate (pH 7.0) and an internal standard (DiAla for acidic BGE) to generate a final concentration of 200 mM and 50  $\mu$ M, respectively. Samples were prepared similarly for anionic CE conditions under negative-ion mode ESI-MS except that HQSA was used as the internal standard which was diluted in 10 mM HCl/5 mM ammonium acetate, pH 2.0. All samples were then frozen at -40°C and thawed only once prior to CE-ESI-MS analysis. These studies serve to assess the intrinsic global antioxidant capacity of all low molecular weight (< 3 kDa) cytosolic constituents (*e.g.*, metal ions, metabolites/peptides, nutrients *etc.*) within erythrocytes as reflected by relative differences in the apparent rates of GSH depletion and/or GSSG formation.

**3.3.5. *In-vitro* Incubation of Intact RBCs with Extrinsic Reagents.** 200  $\mu$ L of isolated RBCs were incubated with 400  $\mu$ L PBS solution containing either 3 mM CDNB or 10 mM NAC. The solution was vortexed and incubated at 37°C for 5 min, which allowed for uptake of extrinsic reagents by RBCs without causing

hemolysis. In the case of CDNB, an equilibrium concentration of approximately 800  $\mu\text{M}$  diffused within RBCs after preincubation as deduced by the extent of GSH depletion upon formation of the dinitrobenzene-glutathione thioether conjugate (DNB-SG). *Ex-vivo* incubation of NAC with intact RBCs resulted in an intra-cellular concentration of about 2 mM, which was similar in magnitude to physiological GSH levels in normal RBC lysates. Although NAC is anionic under physiological conditions with little tendency for passive membrane diffusion,<sup>43</sup> our studies clearly indicate that active-transport processes for NAC are operative *in-vitro* for RBCs. In contrast to CDNB, NAC functions as a competitive free-radical scavenging agent and reducing agent which was found not to significantly alter glutathione equilibrium concentration levels. All incubation studies with extrinsic reagents were terminated by centrifugation at 4°C under 7000 rpm for 1 min to isolate RBCs, which were then washed in PBS solution three-times prior to RBC lysate preparation as described previously. These studies were performed to mimic oxidative stress conditions within erythrocytes, as well as assess the efficacy of antioxidant supplementation.

**3.3.6. Protein-bound Glutathione Sample Preparation.** Protein retained on the 3kDa filter was processed to quantify the fraction of protein-bound glutathione (PSSG) following a modified protocol by Rossi *et al.*<sup>12, 44</sup> Briefly, 100  $\mu\text{L}$  of PBS was added to reconstitute the protein retentate after filtration of the RBC lysate. This protein solution was transferred into a microtube and 77  $\mu\text{L}$  of 920 mM trichloroacetic acid (TCA) was added to precipitate protein. The solution was

then centrifuged and the supernatant was removed to eliminate any residual sample matrix. The protein precipitate was reconstituted in 800  $\mu\text{L}$  of 3 mM EDTA prepared in PBS. Then 12  $\mu\text{L}$  of 50 mM DTT was added and sonicated for 5 min to chemically reduce PSSG in order to generate free GSH. Lastly, 80  $\mu\text{L}$  of 920 mM TCA was added and the precipitate protein allowing for the supernatant containing GSH to be isolated and analyzed by CE-ESI-MS as described previously. Since excess GSH was already removed after initial RBC lysate filtration, the use of acidic deproteinization with TCA did not generate oxidation artifacts on glutathione measurements, which was confirmed by the lack of GSSG detected when using the PSSG protocol described above.

**3.3.7. Hemoglobin Assay.** Hemoglobin (Hb) was quantified using Drabkin's reagent following the protocol outlined by the supplier (Sigma-Aldrich Inc.). Absorbance of hemoglobin was monitored at 400 nm using a Cary 50 UV-VIS spectrophotometer (Varian Inc., Palo Alto, CA, USA), which was used to normalize blood samples collected at different time intervals during the study based on total hemoglobin content.

### **3.4. Results and Discussion**

**3.4.1. CE-MS Optimization for Artifact-free Glutathione Analysis.** To date, there have been only two previous reports for glutathione analysis using CE-ESI-MS,<sup>8,45</sup> however adequate method validation was not performed to ensure reliable

and artifact-free quantification. CE-ESI-MS in conjunction with on-line sample preconcentration and desalting<sup>36-38</sup> offers a simple strategy to extend concentration sensitivity for the simultaneous analysis of GSH, GSSG and various glutathione adducts in biological samples without chemical derivatization. However, a potential instrumental artifact unique to CE is oxidation of redox-active analytes in the sample plug injected at the anodic end of the capillary inlet upon voltage application (30 kV), such as the case when analyzing low levels of GSSG in the presence of excess GSH. This bias is significant when using commercial CE instrument configurations where the capillary is inserted through a hollow electrode in order to make electrical contact with the buffer reservoir. Due to the close proximity of the electrode surface with the sample plug at the capillary inlet as depicted in Figure 3.1(a), highly variable ion responses ( $CV \approx 22\%$ ,  $n = 4$ ) were observed for GSSG (3  $\mu\text{M}$ ) when analyzing consecutive injections of a sample also containing a 500-fold excess of GSH despite the use of an internal standard (DiAla). In contrast, good precision ( $CV \approx 7.8\%$ ,  $n = 4$ ) was realized when performing a direct analysis of GSSG without GSH in the sample plug as a control (data not shown). In order to eliminate in-capillary oxidation artifacts by CE, the sample plug ( $\approx 6.6$  cm) was first displaced away from the electrode assembly by a subsequent injection with BGE prior to voltage application. The benefit of this modified injection sequence is shown in Figure

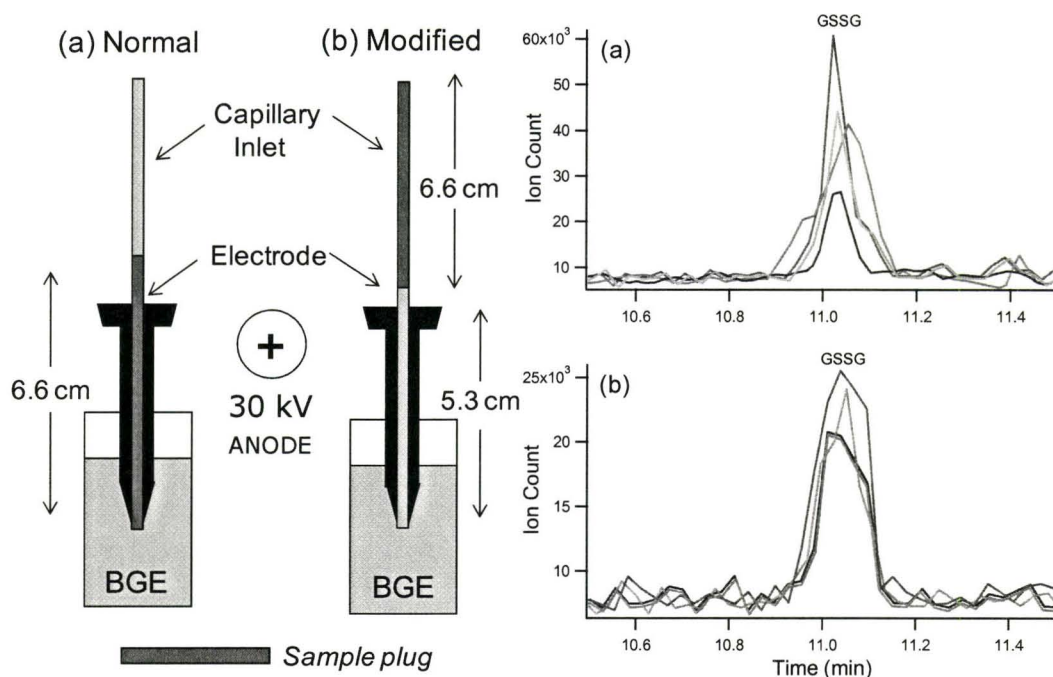


**Figure 3.1.** A comparison of (a) normal and (b) modified hydrodynamic sample injection sequences for avoiding oxidation artifacts at the anodic electrode interface when analyzing low micromolar levels of GSSG in the presence of a 500-fold excess of GSH by CE-ESI-MS with on-line sample pre-concentration. A series of extracted ion electropherogram overlays demonstrate a 3-fold improvement in method precision via the modified sample injection ( $CV \approx 6.9\%$ ,  $n = 4$ ) when quantifying  $3 \mu\text{M}$  GSSG ( $\text{MH}_2^{2+} = 307 \text{ m/z}$ ) that was independent of GSH concentration.

3.1(b), where reliable GSSG analysis was achieved with a three-fold improvement in method precision ( $CV \approx 6.9\%$ ,  $n = 4$ ) that was independent of GSH concentration (*e.g.*,  $3 \mu\text{M}$ - $1.5 \text{ mM}$ ). Enhanced concentration sensitivity was also realized by this method with a limit of detection (LOD) of  $25 \text{ nM}$  ( $S/N \approx 3$ ) for GSSG over a 750-fold linear dynamic range ( $0.01$ - $75 \mu\text{M}$ ) with good linearity ( $R^2 = 0.997$ ) when using an 3D ion trap mass analyzer in full scan mode. In this work, about a 10-fold higher relative response factor<sup>36</sup> was observed for GSSG relative to GSH (LOD =  $250 \text{ nM}$ ) due to faster ion desorption kinetics related to

its divalent positively charge state (*i.e.*,  $\text{MH}_2^{2+} = 307 \text{ m/z}$  for GSSG,  $\text{MH}^+ = 308 \text{ m/z}$  for GSH) under positive-ion mode ESI-MS conditions. Overall, CE-ESI-MS offers improved concentration sensitivity for the direct analysis of low abundance glutathione species (*i.e.*, GSSG) with comparable precision relative to CE-UV,<sup>30</sup> LC-UV<sup>19</sup> or LC-ESI-MS<sup>20, 46, 47</sup> while avoiding complicated off-line sample handling protocols involving chemical derivatization and/or thiol quenching.

#### **3.4.2. Ultrafiltration for Accurate Glutathione Determination in RBC**

**Lysates.** Acid deproteinization of biological samples in the presence of heme-containing proteins has been shown to induce oxidation artifacts resulting in erroneous glutathione quantification that still goes unheeded in the majority of reports published in the literature.<sup>12, 18</sup> Although several research groups have advocated the use of thiol protection reagents prior to sample acidification, such as *N*-ethylmaleidimide,<sup>18, 20</sup> iodoacetic acid<sup>48, 49</sup> or Ellman's reagent,<sup>50</sup> membrane ultrafiltration offers a simpler approach for avoiding bias caused by protein denaturation or perturbations in the GSH/GSSG equilibrium without covalent modification of free thiols. Table 3.1 compares the efficacy of three different sample pretreatment protocols on apparent GSH and GSSG concentration levels in RBC lysates measured by CE-ESI-MS following deproteinization by TCA, ACN and ultrafiltration. It is apparent that both TCA and ACN sample pretreatment result in significant oxidation of glutathione relative to ultrafiltration as reflected by a 9-20% decrease in GSH, but with a dramatic 6-to-10-fold

**Table 3.1.** Impact of deproteinization method on the accuracy of glutathione determination from hemolysates by CE-ESI-MS.

Method of deproteinization <sup>a</sup>	GSH (μM)	GSSG (μM)	GSH/GSSG	$E_{GSH^2/GSSG}^b$ (mV)	% Oxidation <sup>b</sup>
3kDa ultrafiltration	1660 ± 55	3.5 ± 0.2	474 ± 31	-260 ± 2	0.42 ± 0.03
TCA precipitation	1510 ± 70	37 ± 5	41 ± 6	-228 ± 2	4.7 ± 0.9
CH <sub>3</sub> CN denaturation	1310 ± 30	21 ± 1	62 ± 3	-231 ± 2	3.1 ± 0.2

<sup>a</sup> The same blood sample collected was used for all three comparative deprotenization methods, where error represents  $\pm 1\sigma$  ( $n=3$ ).

<sup>b</sup> Half-cell reduction potential estimated by Nernst equation:  
 $E_{GSH^2/GSSG} = E^o - 59.1/2 \cdot \log([GSH]^2/[GSSG])$  with  $E^o = -264$  mV at pH 7.4, whereas % oxidation of glutathione calculated by  $2[GSSG] \times 100 / (2[GSSG] + [GSH])$ .<sup>11</sup>

apparent increase in GSSG that is consistent with previously validated reports.<sup>12,</sup>

<sup>18</sup> Although GSH/GSSG is routinely used as a ratiometric biomarker of oxidative stress,  $E_{GSSG/2GSH}$  better reflects the redox status of a cell since it takes into account the reaction stoichiometry of the glutathione redox couple which is highly correlated with cell phenotype.<sup>10, 11, 51-53</sup> Table 3.1 confirms that glutathione analysis by CE-ESI-MS can provide an accurate assessment of the highly reduced environment of healthy erythrocytes with a  $E_{GSSG/2GSH}$  (pH 7.4) and degree of oxidation of (-260 ± 2) mV and (0.42 ± 0.03)%, respectively. In addition, spike and recovery studies using glutathione ethyl ester (GSH-EE) were performed on RBCs when using ultrafiltration to unambiguously confirm the lack of oxidation artifacts occurring during sample processing. The overall recovery for GSH-EE from filtered RBC lysates ( $n=3$ ) was good at (109 ± 2)% with no evidence of auto-oxidation (GSEE-GSEE) or glutathione-mixed disulfide (GS-GSEE) formation as shown in Figure 3.2. Further studies also examined the impact of

sample storage conditions on filtered RBC lysate samples frozen after ultrafiltration (refer to Table 3.2), which concluded that significant glutathione oxidation was only found to occur after the second and third rounds of freeze/thaw cycles, which were avoided in subsequent experiments. Thus, CE-ESI-MS together with fingerprick micro-sampling and ultrafiltration offers a convenient, reliable yet accurate method for glutathione determination in RBCs that avoids complicated sample handling, chemical labeling and oxidation artifacts pervasive with conventional assays.

#### **3.4.3. Equilibrium Free and Bound Glutathione Levels in Normal RBCs.**

Table 3.3 in the supporting information section summarizes the average equilibrium concentrations of major glutathione species in RBCs, as well as their normalized concentrations to hemoglobin (Hb) and approximate amount (amol) per cell. Ultrafiltration of RBC lysate samples allows for efficient recovery of total protein as the retentate, which can then be reconstituted and reduced with excess DTT to release protein-bound glutathione (PSSG) for subsequent analysis.<sup>44</sup> Indeed, the average equilibrium free GSH/GSSG of  $(460 \pm 43)$  in RBCs measured by CE-ESI-MS with ultrafiltration in this work is similar to whole blood levels reported by Rossi *et al.*<sup>12, 19</sup> using LC-UV after NEM and TCA pretreatment, which has been employed as an index of whole-organism oxidative status, as well as a ratiometric biomarker of disease risk in humans.<sup>15</sup>

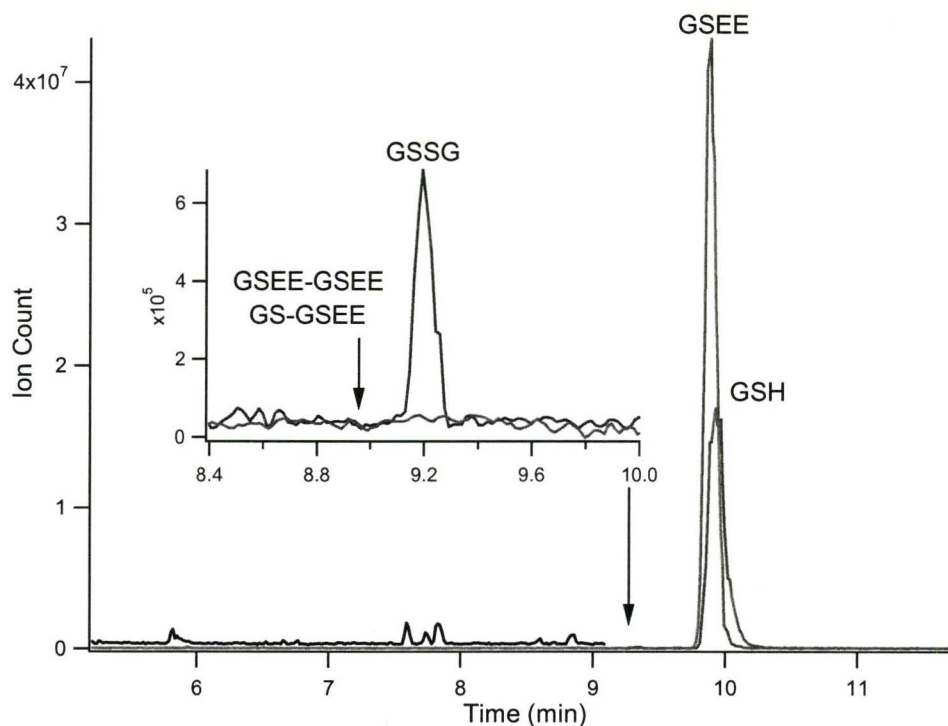


**Figure 3.2.** Recovery study highlighting the lack of oxidation artifacts occurring during sampling processing of filtered RBC lysates with ultrafiltration by spiking 100  $\mu\text{M}$  GSEE in ice-cold de-ionized water which was used for hemolysis. An overall recovery of reduced GSEE was determined to be  $(109 \pm 2)\%$  without detection of the GSEE-GSEE disulfide homodimer ( $\text{MH}^+ = 336$   $m/z$ ) or GS-GSEE disulfide heterodimer ( $\text{MH}_2^{2+} = 321$   $m/z$ ) unlike low micromolar levels of GSSG ( $\text{MH}_2^{2+} = 307$   $m/z$ ) derived from filtered RBC lysates when using CE-ESI-MS. Black trace represents a section of the total ion electropherogram, whereas blue/red traces are extracted ion electropherogram overlays for peptides, which highlights the large dynamic range between high abundance GSH ( $\text{MH}^+ = 308$   $m/z$ ) and minor cationic metabolites present in erythrocytes, including various amino acids and amines.

Glutathionylation of Hb and other classes of protein plays an important role in regulating protein function while representing a significant pool of GSSG during oxidative insult.<sup>54-56</sup> PSSG levels were found to be about three-fold higher than

**Table 3.2.** Impact of sample storage on the accuracy of glutathione analysis from filtered RBC lysates using CE-ESI-MS due to artifactual oxidation.

Storage Condition <sup>a</sup>	GSH (μM)	GSSG (μM)	GSH/GSSG	$E_{GSH^2/GSSG}^b$ (mV)	% Oxidation <sup>b</sup>
Direct analysis	1520 ± 63	3.4 ± 0.3	447 ± 24	-259 ± 2	0.44 ± 0.07
1 <sup>st</sup> freeze-thaw cycle	1550 ± 98	3.5 ± 0.2	443 ± 13	-260 ± 3	0.42 ± 0.04
2 <sup>nd</sup> freeze-thaw cycle	1520 ± 48	17 ± 2	89 ± 6	-238 ± 2	2.2 ± 0.4
3 <sup>rd</sup> freeze-thaw cycle	1430 ± 71	22 ± 1	65 ± 4	-233 ± 2	3.0 ± 0.2

<sup>a</sup> Freeze-thaw comparisons were performed from the same blood sample with the filtered RBC lysate diluted in ammonium acetate, pH 7.0 as described in the methodology, where error represents ± 1σ (n=3).

**Table 3.3.** Artifact-free glutathione analysis of filtered RBC lysates from a healthy adult volunteer using CE-ESI-MS with fingerprick blood microsampling and ultrafiltration.

GSH (μM)	GSSG (μM)	PSSG (μM)	GSH/GSSG	GSH/(GSSG + PSSG)
(1950 ± 130)	(4.2 ± 0.5)	(11.6 ± 0.6)	(461 ± 43)	(123 ± 12)
(6780 ± 470) <sup>a</sup>	(15 ± 2) <sup>a</sup>	(40 ± 2) <sup>a</sup>	--	--
(170 ± 11) <sup>b</sup>	(0.365 ± 0.044) <sup>b</sup>	(1.009 ± 0.052) <sup>b</sup>	--	--

<sup>a</sup> Normalized RBC glutathione levels (nmol/g Hb) derived from a healthy volunteer relative to 288.1 ± 0.4 mg/mL of hemoglobin, where error represents ± 1σ (n=10).

<sup>b</sup> Equivalent RBC glutathione levels per cell (amol/cell) based on an approximate cell volume of 87 fL per RBC (n=10) as reported by B.L. Hogan and E.S. Yeung, *Anal. Chem.* **1992** 64, 2841-2845, where 1 amol = 10<sup>-18</sup> mol.

free GSSG at (11.6 ± 0.6) μM resulting in a GSH/(GSSG+PSSG) ratio of (123 ± 12), which reflects the total oxidized glutathione content within healthy

erythrocytes. These latter results indicate that only about 0.26% of Hb is glutathionylated in healthy RBCs, which is about 10-fold lower than reported in several previous studies for healthy controls.<sup>54, 57, 58</sup> This major discrepancy is most likely associated with oxidation artifacts that produce erroneously elevated levels of PSSG (and GSSG) when sample collection, storage and/or pretreatment steps are not carefully optimized.<sup>44</sup> Our work clearly demonstrates that renewed attention to method validation in assay development is paramount to the successful translation of glutathionylated protein as clinical biomarkers of oxidative stress associated with chronic disease states, ranging from diabetes mellitus, hyperlipidemia, atherosclerosis to human immunodeficiency virus infection.<sup>54</sup>

**3.4.4. Antioxidant Capacity of RBCs via Differential Rates of Glutathione Oxidation.** Overall, glutathione levels were remarkably consistent in normal RBCs (*e.g.*, GSH/GSSG  $\approx$  460) that were collected five different times from the same volunteer over a 8 month interval as summarized in Table 3.4. One of the benefits of direct glutathione analysis by CE-ESI-MS is the ability to perform *ex-vivo* oxidation kinetic studies on unmodified thiols derived from biological samples without chemical labeling. Recently, the apparent pseudo-first order rate constants for oxidation of standard solutions of glutathione and several peptide analogues were determined by CE-UV as a way to compare their antioxidant activity and hydroxyl radical scavenging efficiency.<sup>41</sup> Due to the analytical challenges for global profiling of all antioxidant compounds simultaneously and

their synergistic interactions in complex foods and biological samples, several assays have been developed to estimate total antioxidant capacity using various colorimetric probes and oxidation initiators.<sup>59, 60</sup> Alternatively, endogenous GSH present as the major intra-cellular thiol can serve as a natural substrate for oxidation reactions without extrinsic reporter probes, where the apparent rates of GSH depletion and/or GSSG formation are representative of the total antioxidant capacity for all low molecular weight constituents within the cytosol (*i.e.*, metabolome). In this work, *ex-vivo* metal-catalyzed oxidation (MCO) studies using equimolar concentrations of  $\text{H}_2\text{O}_2/\text{Cu}^{2+}$  (35  $\mu\text{M}$ ) at 37°C was performed for *in-situ* generation of the hydroxyl radical ( $\cdot\text{OH}$ ) as an initiator via a Fenton-like redox reaction mechanism,<sup>41</sup> which has been previously demonstrated to induce oxidative protein modifications that were inhibited by GSH.<sup>40</sup> Although the reaction rate is dependent on the absolute concentration of  $\text{H}_2\text{O}_2$ , concentration ratio of  $\text{H}_2\text{O}_2/\text{Cu}^{2+}$  and/or sample pH,<sup>41</sup> conditions in this work were optimized using healthy erythrocytes as a biological reference in order to generate a steady rate of GSH oxidation within an experimental timeframe convenient for multiple sampling. Figure 3.3(a) highlights a series of extracted ion electropherograms for GSH ( $\text{MH}^+ = 308 \text{ m/z}$ ) and GSSG ( $\text{MH}_2^{2+} = 307 \text{ m/z}$ ) derived from filtered RBC lysates using CE-ESI-MS at different stages of oxidation until near quantitative conversion of free GSH into GSSG. Figure 3.3(b) shows the full oxidation kinetic profile for GSH and GSSG in terms of their time-dependent changes in

**Table 3.4.** Comparison of various thermodynamic and kinetic parameters for assessing the intra-cellular redox status and antioxidant capacity of filtered RBC lysates by DIRGO using CE-ESI-MS.

Experiments/Controls	GSH/GSSG	Oxidation (%)	$E_{GSH^2/GSSG}^a$ (mV)	$k$ (min <sup>-1</sup> ) <sup>b</sup> × 10 <sup>-2</sup>		$t_{CO}^b$ (min)	Hemoglobin (mg/mL)
				GSH	GSSG		
Normal RBC lysate (n=15) <sup>c</sup>	465 ± 38	0.43 ± 0.08	-262 ± 2	-1.27 ± 0.05	1.41 ± 0.05	59.2 ± 1.0	206.6 ± 0.9
CDNB-incubated RBC (n=3)	192 ± 15	1.03 ± 0.14	-238 ± 2	-3.33 ± 0.24	5.87 ± 0.25	13.5 ± 0.5	209.1 ± 0.7
NAC-incubated RBC (n=3)	520 ± 32	0.38 ± 0.05	-263 ± 2	-1.58 ± 0.08	0.79 ± 0.10	124 ± 3	170.2 ± 1.1
Auto-oxidation of RBC lysate <sup>d</sup> (n=3)	423 ± 26	0.47 ± 0.01	-259 ± 2	-0.043 ± 0.003	0.035 ± 0.003	1820 ± 55	216.1 ± 0.8
GSH/GSSG standard mixture <sup>d</sup> (n=3)	500	--	--	-0.24 ± 0.01	0.19 ± 0.03	312 ± 14	--

<sup>a</sup> Half-cell reduction potential estimated by Nernst equation:  $E_{GSH^2/GSSG} = E^o - 59.1/2 \cdot \log([GSH]^2/[GSSG])$  with  $E^o = -264$  mV at pH 7.4, whereas % oxidation of glutathione was calculated by  $2[GSSG] \times 100 / (2[GSSG] + [GSH])$ .<sup>11</sup>

<sup>b</sup> Apparent rate constant ( $k$ ) and cross-over time ( $t_{CO}$ ) for metal-catalyzed ( $H_2O_2/Cu^{2+}$ ) glutathione oxidation reactions based on pseudo-first order reaction kinetics involving  $2GSH + 2 \cdot OH \rightarrow GSSG + 2H_2O$

<sup>c</sup> MCO were performed on RBC lysates collected on 5 separate occasions over an 8 month period. Each trial was performed in triplicate for a total  $n=15$ . Otherwise, all other studies were measured in triplicate ( $n=3$ ) from a single blood sample collection.

<sup>d</sup> Control studies involving the auto-oxidation of GSH in filtered RBC lysates without addition of  $H_2O_2/Cu^{2+}$  catalyst, as well as the oxidation kinetics of a standard solution of GSH/GSSG at 1500  $\mu$ M and 3 $\mu$ M, respectively.

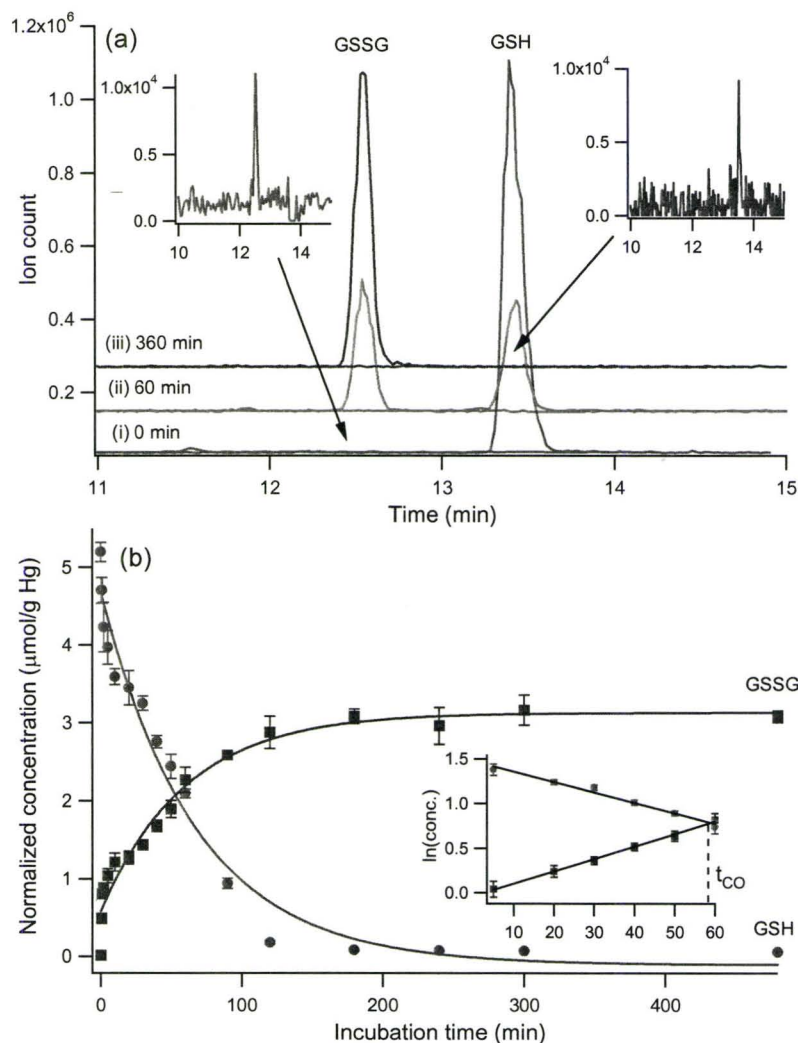


**Figure 3.3.** *Ex-vivo* metal-catalyzed oxidation kinetic studies on filtered RBC lysates (normal) based on the apparent rates of GSH consumption ( $k_{GSH}$ ) and GSSG ( $k_{GSSG}$ ) formation for assessment of intra-cellular redox status and antioxidant capacity by CE-ESI-MS. (a) Extracted ion electropherograms highlighting qualitative changes in GSH and GSSG levels due to oxidation by  $\cdot\text{OH}$  as a function of incubation time. (b) Non-linear oxidation kinetic plots measured for GSH and GSSG in healthy RBCs as a biological reference ( $n = 3$ ), where the inset shows adherence to a pseudo-first order rate law ( $R^2 > 0.997$ ) with  $t_{CO}$  defined as the cross-over time interval at the intersection of GSH and GSSG linearized kinetic plots.

normalized concentrations ( $\mu\text{mol/g Hb}$ ) performed in triplicate ( $n = 3$ ). The inset of Figure 3.3(b) demonstrates that a good linear correlation ( $R^2 > 0.995$ ) was

achieved based on a pseudo-first rate law for determination of the apparent rate constants for GSH depletion ( $k_{GSH}$ ) and GSSG formation ( $k_{GSSG}$ ).<sup>41</sup> Interestingly, the  $k_{GSSG}$  of  $(1.41 \pm 0.05) \times 10^{-2} \text{ min}^{-1}$  was significantly ( $P < 0.05$ ) greater than  $k_{GSH}$  within protein-free RBC lysates, however both rates were determined to be over 5-to-7 fold faster relative to a standard solution containing physiological levels of glutathione (*i.e.*,  $\text{GSH}/\text{GSSG} \approx 500$ ) in de-ionized water as shown in Table 3.4. The inset of Figure 3.3(b) also highlights the apparent cross-over time ( $t_{CO}$ ) for oxidation defined as the intersection of GSH and GSSG pseudo-first order rate plots, which represents a characteristic time parameter reflective of overall glutathione reactivity since different observed  $k_{GSH}$  and  $k_{GSSG}$  values translate into non-equivalent half-life times (*i.e.*,  $t_{1/2} = \ln 2/k$ ). For instance,  $t_{CO}$  measured for glutathione oxidation in de-ionized water relative to normal filtered RBC lysates was dramatically shortened over 5-fold from  $(312 \pm 14) \text{ min}$  to  $(59.2 \pm 1.0) \text{ min}$ , respectively. Table 3.4 also indicates that auto-oxidation of GSH in filtered RBC lysates without addition of  $\text{H}_2\text{O}_2/\text{Cu}^{2+}$  catalyst was extremely slow and negligible within the timeframe of MCO experiments. Thus, both  $k_{GSSG}$  (or  $k_{GSH}$ ) and  $t_{CO}$  parameters highlight the significant impact of sample matrix composition in the cytosol (*e.g.*, nutrients, metals, metabolites) on the measured rates of glutathione oxidation with *ex-vivo* RBC lysates having a substantially greater susceptibility to hydroxyl radical oxidation relative to de-ionized water despite equivalent initial glutathione levels in solution.

**3.4.5. *In-vitro* Preincubation of RBCs with Electrophilic Reagents.** *In-vitro* preincubation experiments were performed as a way to assess the impact of different exogenous reagents on the redox status and intra-cellular antioxidant capacity of intact erythrocytes. In this study, 1-chloro-2,3-dinitrobenzene (CDNB) was selected as a model chemical stressor in order to mimic acute oxidative stress conditions induced by electrophilic detoxification and GSH depletion.<sup>61</sup> Upon diffusion across the cell membrane of RBCs, CDNB is efficiently conjugated by glutathione *S*-transferases to form the 2,3-dinitrobenzene-*S*-glutathione (DBN-SG) adduct.<sup>62</sup> Figure 3.4(a) highlights a series of extracted ion electropherograms at different stages of MCO when using filtered RBC lysates pre-incubated with CDNB, confirming the formation of the stable DBN-SG thioether conjugate ( $MH^+ = 474\ m/z$ ) that resisted further oxidation during the experiment. Table 3.2 shows that the intra-cellular concentration of GSH was considerably depleted in RBCs relative to normal cells by about 40% with a concentration of  $(720 \pm 52)\mu\text{M}$  after CDNB exposure without significant changes to GSSG, which resulted in a decrease in GSH/GSSG to  $(194 \pm 21)$  or an increase of  $E_{GSSG/2GSH}$  to  $(-238 \pm 2)$  mV. Previous studies have demonstrated that relative changes in  $E_{GSSG/2GSH}$  exceeding about +40 mV and +80 mV can trigger cell differentiation and programmed cell death respectively,<sup>10, 11, 52</sup> which were avoided in this work by the short incubation times used to avoid hemolysis. In addition to significant changes in the initial redox status, Figure 3.4(b) also shows that CDNB pre-

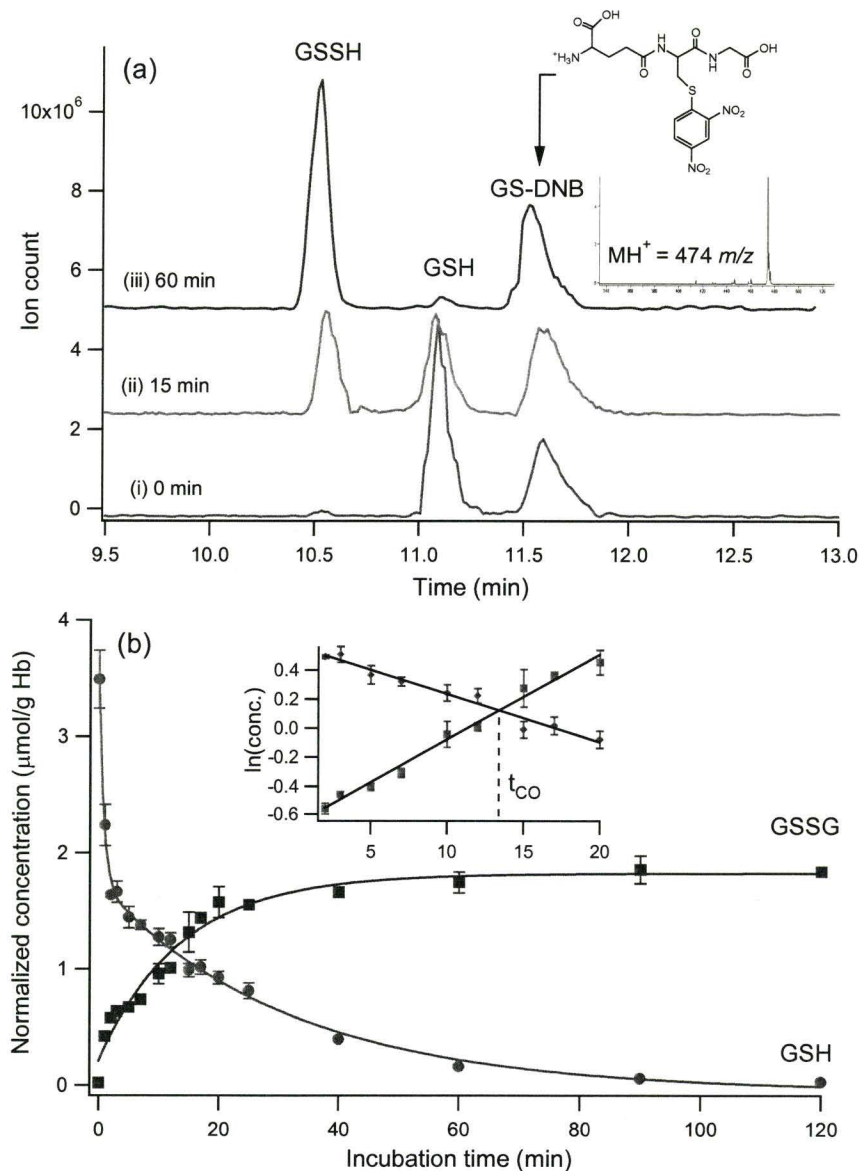


**Figure 3.4** *Ex-vivo* metal-catalyzed oxidation kinetic studies on filtered RBC lysates after preincubation of intact erythrocytes with CDNB. (a) Extracted ion electropherograms highlighting qualitative changes in GSH and GSSG due to oxidation by  $\cdot\text{OH}$  as a function of incubation time, which confirms the formation of the stable/unreactive GS-DNB thioether conjugate. (b) Overall, accelerated oxidation kinetics were observed for CDNB-stressed RBCs relative to normal cells due to GSH depletion as reflected by significantly faster apparent  $k_{GSSG}$  and shorter  $t_{CO}$  as compared to Figure 3.3.

incubated RBC lysates also display considerably faster rates of oxidation with near complete conversion of depleted GSH to GSSG within about 60 min. Table 3.2 highlights that CDNB-stressed RBCs were observed to have over a four-fold faster oxidation rate relative to normal cells as reflected by  $k_{GSSG}$  and  $t_{CO}$  of  $(5.87 \pm 0.25) \times 10^{-2} \text{ min}^{-1}$  and  $(13.5 \pm 0.5) \text{ min}$ , respectively. Vaher *et al.* previously measured the concentration-dependence of GSH oxidation kinetics with  $\text{H}_2\text{O}_2/\text{Cu}^{2+}$  using a pseudo-first order rate law that showed faster reaction rates for GSSG formation upon peptide dilution under similar reaction conditions.<sup>41</sup> Similarly, our studies reveal that cellular oxidative stress caused by GSH depletion from electrophilic reagents can be inferred by the differential rates of glutathione oxidation (DIRGO), where a relative shorter  $t_{CO}$  is indicative of an increased susceptibility to cellular damage from reactive free radicals as compared to healthy controls. Thus, multiple thermodynamic and kinetic parameters associated with glutathione metabolism can serve as complementary indicators of oxidative stress status with improved diagnostic value for early detection of chronic diseases prior to clinical symptoms.<sup>9</sup>

#### **3.4.6. *In-vitro* Preincubation of RBCs with Antioxidant Supplements.**

*N*-acetyl-*L*-cysteine (NAC) is a widely used thiol nutritional supplement<sup>63</sup> and mucolytic agent<sup>64</sup> that has been reported to act as a free radical scavenging agent and/or putative cysteine pro-drug for glutathione biosynthesis.<sup>65</sup> Given this context, *in-vitro* preincubation studies of intact erythrocytes were also performed

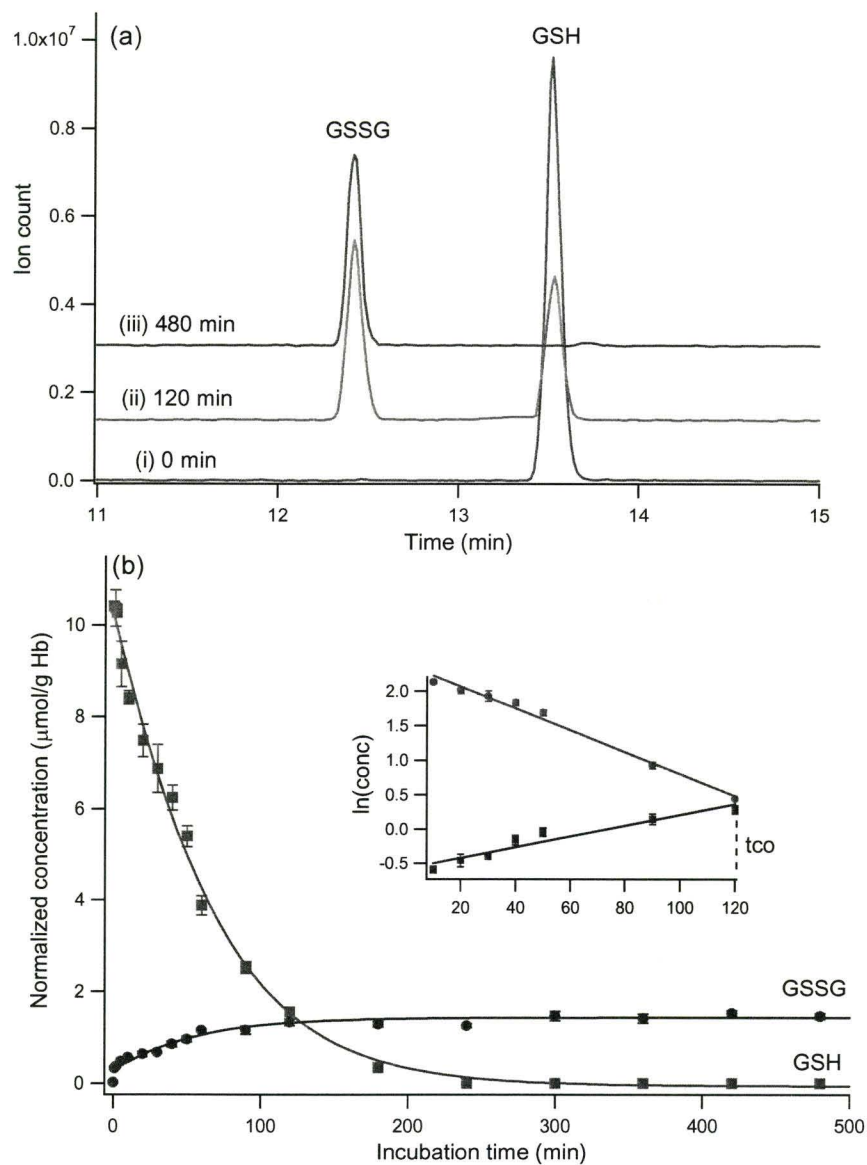


**Figure 3.5.** Metal-catalyzed oxidation kinetic studies on filtered RBC lysates after preincubation of intact erythrocytes with NAC. (a) Extracted ion electropherograms highlighting qualitative changes in GSH and GSSG (initial concentrations unchanged relative to normal cells) due to oxidation by  $\cdot\text{OH}$  as a function of incubation time, which confirms the increased free radical scavenging efficiency of NAC-fortified cells. (b) Overall, attenuated oxidation kinetics were observed for NAC-enriched RBCs relative to normal cells as reflected by significantly slower apparent  $k_{GSSG}$  and longer  $t_{CO}$  in comparison to Figure 3.3.

with NAC after which filtered RBC lysates were subsequently analyzed by DIRGO using CE-ESI-MS. Figure 3.5 of the supporting information section depicts a series of electropherograms at different stages of oxidation for NAC-enriched erythrocytes, as well as pseudo-first order kinetic plots showing a markedly attenuated rate for GSSG formation. Table 3.4 summarizes both thermodynamic and kinetic parameters for characterizing the impact of NAC uptake by RBCs, which was present at a similar concentration level ( $\approx 2$  mM) as endogenous GSH. Overall, there was no significant change in initial GSH concentration levels ( $P < 0.05$ ), GSH/GSSG, nor  $E_{GSSG/2GSH}$  based on the conditions used in the study. However, DIRGO experiments revealed that  $k_{GSSG}$  was considerably slower relative to normal RBCs, which resulted in a 2-fold increase in  $t_{CO}$  to  $(124 \pm 3)$  min. Further investigations using CE under alkaline conditions with negative ion-mode ESI-MS confirmed the generation of the NAC-NAC homodimer ( $M-H^+ = 323$   $m/z$ ) and GS-NAC glutathione-mixed disulfide ( $M-H^+ = 467$   $m/z$ ) that reached steady-state levels during early and late-stages of MCO (refer to Figure 3.6). Thus, the slower observed rate in GSSG formation can be attributed to the competitive yet additive free radical scavenging capacity of NAC in the presence of endogenous GSH, which results in the formation of a GS-NAC mixed disulfide adduct. These results are consistent with the widely accepted clinical practice of emergency intravenous NAC administration as an antidote for acetaminophen poisoning,<sup>66</sup> where its efficient free radical scavenging properties coupled with its thiol-disulfide exchange reactivity can

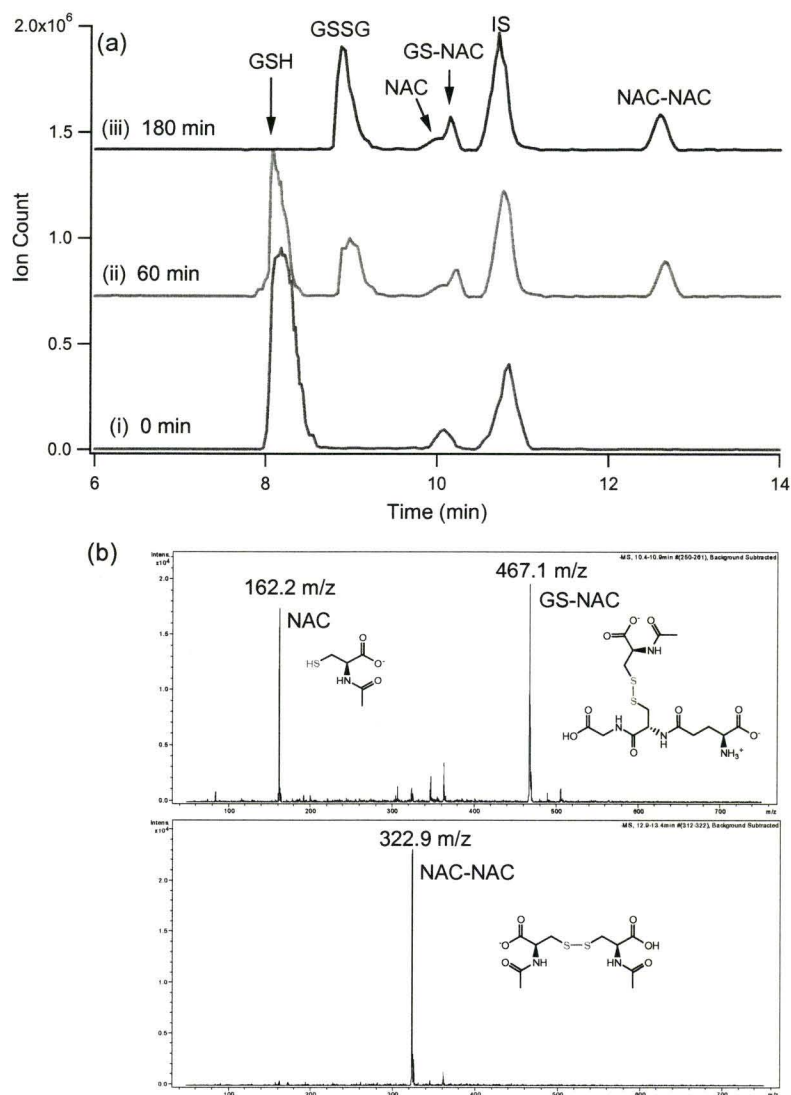


**Figure 3.6.** (a) Series of extracted ion electropherograms when using anionic CE conditions with negative-ion mode ESI-MS detection for simultaneous analysis of GSH and GSSG from NAC-enriched RBCs, as well as acidic metabolites not amenable to separations under acidic CE conditions, including NAC, NAC-NAC and GS-NAC (where IS represents HQSA). Note that NAC-NAC and GS-NAC disulfide levels rapidly increase at early stages of metal-catalyzed oxidation (not detectable at  $t = 0$  min), but do not significantly change from 60 min to 180 min unlike GSH, GSSG and NAC. (b) ESI-MS spectra confirming the identification of disulfide adducts formed during metal-catalyzed oxidation reactions, namely NAC-NAC and GS-NAC.

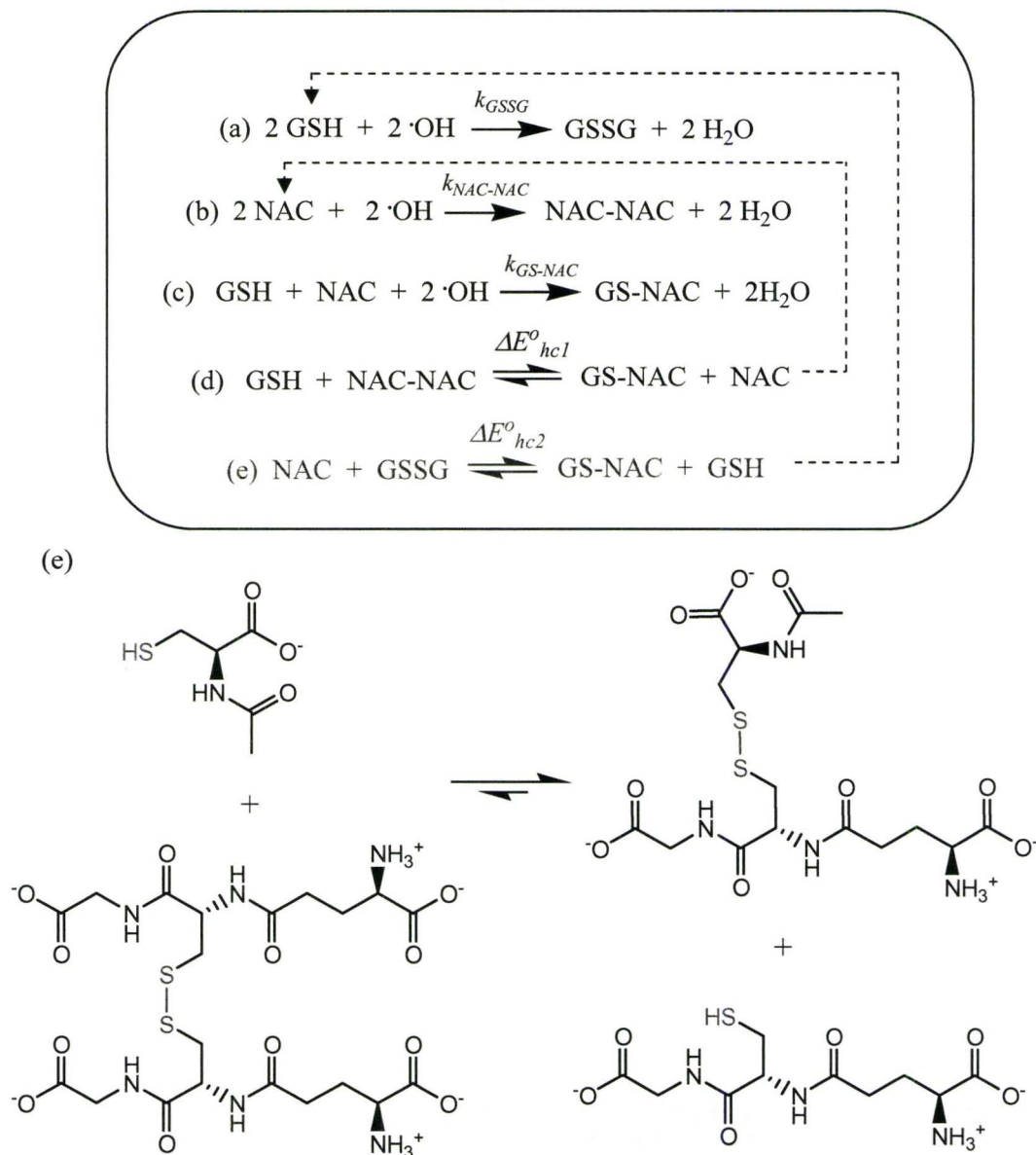


**Figure 3.7.** Proposed mechanism for describing the enhanced antioxidant capacity of NAC-enriched RBCs relative to normal cells based on competitive irreversible reactions (a-c) involving the direct reduction of free radicals ( $\cdot\text{OH}$ ) by GSH and/or NAC, as well as a reversible thiol-exchange reactions (d, e) associated with GSH/NAC-NAC and NAC/GSSG. The latter reversible reaction is thermodynamically favored towards the forward direction with  $\Delta E_{hc2}^{\circ} \approx +63 \text{ mV}$ .<sup>43</sup> The greater reduction potential of NAC provides a driving force for catalytic renewal of GSH during oxidative insult that is reflected by slower apparent  $k_{\text{GSSG}}$  and longer  $t_{\text{CO}}$  shown in Figures 3.5/3.6 of the supporting information section relative to normal RBCs.

contribute to a rapid re-establishment of cellular redox homeostasis. Figure 3.7 summarizes the competitive irreversible and coupled reversible reactions in this system, as well as the putative biological mechanism of NAC for replenishing intra-cellular GSH levels during oxidative insult, which is driven by the greater half-cell standard reduction potential of NAC ( $\Delta E_{hc}^{\circ} \approx +63$  mV for NAC relative to GSH),<sup>43</sup> thus favoring GSH regeneration via a reversible thiol-exchange reaction with rising levels of GSSG (refer to step e of Figure 3.7). This catalytic mechanism for supporting GSH levels while slowing down the rate of GSSG formation during acute oxidative stress is distinct from the hypothesized mechanism of NAC action involving deacetylation for increasing intra-cellular cysteine concentration levels as the rate-determining step in *de novo* GSH biosynthesis.<sup>64, 65</sup> Indeed, future *in-vivo* studies using validated analytical assays are warranted to better understand the specific mechanisms and therapeutic benefits of antioxidant supplementation and drug detoxification in relation to oxidative stress, glutathione metabolism and human health.

### 3.5 Conclusions

CE-ESI-MS in conjunction with ultrafiltration offers an artifact-free method for reliable analysis of glutathione metabolites in biological samples with high selectivity and sensitivity without complicated off-line sample pretreatment. A rigorous validation of the optimized assay was performed to avoid oxidation

artifacts generated during sample processing and chemical analysis that can bias measurements of GSSG, PSSG and GSH/GSSG or  $E_{GSSG/2GSH}$  due to the lability and high concentration levels of GSH in most cell types. DIRGO was explored as an alternative strategy to assess intra-cellular antioxidant capacity using GSH as an endogenous redox-active probe in filtered RBC lysate samples. Multiple thermodynamic and kinetic parameters associated with glutathione metabolism/reactivity can be used to deduce the impact of intrinsic metabolomic contents or extrinsic reagents on the redox status and hydroxyl radical scavenging efficacy of cells. For instance, oxidative stress conditions associated with GSH depletion due to uptake of electrophilic reagents (*e.g.*, CDNB) was inferred by a significant increase in  $E_{GSSG/2GSH}$  and  $k_{GSSG}$  but a shorter  $t_{CO}$  as compared to normal RBCs, which is consistent with detoxification via GS-DNB thioether conjugate formation. In contrast, active-transport of thiol-based antioxidants (*e.g.*, NAC) within RBCs resulted in no significant perturbations in  $E_{GSSG/2GSH}$  however a considerable decrease in  $k_{GSSG}$  with a longer  $t_{CO}$  was measured relative to normal RBCs. The latter observations together with the detection of NAC-NAC homodimer and GS-NAC mixed disulfide indicate that NAC functions both as a competitive antioxidant and reducing agent with greater disulfide formation tendency to replenish GSH levels via a thiol/disulfide exchange mechanism with GSSG during acute oxidative insult. Future studies will survey the inter-individual variability of thermodynamic and kinetic parameters associated with glutathione metabolism using DIRGO among a larger population of healthy

controls relative to various clinical samples. In addition, *in-vitro* studies involving direct oxidant exposure to intact cells will also be performed in order to assess the relative contribution of protein (*i.e.*, hemoglobin) in maintaining intra-cellular redox homeostasis. The advent of nutritional metabolomics<sup>67</sup> in concert with validated analytical techniques for the quantification of biomarkers of oxidative stress<sup>68</sup> promise new breakthroughs in health promotion, disease prognosis and personalized medicine, while offering deeper insight into the etiology of diseases associated with oxidative stress and impaired glutathione metabolism.

### **Acknowledgements**

This work is supported by funds provided by the National Science and Engineering Research Council of Canada and the Canada Foundation for Innovation. R.L. acknowledges support in the form of an Ontario Graduate Scholarship. The authors thank Dr. Adam S. Ptolemy for assistance with the development of the fingerprick microsampling procedure.

### **3.6 References**

- (1) Wu, G.; Fang, Y.-Z.; Yang, S.; Lupton, J. R.; Turner, N. D. *J. Nutrition* **2004**, *134*, 489-492.
- (2) Hayes, J. D.; McLellan, L. I. *Free Radic. Res.* **1999**, *31*, 273-300.
- (3) Sies, H. *Free Radic. Biol. Med.* **1999**, *27*, 916-921.

- (4) Winkler, B. S.; Orselli, S. M.; Rex, T. S. *Free Radic. Biol. Med.* **1994**, *17*, 333-349.
- (5) Dalle-Donne, I.; Rossi, R.; Giustarini, D.; Colombo, R.; Milzani, A. *Free Rad. Biol. Med.* **2007**, *43*, 883-898.
- (6) Singh, S. P.; Wishnok, J. S.; Keshive, M.; Deen, W. M.; Tannenbaum, S. R. *Proc. Natl. Acad. Sci. USA* **1996**, *93*, 14428-14433.
- (7) Vale, N.; Moreira, R.; Gomes, P. *Eur. J. Med. Chem.* **2008**, *44*, 937-953.
- (8) Soga, T.; Baran, R.; Suematsu, M.; Ueno, Y.; Ikeda, S.; Sakurakawa, T.; Kakazu, Y.; Ishikawa, T.; Robert, M.; Nishioka, T.; Tomita, M. *J. Biol. Chem.* **2006**, *281*, 16768-16776.
- (9) Mirochnitchenko, O.; Weisbrot-Lefkowitz, M.; Ruehl, K.; Chen, L.; Yang, C.; Inouye, M. *J. Biol. Chem.* **1999**, *274*, 10349-10355.
- (10) Kranner, I.; Birtic, S.; Anderson, K. M.; Pritchard, H. W. *Free Radic. Biol. Med.* **2006**, *40*, 2155-2165.
- (11) Schafer, F. Q.; Buettner, G. R. *Free Radic. Biol. Med.* **2001**, *30*, 1191-1212.
- (12) Rossi, R.; Dalle-Donne, I.; Milzani, A.; Giustarini, D. *Clin. Chem.* **2006**, *52*, 1406-1414.
- (13) Galleman, D.; Eyer, P. *Anal. Biochem.* **1990**, *191*, 347-353.
- (14) Camera, E.; Picardo, M. *J. Chromatogr. B* **2002**, *781*, 181-206.
- (15) Pastore, A.; Federici, G.; Bertini, E.; Piemonte, F. *Clinica Chimica Acta* **2003**, *333*, 19-39.

- (16) Santori, G.; Domenicotti, C.; Bellocchio, A.; Pronzato, M. A.; Marinari, U. M.; Cottalasso, D. *J. Chromatogr. B* **1997**, *695*, 427-433.
- (17) Nemeth, I.; Orvos, H.; Boda, D. *Free Radic. Biol. Med.* **2001**, *30*, 715-721.
- (18) Rossi, R.; Milzani, A.; Dalle-Donne, I.; Giustarini, D.; Lusini, L.; Colombo, R.; Di Simplicio, P. *Clin. Chem.* **2002**, *48*, 742-753.
- (19) Giustarini, D.; Dalle-Donne, I.; Colombo, R.; Milzani, A.; Rossi, R. *Free Radic. Biol. Med.* **2003**, *35*, 1365-1372.
- (20) Steghens, J. P.; Flourie, F.; Arab, K.; Collombel, C. *J. Chromatogr. B* **2003**, *798*, 343-349.
- (21) Raththagala, M.; Root, P. D.; Spence, D. M. *Anal. Chem.* **2006**, *78*, 8556-8560.
- (22) Srivastava, S. K.; Beutler, E. *Anal. Biochem.* **1968**, *25*, 75-76.
- (23) Tietze, F. *Anal. Biochem.* **1969**, *27*, 502-522.
- (24) Beutler, E.; Srivastava, S. K.; West, C. *Biochem. Biophys. Res. Commun.* **1970**, *38*, 341-347.
- (25) Carru, C.; Zinellu, A.; Pes, G. M.; Marongiu, G.; Tadolini, B.; Deiana, L. *Electrophoresis* **2002**, *23*, 1716-1721.
- (26) Piccoli, G.; Florani, M.; Biagiarelli, B.; Palma, F.; Amicucci, A.; Stocchi, V. *J. Chromatogr. A* **1994**, *676*, 239-246.
- (27) Jones, D. P. *Am. J. Physiol. Cell Physiol.* **2008**, *295*, C849-C868.
- (28) Jones, D. P. *Antioxidants & Redox Signalling* **2006**, *8*, 1865-1879.

- (29) Zinellu, A.; Sotgia, S.; Posadino, A. M.; Pasciu, V.; Zinellu, E.; Usai, M. F.; Scanu, B.; Chessa, R.; Gaspa, L.; Tadolini, B.; Deiana, L.; Carru, C. *Electrophoresis* **2007**, *28*, 3277-3283.
- (30) Maeso, N.; Garcia-Martinez, D.; Ruperez, F. J.; Cifuentes, A.; Barbas, C. *J. Chromatogr. B* **2005**, *822*, 61-69.
- (31) Wang, W.; Xin, H.; Shao, H.; Jin, W. *J. Chromatogr. B* **2003**, *789*, 425-429.
- (32) Serru, V.; Baudin, B.; Ziegler, F.; David, J.-P.; Cals, M.-J.; Vaubourdolle, M.; Mario, N. *Clin. Chem.* **2001**, *47*, 1321-1324.
- (33) Shihabi, Z. K.; Hinsdale, M. E.; Cheng, C. P. *Electrophoresis* **2001**, *22*, 2351-2354.
- (34) Jin, W.; Li, W.; Xu, Q. *Electrophoresis* **2000**, *21*, 774-779.
- (35) Novatchev, N.; Holzgrabe, U. *Chromatographia* **2003**, *57*, 345-349.
- (36) Chalcraft, K. R.; Lee, R.; Mills, C.; Britz-McKibbin, P. *Anal. Chem.* **2009**, *81*, 2506-2515.
- (37) Chalcraft, K. R.; Britz-McKibbin, P. *Anal. Chem.* **2009**, *81*, 307-314.
- (38) Lee, R.; Ptolemy, A. S.; Niewczas, L.; Britz-McKibbin, P. *Anal. Chem.* **2007**, *79*, 403-415.
- (39) Huang, D.; Ou, B.; Priot, R. L. *J. Agric. Food Chem.* **2005**, *53*, 1841-1856.
- (40) Kato, Y.; Kitamoto, N.; Kawai, Y.; Osawa, T. *Free Radi. Bio. Med.* **2001**, *31*, 624-632.

- (41) Vaher, M.; Viirlaid, S.; Ehrlich, K.; Mahlapuu, R.; Jarvet, K.; Soomets, U.; Kaljurand, M. *Electrophoresis* **2007**, *27*, 2582-2589.
- (42) Mahlapuu, R.; Vaher, M.; Ehrlich, K.; Kaljurand, M.; Soomets, U. *J. Pept. Sci.* **2006**, *2006*, 796-799.
- (43) Noszal, B.; Visky, D.; Kraszni, M. *J. Med. Chem.* **2000**, *43*, 2176-2182.
- (44) Giustarini, D.; Dalle-Donne, I.; Colombo, R.; Petralia, S.; Giampaolletti, S.; Milzani, A.; Rossi, R. *Clin. Chem.* **2003**, *49*, 327-330.
- (45) He, T.; Quinn, D.; Fu, E.; Wang, Y. K. *J. Chromatogr. B* **1999**, *727*, 43-52.
- (46) Bouligand, J.; Deroussent, A.; Paci, A.; Morizet, J.; Vassal, G. *J. Chromatogr. B* **2006**, *832*, 67-74.
- (47) Rellan-Alvarez, R.; Hernandez, L. E.; Abadia, J.; Alvarez-Fernandez, A. *Anal. Biochem.* **2006**, *356*, 254-264.
- (48) Reed, D. J.; Babson, J. R.; Beatty, P. W.; Brodie, A. E.; Ellis, W. W.; Potter, D. W. *Anal. Biochem.* **1980**, *106*, 55-62.
- (49) Bouligand, J.; Deroussent, A.; Paci, A.; Marizet, J.; Vassal, G. *J. Chromatogr. B* **2006**, *832*, 67-74.
- (50) Guan, X.; Hoffman, B.; Dwivedi, C.; Mathees, D. P. *J. Pharma. Biomed. Anal.* **2003**, *31*, 251-261.
- (51) Kirilin, W. G.; Cai, J. Y.; Thompson, S. A.; Diaz, D.; Kavanagh, T. J.; Jones, D. P. *Free Radic. Biol. Med.* **1999**, *27*, 1208-1218.

- (52) Hiroi, M.; Ogihara, T.; Hirano, K.; Hasegawa, M.; Morinobu, T.; Tamai, H.; Niki, E. *Free Radic. Biol. Med.* **2005**, *38*, 1057-1072.
- (53) Gutscher, M.; Pauleau, A.-L.; Marty, L.; Brach, T.; Wabnitz, G. H.; Samstag, Y.; Meyer, A. J.; Dick, T. P. *Nature Methods* **2008**, *5*, 553-559.
- (54) Niwa, T. *J. Chromatogr. B* **2007**, *855*, 59-65.
- (55) Sparaco, M.; Gaeta, L. M.; Tozzi, G.; Bertini, E.; Pastore, A.; Simonati, A.; Santorelli, F. M.; Piemonte, F. *J. Neurosci. Res.* **2006**, *83*, 256-263.
- (56) Bursell, S. E.; King, G. L. *Clin. Chem.* **2000**, *46*, 145-146.
- (57) Pastore, A.; Mozzi, A. F.; Tozzi, G.; Gaeta, L. M.; Federici, G.; Bertini, E.; Russo, A. L.; Mannucci, L.; Piemonte, F. *Anal. Biochem.* **2003**, *312*, 85-90.
- (58) Niwa, T.; Naito, C.; Mawjood, A. H. M.; Imai, K. *Clin. Chem.* **2000**, *46*, 82-88.
- (59) Huang, D.; Ou, B.; Prior, R. L. *J. Agric. Food Chem.* **2005**, *53*, 1841-1856.
- (60) Antolovich, M.; Prenzler, P. D.; Patsalides, E.; McDonald, S.; Robards, K. *Analyst* **2002**, 183-198.
- (61) Stoeltinga, M. S.; Tjeerdema, R. S. *Aquatic Toxicology* **2000**, *50*, 177-187.
- (62) Awasthi, Y. C.; Garg, H. S.; Dao, D. D.; Partridge, C. A.; Srivastava, S. K. *Blood* **1981**, *58*, 733-738.
- (63) Sen, C. K. *Molec. Cellular Biochem.* **1999**, *196*, 31-42.

- (64) Atkuria, K. R.; Mantovania, J. J.; Herzenberg, L. A.; Herzenberg, L. A. *Current Opinion in Pharmacol.* **2007**, *7*, 355-359.
- (65) Zafarullah, M.; Li, W. Q.; Sylvester, J.; Ahmad, M. *Cell. Mol. Life Sci.* **2003**, *60*, 6-20.
- (66) Prescott, L. *Ann. Emerg. Med.* **2005**, *45*, 409-413.
- (67) Rezzi, S.; Ramadan, Z.; Fay, L. B.; Kochhar, S. *J. Prot. Res.* **2007**, *6*, 513-525.
- (68) Dalle-Donne, I.; Rossi, R.; Colombo, R.; Giustarini, D.; Milzani, A. *Clin. Chem.* **2006**, *52*, 601-623.

*Chapter IV*

Differential Metabolomics for Quantitative Assessment of Cellular Oxidative Stress and Antioxidant Efficacy with Strenuous Aerobic Exercise: Redox-Control of Cellular Metabolism by N-acetyl-L-Cysteine

#### **IV. Differential Metabolomics for Quantitative Assessment of Cellular Oxidative Stress and Antioxidant Efficacy with Strenuous Aerobic Exercise: Redox-Control of Cellular Metabolism by N-Acetyl-L-Cysteine.**

##### **4.1 Abstract**

Currently there is conflicting evidence on the causative role that oxidative stress plays in human health given the beneficial and detrimental effects of reactive oxygen/nitrogen species (RONS) in cellular metabolism. Herein, we introduce a differential metabolomics strategy using capillary electrophoresis-electrospray ionization-mass spectrometry (CE-ESI-MS) for quantitative assessment of oxidative stress and antioxidant efficacy in erythrocytes with strenuous aerobic exercise as a model system. A healthy untrained volunteer was recruited to perform a sub-maximal prolonged ergometer cycling trial until exhaustion with frequent blood collection over a six hour time interval, which included pre-, during and post-exercise periods while at rest. A follow-up study was subsequently performed by the subject after a high-dose oral supplementation with *N*-acetyl-*L*-cysteine (NAC) prior to performing the same exercise protocol under standardized conditions. Differential metabolomic analyses of filtered red blood cell (RBC) lysates by CE-ESI-MS in conjunction with univariate/multivariate data analysis revealed a significant attenuation of oxidative stress associated with high-dose oral NAC intake, which allowed for the discovery of multiple early- and late-stage biomarkers of oxidative stress. Several quantitative parameters associated with the early-stage biomarkers, reduced glutathione (GSH) and oxidized glutathione (GSSG), were explored to assess the

efficacy of NAC intervention to attenuate oxidative stress relative to the control, such as a greater half-cell reduction potential for glutathione at peak oxidation ( $\Delta E_{peak} \approx +15$  mV) and a shorter recovery time to return to redox homeostasis similar to pre-exercise conditions ( $\Delta t_{rec} \approx 100$  min). Noteworthy, late-stage biomarkers of oxidative stress were markedly downregulated following high-dose oral NAC intake as well as remaining at lower levels post-exercise relative to the control, namely 3-methylhistidine (3-MeHis), *L*-carnitine (C0), *O*-acetyl-*L*-carnitine (C2) and creatine (Cre). Our preliminary results suggest that NAC is effective at mediating acute episodes of oxidative stress with reduced fatigue by modulating cellular metabolism transiently towards lower energy requirements and a pro-anabolic metabolic state. This work demonstrates the proof-of-principle that timely nutritional intervention can effectively attenuate exercise-induced oxidative stress by unanticipated yet reversible global perturbations in metabolism that has important implications in human health, ranging from athletic training to disease prevention.

## 4.2. Introduction

The oxidative stress hypothesis represents a dominant yet contentious paradigm in biology derived from the free radical generation theory for aging,<sup>1,2</sup> which can be described as a deleterious perturbation in the prooxidant-antioxidant balance leading to cellular degeneration and death.<sup>3</sup> Energy harnessed by aerobic organisms via oxidative phosphorylation results in the generation of reactive

oxygen/nitrogen species (RONS) that must be controlled by antioxidant systems evolved to prevent or repair oxidative damage to macromolecules.<sup>4</sup> Earlier studies have demonstrated that obligate anaerobes display low tolerance of oxygen due to the lack of key enzymes (*e.g.*, superoxide dismutase) for scavenging oxidative by-products of aerobic respiration, whereas air-tolerant microbes exhibit increased susceptibility to oxidative injury with growth inhibition under hyperoxic conditions.<sup>5</sup> Other pathways of oxygen toxicity due to superoxide anion, hydrogen peroxide and hydroxyl radical formation occur during oxygen transport,<sup>6</sup> host immune response,<sup>7</sup> xenobiotic biotransformation,<sup>8</sup> as well as other mechanisms involving the interaction of redox-active enzymes with molecular oxygen. Indeed, considerable energy resources are devoted by the cell to maintain homeostasis within a highly reduced environment by recycling low molecular weight reducing agents during oxidative insult.<sup>9</sup> Glutathione metabolism plays a central role in intra-cellular antioxidant defense, redox regulation and detoxification based on the dynamic interplay of the reduced glutathione (GSH)-oxidized glutathione disulfide (GSSG) redox couple in conjunction with various glutathione-dependent enzymes and transporter systems.<sup>10-12</sup> However, a fundamental understanding of the mechanism(s) of oxidative stress remains elusive due to inconsistent results from large-scale clinical trials using antioxidants,<sup>13</sup> as well as the seemingly contradictory and synergistic activities of RONS *in-vivo*. For instance, nitric oxide serves both as an important signaling molecule associated with vasodilation and a precursor

together with the superoxide anion for the cytotoxic oxidant, peroxynitrite.<sup>14</sup> Consequently, there is growing recognition that oxidative stress is better conceived as a global disruption in redox signaling and control.<sup>15, 16</sup> New developments in stress-response hormesis theory<sup>17</sup> may provide deeper insight into the impact of free radical and non-radical chemical stressors on aging and disease pathogenesis.

Exhaustive physical exercise provides a useful model for studying oxidative stress and dietary intervention due to the increased energy demands and oxygen requirements triggered by intense aerobic activity. There is mounting evidence demonstrating that exhaustive exercise without training can illicit deleterious oxidative injury as reflected by structural damage/inflammation of muscle tissue with poor health outcomes.<sup>18</sup> In contrast, regular bouts of moderate exercise with sufficient recovery allows for an adaptive response by upregulation of antioxidant enzymes with improved health benefits that can be ironically dampened with antioxidant supplementation.<sup>19</sup> To date, the majority of exercise-induced oxidative stress studies reported in the literature have relied on classical assays that target specific biomarkers associated with oxidative damage, such as products of lipid peroxidation, DNA and protein modifications, antioxidant enzymes and/or nutrients.<sup>20-23</sup> In addition, protein glutathionylation, GSH/GSSG ratio and/or the equilibrium half-cell reduction potential for glutathione ( $E_{GSSG/2GSH}$ ) represent sensitive indices of oxidative stress complementary to terminal end-products of oxidative insult.<sup>24-26</sup> Nevertheless, careful attention to

method validation is critical to achieving quantitative, reliable and meaningful data interpretations when analyzing oxidative stress biomarkers in complex biological samples. For instance, acid deproteinization of whole blood, tissue or cell lysate samples can induce oxidation artifacts upon protein denaturation resulting in highly biased glutathione levels that is widely reported in the literature with remarkably few exceptions.<sup>26-29</sup> Thus, rigorous assay validation is required during sample collection, sample pretreatment and/or chemical analysis to ensure artifact-free quantification of labile metabolites susceptible to oxidation.<sup>30</sup> Given the diverse classes of metabolites putatively modified as a result of oxidative stress, metabolomics<sup>31</sup> offers a hypothesis-generating strategy for untargeted metabolite profiling relevant to the discovery of novel diagnostic biomarkers<sup>32, 33</sup> and evaluation of dietary adjustments on metabolite phenotype (*i.e.*, metabotype).<sup>34, 35</sup> Recently, Chorell *et al.*<sup>36</sup> introduced a predictive metabolomics model using human serum samples for studying the effects of nutrition modulation following a strenuous ergometer cycling regime, which revealed that a low carbohydrate-protein beverage taken immediately after exercise was able to improve the metabolic status of less fit subjects during recovery. However, blood sampling and metabolite profiling was not performed during strenuous aerobic exercise,<sup>37, 38</sup> which can offer improved understanding of cellular responses to acute oxidative insult and its subsequent return to homeostasis upon recovery.

Herein, we describe a differential metabolomics strategy for quantitative assessment of oxidative stress and antioxidant efficacy with strenuous aerobic exercise using capillary electrophoresis-electrospray ionization-mass spectrometry (CE-ESI-MS)<sup>39, 40</sup>. A healthy untrained volunteer was recruited to perform an ergometer cycling trial for 45 min at peak oxygen consumption (70%  $VO_{2peak}$ ) which was increased to 90%  $VO_{2peak}$  for 6.5 min until exhaustion. Frequent blood collection was performed using a forearm catheter over six hours at sixteen different time intervals pre-, during and post-exercise while at rest. Sampling time was critical for revealing time-dependent changes in global metabolism from filtered red blood cell (RBC) lysates by CE-ESI-MS without oxidation artifacts,<sup>30</sup> which allowed for the identification of putative biomarkers of oxidative stress when using univariate/multivariate analysis. In this study, GSH and notably GSSG levels were found to be highly modulated during the onset of exercise yet tightly regulated within the early phase of recovery (< 2 hrs), whereas *L*-carnitine (C0), *O*-acetyl-*L*-carnitine (C2) and creatine (Cre) remained persistently elevated relative to their initial concentration levels that was indicative of fatigue caused by physical overexertion. A follow-up trial was subsequently performed by the subject after a high-dose oral administration (75 mg/kg/day) of the antioxidant *N*-acetyl-*L*-cysteine (NAC)<sup>41</sup> over five days prior to performing the same exercise protocol under standardized conditions. Differential metabolomics revealed significant attenuation of cellular oxidative stress in RBCs after oral NAC intake relative to the control trial as reflected by a greater half-cell

reduction potential for glutathione ( $\approx +15$  mV) at the peak oxidative, which was also associated with a shorter recovery time ( $\approx 100$  min) to redox homeostasis. An attenuated oxidative response with antioxidant supplementation was also confirmed by lower yet unmodulated concentration levels of C0, C2 and Cre in filtered RBC lysates, including a dramatic ten-fold lowering in 3-methylhistidine (3-MeHis) concentration, which is a diagnostic marker of muscle protein breakdown.<sup>42</sup> Unexpectedly, high-dose oral intake of NAC was found to downregulate the majority of detectable metabolites within erythrocytes (average decrease  $\approx 30\%$ ), whose effect was reversible once supplementation was discontinued. However, there was no direct impact on glutathione metabolism in contrast to the proposed mechanism of NAC action as a glutathione pro-drug.<sup>43-45</sup> This proof-of-concept investigation demonstrates that differential metabolomics provides a quantitative approach for testing the hypothesis of oxidative stress while elucidating the mechanism of antioxidant action, which heralds effective translation of nutritional intervention strategies for improved health outcomes during chronic or acute episodes of oxidative insult relevant to the early treatment of chronic degenerative disorders<sup>46</sup> or as a prophylaxis prior to major surgery,<sup>47</sup> respectively. To the best of our knowledge, this is the first untargeted and artifact-free metabolomics investigation that employs high frequency blood sampling with erythrocytes as reporter cells for probing perturbations in global metabolism induced by prolonged endurance exercise and/or antioxidant supplementation.

### 4.3 Materials and Methods

**4.3.1. Chemicals and Reagents.** De-ionized water used for buffer and sample preparations was obtained using a Barnstead EASYpureII LF ultrapure water system (Dubuque, IA). All buffers, solvents and chemical standards were purchased from Sigma-Aldrich (St. Louis, MO). Individual stock solutions of metabolites (10 mM) were diluted in 1:1 methanol/water, whereas all thiol standards were prepared fresh daily. All solutions and solvents were degassed and chilled to 4°C prior to use. USP/EP-grade *N*-acetyl-*L*-cysteine (NAC) was also purchased from Sigma-Aldrich (Ajinomoto Amino Acid, Product#: A5099, purity > 98.5%) which was used for preparation of high-dose solutions for oral administration by a healthy male volunteer.

**4.3.2. Apparatus and Conditions.** CE-ESI-MS studies were performed on an automated Agilent CE system equipped with an XCT 3D ion trap mass spectrometer, an Agilent 1100 series isocratic pump, and a G16107 CE-ESI-MS sprayer kit (Agilent Technologies, Waldbronn, Germany). All separations were performed on uncoated fused-silica capillaries (Polymicro Technologies Inc., Phoenix, USA) with 50- $\mu$ m i.d. and 80-cm total length. 1.0 M formic acid, pH 1.8 was used as the acidic background electrolyte (BGE) for cationic metabolite separations in CE, such as peptides, amino acids and amines. An Agilent 1100 series pump with a 1:100 splitter was used to supply a volume of 10  $\mu$ L/min of 0.1 % formic acid in 1:1 MeOH/H<sub>2</sub>O as the sheath liquid. Prior to first use, open tubular fused-silica capillaries were conditioned for 20 min with MeOH,

deionized H<sub>2</sub>O and background electrolyte (BGE). In order to achieve broad coverage of polar metabolites in filtered RBC lysates, CE-ESI-MS was performed under both acidic (acidic BGE: 1M formic acid, pH 1.8) and alkaline (alkaline BGE: 50 mM ammonium acetate, pH 8.5) conditions to analyze cationic and anionic metabolites under either positive-ion and negative-ion ESI-MS mode, respectively.<sup>30</sup> All samples were introduced into the capillary using a low-pressure (50 mbar) hydrodynamic injection. On-line sample preconcentration using a discontinuous electrolyte system under acidic conditions was performed to improve concentration sensitivity for the detection of amines, amino acids, peptides and carnitines.<sup>30, 48-51</sup> by first injecting a sample prepared in 200 mM ammonium acetate, pH 7.0 for 75 s at 50 mbar followed by a 60 s injection of the acidic BGE at 50 mbar prior to voltage application. The latter (second) injection sequence was used to displace the original sample plug within the capillary past the electrode interface at the inlet (anode), which was required to avoid CE-induced oxidation artifacts when analyzing low micromolar levels of GSSG in the presence of excess GSH.<sup>30</sup> On-line sample preconcentration of acidic metabolites, such as nucleotides, sugar phosphates and organic acids was performed by first injecting a sample prepared in 10 mM HCl/5 mM ammonium acetate, pH 2.0 for 150 s at 50 mbar followed by a 60 s injection of the alkaline BGE at 50 mbar prior to voltage application. In most cases, filtered RBC lysates were diluted two-fold with acidic or alkaline ammonium acetate solution prior to CE-ESI-MS analysis. An Agilent 1100 series pump equipped with a 1:100 splitter was used to supply a

volume of 10  $\mu\text{L}/\text{min}$  of 5 mM ammonium acetate in 1:1 MeOH/H<sub>2</sub>O as the sheath liquid. Separations were performed at 20°C with an applied voltage of 30 kV. All MS analysis was performed at 300°C using  $\pm 4$  kV as the capillary voltage depending on the ionization mode. Nitrogen gas was used as the nebulizing gas and drying gas at 5 psi and 10 L/min, respectively, whereas helium was employed as the damping gas for the ion trap mass analyzer. All MS data were recorded with a range of 50-750  $m/z$  using the ultrascan mode of 26 000  $m/z$  per second.

**4.3.3. Strenuous Aerobic Exercise Regime.** A healthy untrained male volunteer (22 yrs old, 76 kg, non-smoker) was recruited to perform two trials of a strenuous endurance cycling exercise after the subject was informed of the goals of the study, experimental procedures and rare possible adverse effects from high-dose oral NAC administration<sup>52</sup> (*e.g.* nausea, vomiting) who gave signed consent to participate. The ergometer cycling study and blood sampling protocol were approved by the Hamilton Health Science Research Ethics Board. The subject was informed to abstain from alcohol for 48 hrs prior to each trial, as well as refrain from coffee or caffeine-related products the day of the test. The subject was also requested to keep a meal journal prior to the first trial in order to maintain a similar diet 48 hrs before the subsequent second trial. Prior to beginning all trials the subject initially performed a progressive exercise test (increasing 1 W every 2 s) on an electronically braked stationary cycle ergometer (Lode BV, Excalibur Sport V2.0, the Netherlands) in order to determine his peak

oxygen uptake capacity ( $VO_{2\text{peak}}$ ) using an on-line gas collection system (Moxus Modular  $VO_2$  System, AEI Technologies Inc., Pittsburgh, PA, USA). The value used to determine  $VO_{2\text{peak}}$  corresponded to the highest value achieved over a 30 s collection period, which was then used to set the workload for subsequent tests. All trials were performed by the subject each morning at 8AM while fasting prior to arriving to the testing facility. A prolonged sub-maximal exercise was programmed on the ergometer cycle to generate a workload corresponding to 70%  $VO_{2\text{peak}}$  for 45 min, which was then increased to 90%  $VO_{2\text{peak}}$  for 6.5 min until exhaustion. The latter time interval was determined by volitional fatigue of the subject on the first trial period which was fixed for the subsequent high-dose oral NAC trial. A cycling exercise was designed to achieve sufficient oxidative stress upon exhaustion while minimizing muscle trauma induced by eccentric muscle contractions common with running. Whole blood samples were collected from the volunteer via forearm catheter using vacuum blood collection tubes coated with  $K_2EDTA$  over a 6 hour timeframe pre-, during and post-exercise during recovery while at rest. Water was consumed *ad libitum* during exercise, however no food or water was consumed during recovery. The same subject was then placed on 5 day high-dose oral supplementation corresponding to about 75 mg/kg of NAC which was consumed on a daily basis. The high-dose solutions were prepared by dissolving 5.7 g of NAC in 250 mL of  $H_2O$  together with 1 packet (220 mg) of a low-caloric Crystal Light (Kraft Foods Inc., USA) drink powder to improve palatability. The participant was provided five labeled bottles (1/day)

that were stored in a refrigerator prior to consumption each morning. The subject reported good tolerance of the high-dose oral NAC supplement without any noticeable side-effects. After five consecutive days of NAC intake including a final dose consumed 30 min prior to start of the second trial, the same standardized stationary ergometer cycling series was repeated as the first trial. Both trials of this study were performed over a 6 week time interval without explicit restriction of diet or physical activity of the volunteer except for 48 hrs prior to the second trial. The major objective of this investigation was to develop a robust analytical strategy for quantitative analysis and qualitative identification of putative biomarkers of oxidative stress, which can be used to assess efficacy of antioxidant supplementation with strenuous physical exercise. Although relative changes in erythrocyte metabolism was performed on a single subject in this work, nutritional intervention studies are often designed as cross-over designs where each individual serves as their own control<sup>53</sup> due to large inter-individual group variations influenced by several factors, including gender, training status and dietary intake.<sup>54</sup> Since informed consent was provided to the subject for ethical reasons, including background information regarding the chemical properties and clinical applications of NAC, potential ergogenic effects influencing performance on the second trial could not be eliminated.

**4.3.4. Blood Collection and Filtered RBC Lysate Preparation.** Whole blood was collected from the subject at 16 different time intervals over 6 hrs for both programmed cycle trials. A venous catheter inserted in the ante-cubital vein was

used for blood sampling. This catheter was kept patent using a saline (0.9% w/v) solution. Each blood sample ( $\approx 2$  mL) was immediately kept on ice and subsequently centrifuged using 2000 rpm at 4°C for 5 min to fractionate plasma from erythrocytes. The plasma was removed and RBCs were washed with phosphate buffer saline (10 mM NaH<sub>2</sub>PO<sub>4</sub>, 150 mM NaCl, pH 7.4, 4°C), vortexed and centrifuged using 7000 rpm at 4°C for 1 min to isolate RBCs. The washing steps were repeated 3 times until the supernatant was clear without evidence of hemolysis. Then 200  $\mu$ L of RBCs were hemolysed by adding 600  $\mu$ L of pre-chilled deionized water, which was subsequently centrifuged using 7000 rpm at 4°C for 1 min to sediment cell debris. Next, 100  $\mu$ L of RBC lysate was ultrafiltrated with a 3kDa filter (PALL Corporation, Ann Arbor, USA) using 14,000 rpm at 4°C for 10 min to remove excess hemoglobin. All filtered protein-free RBC lysates were then diluted two-fold in ammonium acetate, stored frozen at -80C and thawed only once prior to analysis ( $n = 3$ ) by CE-ESI-MS under both acidic and alkaline conditions for cationic and anionic metabolites, respectively. Additional blood samples were also collected during oral NAC administration, as well as several days after NAC intake was terminated after completion of the second trial. Our previous study validated that this sample collection, storage and deproteinization protocol is a reliable method for quantification of glutathione metabolites and other labile thiols without oxidation artifacts, while avoiding complicated chemical derivatization/thiol quenching steps required by conventional assays.<sup>30</sup>

**4.3.5. Data Processing and Statistical Analysis.** Data analysis was performed first by manually processing extracted ion electropherograms (EIE) over a range 50-750  $m/z$ , which yielded 700 traces for each run. All filtered RBC lysate samples collected for the two trials (control VS NAC) were analyzed in triplicate ( $n=3$ ) over 16 different time intervals (0-6 hrs) resulting in a total of 134 400 EIE traces. Due to the significant drift in apparent migration times in CE caused by run-to-run variations in the electroosmotic flow (EOF), internal standards were used for normalizing metabolite migration times ( $CV < 2\%$ ) under both acidic and alkaline conditions based on their relative migration time (RMT).<sup>30</sup> The same internal standards were also used for normalization of integrated peak areas of metabolites for improved precision in quantification. Noise filtering and data normalization was performed prior to multivariate analysis by processing each metabolite signal as a single paired variable denoted as  $m/z$ :RMT, which facilitated data alignment among replicates, time intervals and exercise trials. Each EIE was manually integrated with a minimum signal threshold over background noise of  $S/N \approx 10$  in order to avoid signal artifacts, which yielded about one hundred-forty putative ion signals. Subsequent data preprocessing was performed to eliminate redundant responses originating from the same ion, including isotope contributions, fragment ions, salt adducts, as well as common ions detected under both +/- ESI-MS conditions, resulting in unequivocal quantification of forty-two unique metabolite signatures from erythrocytes, which were consistently detected across all time intervals for both trial stages of the

study. This stringent approach towards data analysis was applied in order to enhance data quality for multivariate analyses, as well as avoid the tendency to overestimate total numbers of metabolite detected.<sup>55</sup> Principal component analysis (PCA) was also applied as an unsupervised data exploration method using a multivariate analysis add-in for Excel developed by Dr. Richard Brereton at Bristol University that is freely available for download.<sup>56</sup> The X-data matrix consisted of two cycling trials (control VS NAC) using measured average relative peak areas (*i.e.*, metabolite responses normalized to IS) as responses that was arranged as 42 different ions ( $m/z$ :RMT) as rows or objects over 16 time intervals as columns or variables. All multivariate analyses were preprocessed as standardized data sets, where mean-centered responses were normalized to the inverse of the standard deviation determined at each time variable/column, which provided an effective way to scale different ion responses having different absolute values and ranges. PCA was useful for identifying outliers and putative biomarkers of oxidative stress undergoing systematic changes in responses as a function of time with strenuous exercise and/or oral supplementation. In addition, hierarchical cluster analysis (HCA) was performed using MatLab R2008b (The Mathworks, Inc. Natick, MA, USA) as an unsupervised method for grouping time-dependent changes in standardized responses among metabolites for each trial that was visualized in the form of a dendrogram on a 3D heat map. All data analyses and figures were processed using Excel 2006 (Microsoft Inc., Redmond, WA, USA) and Igor Pro 5.0 (Wavemetrics Inc, Lake Oswego, OR).

#### 4.4. Results

##### 4.4.1. Unsupervised Data Exploration of Exercise-induced Oxidative Stress.

Figures 4.1 and 4.2 summarize overall changes in intra-cellular metabolism based on forty-two unique metabolite signatures derived from filtered RBC lysates consistently quantified across all sixteen time intervals during both standardized cycling trials. The major goal of this study was to quantitatively analyze global changes in erythrocyte metabolism during strenuous aerobic exercise, as well as monitor cellular responses post-exercise during recovery while the subject was at rest. 3D heat maps (Figure 4.1) were used to visualize overall changes in the measured standardized response (*i.e.*, average relative peak area standardized at each time interval) for each metabolite defined as a paired variable ( $m/z$ :RMT) over a six hour time interval, which were arranged in a dendrogram using a HCA algorithm as an unsupervised method for pattern recognition. Each trial involving the subject was performed under the same operating conditions using an exercise regime programmed on a stationary ergometer cycle between the 30 min and 81.5 min time interval, where the first 45 min was maintained at a constant workload of 70%  $VO_{2peak}$  which was then ramped to 90%  $VO_{2peak}$  for the final 6.5 min until exhaustion. Figure 4.1(a) depicts the 3D heat map for the control trial without oral NAC supplementation, which reveals a complex and oscillating pattern of metabolite profiles changing

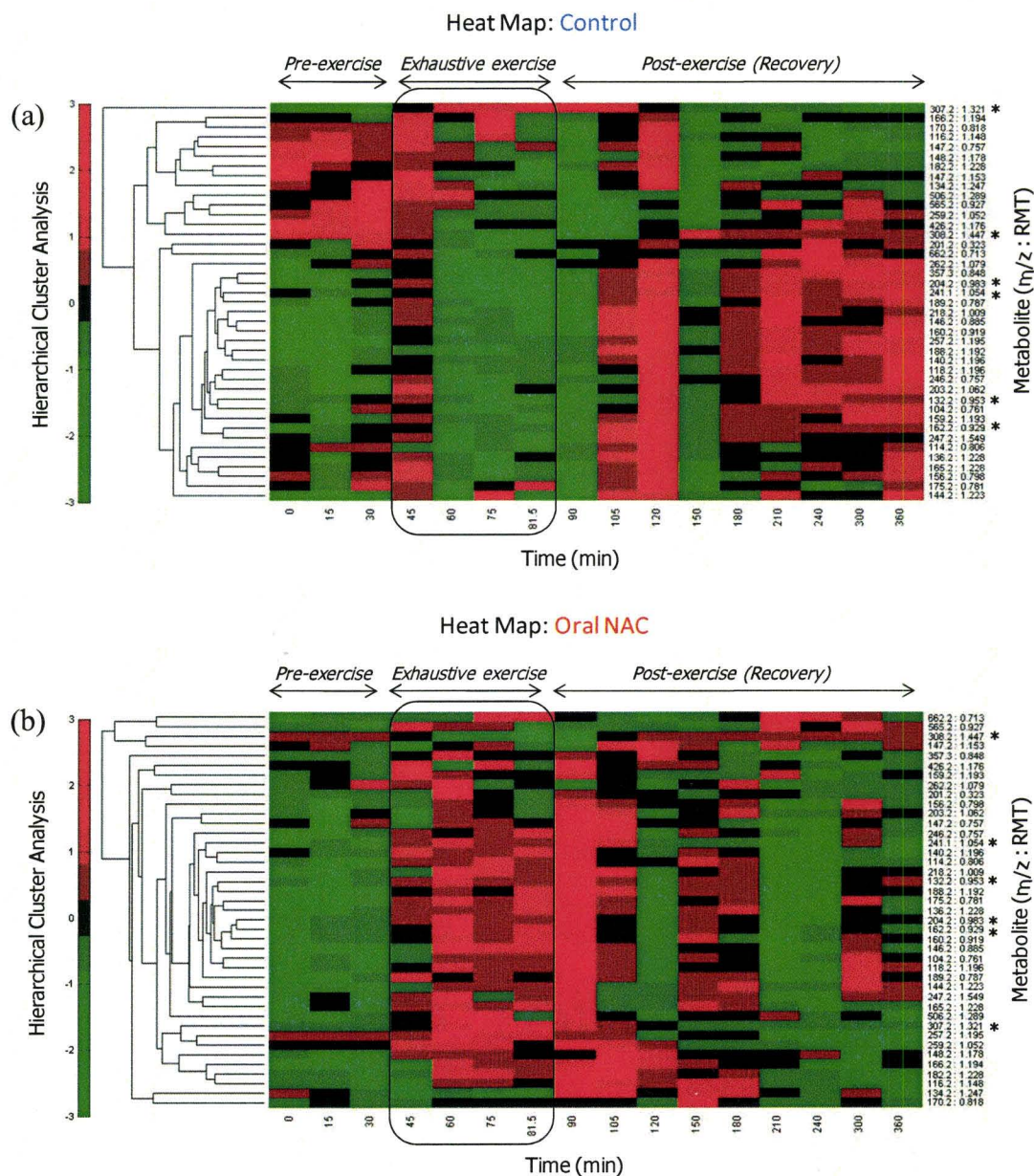


**Figure 4.1.** 3D heat maps qualitatively display changes in the measured standardized response (*i.e.*, average relative peak area standardized at each time interval) for each metabolite defined as a paired variable ( $m/z$ :RMT) over a six hour time interval, which were arranged in a dendrogram using a HCA algorithm as an unsupervised method for pattern recognition. (a) The control trial without oral NAC supplementation, exhibits and oscillating pattern of metabolite profiles changing over the duration of the experiment that can be qualitatively classified into five distinctive groups. (b) Depicts the trial with NAC supplementation which illustrates the attenuation of metabolite fluctuations.

over the duration of the experiment that can be qualitatively classified into five distinctive groups. The major cluster of metabolites was expressed at low levels prior to the onset of strenuous exercise and then detected at elevated levels (*i.e.*, upregulated) three hours after completion of the exercise upon recovery. In contrast, a second minor cluster of metabolites was found to be expressed at high levels prior to the onset of exercise, but then measured at significantly lower levels (*i.e.*, downregulated) during recovery. In addition, two smaller sub-classes of metabolites had responses that were not significantly modulated (*i.e.*, unchanged) or were found to be elevated both prior to and after strenuous exercise (*i.e.* regulated). However, the ion corresponding to  $307m/z:1.321RMT$  was identified as the most significant and regulated concentration profile among all other metabolites detected, which was present at low levels both prior to and after exercise, but was highly elevated during prolonged endurance exercise and the early phase of recovery. Figure 4.1(b) shows the same 3D heat map and HCA dendrogram for the subject after a 5 day high-dose oral intake of NAC prior to performing the same exercise protocol, which revealed a less distinctive cluster of metabolite profiles changing as a function of time. Overall, a comparison of Figures 4.1(a) and (b) qualitatively suggests that oral NAC administration resulted in a less perturbed metabolic status for erythrocytes with the majority of metabolites returning back to initial pre-exercise levels by the late-phase of recovery.

PCA was next performed on the standardized data sets involving the control and oral NAC trials as a way to identify putative biomarkers of oxidative stress significantly modulated by strenuous exercise and/or antioxidant supplementation as a function of time while reducing noise and data dimensionality. Figure 4.2(a) highlights that the majority of systematic data variance (> 98%) in the experiment can be effectively represented by the first two orthogonal principle components (*i.e.*, PC1 and PC2), which revealed six metabolites denoted by their characteristic  $m/z$ :RMT as significant outliers and major objects influencing the explained data variation. The overlay 2D PCA scatter plot confirms that these same metabolites were consistently identified in both cycling trials, although they possessed different scores values that shifted their relative coordinates on the graph indicative of the significant impact of oral NAC on attenuating perturbations in global metabolism with strenuous cycling. A differential PCA was also performed in this study as shown in the inset of Figure 4.2(a), where a single convoluted data matrix was preprocessed by measuring the difference in normalized ion responses (*i.e.*, relative peak areas) for a specific metabolite at each time interval between oral NAC and control trials, which was then standardized prior to multivariate statistical analyses. This type of cross-over data exploration strategy is aimed at identifying metabolites in erythrocytes most significantly modulated by oral NAC supplementation relative to the control as a function of time. Similarly, six specific metabolites were again distinguished as putative biomarkers of oxidative stress, namely ions corresponding to

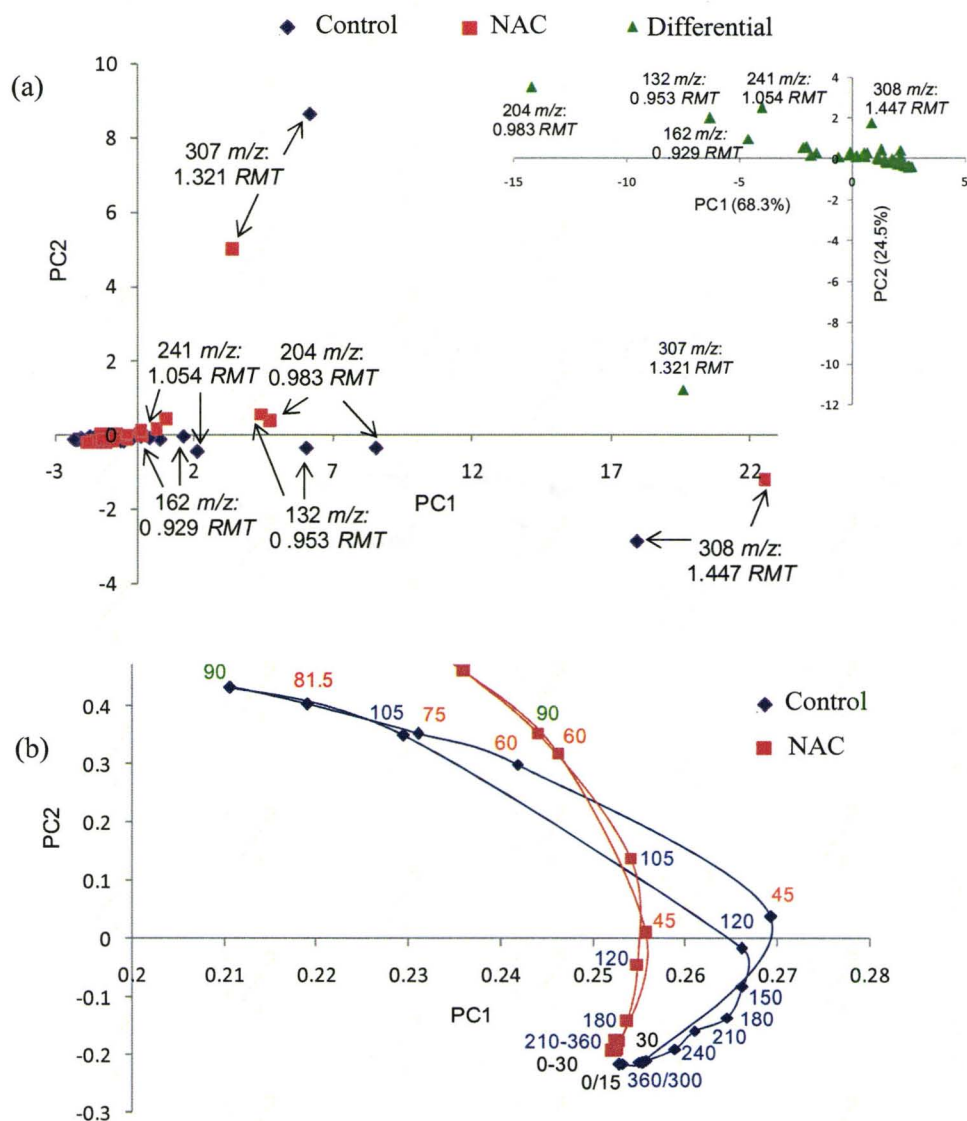


**Figure 4.2** Principle component analysis of all metabolites detected in control (blue) and oral NAC trials (red) (a) The scores plot of both control and NAC trails were overlaid on one PCA plot which revealed six metabolites denoted by their characteristic  $m/z$ :RMT as significant outliers which were observed for both trials. The inset represents the differential PCA which illustrates the same metabolites identified in (a) which undergoes significant change during the exercise regime. (b) Loadings plot of both control and oral NAC trials illustrates the global cellular stress during the oxidative stress event and the return to homeostatic levels after the event. The distinct metabolic attenuation of NAC can be seen by the reduction of the breath/elongation of its loadings curve along PC1.

307 $m/z$ :1.321RMT, 204 $m/z$ :0.983RMT, 132 $m/z$ :0.952RMT, 162 $m/z$ :0.929RMT, 241 $m/z$ :1.054RMT and 308 $m/z$ :1.447RMT. Figure 4.2(b) depicts an overlay of the loadings curve plots for both control and oral NAC trials highlighting the covariance of time variables (*i.e.*, blood collection time) that were associated with the systematic changes in standardized ion responses for metabolites as shown in the scores plot in Figure 4.2(a). Interestingly, both trials show a reversible yet distinct pattern, where initial conditions prior to the onset of exercise (0-30 min) and the late-phase recovery period (> 300 min) represent an equivalent resting metabolic status for erythrocytes. However, the loadings plots also clearly reflect an increasing perturbation in global cellular metabolism upon the onset of strenuous exercise (*i.e.*, 45-81.5 min) with increasing oxidative stress that peaks near the end of the cycling trials. In addition, Figure 4.2(b) also demonstrates that both trials can be readily differentiated since increased susceptibility to fatigue due to oxidative stress can be inferred in the control trial by the wider breadth/elongation of its loadings curve along the PC1 axis, as well as its longer recovery time needed to return to initial/resting conditions relative to the oral NAC trial. For instance, high-dose oral NAC administration was associated with a peak disturbance in global metabolism immediately at the end of the exercise regime (*i.e.*, 81.5 min), which quickly recovered while at rest within 100 min after the end of the cycling trial (> 180 min) in contrast to the delayed recovery measured for the control. Consequently, the latent significance of PC1 is inferred as being associated with the magnitude of exercise-induced cellular oxidative

stress, whereas PC2 is reflective of the underlying time sequence used in the experimental protocol for collecting blood samples as related to the start and end of the cycling trials.

#### **4.4.2. Glutathione Metabolites as Early-stage Biomarkers of Oxidative Stress.**

Given the high natural abundance of reduced glutathione (GSH) in most cell types and its central role in antioxidant defense,<sup>30</sup> two of the ions detected in Figure 4.2 as  $307m/z:1.321RMT$  and  $308m/z:1.447RMT$  from filtered RBC lysate samples were subsequently confirmed as GSSG and GSH, respectively. Due to the large dynamic range in glutathione concentration levels in RBCs, Figure 4.3(a) depicts an overlay plot based on the average relative ion response measured for GSH and GSSG by CE-ESI-MS during both ergometer cycling trials that highlights major changes in glutathione levels for the subject during the onset of strenuous exercise and early phase of recovery. In the case of the control study, GSH underwent a 34% decrease in measured response at its peak minimum (*i.e.*, GSH consumption) shortly after completion of the exhaustive exercise trial, whereas GSSG was measured to be elevated over 20-fold above normal/resting basal levels. Figure 4.3(a) also demonstrates that oral NAC supplementation effectively attenuated the extent of cellular oxidative stress for the subject, which is evident by the significantly lower decrease in GSH or less greater increase in GSSG responses

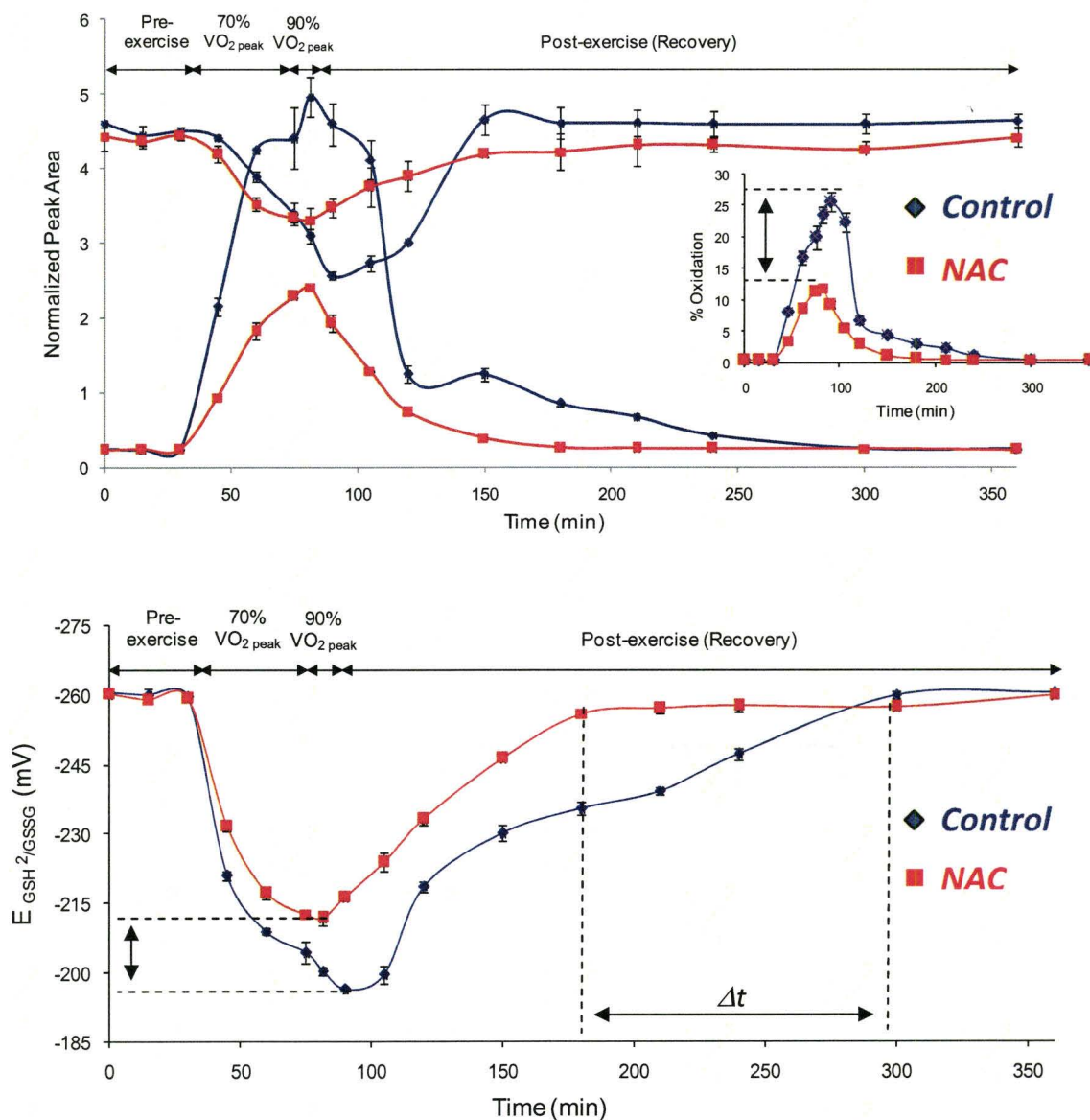


**Figure 4.3.** (a) Depicts the overlay plot of relative ion response for GSH and GSSG during the exhaustive exercise regime. GSH and GSSG undergo significant changes during the exercise protocol as demonstrated by the over 20 fold increase of GSSG and the concomitant decrease of GSH in the control trial. GSH depletion and GSSG formation is modulated during the oral NAC trial. The inset displays the reduction of total RBC oxidation by 14% by oral supplementation of NAC. (b) Illustrates the half cell reduction potential of GSH, ( $E_{GSSG/2GSH}$ ). Both trials initially start with highly reduced state then undergo oxidation during the exhaustive exercise regime. This highly reversible process is attenuated by the consumption of NAC as shown by the more reduced state at the peak oxidation levels and the significantly shorter recovery time.

for the second cycling trial. The inset of Figure 4.3(a) shows a more effective comparison of the two cycling trials by plotting changes in the %oxidation as determined by the fraction of GSSG generated (*i.e.*,  $2[\text{GSSG}]/2[\text{GSSG}]+[\text{GSH}]$ ) in erythrocytes due to exercise-induced oxidative stress.<sup>9</sup> Overall, a absolute decrease in the extent of RBC oxidation of about 14% from a peak maximum of  $(25.7 \pm 1.6)\%$  for the control trial was measured with oral NAC supplementation. Interestingly, there were no significant changes in initial or final concentrations levels for GSH or GSSG in RBCs with high-dose oral NAC supplementation, which is reflected by a low yet consistent degree of cellular oxidation of  $(0.43 \pm 0.02)\%$  while at rest or at full recovery. Similarly, Figure 4.3(b) compares changes in the measured equilibrium half-cell reduction potential for glutathione ( $E_{\text{GSSG}/2\text{GSH}}$ ) with strenuous exercise for the two cycling trials based on the Nernst equation, which provides a quantitative parameter indicative of the redox status of cells.<sup>9, 57, 58</sup> Similar to the pattern revealed in the loadings plot overlay in Figure 4.2(b), the redox potential of RBCs was in a highly reduced state  $(-260 \pm 1)\text{mV}$  while at rest during pre-exercise in both trials, which was fully reversible within 3 hrs post-exercise. Moreover, Figure 4.3(b) also highlights the positive impact of NAC for attenuating oxidative stress in erythrocytes as determined by the relative change in half-cell reduction potential at peak oxidation for glutathione ( $\Delta E_{\text{peak}}$ ) equivalent to  $\approx +15 \text{ mV}$  that implied a more reduced and resistant redox environment relative to the control trial. Figure 4.3(b) also clearly depicts a significantly shorter return to redox homeostasis after strenuous cycling was

completed with a recovery time difference of about 100 min ( $\Delta t_{rec}$ ) with oral NAC relative to the control trial. Consequently, multiple parameters associated with glutathione metabolism can provide sensitive, reliable and quantitative indices for assessing oxidative stress, fatigue and antioxidant efficacy when using standardized ergometer cycling exercise trials.

**4.4.3. Discovery of Unknown Biomarkers of Oxidative Stress.** Although GSSG was determined to be the most significant metabolite modulated by exercise-induced oxidative stress, several other putative biomarkers were also revealed by multivariate analyses when using PCA. In addition, a univariate fold-change comparison with unpaired student's t-test was also used to rank potential biomarkers that were highly modified (*i.e.*, downregulated) after high-dose oral NAC intake (*i.e.*, 30 min prior to exercise) relative to the control while at rest (refer to Figure 4.6). In this study, unambiguous metabolite identification was realized by a series of experiments involving the acquisition/interpretation of multi-stage mass spectra when using a 3D ion trap mass analyzer, which was followed by an extensive search for candidate metabolites on public databases, including the Kyoto Encyclopedia of Genes and Genomes (KEGG) Ligand Database<sup>59</sup> and the Human Metabolome Database (HMDB).<sup>60</sup> Lead metabolite candidates were rationally selected based on several criteria, including equivalent nominal mass, characteristic fragments/isotope patterns as well as a relevant intrinsic charge state deduced by their putative chemical structure. In fact, the latter criterion was effective at excluding a large number of isobaric candidates

that lacked suitable weakly ionic functional groups required for their electromigration in CE, such as the presence of an amino group for cationic metabolite separations under acidic BGE conditions. Once a series of lead candidates were selected, a comparison of their measured (or predicted) RMTs by CE,<sup>51</sup> as well as spiking of filtered RBC lysate samples with authentic standards (if available) allowed for their unequivocal identification and subsequent quantification. The inset of Figure 4.4(a) shows an overlay of extracted ion electropherogram (EIE) traces for six cationic metabolites (including GSH and GSSG) that were as identified putative biomarkers of exercise-induced oxidative stress in RBCs when using an internal standard (IS, *D*-alanyl-*D*-alanine) for data normalization. Three of the four unknown biomarkers were identified after multivariate analysis using PCA in Figure 4.2 (*i.e.*, 204 $m/z$ :0.983RMT, 132 $m/z$ :0.952RMT, 162 $m/z$ :0.929RMT), whereas the other unknown biomarker (*i.e.*, 170 $m/z$ :0.818RMT) was selected after univariate statistical analysis of fold-changes in global metabolism after oral NAC administration while at rest (refer to Figure 4.6). It is important to note the large dynamic range in responses measured for intra-cellular metabolites in filtered RBC lysates by CE-ESI-MS as shown in the total ion electropherogram (TIE) of Figure 4.4(a), where all the putative unknown biomarkers represent low abundance metabolites relative to GSH. Figure 4.4(b) shows multi-stage MS<sup>2</sup> spectra acquired for the four unknown biomarkers of oxidative stress, where their molecular ions (MH<sup>+</sup>) and major fragment ions and/or neutral losses were consistent with the proposed chemical

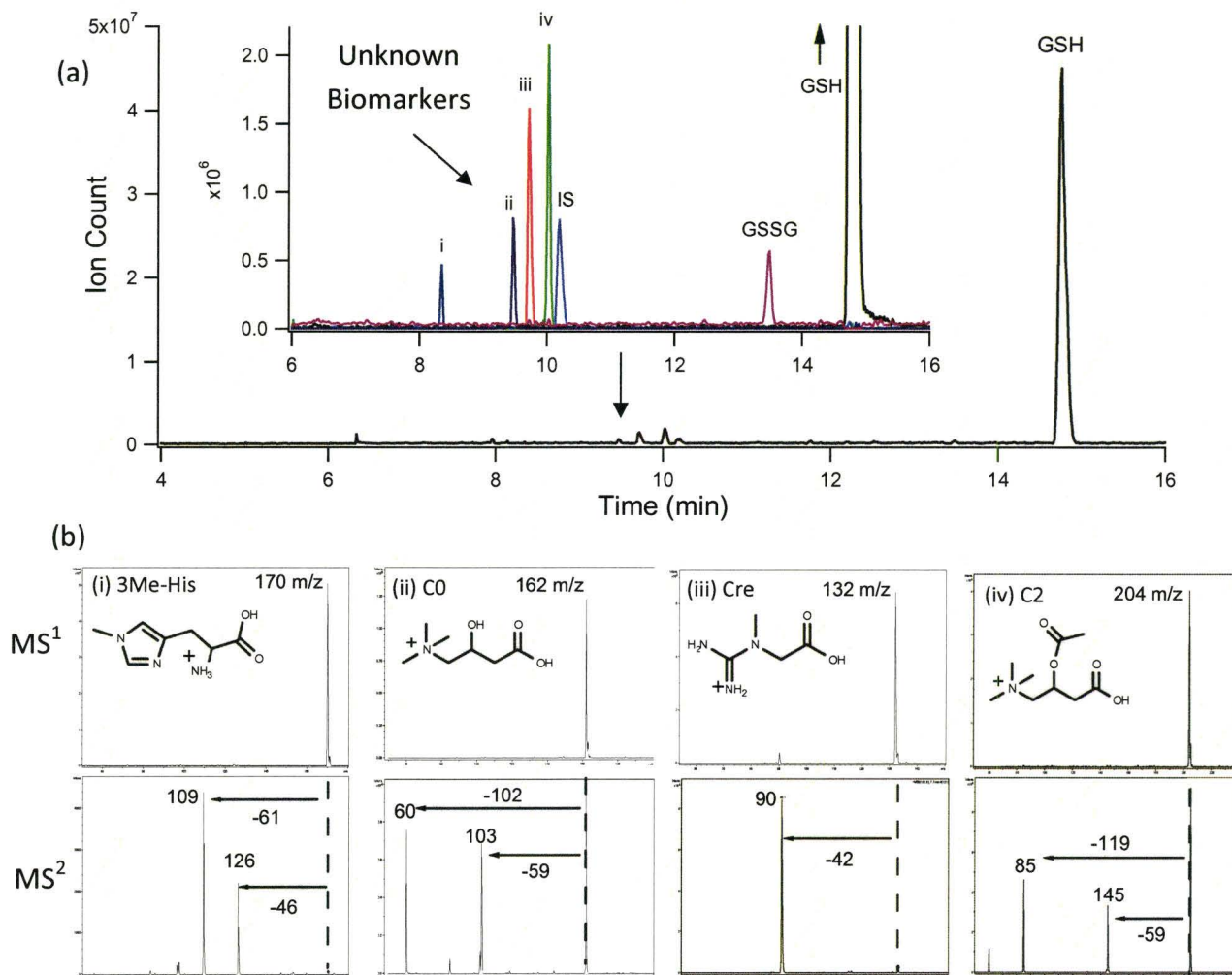


**Figure 4.4** (a) Base peak electropherogram of BRC lysate during T=0 min of control trial. Inset illustrates the extracted ion electropherograms of putative unknown biomarkers of oxidative stress. A large dynamic range is observed for the metabolites in RBC lysate with GSH in excess with the putative biomarkers in low abundance. (b) Multistage MS<sup>n</sup> spectra were acquired for the unknown biomarkers and compared against available database spectra. Identification of metabolites were (i) 3Me-His, (ii) C0, (iii) Cre, and (iv) C2.

structures after thorough ligand database searches, namely 3-methyl-*L*-histidine (3-MeHis), *L*-carnitine (C0), creatine (Cre) and *O*-acetyl-*L*-carnitine (C2). In the case of 3-MeHis, two other potential isomeric ions (*i.e.*, 1-MeHis and *N*-MeHis) were ruled out by performing spiking experiments and computer electrophoretic simulations<sup>51</sup> that were consistent with the experimental RMTs measured by CE (data not shown). However, the unknown ion corresponding to 241 $m/z$ :1.054RMT from Figure 4.2 was not successfully identified because of its low abundance which hampered the acquisition of useful multi-stage MS spectra due to inadequate sensitivity. Overall, the relative migration order of metabolites in CE can be predicted based on their effective charge density, where divalent modified cationic amino acids such as 3-MeHis migrate faster than bulkier monovalent cations under strongly acidic conditions, such as the acylcarnitine C2.<sup>48, 49, 51</sup>

**4.4.4. Concentration Profiles of Lead Biomarkers of Oxidative Stress.** Figure 4.5 summarizes the time-dependent concentration profiles for all six lead biomarkers of oxidative stress identified in this investigation when performing control (blue) and oral NAC (red) trials of standardized sub-maximal prolonged cycling trials. Overall, there was up to a 1000-fold concentration difference among biomarkers detected in RBCs when using CE-ESI-MS ranging from the most abundant (GSH) to the least abundant (C2) which were present at about 1.6 mM (both trials at rest) and 1.7  $\mu$ M (oral NAC trial at rest), respectively. Similar to Figure 4.3, the concentration profiles for GSH and notably GSSG clearly demonstrate their suitability as sensitive “early-stage” biomarkers of cellular

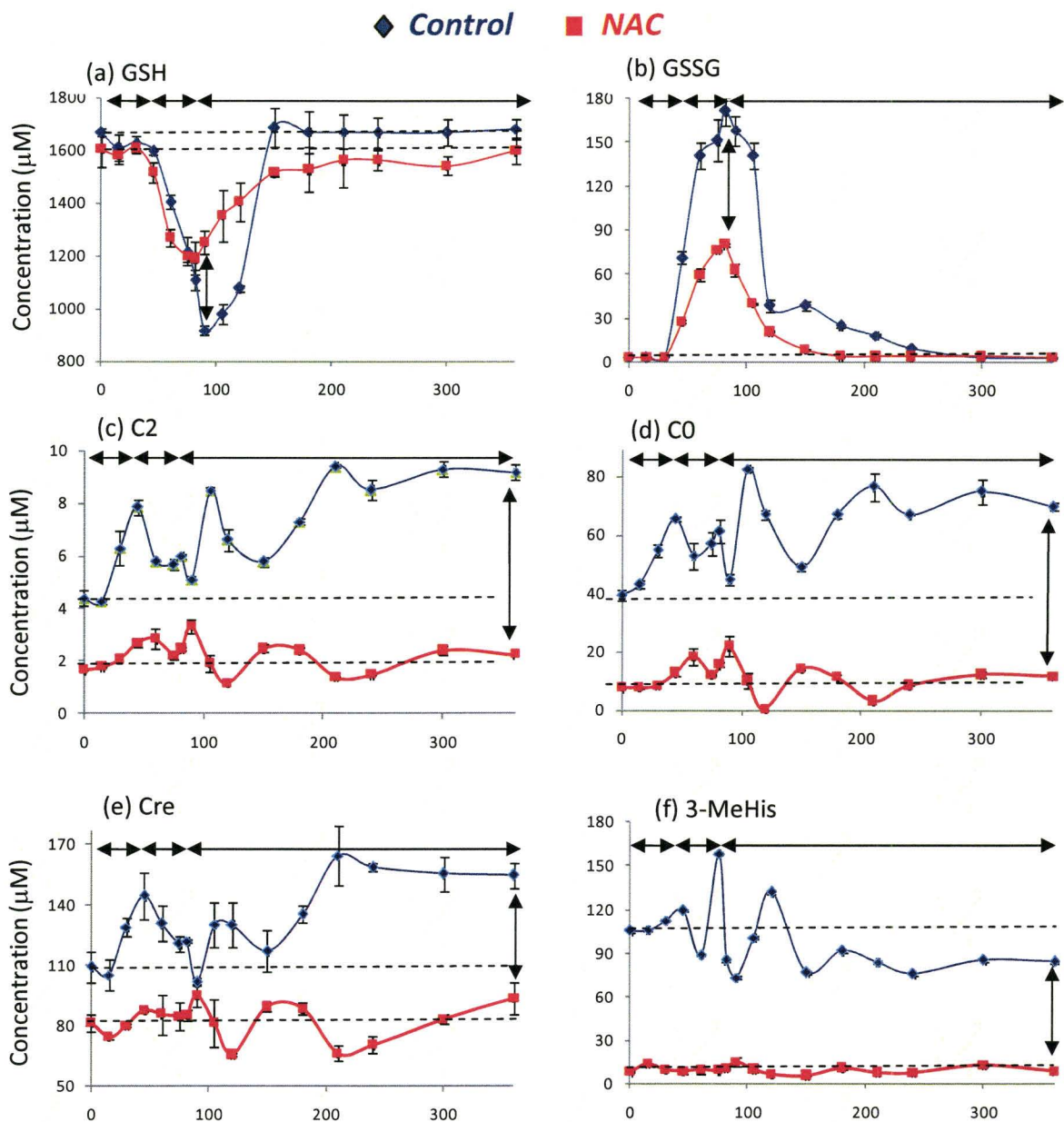


**Figure 4.5.** Time-dependent concentration profiles of six lead biomarkers of oxidative stress in control (blue) and oral NAC trials (red). (a) GSH and (b) GSSG profile depicts the enormous change during the oxidative stress event but returns to baseline levels during the recovery period for both control and oral NAC trials. (c) C2, (d) C0, and (e) Cre shared similar oscillating patterns during exhaustive exercise in the control trial until stabilizing the end of the recovery period but were significantly elevated. During oral NAC trial C2, C0, and Cre were downregulated and did not exhibit significant increase at the end of the exercise protocol. (f) 3-MeHis was observed to have a unique concentration profile as it was not elevated at the end of the exercise protocol during the control trial but was downregulated and greatly attenuated by oral NAC supplementation.

oxidative stress that respond rapidly with the onset of strenuous exercise until its early-phase recovery. In fact, GSSG levels undergo a massive 48-fold and 24-fold increase in concentration during the peak oxidative stress phase from a low resting/basal concentration of about 3.5  $\mu\text{M}$  when comparing the control and oral NAC cycling trials, respectively. Figure 4.5 also shows that the concentration profiles for C0, C2 and Cre share a common oscillating pattern during exhaustive exercise notably in the control trial until eventually stabilizing near the end of the recovery period, but at significantly elevated levels ( $P < 0.001$ ) relative to initial conditions by about 208%, 76% and 41%, respectively. Thus, this latter group of metabolites was designated as promising “late-stage” biomarkers of oxidative stress since there were persistently elevated 3 hrs after completion of the exercise in the control trial. Moreover, C0, C2 and Cre were also found to be markedly downregulated after oral NAC intake at rest prior to performing the second trial (refer to Figure 4.6). Figure 4.5 also demonstrates that this same group of metabolites exhibit lower amplitude oscillations during exercise-induced oxidative stress with oral NAC intake, as well as returning close to initial concentration levels towards the end of recovery/sampling period. The large decrease in absolute concentrations for C2 ( $\approx$  6-fold), C0 ( $\approx$  4-fold) and Cre ( $\approx$  1.3-fold) between the two cycling trials at 3 hrs post-exercise (refer to double arrows in Figure 4.5) further validate the classification of these metabolites as promising late-stage biomarkers of oxidative stress. In addition, Figure 4.5 depicts the unique concentration profile of 3-MeHis which had over a 12-fold

decrease in resting concentration level in RBCs after oral NAC supplementation from about 106  $\mu\text{M}$  (control) to only 8.3  $\mu\text{M}$ . In contrast to C2, C0 and Cre, 3-MeHis was not found to undergo significant oscillations in concentration with prolonged endurance exercise while being present at lower concentration levels post-exercise while at rest relative to initial conditions. However, 3-MeHis was considered to be the most sensitive late-stage biomarker of oxidative stress that was greatly impacted by antioxidant supplementation as reflected by its drastically lower absolute concentration level (*e.g.*, 10-fold lower than control at end of sampling) with a more attenuated (*i.e.*, flat) concentration profile when comparing the time-dependent concentration profiles of the oral NAC relative to control trials. 3-MeHis was not initially identified by PCA presumably due to its lower amplitude oscillations (notably with oral NAC) with strenuous exercise relative to the dominant changes in glutathione levels that were occurring within a similar time interval for the control trial. Thus, a combination of univariate and multivariate statistical tools with appropriate data preprocessing are critical elements for unbiased discovery of novel biomarkers in metabolomics research that are expressed over a wide dynamic range.

#### **4.4.5. Reversible Global Metabolite Perturbations with NAC Pretreatment.**

One the most surprising findings in this work was the inability to directly detect NAC or its potential disulfide adducts<sup>30</sup> (*i.e.*, NAC-NAC, GS-NAC) in filtered RBC lysate samples after high-dose oral administration during the second exercise trial. Blood samples were collected and analyzed on days 3 and 5 (trial

date) of the high-dose oral NAC regime, however NAC was not detectable in erythrocytes which suggested that its concentration level was under 2  $\mu\text{M}$ , which corresponds to the approximate limit of detection (LOD) for NAC when using CE-ESI-MS under alkaline BGE conditions. Despite the high-dose consumed ( $\approx$  6000 mg/day) in this study, NAC in its reduced free form has been previously reported to have a poor oral bioavailability and fast pharmacokinetics with peak concentration levels circulating in plasma within the first hour of about 4  $\mu\text{M}$  after a 400 mg oral dose using effervescent tablets.<sup>61</sup> In addition, recent studies of intra-venously administered NAC showed a significantly lower uptake of reduced NAC by RBCs relative to its circulating levels measured in plasma.<sup>62</sup> Nevertheless, Figure 4.6 clearly demonstrates that high-dose oral NAC intake by the subject about 30 min prior to the start of the second cycling trial had a pronounced yet indirect impact at downregulating global metabolism in erythrocytes (refer to blue bars) as reflected by the magnitude in the fold-change of normalized ion responses relative to the pre-exercise control trial without NAC. Noteworthy, 3-MeHis was found to be most dramatically depleted with oral NAC intake among all other metabolites detected/identified in RBCs, whereas both GSH and GSSG levels were not significantly changed (refer also to Figure 4.5). Figure 4.6 also demonstrates the overall reversibility in global metabolomic perturbations that largely return back to levels detected in the original pre-exercise control trial (*i.e.*, performed 7 weeks previously) when blood samples from the subject were collected 5 days after oral NAC was discontinued (refer to

red bars). Noteworthy, analysis of filtered RBC lysates on day 3 of high-dose oral NAC supplementation (data not shown) which were acquired several hours after the subject consumed the morning dosage was found to have a similar metabolite profile as control and discontinued oral NAC sample (refer to red bars). These observations confirm the rapid yet reversible perturbations in global metabolism upon high-dose oral NAC intake prior to excretion, which is most effectively administered shortly prior to the start of the exercise trial. Table 4.1 summarizes the relative fold-change in responses and their statistical significance for all metabolites detected in RBCs, where there was about a 30% overall decrease in average measured responses for metabolites after oral NAC supplementation as compared to the control trial and sample collected 5 days after oral NAC intake was discontinued. Consequently, our investigation supports a causal link between NAC supplementation, global metabolomic downregulation and attenuation in oxidative stress with prolonged sub-maximal exercise that effectively reduced fatigue due to physical overexertion.

## **4.5. Discussion**

### **4.5.1. Global Metabolite Profiling of Erythrocytes by CE-ESI-MS.**

Metabolomics is a rapidly expanding area of systems biology for functional understanding of the impact of extrinsic stressors on an organism that is relevant to new advances in drug development,<sup>63</sup> environmental toxicology<sup>64</sup> and human

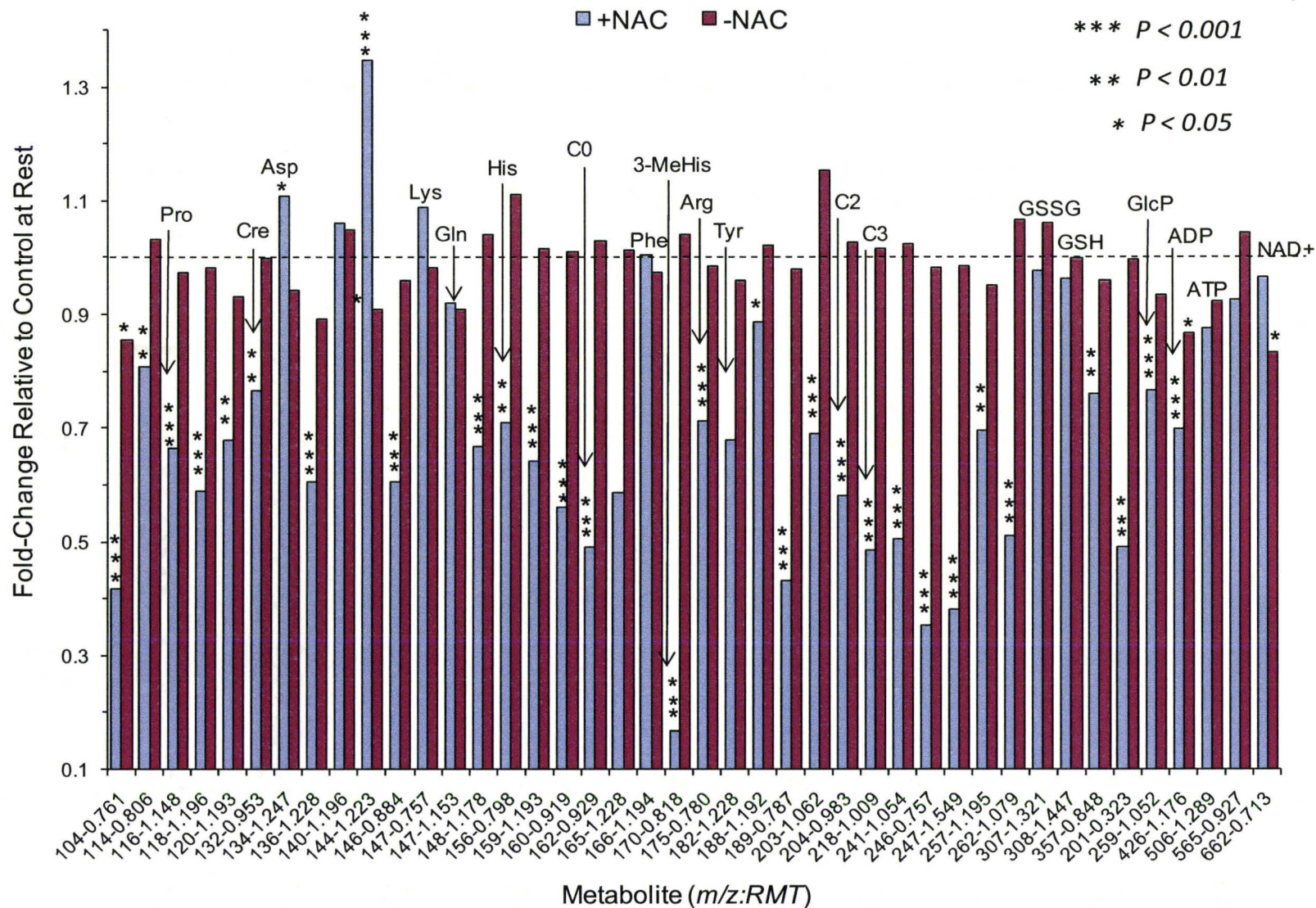


**Figure 4.6.** Univariate analysis comparing the fold change of oral NAC trial at rest (blue) and 5 days after NAC trial (purple) relative to control trial at rest. Identified metabolites are labeled above their corresponding (m/z:RMT) values. Metabolites exhibited an overall significant down regulation with oral NAC supplementation but surprisingly recovered to pre-NAC levels 5 days after last consumption of NAC. Recovery to control levels suggest that efficacy of NAC supplementation is transient and reversible.

**Table 4.1.** Summary of forty-two identified and unknown metabolites reliably quantified in RBCs during both exercise-induced oxidative stress trials by CE-ESI-MS, which highlights the global impact of high-dose oral NAC intake in downregulating metabolite levels that is reversible with its discontinued use.

Metabolite identification	m/z:RMT	Fold-change relative to control	
		+Oral NAC <sup>a</sup>	-Oral NAC <sup>a</sup>
X1	104:0.761	0.42 (15.51)**	0.86 (2.62)*
X2	114:0.806	0.81 (4.28)**	1.03 (-0.741)
L-Proline (Pro)	116:1.148	0.66 (8.23)**	0.97 (1.39)
X3	118:1.196	0.59 (22.4)**	0.98 (0.788)
X4	120:1.193	0.68 (6.94)**	0.93 (1.40)
Creatine (Cre)	132:0.953	0.77 (5.20)**	1.00 (0.019)
L-Aspartic acid (Asp)	134:1.247	1.11 (-3.71)**	0.94 (1.32)
X5	136:1.228	0.60 (7.87)**	0.89 (1.32)
X6	140:1.196	1.06 (-0.517)	1.05 (-0.603)
X7	144:1.223	1.35 (-10.01)**	0.91 (2.76)*
X8	146:0.884	0.61 (18.30)**	0.96 (0.990)
L-Lysine (Lys)	147:0.757	1.09 (-1.62)	0.98 (0.217)
L-Glutamine (Gln)	147:1.153	0.92 (0.881)	0.91 (1.30)
L-Glutamic acid (Glu)	148:1.178	0.67 (17.24)**	1.04 (-1.28)
L-Histidine (His)	156:0.798	0.71 (4.87)**	1.11 (-1.41)
X9	159:1.193	0.64 (8.65)**	1.02 (-0.471)
X10	160:0.919	0.56 (18.15)**	1.01 (0.496)
L-Carnitine (C0)	162:0.929	0.49 (16.58)**	1.03 (-0.963)
X11	165:1.228	0.59 (10.36)**	1.01 (-0.328)
L-Phenylalanine (Phe)	166:1.194	1.01 (-0.153)	0.97 (0.429)
3-Methyl-L-Histidine (3-MeHis)	170:0.818	0.17 (14.62)**	1.04 (-0.669)
Arginine (Arg)	175:0.781	0.71 (8.02)**	0.98 (0.276)
Tyrosine (Tyr)	182:1.228	0.68 (10.12)**	0.96 (0.580)
X12	188:1.192	0.89 (2.51)*	1.02 (-0.480)
X13	189:0.787	0.43 (12.29)**	0.98 (0.308)
X14	203:1.062	0.69 (1.68)	1.15 (-0.726)
O-Acetyl-L-Carnitine (C2)	204:0.983	0.58 (10.59)**	1.03 (-0.612)
O-Propionyl-L-Carnitine (C3)	218:1.009	0.49 (9.82)**	1.02 (-0.232)
X15	241:1.054	0.50 (9.61)**	1.02 (-0.403)
X16	246:0.757	0.35 (8.71)**	0.98 (0.239)
X17	247:1.549	0.38 (26.91)**	0.99 (0.644)
X18	257:1.195	0.70 (3.96)**	0.95 (0.881)
X19	262:1.079	0.51 (9.25)**	1.07 (-0.873)
Glutathione disulfide (GSSG)	307:1.321	0.98 (1.19)	1.06 (-0.942)
Glutathione (GSH)	308:1.447	0.96 (1.55)	1.00 (-0.009)
X20	357:0.848	0.76 (2.85)*	0.96 (0.842)
X21	201:0.323	0.49 (16.64)**	1.00 (0.059)
D-Glucose-6-phosphate (GlcP)	259:1.052	0.77 (10.20)**	0.94 (0.119)
ADP	426:1.176	0.70 (7.71)**	0.87 (2.96)*
ATP	506:1.289	0.88 (1.94)	0.92 (0.984)
X22	565:0.927	0.93 (1.12)	1.04 (-0.663)
NAD <sup>+</sup>	662:0.713	0.97 (0.736)	0.83 (3.21)*
<b>Average</b>		<b>0.71 ± 0.25</b>	<b>0.986 ± 0.058</b>

<sup>a</sup>Fold-change in measured average ion responses relative to their control trial (no NAC) at time 0 min, where numbers in parentheses represent students *t*-values with confidence levels indicated by \* *P* < 0.05 and \*\* *P* < 0.01 and \*\*\* *P* < 0.001.

nutrition.<sup>35</sup> Due to the wide chemical diversity and dynamic range of metabolites in biological samples, several complementary analytical platforms have been developed in order to quantify a broad range of metabolites when using NMR and increasingly MS technology.<sup>65, 66</sup> Both LC-MS and CE-MS techniques offer similar selectivity for the direct analysis of polar metabolites without chemical derivatization unlike GC-MS<sup>67, 68</sup> while allowing for the resolution of isobaric and/or isomeric interferences not feasible by direct infusion ESI-MS.<sup>69</sup> A unique feature of CE-ESI-MS is the ability to integrate on-line sample preconcentration with desalting prior to ionization as a way to improve concentration sensitivity for a wide class of polar metabolites without complicated sample handling.<sup>48</sup> In addition, computer electrophoretic simulations of ion migration behavior can be performed *in silico* to support MS for unambiguous identification of unknown metabolites based on their putative chemical structure in cases when chemical standards are unavailable.<sup>51</sup> Nevertheless, a common constraint of all liquid-infused MS platforms is the lack of a universal ion source for gas-phase desorption<sup>70</sup> since ionization efficiency in ESI is highly dependent on the intrinsic physicochemical properties of metabolites with relative response factors that can vary up to three-orders of magnitude.<sup>49</sup> Given the selectivity constraints of the separation technique and ion source, CE-ESI-MS is primarily amenable to the analysis of polar and weakly ionic metabolites, which comprise a majority (>

60%) of known metabolites or degradation products in primary metabolism.<sup>71</sup> Although metabolomics strives for the quantitative analysis of all low molecular weight metabolites (< 1000 Da) in a cell or biofluid, in most cases chemometric methods are applied on preprocessed data sets for revealing a sub-set of biologically significant metabolites for subsequent characterization that are relevant to the experimental design, such as diagnostic biomarkers.<sup>72</sup> Despite recent advances in analytical instrumentation, method validation still remains a critical yet often overlooked component of metabolomics research that is required for reliable quantification of labile metabolites as putative biomarkers of oxidative stress.<sup>30</sup> In this work, a differential metabolomics strategy is introduced for the quantification of cellular oxidative stress and antioxidant efficacy with sub-maximal prolonged exercise using erythrocytes as a model reporter cell system.

**4.5.2. Erythrocytes as Reporter Cells to Oxidative Stress.** Red blood cells (RBCs) represent the most common circulating cell type susceptible to oxidative stress due to their role in oxygen and nitric oxide transport, high abundance of iron and hemoglobin and lack of nucleus/organelles required for adaptive responses triggered by oxidative insult.<sup>6</sup> However, because of their unique cellular structure and biological functions, erythrocytes are also equipped with potent defenses to resist oxidative stress due to high expression of various enzymatic and non-enzymatic antioxidants during erythropoiesis. RBCs can serve not only as reporter cells relevant to cardiovascular system health,<sup>6</sup> but also reflect oxidative stress status in the whole organism due to their pervasive

circulation and interaction with peripheral tissues/organs (*e.g.*, lungs, liver, muscle *etc.*). In this respect, erythrocytes can serve as convenient surrogate cells for other tissues that can only be accessed through invasive biopsies. In this work, untargeted metabolomics in conjunction with univariate/multivariate analysis of preprocessed data sets allowed for the discovery of six promising biomarkers of oxidative stress, namely two early-stage biomarkers sensitive to the onset of aerobic activity (*i.e.*, GSSG and GSH) and four late-stage biomarkers responsive to high-dose oral NAC administration, which were significantly downregulated at pre-exercise and post-exercise intervals relative to the control (*i.e.*, 3-MeHis, C0, C2 and Cre). Although our studies confirmed that GSH and GSSG represent useful biomarkers of exercise-induced oxidative stress studies, regrettably most reports published in the literature to date have used inappropriate sample pretreatment protocols and/or biased assays that induce oxidation artifacts<sup>26</sup> resulting in highly variable and elevated basal levels of GSSG (> 40  $\mu\text{M}$ ) that do not accurately reflect cellular redox status.<sup>21, 37, 38, 73-76</sup> Figure 4.3 and Figure 4.5(b) clearly demonstrate that GSSG represents an extremely sensitive early-stage biomarker of oxidative stress that can be reliably quantified in erythrocytes when using an artifact-free and rigorously validated analytical strategy.<sup>30</sup> Indeed, acute oxidative stress resulting in severe depletion of intra-cellular GSH has been shown to regulate cell differentiation and signaling that can trigger apoptosis in cases when  $E_{GSSG/2GSH}$  exceeds the range of -180 mV to -160 mV at pH 7.4.<sup>9, 57</sup> In our study, the control trial was associated with the greatest extent of oxidative

stress in erythrocytes which peaked shortly after termination of prolonged endurance cycling (*i.e.*, 90 min) to a maximum voltage of about -196 mV, whereas oral NAC supplementation attenuated oxidation to a maximum of -212 mV as illustrated in Figure 4.3(b). Thus, the severity of exercise-induced oxidative stress in both trials was not sufficient to induce hemolysis allowing RBCs to recover back to redox homeostasis ( $\approx$  -260 mV) within 3 hrs due to regulation of GSSG levels by glutathione reductase in concert with the pentose phosphate pathway for biosynthesis of NADPH. In addition, the time for recovery in the case of the oral NAC trial as inferred in the plot in Figure 4.3(b) was significantly shortened by about 100 min relative to the control implying that high-dose oral NAC intervention delays fatigue during prolonged cycling exercise. Indeed, these observations are consistent with a series of reports by McKenna *et al.*<sup>62, 76, 77</sup> who reported a significant attenuation in muscle fatigue among subjects performing endurance cycling after intra-venous NAC administration.

**4.5.3. Biological Interpretations of Metabolism Downregulation.** Since erythrocytes are not directly involved in metabolic reactions associated with 3-MeHis, C0, C2 or Cre, this supports the premise that these metabolites were likely uptaken by RBCs from plasma or during circulation through skeletal muscle and other major tissues/organs. Surprisingly, neither GSH nor GSSG in erythrocytes were directly modulated while at rest after high-dose NAC administration (*i.e.*, GSSG levels were attenuated 2-fold during strenuous exercise) despite its

reported claim to function as a glutathione pro-drug with remarkable and versatile clinical properties.<sup>43, 44, 52</sup> In contrast, C0 and C2 were significantly downregulated with the resting C0/C2 ratio lowered by about 2-fold with NAC pretreatment whose concentrations remained unchanged after prolonged cycling exercise, unlike the control trial where they were found to be highly oscillating and persistently elevated up to 3 hrs post-exercise. The latter observation is consistent with previous findings demonstrating that high-intensity exercise can elicit a significant increase in short-chain acylcarnitine content in muscle tissue, as well as circulating levels in plasma.<sup>79</sup> Since  $\beta$ -oxidation pathway is the primary energy source in skeletal muscle tissue involving C0 as a cofactor for transport of activated fatty acyl groups across the inner mitochondrial or peroxisomal membrane by acyltransferases for ATP generation, lower levels of C0 and short-chain acylcarnitines (*i.e.*, C2, C3) measured in this study are indicative of enhanced fat catabolism and reduced lipid-induced oxidative stress following NAC pretreatment.<sup>80</sup> Accumulating evidence has demonstrated that NAC can protect mitochondrial respiratory chain proteins from oxidative damage while supporting mitochondrial energetic capacity<sup>81</sup>. Similarly, Cre is also involved in energy metabolism as well as cellular ATP regulation, where it is found in large pools within muscle tissue that have high creatine kinase activity.<sup>82</sup> Although creatine phosphate is the preferred energy reserve in skeletal muscle while at rest or during low-level physical exercise, it is rapidly depleted during strenuous exercise to generate ATP and creatine. Thus, the characteristic build-up

of creatine detected in erythrocytes post-exercise during the control trial is suggestive of heightened energy demands and possible muscle damage due to physical overexertion in the control trial that were effectively suppressed with NAC pretreatment. The inhibitory effect of NAC is supported by recent studies that have demonstrated that creatine kinase can be transiently inactivated by low molecular weight thiols during oxidative insult via protein *S*-thiolation of the active-site cysteine residue of the enzyme.<sup>83</sup> In addition, 3-MeHis was found to be markedly depleted following NAC intake, as well as exhibiting a 10-fold lower relative concentration in RBCs post-exercise relative to the control. Since 3-MeHis is a recognized diagnostic marker of muscle protein (myofibrillar) proteolysis that is not recycled or further metabolized,<sup>42, 84</sup> this infers a significant attenuation in the rate of protein breakdown with NAC pretreatment both at rest and during strenuous exercise. For instance, the enzymes and organelles that comprise the proteasome serve to selectively degrade irreversibly oxidized protein prior to their detrimental accumulation in cells.<sup>85</sup> Recently, a similar decrease in 3-MeHis levels in serum was identified using a predictive metabolomics model when ingesting a low carbohydrate-protein beverage immediately after strenuous cycling that modulated metabolic responses into a pro-anabolic state thereby decreasing the extent of muscle protein turn-over.<sup>36</sup> In our work, downregulation of 3-MeHis was realized with NAC prior to exercise that is consistent with an overall reduction in cellular oxidative stress and lower muscle fatigue.<sup>58</sup> These observations are also consistent with previous studies that have demonstrated that

thiol supplements (*e.g.*, cysteine and NAC) can significantly decrease 3-MeHis levels by attenuating oxidative modifications to protein with a concomitant decrease in proteolysis activity.<sup>86, 87</sup> Figure 4.7 summarizes the major metabolic pathways involving the early and late-stage biomarkers of oxidative stress identified in this study, which are associated with primary antioxidant defense (GSH/GSSG) in erythrocytes, as well as energy metabolism (C0/C2, Cre) and protein turn-over (3-MeHis) processes in skeletal muscle. Although regular high-meat consumption has been reported to elevate these same metabolites in urine,<sup>34</sup> dietary impacts on this study were minimized by performing exercise trials while fasting while maintaining a similar diet for 48 hrs prior to both cycling trials. In addition, the reversibility in global erythrocyte metabolism after NAC was discontinued relative to the control trial that was performed seven weeks earlier, further supports the causal role of NAC to transiently induce a pro-anabolic status with enhancement of energy metabolism that attenuates cellular oxidative stress while delaying the onset of muscle fatigue.

**4.5.4. Redox-control of Global Metabolism and Future Directions.** NAC represents one of the most widely investigated antioxidants to date with a long clinical history serving as a mucolytic agent for treatment of chronic bronchitis and antidote for acute acetaminophen poisoning.<sup>52</sup> Although there have been documented adverse health effects with intravenous NAC administration, high-dose oral NAC is a safe and well-tolerated mode of intake albeit less efficient due to its poor bioavailability.<sup>61</sup> In addition to its known biological functions as a free

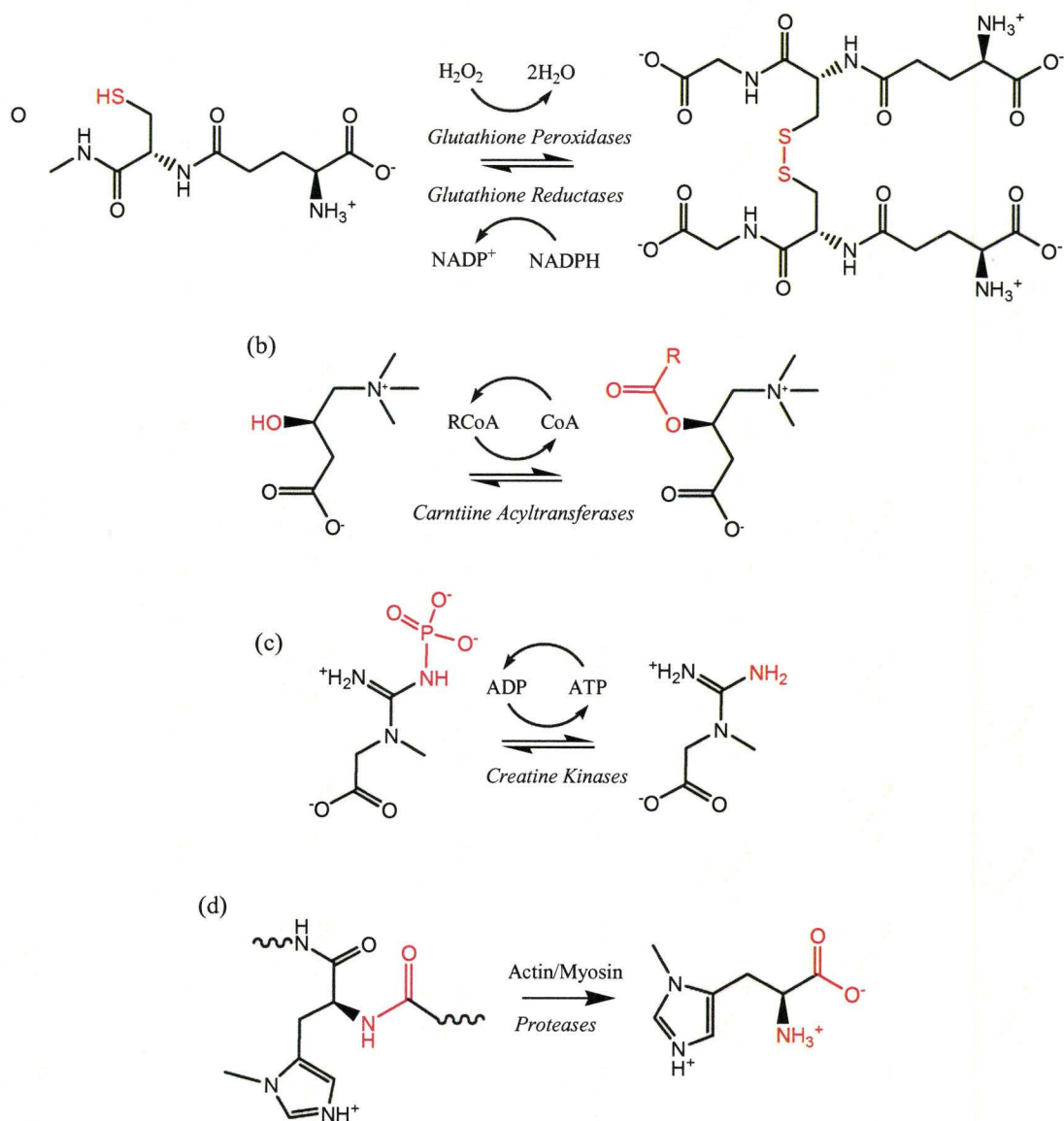


**Figure 4.7.** A summary of four major metabolic reactions associated with oxidative stress biomarkers identified in this study, namely GSH, GSSG, C0, C2, Cre and 3-MeHis. The efficacy of NAC pretreatment in attenuating oxidative stress while delaying the onset of fatigue during strenuous exercise is associated with inhibition of key cellular energy metabolic pathways involving skeletal muscle tissue, such as fatty acid catabolism involving acylcarnitine transport and creatine kinase activity for ATP regulation. Reduced energy demands at rest and during prolonged cycling with NAC pretreatment generates lower levels of RONS corresponding to a decrease in the extent of glutathione oxidation (GSSG) and a slower rate of proteolysis in muscle tissue as indicated by lower amounts of 3-MeHis uptaken by RBCs.

radical scavenger, reducing agent and metal chelator, there is growing recognition that its many therapeutic benefits originates from multiple and non-specific actions associated with redox signaling and control as mediated by protein *S*-thiolation inhibition.<sup>44</sup> Indeed, increasing evidence suggests that oxidative stress and redox regulation play essential roles in determining muscle fatigue which impact exercise performance, although most nutritional antioxidants to date have not been shown to reduce fatigue as significantly as NAC.<sup>58</sup> Our preliminary studies have demonstrated that metabolomics provides a unique and unbiased approach for elucidating the systemic impact that nutritional supplements can have on cellular metabolism when using erythrocytes as model reporter cells of whole-organism oxidative stress status. Future work will investigate a larger cohort of subjects to better evaluate inter-individual biological variability with high-dose oral NAC administration for attenuating exercise-induced oxidative stress. Further improvements to method sensitivity when using CE-ESI-MS are still needed for the detection of sub-micromolar levels of free thiols (*e.g.*, Cys, NAC) in filtered RBC lysates that have poor ionization efficiency in ESI-MS.<sup>49</sup> Moreover, new strategies for qualitative identification of unknown low abundance metabolites using high resolution MS technology in conjunction with computer simulations are also a critical feature to biomarker discovery in metabolomics research since ligand database entries are incomplete and access to authentic standards is still lacking.

#### 4.6. Conclusions

Differential metabolomics by CE-ESI-MS offers a novel strategy for quantitative assessment of oxidative stress and antioxidant efficacy with strenuous exercise based on standardized ergometer cycling trials. Rigorous method validation and careful data preprocessing were key features required for generating artifact-free analysis of labile metabolites without overestimating total numbers of authentic metabolites detected prior to unsupervised data exploration using multivariate analysis. PCA of standardized data sets was used to reveal several early (*i.e.*, GSSG and GSH) and late-stage (*e.g.*, C0, C2 and Cre) biomarkers of oxidative stress that were highly modulated during prolonged endurance exercise or post-exercise during recovery (< 3 hrs), respectively. Univariate data analysis of forty-two metabolites reliably quantified throughout the experimental trials was performed to assess specific metabolites that were modulated with high-dose oral NAC administration relative to the control, such as 3-MeHis. Unexpectedly, the majority of metabolites detected in erythrocytes were transiently downregulated with oral NAC intake by about 30% relative to the control when consumed shortly before the start of the exercise, however this perturbation was reversible once supplementation was discontinued. Although GSH and GSSG were found not to be directly modified with NAC supplementation in this work, they did reflect attenuation of oxidative stress in erythrocytes with strenuous exercise based on the change in half-cell reduction potential for glutathione at peak oxidation and/or the time-lag required to recover to redox homeostasis after acute

oxidative insult. In addition, 3-MeHis, C0, C2 and Cre uptaken by erythrocytes during circulation were all found to be significantly depleted and largely unmodulated during strenuous exercise with NAC pretreatment relative to the control, which indicated oxidative stress inhibition and suppressed energy metabolism/protein turn-over resulting in a corresponding delay in the onset of fatigue. Metabolomics offers an exciting approach for revealing non-specific, systemic and unanticipated perturbations on cellular metabolism that can accompany nutritional intervention, while elucidating the mechanisms of action of widely used yet poorly understood redox-active antioxidants, such as NAC. Further investigations of the time and dose-dependence of oral NAC administration, protein targets of inhibition, as well as the long-term impacts of thiol-based therapy are warranted for better understanding of redox-control mechanisms of protein activity and cellular metabolism.

### **Acknowledgements**

This work is supported by funds provided by the National Science and Engineering Research Council of Canada and the Canada Foundation for Innovation. R.L. acknowledges support in the form of an Ontario Graduate Scholarship. The authors thank Dr. Matthew Henderson for his assistance with multivariate data visualization of metabolite profiles using 3D heatmaps.

#### 4.7. References

- (1) Harman, D., *J. Gerontol.* **1956**, 11, 298-300.
- (2) Harman, D., 1954-2009. *Biogerontology* **2009**, DOI: 10.1007/s10522-009-9234-2.
- (3) Sies, H., Ed. Academic Press: London, 1985; pp 1-8.
- (4) Ott, M.; Gogvadze, V.; Orrenius, S.; Zhivotovsky, B., *Apoptosis* **2007**, 12, 913-922.
- (5) Implay, J. A., *Annu. Rev. Microbiol.* **2003**, 57, 395-418.
- (6) Minetti, M.; Agati, L.; Malorni, W., *Cardiovascular Res.* **2007**, 75, 21-28.
- (7) Fang, F. C., *Nature Rev. Microbiol.* **2004**, 2, 820-832.
- (8) Winzer, K.; Noorden, C. J. F. V.; Kohle, A., *Aquatic Toxicity* **2002**, 59, 17-33.
- (9) Schafer, F. Q.; Buettner, G. R. *Free Radic. Biol. Med.* **2001**, 30, 1191-1212.
- (10) Franco, R.; Schoneveld, O. J.; Pappa, A.; Panayiotidis, M. I., *Arch. Physiol. Biochem.* **2007**, 113, 234-258.
- (11) Pastore, A.; Federici, G.; Bertini, E.; Piemonte, F., *Clinica Chimica Acta* **2003**, 333, 19-39.
- (12) Sies, H., *Free Radic. Biol. Med.* **1999**, 27, (9-10), 916-921.
- (13) Sohal, R. S.; Mockett, R. J.; Orr, W. C., *Free Radic. Biol. Med.* **2002**, 33, 575-586.

- (14) Pryor, W. A.; Squadrito, G. L., *Am J Physiol Lung Cell Mol Physiol* **1995**, 268, L699-L722.
- (15) Jones, D. P., *Antioxidants & Redox Signalling* **2006**, 8, 1865-1879.
- (16) Jones, D. P., *Am. J. Physiol. Cell Physiol.* **2008**, 295, C849-C868.
- (17) Gems, D.; Partridge, L., *Cell Metabolism* **2008**, 8, 200-203.
- (18) Radak, Z.; Chung, H. Y.; Koltai, E.; Taylor, A. W.; Goto, S., *Ageing Res. Rev.* **2008**, 7, 34-42.
- (19) Gomez-Cabrera, M.-C.; Domenech, E.; Vina, J., *Free Radic. Biol. Med.* **2008**, 44, 126-131.
- (20) Dalle-Donne, I.; Rossi, R.; Colombo, R.; Giustarini, D.; Milzani, A., *Clin. Chem.* **2006**, 52, 601-623.
- (21) Bloomer, R. J.; Goldfarb, A. H.; Wideman, L.; McKenzie, M. J.; Consitt, L. A., *J. Strength Cond. Res.* **2005**, 19, 276-285.
- (22) Urso, M. L.; Clarkson, P. M., *Toxicology* **2003**, 189, 41-54.
- (23) Leeuwenburgh, C.; Heinecke, J. W., *Current Med. Chem.* **2001**, 8, 829-838.
- (24) Rossi, R.; Dalle-Donne, I.; Milzani, A.; Giustarini, D., *Clin. Chem.* **2006**, 52, 1406-1414.
- (25) Sparaco, M.; Gaeta, L. M.; Tozzi, G.; Bertini, E.; Pastore, A.; Simonati, A.; Santorelli, F. M.; Piemonte, F., *J. Neurosci. Res.* **2006**, 83, 256-263.
- (26) Rossi, R.; Milzani, A.; Dalle-Donne, I.; Giustarini, D.; Lusini, L.; Colombo, R.; Di Simplicio, P., *Clin. Chem.* **2002**, 48, 742-753.

- (27) Giustarini, D.; Dalle-Donne, I.; Colombo, R.; Milzani, A.; Rossi, R., *Free Radic. Biol. Med.* **2003**, *35*, 1365-1372.
- (28) Steghens, J. P.; Flourie, F.; Arab, K.; Collombel, C., *J. Chromatogr. B* **2003**, *798*, 343-349.
- (29) Jones, D. P.; Carlson, J. L.; Samiec, P. S.; Jr., P. S.; Mody, V. C.; Reed, R. L.; Brown, L. A., *Clin. Chim. Acta* **1998**, *275*, 175-184.
- (30) Lee, R.; Britz-McKibbin, P., *Anal. Chem.* **2009**, *81*, 7047-7056.
- (31) Lindon, J. C.; Nicholson, J. K.; Holmes, E., *The handbook of Metabonomics and Metabolomics*. 1st edition ed.; Elsevier Science: Amsterdam, 2006.
- (32) Sreekumar, A.; Poisson, L. M.; Rajendiran, T. M.; Khan, A. P.; Cao, Q., *Nature* **2009**, *457*, 910-914.
- (33) Soga, T.; Baran, R.; Suematsu, M.; Ueno, Y.; Ikeda, S.; Sakurakawa, T.; Kakazu, Y.; Ishikawa, T.; Robert, M.; Nishioka, T.; Tomita, M., *J. Biol. Chem.* **2006**, *281*, 16768-16776.
- (34) Stella, C.; Beckwith-Hall, B.; Cloarec, O.; Holmes, E.; Lindon, J. C.; Powell, J.; Ouderaa, F. v. d.; Bingham, S.; Cross, A. J.; Nicholson, J. K., *J. Prot. Res.* **2006**, *5*, 2780-2788.
- (35) Rezzi, S.; Ramadan, Z.; Fay, L. B.; Kochhar, S., *J. Prot. Res.* **2007**, *6*, 513-525.
- (36) Chorell, E.; Moritz, T.; Branth, S.; Antti, H.; Svensson, M. B., *J. Prot. Res.* **2009**, *8*, 2966-2977.

- (37) Michailidis, Y.; Jamurtas, A. Z.; Nikolaidis, M. G.; Fatouros, I. G.; Koutedakis, Y.; Papassotiriou, I.; Kouretas, D., *Med. Sci. Sports Exercise* **2007**, 39, 1107-1113.
- (38) Gohil, S.; Viguie, C.; Stanley, W. C.; Brooks, G. A.; Packer, L., *J. Appl. Physiol.* **1988**, 64, 115-119.
- (39) Ramautar, R.; Somsen, G. W.; Jong, G. J. d., *Electrophoresis* **2009**, 30, 276-291.
- (40) Monton, M. R. N.; Soga, T., *J. Chromatogr. A* **2007**, 1168, 237-246.
- (41) Kerksick, C.; Willoughby, D., *J. Inter. Soc. Sports Nutr.* **2005**, 2, 38-44.
- (42) Lukaski, H. C.; Mendez, J.; Buskirk, E. R.; Cohn, S. H., *Am. J. Physiol.* **1981**, 240, E302-E307.
- (43) Atkuri, K. R.; Mantovani, J. J.; Herzenberg, L. A.; Herzenberg, L. A., *Current Opinion Pharmacol.* **2007**, 7, 355-359.
- (44) Zafarullah, M.; Li, W. Q.; Sylvester, J.; Ahmad, M., *Cell. Mol. Life Sci.* **2003**, 60, 6-20.
- (45) Sen, C. K., *Mol. Cell. Biochem.* **1999**, 196, 31-42.
- (46) Adair, J. C.; Knoefel, J. E.; Morgan, N., *Neurology* **2001**, 57, 1515-1517.
- (47) Tossios, P.; Bloch, W.; Huebner, A.; Raji, M. R.; Dodos, F.; Klass, O.; Suedkamp, M.; Kasper, S. M.; Hellmich, M.; Mehlhorn, U., *J. Thorac. Cardiovasc. Surg.* **2003**, 126, 1513-1520.
- (48) Chalcraft, K. R.; Britz-McKibbin, P., *Anal. Chem.* **2009**, 81, 307-314.

- (49) Chalcraft, K. R.; Lee, R.; Mills, C.; Britz-McKibbin, P., *Anal. Chem.* **2009**, 81, 2506-2515.
- (50) Baidoo, E. E. K.; Benke, P. I.; Neussus, C.; Pelzing, M.; Kruppa, G.; Leary, J. A.; Keasling, J. D., *Anal. Chem.* **2008**, 80, 3112-3122.
- (51) Lee, R.; Ptolemy, A. S.; Niewczas, L.; Britz-McKibbin, P., *Anal. Chem.* **2007**, 79, 403-415.
- (52) Kelly, G. S., *Altern. Med. Review* **1998**, 3, 114-127.
- (53) Velzen, E. J. J. v.; Westerhuis, J. A.; Duynhoven, J. P. M. v.; Dorsten, F. A. v.; Hoefsloot, H. C. J.; Jacobs, D. M.; Smit, S.; Draijer, R.; Kroner, C. I.; Smilde, A. K., *J. Prote Res.* **2008**, 7, 4483-4491.
- (54) Bloomer, R. J.; Fisher-Wellman, K. H., *Gender Medicine* **2003**, 5, 218-228.
- (55) Patterson, A. D.; Li, H.; Eichler, G. S.; Krausz, K. W.; Weinstein, J. N.; A.J. Fornace, J.; Gonzalez, F. J.; Idle, J. R., *Anal. Chem.* **2008**, 80, 665-674.
- (56) <http://www.chm.bris.ac.uk/org/chemometrics/addins/index.html>.
- (57) Kirilin, W. G.; Cai, J. Y.; Thompson, S. A.; Diaz, D.; Kavanagh, T. J.; Jones, D. P., *Free Radic. Biol. Med.* **1999**, 27, 1208-1218.
- (58) Ferreira, L. F.; Reid, M. B., *J. Appl. Physiol.* **2008**, 104, 853-860.
- (59) <http://www.genome.jp/ligand/>.
- (60) Wishart, D. S.; Tzur, D.; Knox, C.; Eisner, R.; Guo, A. C.; Young, N.; **2007**, 35, D521-D526.

- (61) Olsson, B.; Johansson, M.; Gabrielsson, J.; Bolme, P., *Eur. J. Clin. Pharmacol.* **1988**, 34, 77-82.
- (62) Medved, I.; Brown, M. J.; Bjorksten, A. R.; McKenna, M. J., *J. Appl. Physiol.* **2004**, 96, 211-217.
- (63) Kell, D. B., *Drug Discovery Today* **2006**, 11, 1085-1092.
- (64) Viant, M. R., *Mol. BioSyst.* **2008**, 4, 980-986.
- (65) Dunn, W. B.; Bailey, N. J.; Johnson, H. E., *Analyst* **2005**, 130, 606-625.
- (66) Want, E. J.; Nordstrom, A.; Morita, H.; Siuzdak, G., *J. Prot. Res.* **2007**, 6, 459-468.
- (67) Buscher, J. M.; Czernik, D.; Ewald, J. C.; Sauer, U.; Zamboni, N., *Anal. Chem.* **2009**, 81, 2135-2143.
- (68) Williams, B. J.; Cameron, C. J.; Workman, R.; Broeckling, C. D.; Sumner, L. W.; Smith, J. T., *Electrophoresis* **2007**, 28, 1371-1379.
- (69) Han, J.; Danell, R. M.; Patel, J. R.; Gumerov, D. R.; Scarlett, C. O.; Speir, J. P.; Parker, C. E.; Rusyn, I.; Zeisel, S.; Borchers, C. H., *Metabolomics* **2008**, 4, 128-140.
- (70) Nordstrom, A.; Want, E.; Northen, T.; Lehtio, J.; Siuzdak, G., *Anal. Chem.* **2008**, 80, 421-429.
- (71) Ohashi, Y.; Hirayama, A.; Ishikawa, T.; Nakamura, S.; Shimizu, K.; Ueno, Y.; Tomita, M.; Soga, T., *Mol. BioSyst.* **2008**, 4, 135-147.
- (72) Bijlsma, S.; Bobeldijk, I.; Verheij, E. R.; Ramaker, R.; Kochhar, S.; Macdonald, I. A.; Ommen, B. v.; Smilde, A. K., *Anal. Chem.* **2006**, 78, 567-574.

- (73) Unt, E.; Kairane, C.; Vaher, I.; Zilmer, M., *J. Sports Sci. Med.* **2008**, *7*, 344-349.
- (74) Vina, J.; Gomez-Cabrera, M.-C.; Lloret, A.; Marquez, R.; Minana, J. B.; Pallardo, F. V.; Sastre, J., *Life* **2000**, *50*, 271-277.
- (75) Sen, C. K.; Rankinen, T.; Vaisanen, S.; Rauramaa, R., *J. Appl. Physiol.* **1994**, *76*, 2570-2577.
- (76) Medved, I.; Brown, M. J.; Bjorksten, A. R.; Murphy, K. T.; Petersen, A. C.; Sostaric, S.; Gong, X.; McKenna, M. J., *J. Appl. Physiol.* **2004**, *97*, 1477-1485.
- (77) Kranner, I.; Birtic, S.; Anderson, K. M.; Pritchard, H. W., *Free Radic. Biol. Med.* **2006**, *40*, 2155-2165.
- (78) McKenna, M. J.; Medved, I.; Goodman, C. A.; Brown, M. J.; Bjorksten, A. R.; Murphy, K. T.; Petersen, A. C.; Sostaric, S.; Gong, X., *J. Physiol.* **2006**, *576*, 278-288.
- (79) Hiatt, W. R.; Regensteiner, J. G.; Wolfel, E. E.; Ruff, L.; Brass, E. P., *J. Clin. Invest.* **1989**, *84*, 1167-1173.
- (80) Koves, T.; Ussher, J.; Noland, R.; Slentz, D.; Mosedale, M.; Ilkayeva, O.; Bain, J.; Stevens, R.; Dyck, J.; Newgard, C., *Cell Metabolism* **2008**, *7*, 45-56.
- (81) Banaclocha, M. M., *Medical Hypotheses* **2001**, *56*, 472-477.
- (82) Wyss, M.; Kaddurah-Daouk, R., *Physiol. Rev.* **2000**, *80*, 1107-1213.
- (83) Reddy, S.; Jones, A. D.; Cross, C. E.; Wong, P. S.-Y.; Vliet, A. v. d., *Biochem. J.* **2000**, *347*, 821-827.

- (84) Long, C. L.; Dillard, D. R.; Bodzin, J. H.; Geiger, J. W.; Blakemore, W. S  
*Metabolism* **1988**, 37, 844-849.
- (85) Friguet, B., *FEBS Letters* **2006**, 580, 2910-2916.
- (86) Nakashima, K.; Masaki, S.; Yamazaki, M.; Abe, H., *Biosci. Biotechnol.  
Biochem.* **2006**, 68, 2326-2331.
- (87) Droge, W.; Gross, A.; Hack, V.; Kinsharf, R.; Schykowski, M.;  
Bockstette, M.; Mihm, S.; Galter, D., *Adv. Pharmacol.* **1996**, 38, 581-600.

*Chapter V*

Metabolomic Studies of Radiation-induced Apoptosis of Human Leukocytes  
by Capillary Electrophoresis-Mass Spectrometry and Flow Cytometry:  
Adaptive Cellular Response to Ionizing Radiation

## **V. Metabolomic Studies of Radiation-induced Apoptosis of Human Leukocytes by Capillary Electrophoresis-Mass Spectrometry and Flow Cytometry: Adaptive Cellular Response to Ionizing Radiation.**

### **5.1. Abstract**

There is growing interest in the development of new methods for elucidating the biological effects of low-dose exposure to ionizing radiation (IR) on human health. Herein, we introduce a new strategy for assessment of the impact of radiation-induced oxidative stress on the intra-cellular metabolism of human leukocytes as a model cell system. Untargeted metabolomic analyses of filtered white blood cell (WBC) lysates were performed by capillary electrophoresis-electrospray ionization-mass spectrometry (CE-ESI-MS) on irradiated-leukocytes exposed to increasing doses of  $\gamma$ -radiation emitted from a Taylor source (*i.e.*, 0, 2, 4, 8 Gy) which were subsequently incubated for 44 hrs to allow for cellular recovery. Flow cytometry (FC) with dual fluorescence staining revealed a major shift from early to late-stage apoptosis associated with cell membrane permeability changes as radiation dosage was increased relative to the control, but with a significant attenuation measured at intermediate dose levels. CE-ESI-MS analysis of filtered WBC lysates was also performed to quantify changes associated with 22 unique intra-cellular metabolites which were consistently measured in leukocytes across all radiation levels. Preliminary experiments demonstrated that there was an overall depletion in metabolites with extended exposure to IR, however there was a non-linear upregulation of specific metabolites at the 4 Gy level relative to pre-irradiated levels, notably for arginine

(Arg), glutamine (Gln), creatine (Cre), proline (Pro) and reduced glutathione (GSH). These *in-vitro* experiments demonstrate that healthy leukocytes exhibit an adaptive oxidative stress response at a minimum threshold radiation dosage that is relevant to new advances in radiobiology and cancer therapy.

## 5.2. Introduction

The theory of hormesis is a contentious hypothesis within toxicology and risk assessment based on a non-linear dose-response model that describes the putative stimulatory effects of low-dose exposure to normally inhibitory or toxic agents.<sup>1-3</sup> Exposure of organisms to extrinsic stressors is not only limited to low levels of xenobiotics in the environment,<sup>4</sup> but also extends to ionizing radiation (IR).<sup>5</sup> Although epidemiological studies have unambiguously demonstrated adverse human health effects with a greater risk for cancer development when subjects are exposed to acute levels of radiation,<sup>6</sup> the biological impacts of chronic low-dose exposure is still unclear despite the increasing use of diagnostic radiology in medicine.<sup>7-9</sup> Radiation toxicity results in increased oxidative stress triggered by the direct ionization of biological polymers (*e.g.*, DNA, protein) and/or indirect modifications to cellular components by reactive oxygen species (ROS) generated by the radiolysis of water, such as the hydroxyl radical.<sup>10</sup> Acute levels of radiation-induced oxidative stress has been demonstrated to cause deleterious cellular injury as measured by an increase in the extent of lipid peroxidation (*e.g.*, malonaldehyde), DNA and aromatic hydroxylation (*i.e.*, 8-

OHdG, *o*-Tyr), as well as the upregulation of various antioxidant enzymes that reflects an adaptive cellular response mechanism to radiation insult.<sup>11-14</sup> Irreversible modifications to DNA, protein and lipid structure that overwhelm intrinsic cellular antioxidant defense and repair mechanisms can ultimately result in radiation-induced programmed cell death (PCD) or apoptosis.<sup>15</sup>

Despite the long-recognized benefit of IR as an adjunctive therapy for treatment of tumours,<sup>16,17</sup> strategies for determination of optimum dose rates to enhance intervention efficacy and long-term survivorship of patients are lacking. For instance, several reports have investigated the therapeutic benefits of low-dose radiation as a means to induce an adaptive response such that subsequent high-dose administration is better tolerated with less adverse health effects. Recently, Day *et al.*<sup>18</sup> demonstrated the enhanced effects of a priming dose 4 hrs prior to a high level challenge dose on chromosomal inversion of mice prostate cells. Similarly, whole body X-ray radiation on mice pretreated with a priming dose has been reported to exhibit fewer instances of chromosomal damage that was associated with extended survival rates.<sup>19</sup> In contrast, several studies have also demonstrated that low-dose radiation (< 0.1 Gy) can induce detrimental perturbations in normal cellular activity.<sup>20-24</sup> For instance, Sakamoto-Hojo *et al.*<sup>25</sup> reported variations of gene expression in human leukocytes from health care workers from chronic exposure of low levels of IR using cDNA microarrays. Kang *et al.*<sup>26</sup> investigated the effects of prolonged IR exposure on peripheral blood lymphocytes in nuclear workers to identify gene aberrations arising from

low-dose exposure, where four putative gene markers were used to estimate radiation exposure. Indeed, the conflicting reports regarding the biological impact of low-dose exposure to IR are likely a function of the experimental design (*e.g.*, dose rate), cell model system and assays used to target a limited set of biomarkers of oxidative damage that are not always representative of cell phenotype.

In this context, new strategies for assessment of global perturbations in cellular metabolism may offer deeper insight into the paradoxical stimulatory and/or detrimental effects of low-dose irradiation. To date, there have been only a limited number of studies investigating the impact of IR on changes in intracellular metabolites<sup>27, 28</sup> often using high-dose irradiation (*i.e.*, > 20 Gy).<sup>29-31</sup> Several research groups have used NMR for targeted profiling of phospholipids, nucleotides and other classes of metabolites associated with cellular apoptosis when using tumour cell lines relative to controls.<sup>32</sup> Metabolomics represents an expanding area of systems biology which can be used to quantitatively assess the functional impact of extrinsic stressors based on the comprehensive analysis of metabolites in a cell or biofluid.<sup>33, 34</sup> Recently, Patterson *et al.*<sup>35</sup> reported an untargeted metabolomics strategy using UPLC-TOF-MS to evaluate the effect of low-dose radiation on cultured cell lines at different dose levels and incubation times, which identified changes in the response of specific metabolites associated with DNA and protein repair, such as reduced glutathione (GSH) and spermine. However, their report did not adequately quantify changes in metabolite concentrations due to IR insult, as well as assess changes in cell membrane

structure associated with apoptosis. In this study, an untargeted metabolomics strategy was developed for the assessment of radiation-induced oxidative stress involving healthy leukocytes exposed to increasing levels of  $\gamma$ -radiation (*i.e.*, 0, 2, 4, 8 Gy), which were subsequently incubated for 44 hrs to allow for adaptive cellular repair and/or recovery. Metabolomic analyses was performed by capillary electrophoresis-electrospray ionization-mass spectrometry<sup>36</sup> (CE-ESI-MS) using filtered white blood cell (WBC) lysates, which revealed an unexpected non-linear change in global metabolism reflected by a significant upregulation of specific metabolites induced at a minimum threshold of radiation (*i.e.* 4 Gy), in contrast to other dose regimes where metabolites were extensively depleted relative to the control. Flow cytometry (FC) using a dual-staining fluorescence method was also performed on irradiated-leukocytes in order to differentiate radiation-induced cell membrane perturbations associated with early and late-stage apoptosis. CE-ESI-MS in conjunction with FC offers a promising approach for assessing metabolite responses to radiation-induced oxidative stress, which can reveal unexpected dose-response relationships for improved understanding of the biological impacts of low-dose IR on cell viability and differentiation.

### **5.3 Materials and Methods**

**5.3.1. Chemicals and Reagents.** De-ionized water used for buffer and sample preparations was obtained using a Barnstead EASYpureII LF ultrapure water system (Dubuque, IA). A 1 M formic acid buffer (pH 1.8) was prepared by dilution of concentrated formic acid derived from Sigma-Aldrich (St. Louis, MO). All metabolite standards were purchased from Sigma-Aldrich. Individual stock solutions of 10 mM were prepared in 1:1 methanol/water. All solutions and solvents were degassed and chilled to 4°C prior to use.

**5.3.2. Cell Culture and Irradiation.** A total of 54 mL of blood was collected into sodium heparin venous blood collection tubes from a healthy volunteer. Leukocytes were separated from whole blood by density gradient (Ficoll-Histopaque-1077, Oakville, Canada) and washed twice with Roswell Park Memorial Institute (RPMI)-1640. Cell concentrations were determined using a Z2 counter (Beckman Coulter, Mississauga, Canada) and adjusted to a final concentration of  $1 \times 10^6$  cells/mL with RPMI media supplemented with 15% heat-inactivated bovine serum 1% glutamine, 1% penicillin/streptomycin. 6 mL of leukocyte culture was placed into 8 flasks and irradiated with 661 keV  $\gamma$ -rays using a Taylor source equipped with a  $^{137}\text{Cs}$  source housed at McMaster University. Two replicate flasks for each dosage (0, 2, 4, 8 Gy) were irradiated on ice at a dose rate of 0.1 Gy/min, where the control cells were sham-irradiated without exposure to the  $^{137}\text{Cs}$  source. All flasks were initially placed together in the same radiation container and then removed at time intervals corresponding to

the appropriate total dosage of radiation, where 2 Gy = 20 min, 4 Gy = 40 min and 8 Gy = 80 min. The cultures were then incubated post-irradiation in a controlled environment at 37°C with a humidified atmosphere of 5% CO<sub>2</sub> for 44 hr in order to allow for adequate time for cellular responses to adapt following oxidative insult.<sup>37, 38</sup> Since healthy leukocytes were used without further fractionation, intra-cellular metabolomic changes measured in this study derive from a heterogeneous mixture of viable WBCs, such as neutrophils, lymphocytes, macrophages and monocytes.

**5.3.3. Flow Cytometric Assay.** Leukocytes were analyzed with a Beckman Coulter EPICS XL Flow Cytometer (Beckman Coulter, Mississauga, Canada) using commercially available Annexin-V-FITC (AnxV) and 7-amino-actinomycin (7-AAD) assay kits (Beckman Coulter). Three samples of  $2.5 \times 10^5$  cells from each flask were placed into 5 mL tubes, centrifuged at 500 rpm for 5 min and supernatant removed. 10 µL of 7-AAD, 5 µL of AnxV and 100 µL of binding buffer were added to each tube and incubated on ice for 15 min. Fluorescence was collected at emission wavelengths of 525 nm and 675 nm for FITC and 7-AAD, respectively. For statistical significance  $1 \times 10^4$  leukocytes were quantified by flow cytometry as reported in previous reports.<sup>37, 38</sup> Flow cytometry data was processed and plotted as 3D contour plots using Microsoft Excel 2007 (Microsoft, Microsoft Inc., Redmond, WA, USA.)

**5.3.4. Metabolite Extraction.** Each flask was vortexed and centrifuged at 4°C, 7000 rpm, for 1 min and supernatant was removed to isolate leukocytes. Leukocytes were washed twice with PBS to remove any residual RPMI media. 20 µL of pre-chilled water was added to each sample to induce hypotonic lysis and centrifuged at 4°C, 7000 rpm, for 1 min to separate cell debris. The WBC lysate was then centrifuged through a 3kDa filter (PALL Corporation, Ann Arbor, Michigan) at 4°C, 14,000 rpm, for 15 min for deproteinization. The protein-free filtered WBC lysate was then stored frozen at -80°C and subsequently thawed for metabolomic analysis by CE-ESI-MS after a two-fold dilution in buffer.

**5.3.5. Apparatus and Conditions.** CE-ESI-MS studies were performed on an automated Agilent CE system equipped with an XCT 3D ion trap mass spectrometer, an Agilent 1100 series isocratic pump, and a G16107 CE-ESI-MS sprayer kit (Agilent Technologies, Waldbronn, Germany). All separations were performed on uncoated fused-silica capillaries (Polymicro Technologies Inc., Phoenix, USA) with 50-µm i.d. and 80-cm total length. 1.0 M formic acid, pH 1.8 was used as the acidic background electrolyte (BGE) for cationic metabolite separations in CE, such as peptides, amino acids and amines. An Agilent 1100 series pump with a 1:100 splitter was used to supply a volume of 10 µL/min of 0.1 % formic acid in 1:1 MeOH/H<sub>2</sub>O as the sheath liquid. Prior to first use, open tubular fused-silica capillaries were conditioned for 20 min with MeOH, de-ionized H<sub>2</sub>O and background electrolyte (BGE). In order to achieve broad

coverage of polar metabolites in filtered RBC lysates, CE-ESI-MS was performed under both acidic (acidic BGE: 1M formic acid, pH 1.8) and alkaline (alkaline BGE: 50 mM ammonium acetate, pH 8.5) conditions to analyze cationic and anionic metabolites under either positive-ion and negative-ion ESI-MS mode, respectively.<sup>39</sup> All samples were introduced into the capillary using a low-pressure (50 mbar) hydrodynamic injection. On-line sample preconcentration using a discontinuous electrolyte system under acidic conditions was performed to improve concentration sensitivity for the analysis of amines, amino acids, peptides and carnitines<sup>40, 41</sup> by first injecting a sample prepared in 200 mM ammonium acetate, pH 7.0 for 75 s at 50 mbar followed by a 60 s injection of the acidic BGE at 50 mbar prior to voltage application. The latter (second) injection sequence was used to displace the original sample plug within the capillary past the electrode interface at the inlet (anode), which was required to avoid CE-induced oxidation artifacts when analyzing low micromolar levels of GSSG in the presence of excess GSH.<sup>39</sup> On-line sample preconcentration of acidic metabolites, such as nucleotides, sugar phosphates and organic acids was performed by first injecting a sample prepared in 10 mM HCl/5 mM ammonium acetate, pH 2.0 for 150 s at 50 mbar followed by a 60 s injection of the alkaline BGE at 50 mbar prior to voltage application. In most cases, filtered WBC lysates were diluted two-fold with acidic or alkaline ammonium acetate solution prior to CE-ESI-MS analysis. An Agilent 1100 series pump equipped with a 1:100 splitter was used to supply a volume of 10  $\mu$ L/min of 5 mM ammonium acetate in

1:1 MeOH/H<sub>2</sub>O as the sheath liquid. Separations were performed at 20°C with an applied voltage of 30 kV. All MS analysis was performed at 300°C using  $\pm 4$  kV as the capillary voltage depending on the ionization mode. Nitrogen gas was used as the nebulizing gas and drying gas at 5 psi and 10 L/min, respectively, whereas helium was employed as the damping gas for the ion trap mass analyzer. All MS data were recorded with a range of 50-750  $m/z$  using the ultrascan mode of 26 000  $m/z$  per second.

**5.3.6. Data Preprocessing and Statistical Analyses.** Data analysis was performed first by manually processing extracted ion electropherograms (EIEs) between  $m/z$  50-750, yielding 700 electropherograms traces for each run. Each sample was analyzed in triplicate ( $n = 3$ ) by CE-ESI-MS under both acidic and alkaline separation conditions, whereas each radiation dose was performed in duplicate resulting in a total of 33 600 EIEs. Noise filtering and data normalization was performed prior to statistical analyses by processing each metabolite signal as a single paired variable denoted as  $m/z$ :RMT, which facilitated data alignment among instrumental and biological replicates. Each EIE was manually integrated with a minimum signal threshold over background noise of  $S/N \approx 10$  in order to avoid signal artifacts, which yielded about one hundred and twenty putative ion signals. Subsequent data preprocessing was performed to eliminate redundant responses originating from the same ion, including isotope contributions, fragment ions, salt adducts, as well as common ions detected under

both +/- ESI-MS conditions, resulting in unambiguous quantification of twenty-two unique metabolite signatures derived from filtered WBC lysates, which were consistently detected across all radiation doses used in the study. This stringent approach towards data analysis was applied in order to enhance data quality for statistical analyses, as well as avoid the tendency to overestimate total numbers of metabolite detected.<sup>35</sup> A two-way parametric student's t-test was applied to compare the significance of changes in measured ion responses for metabolites at increasing levels of irradiation relative to the control. All data analyses and figures were processed using Excel 2007 (Microsoft Inc., Redmond, WA, USA) and Igor Pro 5.0 (Wavemetrics Inc, Lake Oswego, OR).

## **5.4 Results and Discussion**

**5.4.1. Radiation-induced Apoptosis of Leukocytes.** Cells that undergo apoptosis undergo a series of distinctive morphological changes on the outer layer of the membrane which serves as a signaling mechanism for phagocytosis.<sup>42</sup> Depending on the severity of damage to the phospholipid membrane during oxidative insult, cells can be classified as in early or late-stages of apoptosis when exposed to lose-dose IR,<sup>37,38</sup> whereas necrosis is often induced by acute oxidative insult.<sup>43</sup> Healthy cells normally exhibit an asymmetric alignment of phospholipids between the inner and outer layer of the plasma membrane.<sup>43</sup> However, during early-stage apoptosis, phospholipids from the inner membrane are exposed to the surface of the cell, such as phosphatidylserine (PS) which is a

major phospholipid component involved in maintaining cell membrane integrity. Fadok *et al.*<sup>43</sup> reported that PS exposed on the surface of the cellular membrane during apoptosis functions as a molecular signal for recognition by macrophages. In our study, fluorescein isothiocyanate-labeled Annexin-V (AnxV) was used as a probe for assessing early-stage apoptosis<sup>46</sup> based on its selective binding to exposed PS in the presence of  $\text{Ca}^{2+}$  ions. In contrast to more subtle perturbations in cell membrane structure, late-stage apoptosis is characterized by a loss of cellular integrity with increased membrane permeability.<sup>47</sup> To differentiate between early and late-stage apoptosis, a secondary staining method was applied in our work based on 7-amino-actinomycin (7-AAD) as a reporter probe that acts as a DNA intercalating agent.<sup>48</sup> Thus, a dual-staining fluorescence approach based on AnxV and 7-AAD in conjunction with flow cytometry was used to simultaneously distinguish between early and late-stage apoptosis since both probes bind to complementary targets with non-overlapping spectral emissions.<sup>37,</sup>

38

Figure 5.1 illustrates the overall changes in cell viability for leukocytes after exposing cells to increasing doses of  $\gamma$ -irradiation, which was followed by a 44 hr incubation/recovery period prior to sampling. There are three regions of interest when examining the contour plots of cell populations sorted by FC with dual-channel fluorescence detection. The double-negative fluorescence region

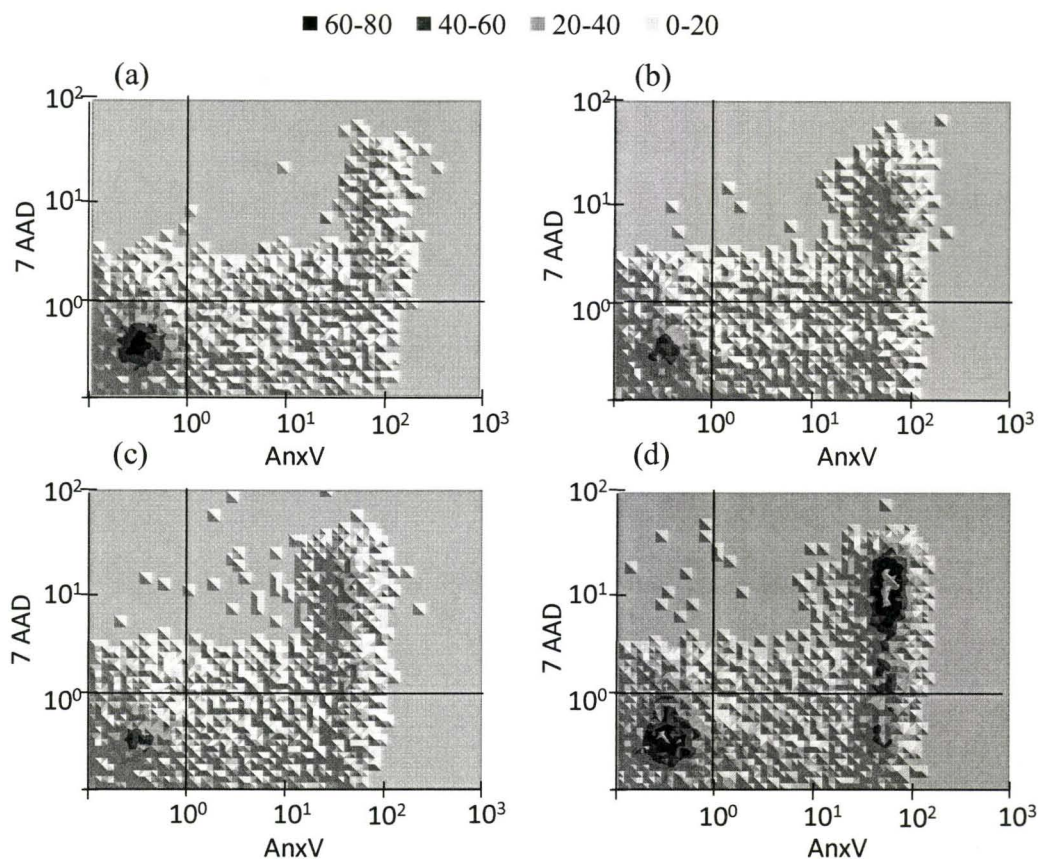


**Figure 5.1.** FC contour plots for differentiating sub-populations of  $\gamma$ -irradiated-leukocytes following a 44 hr incubation period that were exposed to (a) 0, (b) 2, (c) 4 and (d) 8 Gy. Lower left quadrant represents the double-negative staining region of AnxV-/7-ADD- indicating viable cells, lower right quadrant reflects the AnxV+/7-ADD- region corresponding to early-stage apoptosis, whereas the upper right quadrant represents the double-positive staining region of AnxV+/7-ADD+ indicative of late-stage apoptosis. Note that the extent of necrosis (AnxV-/7-ADD+) was not significantly detected in this study (< 0.1%).

(*i.e.*, AnxV-/7-ADD-, bottom left quadrant) represents normal/viable leukocytes with intact cell membrane structures. In contrast, the single AnxV-positive region (*i.e.*, AnxV+/7-ADD-, bottom right quadrant) represents perturbed leukocytes at early-stage apoptosis, whereas the double-positive AnxV/7-AAD region (*i.e.*, AnxV+/7-ADD+, top right quadrant) corresponds to leukocytes associated with irreversible late-stage apoptosis. Duplicate biological samples for each dose level

**Table 5.1.** Dual-staining fluorescence using FC for assessment of fraction of viable cells (AnxV-/7-ADD-), as well as early-stage (AnxV+/7-ADD-), and late-stage (AnxV+/7-ADD+) apoptosis of normal leukocytes exposed to increasing levels of low-dose  $\gamma$ -radiation.

	$\gamma$ -Irradiation Dosage			
	0 Gy (%)	2Gy (%)	4 Gy (%)	8 Gy (%)
AnxV-/7-AAD-	64.6 $\pm$ 1.3	47.0 $\pm$ 1.9	42.8 $\pm$ 0.3	36.9 $\pm$ 1.2
AnxV+/7-AAD-	31.3 $\pm$ 1.1	35.8 $\pm$ 0.5	37.2 $\pm$ 0.3	34.7 $\pm$ 1.4
AnxV+/7-AAD+	4.0 $\pm$ 0.2	16.4 $\pm$ 0.3	20.0 $\pm$ 0.4	28.2 $\pm$ 0.4
<i>Relative increase in late-stage apoptosis</i>	--	12.4 $\pm$ 0.4	3.6 $\pm$ 0.5	8.2 $\pm$ 0.6

were prepared on ice and measured in triplicate, resulting in an overall average of six replicates ( $n = 6$ ) in total for each radiation dose. In this study, necrosis of irradiated-leukocytes under all the dosage levels examined was negligible ( $< 0.1\%$ ) as reflected by the population of cells detected in the single 7-ADD-positive region (*i.e.*, AnxV-/7-ADD+, top left quadrant) in Figure 5.1. However, recent studies have shown that pretreatment of tumour cell lines with epigallocatechin-3-gallate prior to low-dose  $\gamma$ -irradiation can selectively enhance cell death mediated by necrosis.<sup>49</sup> Table 5.1 summarizes the fraction of sub-populations representing viable, early-stage and late-stage apoptotic cells as a function of irradiation dose. The sham-irradiated control cells were found to be predominately viable ( $\approx 65\%$ ) although there was a significant amount of background early-stage apoptosis ( $\approx 31\%$ ) with a low level of late-stage apoptosis ( $\approx 4\%$ ) among *ex-vivo* leukocytes due to the extended *in-vitro* incubation times used for healthy cells.<sup>37, 38</sup> Table 5.1 highlights the dose-dependent shift inviable leukocyte populations which decreased significantly with

longer exposure to  $\gamma$ -radiation, whereas a corresponding increase in late-stage apoptosis was measured ranging from 4-28%. Interestingly, the fraction of cell populations in early-stage apoptosis remained stable and similar to the control throughout all radiation doses, suggesting that radiation-induced oxidative stress primarily triggers irreversible apoptosis after a sufficient incubation time.<sup>50</sup> In addition, a non-linear increase in late-stage apoptosis for leukocytes was observed at higher radiation dose intervals, where cells were exposed to the same dose rate but exposure time was extended. Unexpectedly, a reduced progression in the extent of late-stage apoptosis was observed for cells exposed from 2 Gy to 4 Gy ( $\approx 3.6\%$ ) in comparison to the larger relative increases in cell death determined among other dose intervals. Although the biological effects of radiation are commonly associated with dose-rate, where reduced cellular injury is sustained at longer exposure times when using slower rates of irradiation,<sup>51</sup> our data indicates that leukocytes exhibit increased resistance to late-stage apoptosis *in-vitro* at intermediate exposure times (*i.e.* 4 Gy) sufficient to trigger an adaptive cellular response that was negated at higher dose levels and/or longer exposure times.

**5.4.2. Untargeted Metabolite Profiling by CE-ESI-MS.** Oxidative modifications to biopolymers (*i.e.*, DNA, RNA, protein) upon exposure to high levels of ionizing radiation have been extensively investigated,<sup>52,53</sup> however there have been limited studies examining the effects of low-dose radiation on intracellular metabolites. In order to better understand the apparent changes in cell

viability of irradiated-leukocytes, CE-ESI-MS analyses were performed to quantify global changes in intra-cellular polar metabolites from filtered WBC lysates at three different dose levels. In our work, samples were directly analyzed after initial thawing without complicated off-line sample enrichment or desalting steps. The majority of metabolites detected in leukocytes were identified by comparing their relative migration time (RMT) and molecular ion ( $MH^+$ ) in terms of their paired  $m/z$ :RMT variable similar to previous studies performed on erythrocytes in our laboratory.<sup>39, 41</sup> Unambiguous identification of metabolites were also confirmed by spiking with authentic standards after searching for relevant metabolite candidates in public databases, such as the KEGG Ligand Database<sup>54</sup> and the Human Metabolome Database.<sup>55</sup> Of the 22 polar metabolites which were reliably quantified in filtered WBC lysates, 18 were positively identified with 5 ions representing unknown metabolites. The limited number of detectable metabolites achieved in this study was associated with the low leukocyte densities ( $\approx 1 \times 10^6$ ) required to ensure uniform exposure during  $\gamma$ -irradiation, as well as extensive data preprocessing used to remove redundant and/or artifactual signals from the raw data. Poor sensitivity limited the application of multi-stage  $MS^n$  experiments for characterizing some low abundance unknown metabolites (*e.g.*, X8) using an ion trap mass analyzer, whereas in other cases no consistent candidate was identified after exhaustive database searches based on their putative chemical structure. For instance, metabolites detected by CE-ESI-MS when using acidic buffer conditions with positive-ion mode ionization

restricts likely candidates to cationic or zwitter-ionic metabolites with a weakly basic functional moiety (e.g., amino group) thereby excluding other isobaric species that are either neutral or anionic. An advantage of CE is the ability to accurately predict ion electromigration behavior that can be used to support ESI-MS for the qualitative identification of unknown metabolites *in silico* among several MS-equivalent isobaric and/or isomeric candidates.<sup>56</sup> Nevertheless, qualitative identification of unknown low abundance metabolites represents one of the most significant obstacles in metabolomics research since databases remain incomplete and access to purified commercial standards are often limited.

**5.4.3. Dose-dependent Metabolic Responses to Ionizing Radiation.** Figure 5.2 depicts a series of offset extracted ion electropherograms (EIE) associated with four major unknown metabolites detected in filtered WBC lysates, such as X3 ( $m/z$  116) and its isobaric ions, creatine (Cre) and leucine (Leu), as well as X8 ( $m/z$  132) and its isobaric ion, proline (Pro). Figure 5.2 also highlights the distinctive non-linear changes in apparent ion responses for both unknown and identified metabolites as a function of radiation dose relative to control (refer to arrow direction), where metabolites are depleted at 2 Gy and 8 Gy, but are significantly upregulated at 4 Gy. Figure 5.2(e) quantitatively compares the relative change in concentration of 8 of the most significantly upregulated metabolites at 4 Gy which were identified in filtered WBC extracts. It is apparent that intra-cellular concentration levels for this group of metabolites are increased

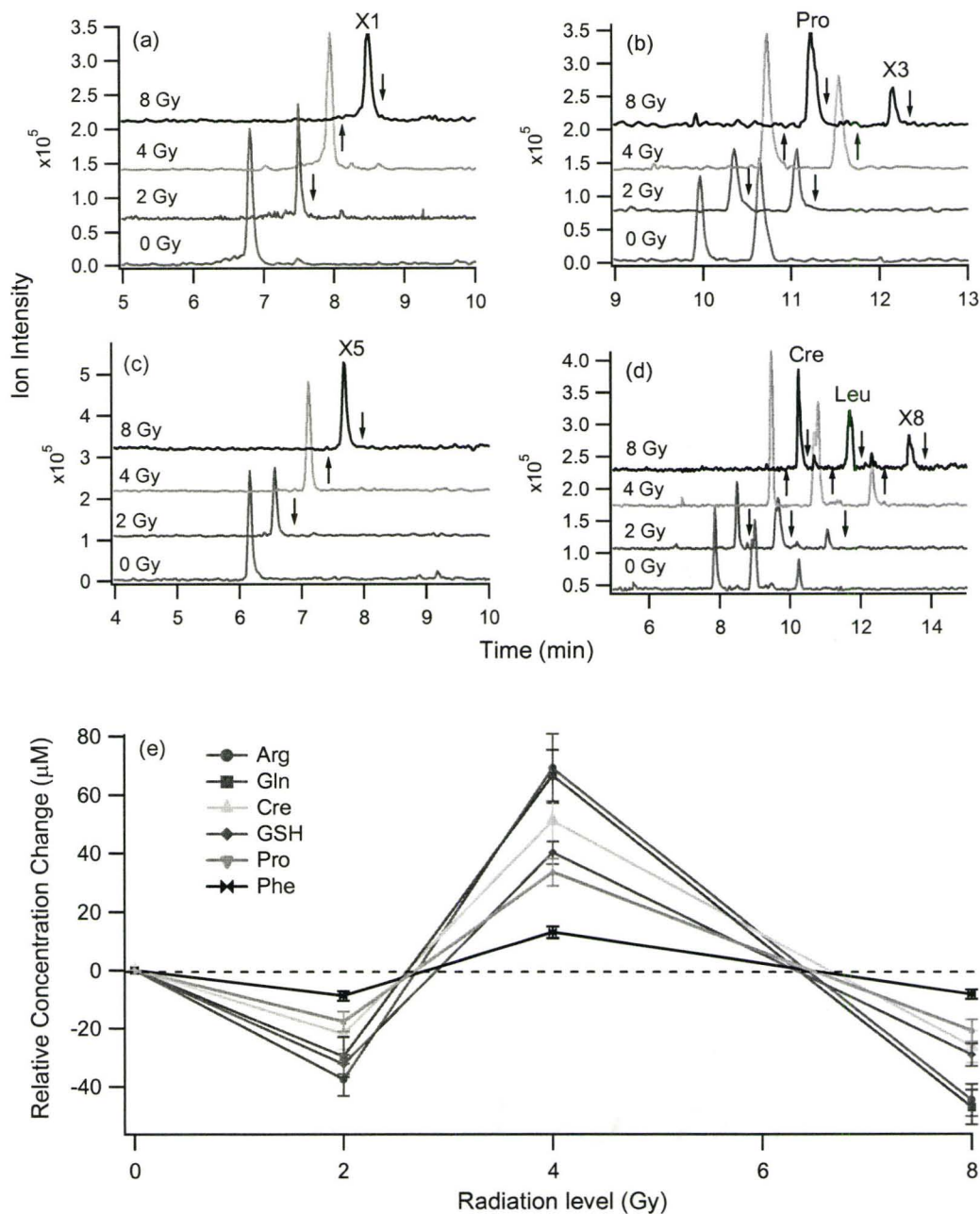


**Figure 5.2.** A series of extracted ion electropherograms (EIE) for four major unknown metabolites and other identified isobaric ions derived from filtered WBC lysates exposed to increasing levels of  $\gamma$ -irradiation. Arrows qualitatively highlight the net depletion or upregulation of metabolites relative to control at increasing radiation dosages when using CE-ESI-MS. (a) unknown X1,  $m/z$  104, (b) unknown X3,  $m/z$  116 with isobar Pro (c) unknown X5,  $m/z$  131 (d) unknown X8,  $m/z$  132 with isobars Cre and Leu, whereas (e) depicts the non-linear dose-response relationship of 6 known metabolites identified from irradiated-leukocytes that exhibited significant upregulation at the 4 Gy level in terms of their relative concentration levels in comparison to the control.

ranging from  $\approx 15\text{-}70\ \mu\text{M}$  above basal levels present in sham non-irradiated control cells, notably arginine (Arg), glutamine (Gln), Cre, Pro and reduced glutathione (GSH). Figure 5.3 provides an overview of the selectivity, magnitude and significance in differences in average ion responses measured for all 22 metabolites relative to the control at 0 Gy. Overall, a significant depletion of metabolites was observed to occur with irradiation from 0 to 2 Gy, where all metabolites were observed to be downregulated ( $P < 0.01$ ) with an average fold-change of  $(0.44 \pm 0.10)$ . Similarly, metabolite responses of leukocytes at the highest dose exposure of 8 Gy also had a significant depletion in metabolite levels relative to the control (except for Cre and X8) albeit to a lower extent than 2 Gy as reflected by an average fold-change of  $(0.61 \pm 0.22)$ . In contrast, irradiated-leukocytes exposed to 4 Gy displayed a selective upregulation in metabolism (except for ATP) with an average fold-change of  $(1.01 \pm 0.30)$  that represents a distinct metabolic state from the control. From the 22 metabolites measured after 4 Gy exposure, 8 were determined to be significantly upregulated ( $P < 0.05$ ), 4 downregulated and 10 recovered back to pre-irradiated levels similar to control as depicted in Figure 5.3. Since ionization efficiency in ESI-MS is highly dependent on intrinsic solute properties that can vary over three-orders of magnitude,<sup>41</sup> changes in apparent relative ion responses for unknown metabolites do not reflect their actual concentration changes in the cell as depicted in Figure 2(e).

**5.4.4. Biological Interpretations of Low-level Irradiation of Leukocytes.** Untargeted metabolite profiling by CE-ESI-MS in conjunction with cell viability studies using FC

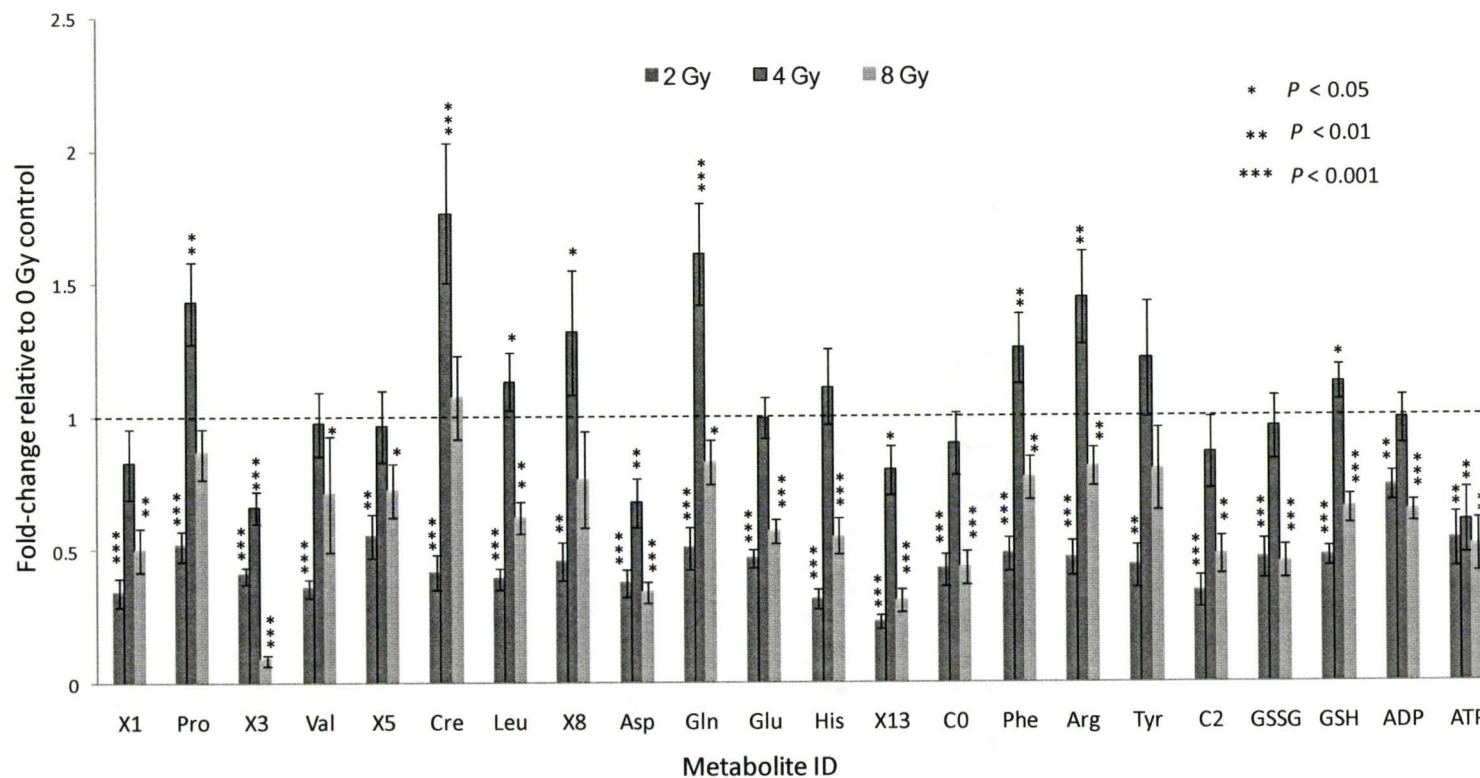


**Figure 5.3.** Histogram illustrating the impact of irradiation dosage on intra-cellular cellular metabolism that shows the non-linear changes in identified and unknown metabolite levels derived from human leukocytes relative to the control at 0 Gy. Blue, red, and green bar graphs represent fold-change in average normalized ion responses measured for metabolites at 2, 4, and 8 Gy radiation relative to the control, where error bars represent  $\pm 1\sigma$  (triplicate measurements from two sets of cell batches,  $n=6$ ). A major depletion in metabolites was consistently measured for most metabolites at the 2 and 8 Gy doses, whereas a significant upregulation or recovery to control levels were detected for the majority of metabolites at the intermediate 4 Gy dose level, notably for Gln, Arg, Pro, Cre and GSH.

with dual-staining fluorescence detection revealed that healthy leukocytes undergo a distinct non-linear dose-response transition *in-vitro* with dose-dose exposure to IR. A reduced progression in late-stage apoptosis reflected by a loss in membrane permeability was correlated with an induction of a significant upregulation and/or recovery of metabolites in viable cells notably at 4 Gy relative to the control or other dose levels. Although overall fold-changes in intra-cellular metabolites at 4 Gy was analogous to the control, significant changes in the concentration profiles of metabolites reflect a distinct cellular phenotype induced above a minimum threshold of radiation ( $> 2$  Gy) after cells were incubated for a fixed time interval of 44 hrs. However, initial exposure of leukocytes to a 2 Gy dose of  $\gamma$ -irradiation resulted in a severe depletion of metabolites that corresponded to a major increase in late-stage apoptosis relative to the control, whereas prolonged exposure to higher doses of radiation ( $> 4$  Gy) negated metabolic responses observed at the intermediate dose levels. These observations are consistent with a biphasic hormetic model which is typically performed using a much slower rate of irradiation as a way to stimulate adaptive cellular responses without triggering apoptosis prior to a subsequent high-dose challenge. Recently, Elmore *et al.*<sup>57</sup> have demonstrated that a minimum threshold of low-dose priming equivalent to about 0.1 Gy delivered at a very low dose rate ranging from 1-4 mGy/day was required to induce adaptive cellular responses that attenuated neoplastic transformation of cells relative to unirradiated controls. Radiation-induced perturbations in metabolic status may reflect cellular

**Table 5.2.** Fold-change in measured ion responses relative to 0 Gy control for twenty-two identified and unknown metabolites quantified in irradiated-leukocytes by CE-ESI-MS as a function of radiation dose. Unidentified metabolites were internally labeled by numerical sequence in their *m/z*:RMT.

Metabolite ID	<i>m/z</i> :RMT	<i>Fold-change response relative to control</i>		
		2 Gy	4 Gy	8 Gy
X1	104:0.793	0.34 ± 0.05	0.83 ± 0.13	0.50 ± 0.08
Pro	116:1.124	0.52 ± 0.06	1.43 ± 0.15	0.87 ± 0.09
X3	116:1.218	0.41 ± 0.03	0.66 ± 0.06	0.09 ± 0.02
Val	118:1.162	0.36 ± 0.04	0.97 ± 0.12	0.71 ± 0.22
X5	131:0.697	0.55 ± 0.08	0.96 ± 0.13	0.73 ± 0.10
Cre	132:0.963	0.42 ± 0.06	1.77 ± 0.26	1.07 ± 0.16
Leu	132:1.087	0.39 ± 0.04	1.13 ± 0.11	0.62 ± 0.06
X8	132:1.232	0.46 ± 0.07	1.32 ± 0.23	0.77 ± 0.18
Asp	134:1.200	0.37 ± 0.05	0.68 ± 0.09	0.34 ± 0.04
Gln	147:1.128	0.51 ± 0.08	1.61 ± 0.19	0.83 ± 0.08
Glu	148:1.144	0.47 ± 0.04	0.99 ± 0.08	0.57 ± 0.05
His	156:0.826	0.32 ± 0.04	1.11 ± 0.14	0.55 ± 0.07
X13	160:0.962	0.23 ± 0.02	0.80 ± 0.09	0.31 ± 0.04
C0	162:0.939	0.43 ± 0.06	0.90 ± 0.12	0.43 ± 0.06
Phe	166:1.159	0.48 ± 0.06	1.25 ± 0.13	0.77 ± 0.08
Arg	175:0.809	0.47 ± 0.07	1.44 ± 0.17	0.81 ± 0.07
Tyr	182:1.187	0.44 ± 0.08	1.21 ± 0.22	0.80 ± 0.15
C2	204:0.986	0.34 ± 0.06	0.86 ± 0.14	0.48 ± 0.07
GSSG	307:1.256	0.47 ± 0.07	0.96 ± 0.12	0.45 ± 0.06
GSH	308:1.359	0.48 ± 0.04	1.13 ± 0.07	0.65 ± 0.05
ADP <sup>a</sup>	426:1.260	0.74 ± 0.05	0.99 ± 0.09	0.64 ± 0.04
ATP <sup>a</sup>	506:1.426	0.54 ± 0.10	0.61 ± 0.12	0.51 ± 0.10
<i>Average fold-change</i>		<b>0.44 ± 0.10</b>	<b>1.03 ± 0.30</b>	<b>0.61 ± 0.22</b>

<sup>a</sup>Metabolites detected by CE-ESI-MS under alkaline separation conditions.

responses associated with adapted changes to antioxidant defense (*e.g.*, GSH, Gln, Pro), cell signaling (*e.g.*, Arg), energy metabolism (*e.g.*, Cre) and/or protein biosynthesis (*e.g.*, Phe). Glutathione metabolism serves as a sensitive biomarker of oxidative stress since it is one most abundant non-enzymatic antioxidant systems that regulates the redox status of cells,<sup>39</sup> where acute GSH depletion has been associated with the regulation of caspase-8-mediated apoptosis.<sup>58</sup> Similarly, Gln can function as an efficient precursor to support GSH biosynthesis, which has been clinically demonstrated to attenuate the extent of oxidative damage with radiotherapy or chemotherapy.<sup>59</sup> In addition, Pro upregulation has recently been shown to be an oxidative stress response in various mammalian cell lines exposed to physiological levels of hydrogen peroxide.<sup>60</sup> Suschek *et al.*<sup>61</sup> have demonstrated that elevated nitric oxide levels protects endothelial cells from oxidative stress-induced apoptotic or necrotic cell death that is dependent on Arg that serves as the key substrate for inducible-nitric oxide synthase. These studies emphasize the various biological functions that amino acids are implicated for regulating cell viability and differentiation during oxidative insult. Since mitochondrial enzymes (*e.g.*, creatine kinase) and transport protein (*e.g.*, carnitine/acylcarnitine translocase) associated with energy homeostasis represent key targets that are inhibited by oxidative stress resulting in loss in bioenergetic capacity,<sup>62</sup> downregulation in Cre, as well as carnitine and acetylcarnitine (*i.e.*, C0 and C2) levels with the onset and after prolonged IR exposure along with their transient increases at 4 Gy parallel the upregulation of key amino acids/peptides for mobilizing antioxidant defense in leukocytes. The major

exception to the overall trend in non-linear metabolic responses with increasing low-level radiation exposure was the consistent depleted state of ATP (refer to Figure 5.3). Since regulation of the cell membrane structure is associated with ATP-dependent translocase enzymes which control the internalization of PS within the phospholipid bilayer,<sup>44</sup> the constant depletion of ATP relative to control can be directly associated with the high background level of early-stage apoptosis measured for irradiated-leukocytes in this study. Further metabolomic studies with improved concentration sensitivity are required to better understand the time-dependent metabolic responses of cells associated with radiation-induced apoptosis that can be modulated by pretreatment with various chemical stressors and/or with ultra-low-rates of radiation exposure.

### **5.5. Conclusion.**

The impact of low-dose exposure to IR was explored in this work by untargeted analysis of changes in intra-cellular metabolism in conjunction with dual staining fluorescence used for flow cytometry. CE-ESI-MS analysis of filtered WBC lysates yielded 22 metabolites which were quantified across all radiation dose levels, of which 18 were unambiguously identified. A comparison of metabolite levels suggests that leukocytes displayed a non-linear response mechanism that is associated with low-dose radiation. Unexpectedly, at the lowest radiation exposure (2 Gy), a significant downregulation of all metabolites was observed compared to the sham-irradiated control cells. The increase of metabolic activity detected at the intermediate

radiation dose (4 Gy) indicates that there was an underlying mechanism of cellular repair and defense against oxidative insult which correlated with a related decrease in the progression of late-stage apoptosis from 2 Gy to 4 Gy. Metabolites involved in several metabolic pathways including antioxidant defense, energy homeostasis and cell signaling indicate that at minimum threshold dose is required to induce cellular responses for attenuating radiation-induced oxidative stress. This proof-of-concept study suggests that healthy leukocytes exhibit a biphasic dose-response mechanism of radiation exposure which warrants future investigation when using low-dose priming prior to a high-dose radiation challenge for minimizing the extent of cell death by apoptosis and/or necrosis.

## 5.6. Acknowledgements

This work is supported by funds provided by the National Science and Engineering Research Council of Canada and the Canada Foundation for Innovation. R.L. acknowledges support in the form of an Ontario Graduate Scholarship.

## 5.7. References

- (1) Douglas, H., *Human Experim. Toxicol.* **2008**, *27*, 603-607.
- (2) Calabrese, E. J., Baldwin, L. A., *Nature* **2003**, *421*, 691-692.
- (3) Gems, D., Partridge, L., *Cell Metabolism* **2008**, *7*, 200-203.
- (4) Calabrese, E., Stanek, E. J., Nascarella, M., Hoffmann, G., *Inter. J. Toxicol.* **2008**, *27*, 369-378.

- (5) S.-Z.Liu, *Critical Rev. Toxicol.* **2003**, *33*, 431 - 441.
- (6) Ron, E., *Radiat. Res.* **1998**, *150*, S30-S41.
- (7) Hall, E. J., Brenner, D. J., *British J. Radiol.* **2008**, *81*, 362-378.
- (8) Kleinerman, R. A., *Pediatric Radiol.* **2006**, *36*, 121-125.
- (9) Ron, E., *Health Physics* **2003**, *85*, 47-59.
- (10) Wallace, S. S., *Radiat. Res.* **1998**, *150*, S60-S79.
- (11) Kang, C. M., Park, K. P., Song, J. E., Jeoung, D. I., *et al.*, *Radiat. Research* **2003**, *159*, 312-319.
- (12) Peker, S., Abacioglu, U., Sun, I., Konya, D., *et al.*, *Life Sciences* **2004**, *75*, 1523-1530.
- (13) Hardmeier, R., Hoeger, H., FangKircher, S., Khoschsorur, A., Lubec, G., *Proc. Nat. Acad. Sci. USA* **1997**, *94*, 7572-7576.
- (14) Navarro, J., Obrador, E., Pellicer, J. A., Asensi, M., *et al.*, *Free Radic. Biol. Med.* **1997**, *22*, 1203-1209.
- (15) Roos, W. P., Kaina, B., *Trends Mol. Med* **2006**, *12*, 440-450.
- (16) Stieber, V. W., Mehta, M. P., *Neurologic Clinics* **2007**, *25*, 1005-1033.
- (17) Avanzo, M., Romanelli, P., *Neurosurgical Review* **2009**, *32*, 1-12.
- (18) Day, T. K., Zeng, G., Hooker, A. M., Bhat, M., *et al.*, *Radiat. Res.* **2006**, *166*, 757-766.
- (19) Ito, M., Shibamoto, Y., Ayakawa, S., Tomita, N., *et al.*, *J. Radiat. Res.* **2007**, *48*, 455-460.

- (20) Fachin, A. L., Mello, S. S., Sandrin-Garcia, P., Junta, C. M., *et al.*, *Radiat. Res.* **2007**, *168*, 650-665.
- (21) Woloschak, G. E., *Inter. J. Radiat. Oncol. Biol. Phys.* **1997**, *39*, 951-952.
- (22) Woloschak, G. E., Changliu, C. M., Jones, P. S., Jones, C. A., *Cancer Res.* **1990**, *50*, 339-344.
- (23) Woloschak, G. E., Paunesku, T., *Stem Cells* **1997**, *15*, 15-25.
- (24) Cardoso, R. S., Takahashi-Hyodo, S., Peitl, P., Ghilardi-Neto, T., Sakamoto-Hojo, E. T., *Teratogen. Carcinogen. Mutagen.* **2001**, *21*, 431-439.
- (25) Sakamoto-Hojo, E. T., Mello, S. S., Pereira, E., Fachin, A. L., *et al.*, *Mutation Res.-Rev. Mutation Res.* **2003**, *544*, 403-413.
- (26) Kang, C. M., Park, K. P., Song, J. E., Jeoung, D. I., *et al.*, *Radiat. Res.* **2003**, *159*, 312-319.
- (27) Santini, M. T., Romano, R., Rainaldi, G., Ferrante, A., *et al.*, *Anticancer Res.* **2006**, *26*, 267-281.
- (28) Rainaldi, G., Romano, R., Indovina, P., Ferrante, A., *et al.*, *Radiat. Res.* **2008**, *169*, 170-180.
- (29) Rosi, A., Grande, S., Luciani, A. M., Palma, A., *et al.*, *Radiat. Res.* **2007**, *167*, 268-282.
- (30) Grande, S., Giovannini, C., Guidoni, L., Luciani, A. M., *et al.*, *Radiat. Prot. Dosim.* **2006**, *122*, 205.
- (31) Krokosz, A., Koziczak, R. N., Gonciarz, M., Szweda-Lewandowska, Z., *Radiat. Phys. Chem.* **2006**, *75*, 98-105.

- (32) Lutz, N. W., *Metabolomics* **2005**, *3*, 251-268.
- (33) Metz, T. O., Page, J. S., Baker, E. S., Tang, K. Q., *et al.*, *Trends Anal. Chem.* **2008**, *27*, 205-214.
- (34) Wishart, D. S., *Trends Anal. Chem.* **2008**, *27*, 228-237.
- (35) Patterson, A. D., Li, H., Eichler, G. S., Krausz, K. W., *et al.*, *Anal. Chem.* **2008**, *80*, 665-674.
- (36) Ramautar, R., Somsen, G. W., Jong, G. J. d., *Electrophoresis* **2009**, *30*, 276-291.
- (37) Liberda, J. J., Schnarr, K., Coulibaly, P., Boreham, D. R., *Inter. J. Radiat. Biol.* **2005**, *81*, 827-840.
- (38) Schnarr, K., Dayes, I., Sathya, J., Boreham, D., *Dose-Response* **2007**, *5*, 2207-2022.
- (39) Lee, R., Britz-McKibbin, P., *Anal. Chem.* **2009**, *91*, 7046-7057.
- (40) Chalcraft, K. R., Britz-McKibbin, P., *Anal. Chem.* **2009**, *81*, 307-314.
- (41) Chalcraft, K. R., Lee, R., Mills, C., Britz-McKibbin, P., *Anal. Chem.* **2009**, *81*, 2506-2515.
- (42) Fadok, V. A., de Cathelineau, A., Daleke, D. L., Henson, P. M., Bratton, D. L., *J. Biol. Chem.* **2001**, *276*, 1071-1077.
- (43) Rainaldi, G., Ferrante, A., Indovina, P. L., Santini, M. T., *Anticancer Res.* **2003**, *23*, 2505-2518.
- (44) Connor, J., Pak, C. H., Zwaal, R. F. A., Schroit, A. J., *J. Biol. Chem.* **1992**, *267*, 19412-19417.

- (45) Fadok, V. A., Voelker, D. R., Campbell, P. A., Cohen, J. J., *et al.*, *J. Immunology* **1992**, *148*, 2207-2216.
- (46) Koopman, G., Reutelingsperger, C. P. M., Kuijten, G. A. M., Keehnen, R. M. J., *et al.*, *Blood* **1994**, *84*, 1415-1420.
- (47) Majno, G., Joris, I., *Am. J. Pathology* **1995**, *146*, 3-15.
- (48) O'Brien, M. C., Bolton, W. E., *Cytometry* **1995**, *19*, 243-255.
- (49) McLaughlin, N., Annabi, B., Lachambre, M.-P., Kim, K. S., *et al.*, *J. Neurooncol.* **2006**, *80*, 111-121.
- (50) Meijer, A. E., Saeidi, A. B. B., Zelenskaya, A., Czene, S., *et al.*, *Inter. J. Radiat. Biol.* **1999**, *75*, 1265 - 1273.
- (51) Hall, E. J., *Inter. J. Radiat. Biol.* **1991**, *59*, 595-610.
- (52) Little, M. P., Tawn, E. J., Tzoulaki, I., Wakeford, R., *et al.*, *Radiat. Res.* **2008**, *169*, 99-109.
- (53) Marignol, L., Coffey, M., Hollywood, D., Lawler, M., *Cancer Biol. Ther.* **2007**, *6*, 1005-1012.
- (54) Ogata, H., Goto, S., Sato, K., Fujibuchi, W., Bono, H., *Nucleic Acids Res.* **1999**, *27*, 29.
- (55) Wishart, D. S., Tzur, D., Knox, C., Eisner, R., *et al.*, *Nucleic Acids Res.* **2007**, *35*, D521-526.
- (56) Lee, R., Ptolemy, A. S., Niewczas, L., Britz-McKibbin, P., *Anal. Chem.* **2007**, *79*, 403-415.

- (57) Elmore, E., Lao, X. Y., Kapadia, R., Giedzinski, E., *et al.*, *Radiat. Res.* **2008**, *169*, 311-318.
- (58) Hentze, H., Schmitz, I., Latta, M., Krueger, A., *et al.*, *J. Biol. Chem.* **2002**, *277*, 5588-5595.
- (59) Amores-Sanchez, M. S., Medina, M. A., *Molec. Gen. Metabol.* **1999**, *67*, 100-105.
- (60) Krishnan, N., Dickman, M. B., Becker, D. F., *Free Radic. Biol. Med.* **2008**, *44*, 671-681.
- (61) Suschek, C. V., Schnorr, O., Hemmrich, K., Aust, O., *et al.*, *Circulation* **2003**, *107*, 2607-2614.
- (62) Corstjens, H., Declerq, L., Hellemans, L., Sente, I., Maes, D., *Exp. Gerontol.* **2007**, *42*, 924-929.

*Chapter VI*

Future Directions in Capillary Electrophoresis-Electrospray Ionization-Mass Spectrometry for Biomarker Discovery

## **VI. Future Directions in Capillary Electrophoresis-Electrospray Ionization-Mass Spectrometry for Biomarker Discovery**

The work presented in this thesis has demonstrated that CE-ESI-MS represents a viable platform for metabolomics research which addresses some of the challenges faced by researchers involved in untargeted metabolic profiling investigations. Its unique ability to integrate on-line sample preconcentration with desalting for the analysis of polar metabolites as demonstrated in *Chapter II*, affords it an advantage over traditional LC and GC platforms, where extensive sample pretreatment protocols are often required. Also, one of the major contributions of my research has been the development of an integrative strategy for unknown metabolite identification. Incorporating computer simulations to predict the migration behavior of ions is a unique feature of the CE-MS platform. This approach is particularly valuable for distinguishing among several isobaric and isomeric metabolite candidates, where high resolution MS cannot identify the compound but only its elemental composition. Although tandem MS may be applied to differentiate among potential isobaric ions, interpretation of MS spectra relies on the presence of authentic standards which are often not commercially available. In contrast, computer simulations provide a virtual and complementary strategy for metabolite identification which can support ESI-MS. *Chapter III* demonstrated the importance of method validation with respect to labile metabolites such as GSH that are subject to oxidation artifacts during sample pretreatment. By developing a robust and validated sample pretreatment protocol,

accurate assessment of the redox status of erythrocytes was accomplished that is significant since inaccurate values of GSH and GSSG have plagued literature to date. In addition, the rate of GSH oxidation was introduced as a kinetic parameter reflective of intracellular antioxidant capacity which provided a complementary measure for differentiating different cell states. Building upon the theoretical and methodological foundations developed in the previous two chapters, *Chapters IV* and *V* demonstrated untargeted metabolomic investigations for the discovery of putative biomarkers of oxidative stress. *Chapter IV* demonstrated the integration of all developed strategies to probe the effect of strenuous exercise and antioxidant supplementation on oxidative stress. Over the course of the standardized exercise protocol, blood was frequently sampled from a volunteer to capture the time-dependent changes in metabolites levels within erythrocytes. The use of multivariate analysis was required to identify and rank metabolites which were highly modulated by the exercise regime. The application of our metabolite identification strategy allowed for the characterization of several biomarkers of oxidative stress, such as 3-MetHis, Cre, C0, and C2. Interestingly, GSH and GSSG were highly modulated during the aerobic exercise protocol, but recovered back to normal baseline levels post-exercise during recovery, which indicated that GSH metabolism in the cell during oxidative insult was tightly regulated. The study was repeated again with 6 days of oral NAC supplementation, a reported antioxidant and precursor to GSH biosynthesis. Surprisingly, NAC was found to dramatically downregulate global metabolism

but did not affect the levels of GSH, as previously reported. Nevertheless, attenuation of GSH depletion and GSSG formation was considerably affected by high dose oral NAC intake. Indeed, the effect of NAC was observed to be transient as metabolite levels after NAC consumption was terminated returned to pre-NAC levels. In contrast, *Chapter V*, focused on the identification of metabolites associated with radiation-induced oxidative stress. Lymphocytes were exposed to low level irradiation and metabolite levels were correlated to varying levels of apoptosis as a result of  $\gamma$ -irradiation. Our studies revealed that at low and high levels of ionizing radiation caused a downregulation of all detected metabolites but at the intermediate dosage, metabolites associated with energy production and antioxidant defense were significantly elevated, suggesting increased metabolic activity to counteract the onset of oxidative stress. These two studies have demonstrated the importance of rigorous data processing to avoid overestimation of redundant metabolite signals and the use of multivariate analysis as a tool for biomarker discovery. Based on the methodologies developed in this body of work, there are several directions which can be pursued with respect biomarker discovery and analysis of oxidative stress.

### **6.1 Extension of Strenuous Exercise-induced Oxidative Stress**

The proof of principle study of strenuous exercise induced oxidative stress has laid the foundation for a number of directions with respect to experimental design and analytical methodology. One of the concerns to be addressed would

be the expansion of the population pool to include a significant number of subjects to acquire a statistically relevant response for improved biological interpretation. Investigations have demonstrated metabolic response can vary extensively based on gender, age, and diet. Also it has been shown that trained versus untrained athletes will exhibit different metabolic responses to the onset of oxidative stress.<sup>1-3</sup> In order to account for inter-individual variability, a demographically diverse subject pool would be required. Several experimental factors would have to be considered and monitored to determine the efficacy of NAC or any other supplement to enhance antioxidant capacity. Diet has been shown to alter the metabolite profile of athletes undergoing the same physical exercise protocol,<sup>4</sup> thus, it would be imperative to control diet, including caloric, protein, and carbohydrate intake, and administer equal nutritional contribution. Not only would diet need to be closely monitored, physical exercise outside the bounds of the developed exercise protocol would have to be eliminated to ensure reproducibility of the exhaustive exercise routine. In addition, prior to any investigations of supplement efficacy, pharmacokinetics studies should be performed to determine the bioavailability of the supplement. In the case of NAC, pharmacokinetics was able to show the clearance of NAC within a two hour period although time was dependent on each individual.<sup>5</sup> To assess the efficacy of any supplement a thorough investigation on the pharmacokinetics should be performed to determine if any changes in the metabolic profile is a result of accumulation or a response to an acute dose.

## 6.2 Integrated Sample Pretreatment of Labile Thiol Metabolites

The analytical methodology developed for the analysis of labile metabolites found within erythrocytes, in particular thiol containing metabolites, requires immediate processing by an experienced and proficient chemist. The number of blood samples that are collected during the exercise regime can be numerous, and can allow for blood samples to be compromised due to the processing time required for each sample and as a consequence small molecule thiols such as cysteine and GSH can inadvertently become oxidized. Peptide chemists have introduced the use of the maleimide group to protect conjugate numerous compounds the thiol moieties of cysteine residues on peptides and proteins forming a covalent thiol-maleimide bond via the reaction scheme illustrated in Figure 6.1.

Preliminary results indicate the incorporation of maleimide derivatization is feasible as a blocking agent when dissolved in phosphate buffer solution (PBS) during the washing phase of erythrocytes. The inclusion of maleimide does not compromise the cellular integrity and the reaction is quite efficient as it crosses the cellular membrane through passive diffusion. The reaction between GSH and maleimide results in the formation of the GSH-maleimide (GSH-MM) conjugate which is thermally stable throughout the sample processing procedure and subsequent CE-MS analysis. This integrated whole blood isolation will allow for

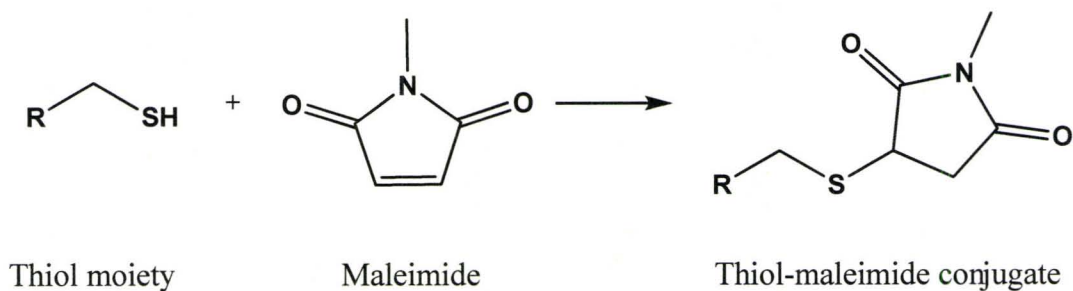


**Figure 6.1.** Reaction of maleimide with thiol moiety to form the stable thiol-maleimide conjugate.

accurate assessment of not only GSH but other low abundance and poorly responsive thiols including cysteine and  $\gamma$ -GluCys (biosynthetic precursors of GSH). Although preliminary results suggest that GSH is protected, a thorough investigation would be needed to determine if any unanticipated reactions occurs.

One further potential advantage that maleimide derivatization could address for small thiol metabolites is enhancement of ionization efficiency for improved sensitivity.<sup>6</sup> The reaction of methyl maleimide not only blocks thiol reactivity but also has shown to increase apparent ion responses. Figure 6.2a illustrates a moderate increase in ionization efficiency of approximately 20 % for NAC under alkaline CE-MS conditions and negative mode ESI. However, maleimide conjugation to hCys and Cys dramatically enhances response by approximately 40 and 19 fold increase, respectively, under acidic CE-MS conditions and positive mode ESI as demonstrated in Figure 6.2b. A systematic study to explore the ionization efficiency from maleimide derivatives should be investigated as increasing hydrophobicity could enhance ionization efficiency.<sup>6</sup> The integration of methyl maleimide into the validated sample pretreatment

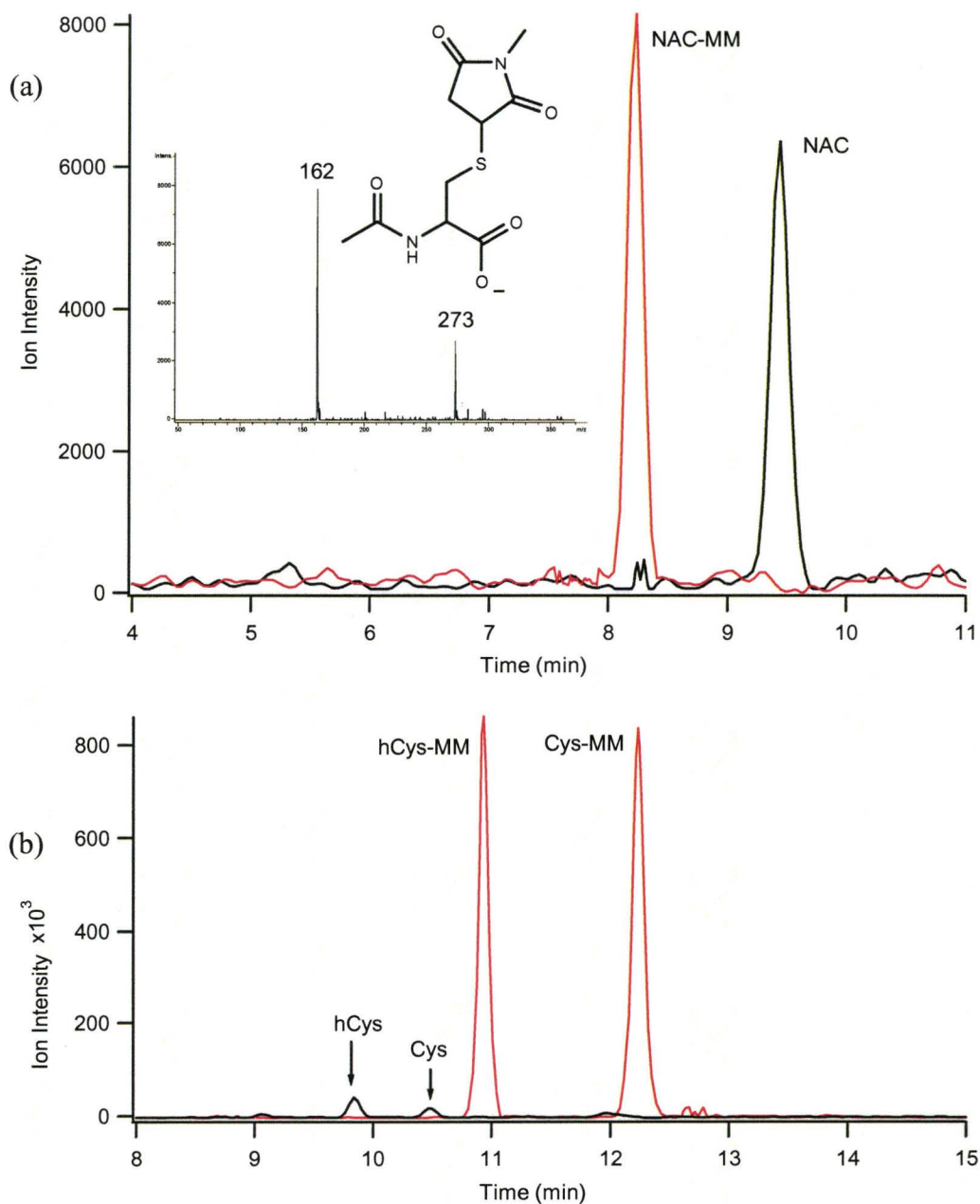


**Figure 6.2.** Extracted ion electrophorograms of free thiol (black) and thiol-MM conjugate (red). (a) Standard 20  $\mu\text{M}$  solution of both NAC and NAC-MM conjugate under alkaline conditions and negative ESI conditions. Approximately 20% increase in signal for NAC-MM compared to NAC. The inset illustrates the mass spectrum of the NAC-MM conjugate with  $[\text{M}-\text{H}]^-$  at  $m/z$  273 (b) Standard 20  $\mu\text{M}$  solution of hCys-MM and Cys-MM both display a dramatic increase in ionization efficiency with maleimide conjugation. Enhancement of 40 and 19 fold increase is exhibited by hCys-MM and Cys-MM, respectively.

protocol should allow for future studies of reactive thiol containing metabolites found within erythrocytes or any mammalian cell type.

### **6.3. Radiation-induced Metabolic Response**

The consequences of low-dose radiation exposure still remain uncertain. Evidence suggests radiation does indeed alter the metabolite profile but the degree of modification is unknown. Much of the work that has been done to study the effect of ionizing radiation has been performed on specific cell lines, and in particular their effects on cancerous cell lines. Patterson *et al.* observed varied responses to ionizing radiation depending on the cell type used.<sup>7</sup> Not only is cell type critical but previous reports have demonstrated the method in which cells are cultured will affect response, monolayer vs. spheroid,<sup>8</sup> as well, the medium in which the cells are cultured can influence their response to ionizing radiation.<sup>9</sup> Time-dependent radiation studies can be explored to observe the changes in the metabolome of WBC post-irradiation as a result of various dose levels. This study could reveal if there a time dependency for which a metabolomic response to ionization radiation which would further offer insight into the dose-dependent response observed in *Chapter V*. To minimize experimental variation, *in vivo* radiation studies may provide a more representative response to low dose radiation. Animal studies have been previously used to study the effects of radiation on gene and chromosome aberrations,<sup>10-13</sup> and an extension to study the metabolome appears to be a natural progression. Untargeted metabolomic studies to correlate traditional chromosome and gene modification experiments could be

used to generate a predictive model to describe the degree of cellular damage by low dose radiation which may reveal a much more integrated landscape of cellular response by ionizing radiation.

#### **6.4. Critical Aspects of Metabolomics and Future Directions of CE-MS**

As illustrated in Figure 1.3 of *Chapter I*, metabolomic investigations have exponentially increased since the completion of the human genome project. The utility of metabolomics to understand disease pathology<sup>14</sup> as well as to further understand protein and enzyme activity<sup>15</sup> is apparent but there are still challenges to overcome. One of the major issues that still plague metabolomics studies is chromatographic alignment. Several programs have attempted to address this issue<sup>16, 17</sup> and work relatively well for LC or GC based separation where absolute retention times are more reproducible but these software packages cannot account for the variation found in electrokinetic separations due to the variable EOF. Software development designed specifically for CE based separations could increase the speed and automation of data mining especially for CE-MS based metabolomic studies where hundreds of thousands of chromatograms can be generated as seen *Chapters IV and V*. Although the relative migration times for CE-MS have been shown to be reliable, fluctuations in absolute migration times of analytes as a result of unreliable EOF has hampered the adoption of CE-MS, particularly in the biotechnology and pharmaceutical industries. Future investigations focusing on the development of more reliable fused silica

capillaries by introducing coated capillaries<sup>18</sup> to eliminate or stabilize the EOF could greatly enhance CE-MS as a viable alternative to more traditional LC/GC-MS platforms.

### 6.5. References

- (1) Medved, I.; Brown, M. J.; Bjorksten, A. R.; Leppik, J. A.; Sostaric, S.; McKenna, M. J. *J. Appl. Physiol.* **2003**, *94*, 1572-1582.
- (2) Medved, I.; Brown, M. J.; Bjorksten, A. R.; McKenna, M. J. *J. Appl. Physiol.* **2004**, *96*, 211-217.
- (3) Medved, I.; Brown, M. J.; Bjorksten, A. R.; Murphy, K. T.; Petersen, A. C.; Sostaric, S.; Gong, X.; McKenna, M. J. *J. Appl. Physiol.* **2004**, *97*, 1477-1485.
- (4) Chorell, E.; Moritz, T.; Branth, S.; Antti, H.; Svensson, M. B. *J. Prot. Res., ASAP*.
- (5) Olsson, B.; Johansson, M.; Gabrielsson, J.; Bolme, P. *Euro. J. Clin. Pharmacol.* **1988**, *34*, 77-82.
- (6) Chalcraft, K. R.; Lee, R.; Mills, C.; Britz-McKibbin, P. *Anal. Chem.* **2009**, *81*, 2506-2515.
- (7) Patterson, A. D.; Li, H.; Eichler, G. S.; Krausz, K. W.; Weinstein, J. N.; Formace, A. J.; Gonzalez, F. J.; Idle, J. R. *Anal. Chem.* **2008**, *80*, 665-674.
- (8) Santini, M. T.; Romano, R.; Rainaldi, G.; Ferrante, A.; Indovina, P.; Motta, A.; Indovina, P. L. *Anticancer Res.* **2006**, *26*, 267-281.

- (9) Adzic, M.; Niciforovic, A.; Zaric, B.; Neskovic-Konstatinovic, Z.; Spasic, S. D.; Jones, D. R.; Radojcic, M. B. *Redox Report* **2008**, *13*, 17-22.
- (10) Bhatia, A. L.; Jain, M. *Phytomedicine* **2004**, *11*, 607-615.
- (11) Brown, A. P.; Robosky, L. C.; Okerberg, C. V.; Merriman, R.; Howard, C.; Tecele, H.; Reily, M. D. *Toxicol. Sci.* **2004**, *78*, 854.
- (12) Munson, G. P.; Woloschak, G. E. *Cancer Res.* **1990**, *50*, 5045-5048.
- (13) Tanaka, I. B.; Tanaka, S.; Ichinohe, K.; Matsushita, S.; Matsumoto, T.; Otsu, H.; Oghiso, Y.; Sato, F. *Radiat. Res.* **2007**, *167*, 417-437.
- (14) Kaddurah-Daouk, R.; Kristal, B. S.; Weinshilboum, R. M. *Annu. Rev. Pharm. Tox.* **2008**, *48*, 653-683.
- (15) Saito, N.; Robert, M.; Kitamura, S.; Baran, R.; Soga, T.; Mori, H.; Nishioka, T.; Tomita, M. *J. Prot. Res.* **2006**, *5*, 1979-1987.
- (16) Katajamaa, M.; Oresic, M. *J. Chromatogr. A* **2007**, *1158*, 318-328.
- (17) Baran, R.; Kochi, H.; Saito, N.; Suematsu, M.; Soga, T.; Nishioka, T.; Robert, M.; Tomita, M. *BMC Bioinform.* **2006**, *7*.
- (18) Kodama, S.; Yamamoto, A.; Terashima, H.; Honda, Y.; Taga, A.; Honda, S. *Electrophoresis* **2005**, *26*, 4070-4078.